MOLECULAR/MICRO-MACROSCOPIC CHARACTERISTICS OF EFFERVESCENT EUTECTIC IBUPROFEN-POLOXAMER MATRICES FABRICATED WITH MELT GRANULATION

By
Mr. Pornsit CHAIYA

A Thesis Submitted in Partial Fulfillment of the Requirements
for Doctor of Philosophy PHARMACEUTICAL ENGINEERING
(INTERNATIONAL PROGRAM)
Silpakorn University
Academic Year 2023

คุณลักษณะระดับโมเลกุล จุลภาคและมหภาคของเมทริกซ์ยาไอบูโพรเฟน-พอล็อกซาเม อร์ชนิดยูเทคติกฟองฟู่ที่เตรียมด้วยวิธีทำแกรนูลแบบหลอม

โดย
Mr.Pornsit Chaiya

วิทยานิพนธ์นี้เป็นส่วนหนึ่งของการศึกษาตามหลักสูตรปรัชญาดุษฎีบัณฑิต
วิศวเภสัชกรรม แบบ 1.2 ปริญญาปรัชญาดุษฎีบัณฑิต (หลักสูตรนานาชาติ)
มหาวิทยาลัยศิลปากร
ปีการศึกษา 2566

MOLECULAR/MICRO-MACROSCOPIC CHARACTERISTICS OF EFFERVESCENT EUTECTIC IBUPROFEN-POLOXAMER MATRICES FABRICATED WITH MELT GRANULATION

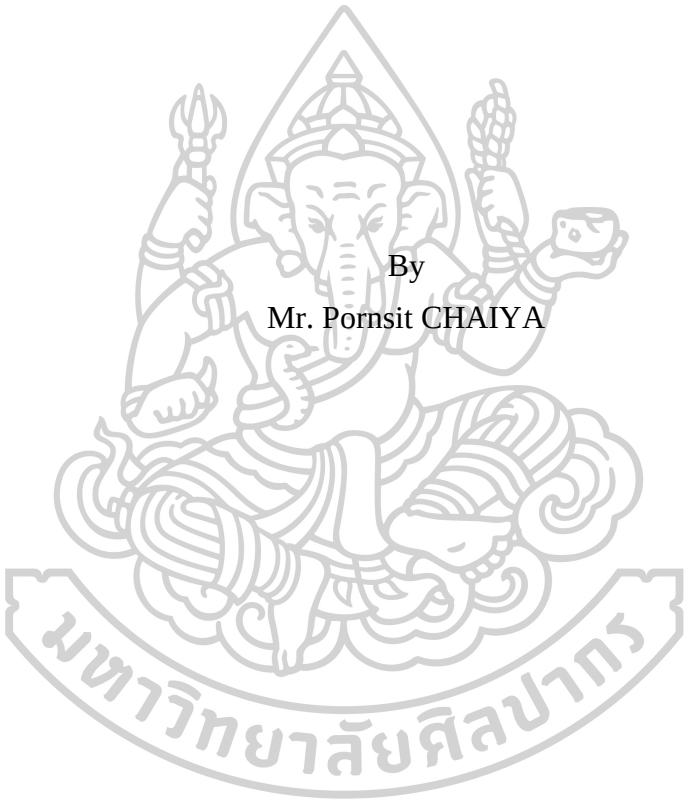

By

Mr. Pornsit CHAIYA

A Thesis Submitted in Partial Fulfillment of the Requirements
for Doctor of Philosophy PHARMACEUTICAL ENGINEERING
(INTERNATIONAL PROGRAM)
Silpakorn University
Academic Year 2023

Title	Molecular/micro-macroscopic characteristics of effervescent eutectic ibuprofen-poloxamer matrices fabricated with melt granulation
By	Mr. Pornsit CHAIYA
Field of Study	PHARMACEUTICAL ENGINEERING (INTERNATIONAL PROGRAM)
Advisor	Professor Thawatchai Phaechamud, Ph.D.
Co advisor	Associate Professor Pornsarp Pornsawad, Ph.D.

Faculty of Pharmacy, Silpakorn University in Partial Fulfillment of the Requirements for the Doctor of Philosophy

.....Dean of Faculty of Pharmacy
(Professor Pornsak Sriamornsak, Ph.D.)

Approved by

.....Chair person
(Associate Professor Pakorn Kraisit, Ph.D.)

.....Advisor
(Professor Thawatchai Phaechamud, Ph.D.)

.....Co advisor
(Associate Professor Pornsarp Pornsawad, Ph.D.)

.....Committee
(Professor Sontaya Limmatvapirat, Ph.D.)

.....Committee
(Associate Professor Prasert Akkaramongkolporn, Ph.D.)

.....Committee
(Assistant Professor Vipaluk Patomchaiviwat, Ph.D.)

620830005 : Major PHARMACEUTICAL ENGINEERING (INTERNATIONAL PROGRAM)
Keyword : Effervescent matrices, Eutectic mixture, UV-vis imaging, Numerical, Melt granulation, Ibuprofen, Poloxamer 407

Mr. Pornsit CHAIYA : Molecular/micro-macroscopic characteristics of effervescent eutectic ibuprofen-poloxamer matrices fabricated with melt granulation Thesis advisor : Professor Thawatchai Phaechamud, Ph.D.

Employing a combination of conventional and advanced techniques, the multiscale characterization of effervescent matrix tablets containing the ibuprofen (IBU)-poloxamer 407 (P407) eutectic mixture yielded valuable insights into their molecular, microscopic, and macroscopic characteristics. Traditional methods, such as thermal analysis, powder X-ray diffractometry (PXRD), and Fourier-transformed infrared (FT-IR) spectroscopy, confirmed the dispersion of IBU as a solid solution in the eutectic system with hydrogen bonding interaction with P407. Stereomicroscope and imaging analysis demonstrated enhanced wetting properties in IBU tablets with P407. Effervescent agents in eutectic tablets, observed under stereomicroscopy, facilitated CO_2 liberation, augmenting tablet surface roughness through matrix erosion. The interplay of effervescent agents and P407 in enhancing IBU dissolution was suggested by the relationship between observed physical properties and dissolution parameters. According to the impact of effervescent agents on tablet surface modification, it is interesting to incorporate into hydroxypropyl methylcellulose (HPMC) matrix tablets containing IBU-P407 eutectic mixture. The eutectic effervescent matrix tablets were successfully developed with controlled drug release characteristic. The impact of effervescent agents on tablet characteristics was explored using texture analysis and imaging approaches. Effervescent agents (5-10% (w/w)) promoted a rapid effervescence reaction, leading to high gel layer formation with low gel strength, as evidenced by texture analysis. Digital microscope and scanning electron microscope (SEM) revealed enhanced surface roughness, porosity, and a microporous structure in the gel layer. Three-dimensional images from synchrotron radiation X-ray tomographic microscopy (SRXTM) displayed interconnected pores in microporous networks, influencing the gel layer's strength, drug release patterns, and release mechanism. Furthermore, simultaneous real-time monitoring of tablet behavior and drug release using UV-visible imaging provided microscopic insights. Effervescent matrix tablets exhibited increased water penetration when exposed to HCl buffer, as indicated by the development of finger-like structures and gel layer structures with high porosities. Changing the medium to phosphate buffer at pH 6.8 led to modified gel layer structures, resulting in a significantly decreased drug release rate and a more prolonged release. Numerical approximation based on developed mathematical model was employed to estimate diffusion parameters during drug liberation studies. The mechanistic nature of effervescent agents and HPMC in controlling the release of drug in effervescent matrix tablets was clearly elucidated by determining the correlation between the estimated diffusion parameters and drug release profiles. To extend preformulation knowledge to the manufacturing phase, scaling up *via* high-shear melt granulation was conducted, varying process parameters. The IBU-P407 eutectic mixture served as a meltable binder, aiding particle agglomeration into granules. Granules and tablets prepared at 70 ºC displayed satisfactory appearance and physical characteristics. Changes in processing temperature notably influenced granule properties, subsequently modifying the physical attributes and dissolution behavior of the eutectic tablets. Comprehending the multiscale characteristics in pharmaceutical development provides valuable insights that can influence and guide the direction of future developments in pharmaceutical product design.

ACKNOWLEDGEMENTS

Completing a PhD is a remarkable accomplishment, and sometimes I can hardly believe that I have finally reached this significant milestone. I would like to propose a toast to everyone who has been a part of this incredible journey with me. First and foremost, I extend my heartfelt appreciation to my advisor, Prof. Thawatchai Phaechamud, Ph.D. for generously sharing his extensive academic knowledge and playing a pivotal role in helping me establish myself within the academic community. I am truly thankful for his firm yet compassionate guidance, which not only facilitated significant contributions to publications during my PhD but also opened doors I never thought possible. I am deeply thankful to Assoc. Prof. Pornsarp Pornsawad, Ph.D., from the Department of Mathematics, Faculty of Science, Silpakorn University, for their support especially in the numerical aspect. I extend my gratitude to Prof. Jesper Østergaard from the Department of Pharmacy, University of Copenhagen, Denmark, for his invaluable advice on the UV-vis imaging experiments. His guidance has greatly benefited my work and has been instrumental in my success. My heartfelt thanks go to Assoc. Prof. Pakorn Kraisit, Ph.D., Prof. Sontaya Limmatvapirat, Ph.D., Assoc. Prof. Prasert Akkaramongkolporn, Ph.D., Asst. Prof. Vipaluk Patomchaiviwat, Ph.D., Assoc. Prof. Chatchai Chinpaisal, Ph.D., and Catleya Rojviriya, Ph.D. for their contribution, invaluable guidance, constructive feedback, and consistent motivation, all of which significantly contributed to the development of this thesis. I am grateful to the National Research Council of Thailand (NRCT) (Grant No. NRCT5-RGJ63018-155) for supporting the grant and this thesis is partially supported by the Faculty of Pharmacy, Silpakorn University. I extend my appreciation to the committee members and all the faculty members at the Faculty of Pharmacy, Silpakorn University, as well as the staff who provided guidance and contributed to the completeness of this thesis. I am grateful to my lab members (Miss Siraprapa Chansatidkosol, Miss Ei Mon Khaing, Mr. Wantanwa Krongrawa, Mr. Kasitpong Thanawuth, Mr. Nutdanai Lertsuphotvanit, Mr. Napaphol Puyathorn, Mr. Setthapong Senarat, and Mr. Warakon Thammasut) who provided constant encouragement and valuable insights throughout the research journey. Lastly, I would like to express my heartfelt appreciation to my father and my wife. Thank you for being my unwavering support throughout this academic journey, through all the ups and downs. Your unwavering support and belief in me have been a constant source of strength and motivation.

Pornsit CHAIYA

TABLE OF CONTENTS

Page

LIST OF TABLES

Page

LIST OF FIGURES

Page

LIST OF ABBREVIATIONS

%	percentage (s)
% (w/w)	percent weight by weight
±	plus-minus sign
2θ	two theta
3-D	three-dimension
ºC	degree Celsius
µm	micrometer (s)
cm^{-1}	per centimeter
<	less than
r^2	coefficient of determination
AIC	Akaike information criterion
Alst	aluminium monostearate
API	active pharmaceutical ingredient
ATR	attenuated total reflectance
AUC	area under the curve
BA	bioavailability
BSC	biopharmaceutical classification system
CA	citric acid
CCS	crosscarmellose
CI	compressibility index
CLSM	confocal laser scanning microscopy
cm	centimeter (s)
C_{max}	maximum concentration
CMOS	complementary metal oxide semiconductor
CO_2	carbon dioxide
COX	cyclo-oxygenase

CQA	critical quality attributes
DE	dissolution efficiency
DI	deionized
DT	disintegration time
DSC	differential scanning calorimeter
e.g. (Latin);	for example
EO	ethylene oxide
f_2	similarity factor
FBG	fluid bed granulator
FCF	for coloring food
FT-IR	Fourier-transform infrared
g	gram (s)
GI	gastrointestinal
GV	gigavolt
h	hour (s)
HCl	hydrochloric acid
HLB	hydrophile-lipophile balance
HPMC	hydroxypropyl methylcellulose
HR	Hausner's ratio
HSG	high shear granulator
HSM	hot stage microscopy
I_0	initial intensity
IA	Iowa
IBU	ibuprofen
IDR	intrinsic dissolution rate
IL	Illinois
kV	kilovolt
L	lactose monohydrate

LEDs	light emission diodes
M	molarity
MA	Massachusetts
mAU	milli-absorbance unit
MCC	microcrystalline cellulose
MDT	mean dissolution time
mg	milligram (s)
MgSt	magnesium stearate
min	minute (s)
mL	milliliter (s)
mm	millimeter (s)
MO	Missouri
mPa	megapascal
MRI	magnetic resonance imaging
MSC	model selection criterion
MW	molecular weight
N	normality
NaCMC	sodium carboxymethylcellulose
NIR	near infrared
NCEs	new chemical entities
nm	nanometer (s)
NMR	nuclear magnetic resonance
No.	number
NSAID	nonsteroidal anti-inflammatory drug
ODFs	orodispersible films
P	Poloxamer
P407	Poloxamer 407
PEGs	polyethylene glycols

pH	potentia hydrogenii (Latin); power of hydrogen
pKa	acid dissociation constant
PO	propylene oxide
PXRD	powder X-ray diffractometry
RPM	revolutions per minute
SA	stearic acid
SD	solid dispersions
S.D.	standard deviation
SEM	scanning electron microscope
SLRI	Synchrotron Light Research Institute
SPSS	statistical package for social science
SRXTM	synchrotron radiation X-ray tomographic microscopy
SSA	specific surface area
SSG	sodium starch glycolate
TEM	transmission electron microscopy
T_{max}	time to achieve the maximum concentration
TPI	terahertz pulsed imaging
TSG	twin-screw granulator
UK	United Kingdom
USA	United States of America
USP	United State Pharmacopeia
UV	Ultraviolet
UV-vis	Ultraviolet-visible
WA	Washington
WI	Wisconsin

CHAPTER 1
INTRODUCTION

RATIONAL AND PROBLEM STATEMENT:

The oral route is a widely-accepted and convenient method of drug administration. It is non-invasive, painless and easy-to-use, which results in better patient compliance. Solid dosage forms are the most commonly used medication forms due to various advantages over other pharmaceutical dosage forms such as no need to require sterility during production, simple and cost-effective fabrication procedures and remarkable physicochemical stability, making it safe and easy for self-administration [1, 2]. However, dissolution is the rate-limiting step in the absorption of a drug from solid dosage forms in gastrointestinal tract. Unfortunately, many drugs currently used and in development are mostly poorly water-soluble drugs and belonging to Classes II and IV of the biopharmaceutical classification system (BSC) which have low solubility. To improve solubility, dissolution rate and/or oral bioavailability (BA) of poorly water-soluble drugs, various strategies have been explored, such as amorphous solid dispersions (SD), micro and nanoparticles, salt formation, nanocrystals, cocrystals, inclusion complexes and liquisolid pellets [3-9]. The primary emphasis of this study will be on eutectic mixture which is the one type of SD that has been popularly employed as an approach to enhance solubility and dissolution of poorly water-soluble drug compound.

Ibuprofen (IBU), a nonsteroidal anti-inflammatory drug (NSAID), belongs to the propionic acid derivative category. It has anti-inflammatory, analgesic, and antipyretic effects [10, 11] and is classified as highly permeable with a bioavailability of about 100% according to the BCS guidance [12]. However, the solubility of IBU depends on the pH of release medium. It is poorly absorbed in stomach due to its lower pH, whereas small intestine with higher pH is the main site of IBU absorption. This may result in the fluctuation of IBU concentration in local gastrointestinal (GI) tract, leading to side effects such as ulceration [13]. Therefore, to enhance the solubility and dissolution of IBU without any side effects, it is recommended to develop a eutectic mixture of IBU.

Poloxamers (P) are non-ionic block polymers consisting of hydrophobic propylene oxide (PO) and hydrophilic ethylene oxide (EO) arranged in a tri-block structure; EO_x - PO_y - EO_x [14]. These copolymers possess amphiphilic properties characterized by their hydrophile-lipophile balance (HLB) values, which depend greatly on the values of x and y [15]. Due to their surface active property, P can improve the dissolution rate as well as physical and chemical stabilities of supersaturated system by being absorbed onto the outer layer of drug particles and forming micelles that encapsulate drug particles in SD [16]. In this study, poloxamer 407 (P407) was chosen

as the carrier in SD to form the eutectic mixture with IBU. The objective was to improve the solubility and dissolution of IBU, which is categorized as a poorly water-soluble drug. Previous research has shown that using P407 as a water-soluble carrier in formulation can effectively enhance the solubility and dissolution behaviors of IBU [17]. The ratio of drug to carrier is a crucial factor in the solubility and dissolution improvements of poorly water-soluble drugs using eutectic mixture. When using P407 as carrier in a eutectic mixture, previous researches suggested that the ratio of IBU to P407 should be between 1:0.25 to 1:2.5 by weight in order to form the eutectic mixture. This conclusion is supported by differential scanning calorimetry (DSC) thermograms and powder X-ray diffraction (PXRD) patterns of these eutectic mixtures [18-20]. A low IBU:P407 ratio allows for eutectic mixture to be made using fusion method, whereas a higher ratio of 1:1.5 can be made using both physical mixture and fusion methods [20]. Therefore, the binary mixture between IBU and P407 at the ratio of 1:1.5 was chosen to be further investigated in this present study.

Monolithic matrix system is the one type of controlled-release drug delivery systems. The hydrophilic matrix system is more popular in tablet manufacturing process of controlled release drug delivery systems due to low manufacturing cost [21, 22]. Most of researchers concentrate on the drug and polymer properties such as solubility, particle size and viscosity but often neglect to consider the formulation factors such as physical characteristics [23-25]. The alteration of physical characteristics, such as internal structure and porosity, of matrices can have an impact on the pattern of drug release from hydrophilic matrix systems [26-30]. In addition, the effervescent agent which is the mixture of citric acid (CA) and sodium bicarbonate ($NaHCO_3$) can produce the gaseous carbon dioxide (CO_2) when exposed to water and promote the erosion and porosity of the internal structure of tablet [31]. Nevertheless, there have been no reports of effervescent agents being used to modify the microstructure of matrix tablet. Therefore, hydrophilic matrices with effervescent agents containing IBU-P407 eutectic mixture would be developed and determine the effect of effervescent agents on microstructure of systems using various characterization methods.

Various imaging methods are employed in the pharmaceutical realm to comprehend and define drug release from hydrophilic matrix tablets. These techniques encompass near-infrared (NIR), magnetic resonance imaging (MRI), nuclear magnetic resonance (NMR), terahertz, confocal laser scanning microscopy (CLSM), ultraviolet (UV) dissolution imaging, and synchrotron radiation X-ray tomographic microscopy (SRXTM). NIR is applied to observe the gel layer formation in compacts with hydroxypropyl methylcellulose (HPMC) [32] and track the drug release due to erosion [33]. MRI is implemented to monitor the movement of water in pastes [34], model polymer dissolution [35] and studies structural evolution of hypromellose tablets [36]. NMR is used to monitor water penetration [37], water mobility and drug diffusion in hydrophilic matrices [38]. Terahertz pulsed imaging (TPI) tracks swelling and drug diffusion in tablets containing HPMC [39, 40]. CLSM monitors gel layer growth and

water penetration in hydrophilic matrices [41, 42]. UV dissolution imaging serves as an analytical tool for the monitoring various dissolution events. These dissolution events can be events with API [43, 44], release from transdermal patches [45], dissolution behaviour of polymers [46], and swelling behaviour of the matrix tablet containing HPMC as a model hydrophilic matrix former [47]. SRXTM provides advantages in investigating three-dimensional (3-D) structures for solid objects. It quantifies interior porous channels and surfaces in tablets through fractal dimensions, correlating well with the drug release kinetics [48]. SRXTM also studies hydration dynamics and erosion-swelling layer importance, correlated with drug release [49]. It would be intriguing to examine how the effervescent agent affects the microstructure of the tablets when they are immersed in a medium using SRXTM. However, this technique may not offer real-time insight into the characteristics of the tablets during the dissolution experiment. Therefore, it is recommended to use UV-imaging techniques in conjunction with SRXTM to monitor swelling, erosion, and drug release from effervescent matrix tablets in real-time.

Besides tablet microstructure could affect mass transport, disintegration and drug release *via* dissolution of matrix tablet, the water sorption and erosion behaviors are the important quality attributes of matrix tablet which mainly affect the mechanism of drug release of formulations [50]. This investigation employs HPMC K15M grade as hydrophilic matrix-forming agent, where the gel layer thickness increases with water ingress. As water sorption progresses, the outermost polymer chains, hydrating earlier, gradually relax until losing consistency, initiating matrix erosion [51, 52]. Thus, gel formation can be discussed in term of water sorption in several research works [53]. Mathematical models, particularly mechanistic ones, are valuable tools for understanding and predicting drug release in matrix systems. Numerous models have been developed for describing drug release processes from matrices [54-57]. According to the free-volume theory, molecular diffusion rate relies on the amount of free space between the molecules [58]. It can describe the mass transport during dissolution process of hydrophilic monolithic matrix tablets especially water and drug diffusion during swelling of hydrophilic polymer after immersed in the release medium. Fujita (1961) suggested that the diffusivity of drug is sensible to the water concentration. This dependency is defined as the exponential function of the diffusion coefficient which can be linked with drug release from hydrophilic monolithic matrix tablets [59]. Therefore, in this study, the water content obtained from water sorption and erosion studies and drug release profiles are used to approximate the diffusion coefficient of water and drug during drug release studies of effervescent matrices in dissolution medium. To estimate the diffusivity of water and drug, the numerical method is implemented using the least square method with Gauss-Newton iterative algorithm to solve the non-linear function in mathematical model. The estimated diffusion coefficient of water and drug were then correlated with drug release patterns to better understand the influence of effervescent agents on mass transport of HPMC matrix tablets.

Melt granulation is a technique wherein pharmaceutical powders are effectively conglomerated using a substance which melts at relatively low temperature (50-80 ºC). This substance can be introduced to the powders in the form of either a molten liquid (*via* spray-on procedure) or solid that undergoes melting during the process (*in situ* melt granulation or melt-in procedure) [60, 61]. Given the melting characteristics of P407 in formulation, melt granulation appears suitable for producing tablets containing the IBU-P407 eutectic mixture in this study. The suitable formulation is selected to scale up with melt granulation in high shear granulator (HSG) and also investigate the effect of critical process parameters such as impeller and chopper speed and process temperature on physicochemical properties of granule and tablet comprising eutectic mixture of IBU and P407.

The aims of this study were to design the effervescent monolithic matrix tablets containing IBU-P407 eutectic mixture using HPMC K15M as matrix-forming agent and mixture of $NaHCO_3$ and CA as effervescent agents. In order to develop the controlled-release formulation, the understanding of swelling and erosion behaviors and drug release pattern of formulations should be achieved. Thus, the influence of various ratios of effervescent agents and HPMC K15M was studied and discussed in terms of physicochemical properties, swelling and erosion behaviors and drug release pattern of formulations. In addition, the novel characterization methods using stereomicroscope, SRXTM and UV-imaging were employed in this research to investigate the swelling and erosion behaviors and tablet microstructure of formulations. To achieve the profound understanding, a numerical approximation based on mathematical model was performed to investigate the role of effervescent agents and HPMC K15M on drug and water diffusivities. The findings can be linked to the macroscopic characteristics of effervescent monolithic matrix tablet. Furthermore, the suitable formulation was chosen from microscopic and macroscopic characteristics investigation to scale up with melt granulation in HSG and also investigate the effect of critical process parameters on physicochemical properties of granules and tablets containing IBU-P407 eutectic mixture.

OBJECTIVES:

1. To develop effervescent matrix tablets comprising IBU-P407 eutectic mixture with controlled drug release behavior

2. To understand the role of effervescent agents and HPMC K15M on water sorption and erosion behaviors and drug release pattern of IBU-P407 effervescent matrix tablets with novel characterization methods

3. To estimate diffusion parameters of IBU-P407 effervescent matrix tablets based on experimental data of water content and drug release profiles using numerical method implemented on mathematical model

4. To investigate the impact of effervescent agents and HPMC K15M on mass transport and its correlation with water sorption, erosion and drug release behaviors of effervescent matrix tablets comprising IBU-P407 eutectic mixture

5. To scale up the granules containing IBU-P407 eutectic mixture fabricated with melt granulation in HSG and investigate the effect of critical process parameters on physicochemical properties of IBU-P407 granules and tablets

HYPOTHESIS:

1. The ratio of effervescent agents and HPMC K15M are the crucial factors for development of IBU-P407 effervescent monolithic matrix tablets with controlled drug release manner.

2. The influence of effervescent agents and HPMC K15M on the water sorption and erosion behaviors and release pattern of IBU-loaded effervescent monolithic matrix tablets can be characterized using novel characterization methods.

3. The diffusion parameters can be estimated using numerical approximation based on mathematical model to describe the relationship between water-erosion and drug release behaviors of IBU-P407 effervescent matrix tablets.

4. The critical process parameters including processing temperature and chopper and impeller speed of HSG in melt granulation process influence the physicochemical properties of granules and tablets containing IBU-P407 eutectic mixture.

CHAPTER 2
REVIEW LITERATURES

Improvement in solubility of poorly water-soluble drugs

Approximately 40% of newly developed chemical entities in the pharmaceutical industry are practically insoluble in water. These poorly water-soluble drugs can cause insufficient and unpredictable BA, as well as gastrointestinal mucosal toxicity owing to inadequate drug absorption [62]. Drug solubility stands as a critical criterion limiting the rate for orally administered pharmaceutical dosage forms to achieve the required concentration in systemic circulation for pharmacological activities [63]. The BCS classifies drugs into four groups: class I (high solubility and high permeability), class II (low solubility and high permeability), class III (high solubility and low permeability) and class IV (low solubility and low permeability) [12]. Among four groups, drugs belonging to class II and IV exhibit poor aqueous solubility, resulting in poor BA. Therefore, enhancing the solubility and BA of poorly water-soluble drugs in BCS classes II and IV poses a significant challenge in the pharmaceutical industry. Various methods have been developed to improve the solubility and BA of poorly water-soluble drugs, including solid dispersion (SD) [64-66], complexation [67], lipid-based systems [68, 69], micronization [70, 71], nanonization [72-74] and co-crystals [75]. Among these, SD emerges as one of the most potent and successful methods. SD is defined as a mixture comprising a hydrophobic drug dispersed in hydrophilic carrier, resulting in an increased surface area that enhances drug solubility and dissolution rate. Additionally, SD improves wettability and dispersibility while reducing aggregation and agglomeration of drug particles, leading to enhanced drug BA. Molecular-level characterization of SD involves techniques such as Fourier-transform infrared spectroscopy (FTIR), Raman spectroscopy, near-infrared spectroscopy (NIR) and solid-state nuclear magnetic resonance (SSNMR). Particulate-level characterization utilizes powder X-ray diffractometry (PXRD), differential scanning calorimetry (DSC), scanning electron microscopy (SEM), and transmission electron microscopy (TEM) [76]. SD can be fabricated through various methods such as solvent evaporation [64], hot-melt extrusion [77] and spray drying [78].

Eutectic mixture theory and applications

Eutectic mixture represents a form of SD extensively utilized to enhance drug solubility. Different definitions exist for eutectic mixtures, with the most prevalent being a combination of substances that melts at a singular temperature, lower than the melting points of the pure compounds [79, 80]. Another definition describes it as a mixture of two or more components that typically do not interact to form a new chemical compound but, at specific ratios, hinder the crystallization of the other component, resulting in a system with a lower melting point [5, 81]. Eutectic mixtures

can be prepared by mixing a drug and an inert carrier, often a highly hydrophilic compound, or by combining two drugs with different solubilities [82, 83]. The growing interest in using eutectics for pharmaceutical formulations is attributed to the cost-effective preparation method and its ease of production and scalability. Additionally, since eutectics are not considered new chemical entities or crystal forms, they do not necessitate clinical trials [84]. A distinctive property of eutectic mixtures is the simultaneous melting of two components at a lower temperature compared to the pure components. Eutectic mixtures can be seen as intimately physically blended, demonstrating high thermodynamic stability. Examining the thermodynamics of eutectic mixtures suggests that they are entropy-driven. Assuming A and B are two eutectic-forming components, with the eutectic composition being X_A and X_B (where $X_A = 1 - X_B$) and T_m representing the melting point of eutectic mixture. The total entropy change, when compound A and B melt separately, is given by

$$\Delta S_T = X_A \Delta S_A + X_B \Delta S_B \quad (1)$$

where ΔS_T is the total entropy change, and ΔS_A, ΔS_B are the entropies of fusion of compound A and B, respectively. In case of non-ideal mixing, the total entropy change, will be

$$\Delta S_T = X_A \Delta S_A + X_B \Delta S_B + R X_A ln\left(\frac{1}{X_A}\right) + R X_B ln\left(\frac{1}{X_B}\right) + \Delta S_{ex} \quad (2)$$

where ΔS_{ex} is the entropy change due to non-ideal mixing and R is universal gas constant. This relationship shows that ΔS_T must increase in proportion to the mutual solubility [85]. The mixing of eutectic compounds is considered as non-ideal mixing. The total entropy of eutectic system would increase as shown in Equation 2 resulting in the melting temperature of eutectic mixture will decrease as relationship in Equation 3.

$$T_m = \frac{\Delta H_T}{\Delta S_T} \quad (3)$$

where ΔH_T is the total heat of fusion which is constant. According to these equations, intimate contact in the solid state and mutual solubility in the liquid state are the important criteria for eutectic formation. Intimate contact in the solid state is necessary for contact-induced melting point depression to occur. There would be on increase in ΔS_T and no melting point depression, if the eutectic-forming compounds are not in contact [85]. In addition, thermodynamic parameters including melting temperature (T_m), enthalpy or heat of fusion (ΔH_f) and entropy of fusion (ΔS_f) affect solubility. The decrease in ΔH_f of eutectic mixtures indicated that solubility thermodynamically increased according to Van't Hoff 's reaction. Based on the relationship between ΔS_f and T_m in Van't Hoff 's equation (Equation 4), as T_m decreases,

the logarithmic value of the molar fraction of solute approaches zero and becomes large [86].

$$ln(K) = -\frac{\Delta H}{R}\left(\frac{1}{T}\right) + \frac{\Delta S}{R} \quad (4)$$

where K is the equilibrium constant, ΔH is the enthalpy change, T is the absolute temperature, ΔS is the entropy change and R is the universal gas constant. The eutectic mixture exhibits improvements in solubility, dissolution rate, and intrinsic dissolution rate (IDR) when compared to individual drugs. However, the mechanism underlying this enhanced solubility is not always fully elucidated. Currently, there are three hypotheses to describe the enhancement of solubility/dissolution for eutectic mixtures. The first explanation proposes that when a mixture of a drug and a highly water-soluble carrier is dissolved in an aqueous medium, the carrier dissolves rapidly, releasing very fine crystals of the drug. The increased dissolution rate is attributed to the large surface area of the resulting suspension [5]. The role of highly water-soluble carriers in impacting the wettability of the drug has been described in numerous studies, where these carriers and excipients positively influence wettability, leading to solubility improvements. Studies by Haneef and Chadha (2018) emphasized the impact of hydrophilic carriers on enhancing the solubility of eutectic samples. The intrinsic solubility of the carrier significantly influences the solubility profile of eutectic mixtures, with carriers like ascorbic acid, possessing higher intrinsic aqueous solubility, exhibiting better solubility profiles [87].

The second explanation correlates the enhancement of eutectic dissolution to powder wettability. Research by Hyun and colleagues (2019) linked the improved dissolution profiles of celecoxib/adipic acid or saccharin to their superior wettability compared to raw celecoxib. A linear relationship was observed between contact angles and intrinsic dissolution values, suggesting that increased wettability and dissolution rate resulted from the inclusion of hydrophilic molecules in the formation of eutectics [81]. Enhanced wettability and dispersibility of a solid drug are known to improve the chances of non-agglomerated drug particles coming into contact with the medium, contributing to an increased dissolution rate. Additionally, lattice energies influence the dissolution of solid phases, where the prevalence of weaker forces in the crystal lattice of eutectic mixtures can be easily disrupted, and the presence of soluble carriers overcomes the solvation barrier, leading to enhanced aqueous solubility [87]. To validate these explanations, further research is needed to explore the molecular structure, organization, and microstructure of eutectic mixtures.

However, in the development of pharmaceutical solid dosage forms, unintentional eutectic formation (e.g., during pharmaceutical unit operations such as wet granulation and/or compression) has been reported to result in undesired changes in the physical and/or chemical characteristics of the solid dosage forms. These changes

may manifest as sticking, unpredictable hardness, instability, or difficulties in the accelerated assessment of stability [86]. Hence, compatibility studies between the drug substance and excipients in the formulation are crucial during the screening phase of pharmaceutical developments.

Eutectic mixture between IBU and P407

IBU ($C_{13}H_{18}O_2$, molecular weight (MW) = 206.28 g/mol) is a propionic acid derivate and nonsteroidal anti-inflammatory drug (NSAID) with anti-inflammatory, analgesic, and antipyretic effects. IBU inhibits the activity of cyclo-oxygenase (COX) I and II, resulting in a decreased the precursors of prostaglandins which produced during inflammation [11, 88]. The recommended single dose of IBU for the treatment of mild to moderate pain and fever is 200 to 400 mg with a maximum daily dosage of 1,200 mg. The chemical name is (R,S)-2-(*p*-isobutylphenyl) propanoic acid and its structure shown in Figure 1. The physical appearance is white powder with a melting point of 74-77 ºC. It is incredibly slightly soluble in water (<1 mg/mL) and readily soluble in organic solvents such as ethanol and acetone [10]. The pKa of IBU is in the range of 4.5-4.6. Following oral administration of IBU, maximum plasma concentrations are reached within 1–2 h in humans with an absolute BA of about 100% [89]. The BA of about 100% already classifies IBU as highly permeable according to the present BCS guidance [12]. In case of solubility, Potthast and coworkers (2005) reported solubility data at 37 ºC with different pH values. At the pH values below pH 5.5, their dose/solubility ratios exceed the critical value of 250 mL for both strengths (400 mg and 800 mg) of marketed IBU products [13]. Due to high membrane permeability and poor water solubility, IBU is classified as a drug belonging to BCS class II and suitable to select as a model drug to improve its solubility by eutectic mixture approach in this study.

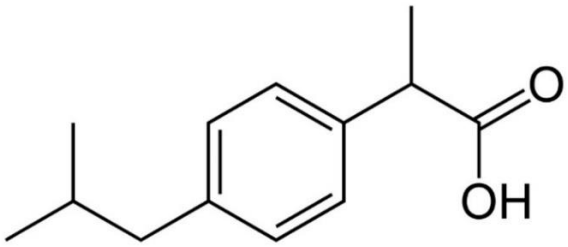

Figure 1. Chemical structure of IBU

Poloxamer (P) are block polymers consisting of hydrophobic propylene oxide and hydrophilic ethylene oxide, forming a central poly(oxypropylene) (PPO) molecule with two chains of poly(oxyethylene) (PEO) on each side [89]. Their chemical structure is $OH[CH_2\text{-}CH_2O]_x - [CH(CH_3)\text{-}CH_2O]_y - [CH_2\text{-}CH_2O]_x$, arranged in a tri-block structure; PEO_x - PPO_y - PEO_x. Registered trademarks of these copolymers (e.g., Pluronic®, Synperonic® or Tetronic®) encompass a range of liquid, paste, and solid

forms. Synthesis involves sequential polymerization of PPO and PEO monomers in the presence of sodium hydroxide or potassium hydroxide [14]. These copolymers have amphiphilic properties characterized by their hydrophilic-lipophilic balance (HLB) values, which highly depend on x and y values. By varying the values of these parameters, size, lipophilicity and hydrophilicity can be easily modified. Poloxamer 407 (P407) principally available in the registered trademark of Pluronic F127® and Synperonic F127® has a MW of about 12,600 (in range of 9,840-14,600) [15], x and y are equal to 95-105 and 54-60, respectively. Its HLB is 22 at 22 ºC [14, 89]. The chemical structure of P407 is shown in Figure 2. Due to surface active property of P, they can improve the dissolution rate as well as physical and chemical stability of supersaturated system. Moreover, it is able to absorb onto the outer layer of drug particles or form micelles encapsulating drug particles, effectively preventing drug precipitation in SD [16]. P are widely used in pharmaceutical formulations such as emulsifiers, wetting agents and solubilizers. They have been introduced into SD to enhance solubility and dissolution profiles of poorly water-soluble drugs from solid dosage forms [90, 91]. In this study, to improve solubility and dissolution of IBU which is classified as drug belonging to BCS Class II, P407 is selected as SD carrier in eutectic formulation.

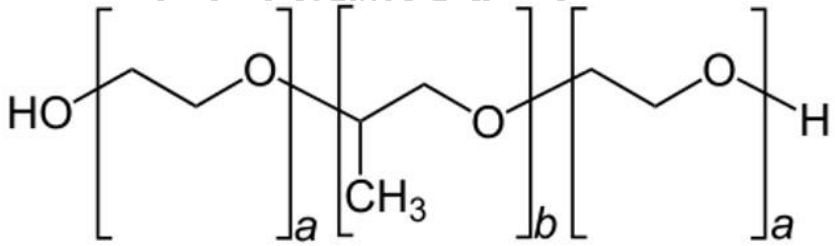

Figure 2. Chemical structure of P407 (a = 95-105 and b = 54-60)

Various researchers have reported to use eutectic mixture approach to improve the solubility and dissolution behavior of IBU remarkably by using P407 as water soluble carrier in formulation. Ali and coworkers (2010) investigated the molecular interactions between model drugs and P that facilitate dissolution rate improvements. IBU and ketoprofen was used as model drugs in SD which were prepared at different mole ratios using P. Fourier-transform infrared (FT-IR) spectra indicated the disruption of IBU dimer concomitant with hydrogen bond formation between the drug and carrier at the mole ratio of 2:1 (3% (w/w) of IBU) due to carbonyl stretching vibration of the IBU dimer shifted to higher wavenumber in the infrared spectra. SD with mole ratios >2:1 drug:carrier (up to 29:1 (33%w/w of IBU)) showed both IBU hydrogen-bonded to the P, and excess drug present as dimers. Thermal analysis of SD between IBU and P407 suggested solid solutions and a eutectic system were formed, depending on drug loading. Moreover, dissolution studies showed fastest release from the solid solutions; dissolution rates from solid solutions were 12-fold greater than the dissolution of IBU powder whereas the eutectic mixture gave a 6-fold improvement over the IBU powder

[17]. Besides of drug loading which affect the interaction in SD, preparation method should be considered as the important factor in SD approach. Al Masum et al. (2013) prepared SD of IBU using P as water-soluble carrier at different ratios and methods. Effect of different methods which were melt dispersion and solvent evaporation techniques on solubility properties and dissolution characteristics was also investigated and compared. The results obtained from the study showed both melt dispersion and solvent evaporation techniques could improve the release rate and extent of IBU from SD. In addition, the higher ratio of drug:carrier about 1:1.5 could form a eutectic system that undergoes melting at comparatively lower temperature region. When the content of P is relatively lower about 1:0.5, some portions of IBU dissolve and hence, a little peak for the remaining drug is obtained from DSC thermogram [18]. This is consistent with the study of Newa et al. (2008) which prepared SD of IBU using different ratios of P with melting dispersion method. Solubility and dissolution of IBU linearly increased as the increment in the ratio of P407 in SD. Moreover, pharmacokinetic study was also performed in twenty male Sprague-Dawley rats. The total plasma concentration (AUC), maximum concentration (C_{max}) and time to achieve the maximum concentration (T_{max}) were significantly higher compared with those in IBU powder. This indicated higher extent of absorption for SD because of their improved dissolution rate in rate intestine [19]. Thus, the fast and complete dissolution resulting from improved solubility of SD is responsible for its enhanced oral absorption. Dugar et al. (2016) prepared SD of IBU with lower levels of P407 giving a chance of higher drug loading without increasing the final formulation weight. Drug to polymer ratios at 1:0.25 to 1:0.75 by weight were selected and high shear mixer was used for carrying out the fusion method. The maximum solubility enhancement was seen in fused formulation with the drug:polymer ratio of 1:0.75 and DSC thermogram and PXRD exhibited decreasing of drug crystalline due to eutectic formation. However, at lower content of P407 in SD (1:0.25 to 1:0.75), DSC thermogram showed two endothermic peaks. The one endothermic peak at lower temperature region represented the eutectic formation between IBU and P and another peak at higher temperature region represented the remaining IBU in SD. Tamman's diagram suggested the exact eutectic composition to be close to 27% by weight of IBU which corresponds roughly to 1:2.5 % w/w ratio [19]. Therefore, the suitable ratios of IBU:P407 that can form eutectic mixture and prepare with both physical mixture and fusion method should be in range of 1:1.5 to 1:2.5 by weight. In this study, the binary mixture between IBU and P407 at the ratio of 1:1.5 is chosen to further investigated.

Effervescent systems

Effervescent systems comprise alkali metal bicarbonates and acids, primarily citric and tartaric acid, engaging in a chemical reaction related to acid-base interactions upon contact with water, leading to the generation of gas bubbles, mainly carbon dioxide (CO_2) [92, 93]. Typical oral dosage forms often face drawbacks such as slow absorption, affecting the onset of drug action. While this challenge can be addressed by administering drugs in liquid form, many drugs encounter limitations in solubility and stability. The implementation of effervescent systems in solid dosage forms presents a solution to enhance the therapeutic outcomes of drugs [94]. The main important property of effervescent products is the adsorption/desorption isotherm of the raw material and, consequently, its moisture content. To avoid a premature effervescent reaction in the tablets, substances with low moisture contents will have to be used. Acid materials in effervescent products can be obtained from three main sources; acid, acid anhydrides and acid salts. The commonly used sources of acid materials are organic acid such as citric acid (CA), tartaric acid and ascorbic acid. A comparison of the formation of carbon dioxide from effervescent tablets based on anhydrous citric acid, ascorbic acid or tartaric acid, and $NaHCO_3$ in stoichiometric proportions indicated that ascorbic acid and anhydrous CA behaved similarly. However, tartaric acid formed the most CO_2, but the disintegration time was longer [95]. In case of ascorbic acid, Schmidt et al. (1988) studied the possibility of using ascorbic acid in effervescent tablet preparation. The results showed that ascorbic acid can be used as the acid source in effervescent tablet. The speed of release of CO_2 from a mixture of ascorbic acid and $NaHCO_3$ is comparable with that produced by CA or tartaric acid–$NaHCO_3$ combinations. Since ascorbic acid is less hygroscopic than citric and tartaric acid, using ascorbic acid as the only acid source makes it possible to produce effervescent tablets in a non-air conditional area [96]. For sources of CO_2, both carbonates and bicarbonates are used as carbonate sources, but the latter is most often used. $NaHCO_3$ is an odorless, white crystalline powder and slightly alkaline taste. It can produce carbon dioxide approximately 52% by weight. At relative humidity (RH) below approximately 80% (at room temperature), the moisture content is less than 1%. Above 85% RH, it rapidly absorbs an excessive amount of water and may start to decompose. When heated to 250-300 ºC, $NaHCO_3$ decomposes and is converted into anhydrous sodium carbonate. However, this process is both time and temperature-dependent [97]. Due to high CO_2 yield of mixture between $NaHCO_3$ and CA, they are chosen as effervescent agents in this study. The chemical structure of $NaHCO_3$ and CA are illustrated in Figure 3.

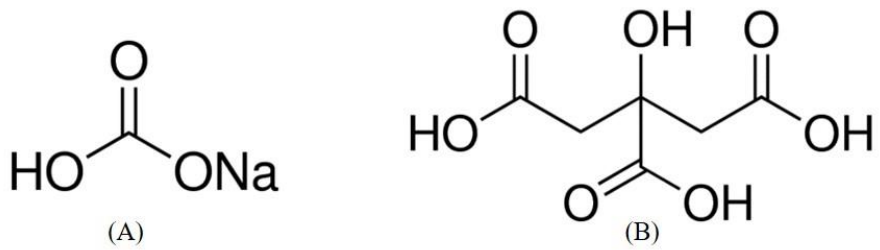

Figure 3. Chemical structure of $NaHCO_3$ (A) and CA (B)

Monolithic matrix systems

Traditionally, oral drug administration has been the predominant method for delivering drugs, primarily due to the flexibility in dosage form design afforded by the gastrointestinal physiology compared to other routes [50, 98]. A controlled release drug delivery system administers the drug either locally or systemically at a predetermined rate for a specified duration [98-100]. The objective of such systems is to achieve therapeutic plasma levels by offering desirable delivery profiles [98]. The controlled release systems have numerous advantages over conventional dosage forms, including reduced dosing frequency due to drug release over a longer period of time [101], avoidance of side effects due to dose dumping and better patient compliance due to reduced dosing [99]. These systems are categorized based on the mechanism of drug release, encompassing diffusion-controlled, dissolution-controlled, erosion-controlled, ion exchange-controlled, and transport-controlled systems, also known as osmotic pump systems [102]. Matrix systems, specifically diffusion-controlled ones, are widely employed for controlled release formulations and are further categorized as reservoir matrix systems, monolithic matrix systems, and osmotic pump systems, based on their mechanisms for prolonging drug release [51].

Monolithic matrix systems involve incorporating the drug into a matrix, which can be created using hydrophobic and/or hydrophilic matrices to regulate drug release [21]. Hydrophobic matrix systems, primarily utilizing waxes, are suitable for highly water-soluble drugs, as demonstrated by Sudha et al. (2010) with a tramadol hydrophobic matrix tablet using hydrogenated cottonseed oil as a sustained release matrix [22, 103]. Although hydrophobic matrices can modulate drug release, the involved processes like hot fusion and thermal treatment highlight the time-consuming nature of tablet formation, posing challenges for cost-effective manufacturing of sustained-release formulations. Conversely, hydrophilic matrix systems are more commonly employed in tablet production for controlled-release drug delivery due to their lower manufacturing costs [22]. Upon contact with water, hydrophilic matrices increase in size due to the entry of the water molecules. This then allows the polymer to swell up forming a barrier to drug release. There has been a lot of research into the mechanisms of drug release from hydrophilic matrices and the critical factors that

influence the release rate. Most of researches focus on the amounts and types of used polymer in hydrophilic matrices. Maggi et al. (2002) studied the effects of different types of polymers, such as different MW of PEO, on the hydration and erosion of matrix tablet, which affect the drug release. The findings revealed that varying MW of PEO influence erosion behavior, which could explain the different efficiencies of the two polymeric products in modulating the release of the water-soluble drug [23]. Conti et al. (2007) investigated drug release behavior of the systems containing a mixture of HPMC and sodium carboxymethylcellulose (NaCMC) and each substance. *In vitro* drug release studies demonstrated that the mixture of HPMC and NaCMC enables better control of the drug release profiles both in terms of rate and mechanism when compare with matrices containing only one polymer [24]. This finding is consistent with the study of Siahi-Shadbad et al. (2011) which used the binary mixtures of psyllium powder and other hydrophilic polymers to produce controlled release profile of propranolol HCl [25]. In addition, the study of Phaechamud (2008) exhibited the geometry dimension of matrix systems also influences the drug release pattern. Layered matrix tablet of propranolol HCl containing HPMC and phytowax as matrix components was prepared using direct compression. Layering with this polymeric matrix could prolong the release of drug and shift the release pattern approach to zero order [21]. In addition to the polymer types and tablet geometry, drug release from hydrophilic matrix systems is influenced by three main factors: drug properties (solubility and particle size), polymer properties (radius of gyration, particle size, viscosity), and formulation factors. Formulation factors, such as tablet characteristics, play a crucial role in affecting the drug release pattern, particularly porosity and air entrapment in the matrix tablet. The presence of pores or channels in the matrix significantly impacts drug release kinetics. Studies, like Dabbagh et al. (1996), have explored the impact of different compression forces on matrix porosity, leading to varied drug release patterns [26]. The study of Nerurkar et al. (2005) indicated the porosity of IBU matrices based in a combination of cellulose derivate and a carrageenan, either the initial porosity from compaction or that due to the rapid dissolution of drug molecules, increases the release rate of the drug, since drug molecules can access the medium more easily through the channels or pores [27]. Pore formation mechanisms in matrices of water-soluble drugs involve rapid dissolution of surface drug particles, creating pores that facilitate increased drug release. In the case of water-insoluble drugs, the formation of pores in the matrix is more limited [104]. Given the poorly water-soluble nature of IBU, the use of a hydrophilic monolithic matrix tablet is considered suitable for this study. Additionally, the inclusion of effervescent agents (NaHCO3 and CA) may induce pore formation through carbonation, potentially altering IBU release from the formulation. Investigating these microstructural properties is a compelling aspect of the present study.

Polymeric materials play a crucial role in pharmaceutical formulations, particularly in controlled-release applications, leveraging their favorable properties. These characteristics stem from the structure and composition of polymers, which are chains formed by covalently bound monomers. The structural variations in these chains include linear, branched, and crosslinked configurations, resulting in diverse polymer types based on complexity.[105]. In recent years, hydrophilic matrices, integral for controlled release, have seen an upsurge in the utilization of various polymers including natural or synthetic, alone or in combinations as effective release retardant excipients. Polymers exhibiting swelling behavior in aqueous media can be categorized into hydrogels, which swell but remain insoluble in water, and hydrophilic polymers, which both swell and dissolve in water. Commonly used polymers in controlled-release matrices are detailed in Table 1.

Table 1. Commonly used polymers in controlled release matrices

Hydrophilic polymers
Cellulose derivatives - Methyl cellulose - Hydroxypropyl methylcellulose (Hypromellose, HPMC) - Hydroxypropylcellulose (HPC) - Hydroxyethylcellulose (HEC) - Ethylhydroxyethylcellulose (E-HEC) - Sodium carboxymethylcellulose (NaCMC)
Non-cellulose derivatives - Sodium alginate - Xanthan gum - Carrageenan - Chitosan - Guar gum - Pectin - Cross-linked high amylose starch - Polyethylene oxide - Homopolymers and copolymers of acrylic acid
Water-insoluble and hydrophobic polymers
- Ethylcellulose - Hypromellose acetate succinate - Cellulose acetate - Cellulose acetate propionate - Methacrylic acid copolymers - Polyvinyl acetate

Among the hydrophilic polymers, HPMC is the one most widely used as a drug release retardant excipient in hydrophilic matrices. HPMC is soluble in water, non-ionic cellulose derivatives and stable over pH range 3-11 [106]. HPMC is the preferred choice for formulating hydrophilic matrix systems. Its non-ionic nature minimizes interaction issues in various pH environments, ensuring consistent release profiles [24]. HPMC is particularly favored for its rapid hydration, excellent compression, and gelling characteristics compared to other swellable polymers used for prolonged drug release. Additionally, it boasts low toxicity and widespread availability [107-109]. Therefore, HPMC has been a material of great importance when used as a matrix-forming agent in monolithic matrix tablets. The chemical structure is shown in Figure 4.

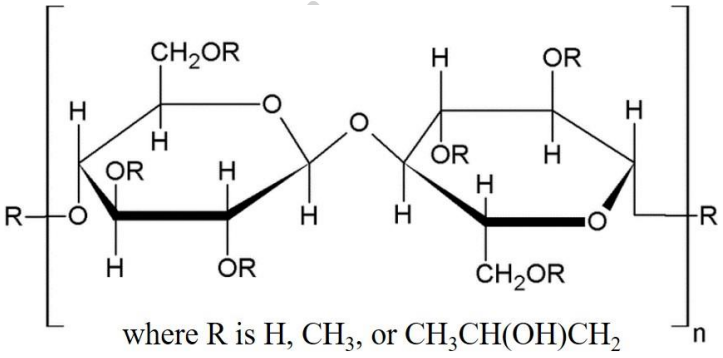

Figure 4. Chemical structure of HPMC

Pharmaceutical tablet characterizations using imaging techniques

The tablet quality relies on several attributes, necessitating rigorous control before market release. Critical quality attributes (CQA), such as drug content, polymorphism, uniformity of drug content, dissolution behaviors, coating state, and physical characteristics, must be regulated within suitable ranges to ensure product safety, efficacy, and impact on *in vivo* drug behaviors [110]. Typically, traditional tablet characterization involves off-line and at-line testing through methods like UV spectroscopy, dissolution apparatus, and tablet hardness tester. While these methods are accurate and standardized, they have limitations in terms of resource consumption, labor intensity, and destructiveness. To overcome these drawbacks, extensive research has explored imaging techniques for tablet characterization [111]. Unlike conventional methods, innovative imaging allows real-time visualization and noninvasive assessment of pharmaceutical dosage form quality. Various imaging techniques, such as optical imaging, terahertz pulsed imaging (TPI), UV imaging, near-infrared spectroscopy (NIR) imaging, Raman imaging, magnetic resonance imaging (MRI), X-ray imaging, attenuated total reflectance-Fourier transform infrared (ATR-FTIR) imaging, and thermal imaging, can be employed for this purpose.

UV imaging has emerged as a valuable tool for real-time monitoring and quantification of drug concentrations during dissolution and release processes [112]. This technique utilizes UV light of specific wavelengths to irradiate pharmaceutical samples, enabling imaging through CMOS. UV imaging facilitates the observation of key events in drug dissolution, including polymer swelling, drug precipitation/recrystallization, and solvent-mediated phase transitions [113]. Multispectral UV imaging, a non-destructive approach, allows for the differentiation of drug compounds or excipients in a compact matrix and rapid visualization of amorphous and crystalline forms. In a study by Wu and co-worker, utilizing glibenclamide in both forms along with MCC and magnesium stearate, UV imaging effectively distinguished between the active pharmaceutical ingredient (API) and excipients, providing a non-invasive mapping of the API in its solid state [114].

Excipients play a crucial role in various aspects of drug manufacturing, including formulation, molding, and absorption in solid dosage forms. UV–vis imaging has emerged as a novel approach for the functional characterization of excipients in solid oral dosage forms [115]. In a study involving tablets containing theophylline anhydrate, magnesium stearate, and either MCC or HPMC, UV–vis imaging, coupled with a UV–vis detector and Sirius SDi2, was employed. The experiment, conducted in 0.01 M HCl at 37 ◦C, revealed that HPMC tablets exhibited greater swelling compared to MCC tablets, with a visible gel layer only in HPMC tablets. UV–vis imaging recorded during release tests showed a significant increase in the diameter of HPMC tablets over time, while the size of MCC tablets changed minimally. Flow rate variations in the dissolution medium had little impact on the swelling of HPMC tablets, whereas for MCC cellulose tablets, different flow rates resulted in size changes, indicating that expansion and erosion were flow rate-dependent [116]. Surface dissolution UV imaging was utilized to examine the swelling behavior of SSG (Sodium starch glycolate) and croscarmellose sodium (CCS) and its impact on drug dissolution. Findings revealed that the rapid swelling of SSG and CCS was influenced by critical formable materials and the pH of the dissolution medium, emphasizing their non-interchangeability in oral solid dosage forms [117]. UV imaging was also applied to study the real-time diffusion and release of Piroxicam and human serum albumin in Pluronic F127 hydrogels. The experiment provided real-time data on the temporal and spatial absorbance distribution, indicating lower diffusion coefficients for formulations with higher polymer content and larger analytes, in accordance with Fick’s second diffusion law [118]. Given the benefits of UV imaging in real-time monitoring of tablet behavior, it is intriguing to apply it in this investigation to examine how tablets change during drug release in the dissolution medium. This could provide insights into the influence of effervescent agents on HPMC matrix tablets.

Mathematic modeling of monolithic matrix tablet based on swelling and erosion behavior

As previously stated, HPMC serves as the matrix-forming agent in the monolithic matrix tablet incorporating IBU. Its notable characteristic, high swellability, significantly influences the release kinetics of the drug in an HPMC-based formulation [119]. Upon introduction of the matrix tablet into an aqueous medium, water permeates the matrix, moistening the polymer and drug particles, and filling the pores. In the hydrated layer, drug particles dissolve, and drug molecules diffuse from the wetted zone, defined by the diffusion front in Figure 5. The hydrated polymer chains gradually relax, forming a gel layer. Notably, drug diffusion in the gel layer is much faster than in the dry glassy core and the slightly hydrated layer [120]. To design controlled drug delivery systems based on HPMC with specific, predefined release profiles, understanding the precise mass transport mechanisms in drug release and the ability to quantitatively predict resulting release kinetics are crucial. An effective mathematical model offers practical benefits by allowing simulation of the impact of design parameters on the release profiles of HPMC-based drug delivery systems [121].

Several mathematical models, ranging from simpler ones like the Higuchi equation to more complex and comprehensive models, have been proposed for predicting drug release rates [122]. A notable model in previous studies was introduced by Siepmann et al. (1999), incorporating simultaneous considerations of polymer swelling, dissolution, and water diffusion, with diffusivity changing in response to variations in water concentration. Recognized as the "sequential layer" model, it stands out for accounting for multiple phenomena concurrently, revealing the strong dependence of water and drug diffusivity on the matrix's swelling ratio [123].

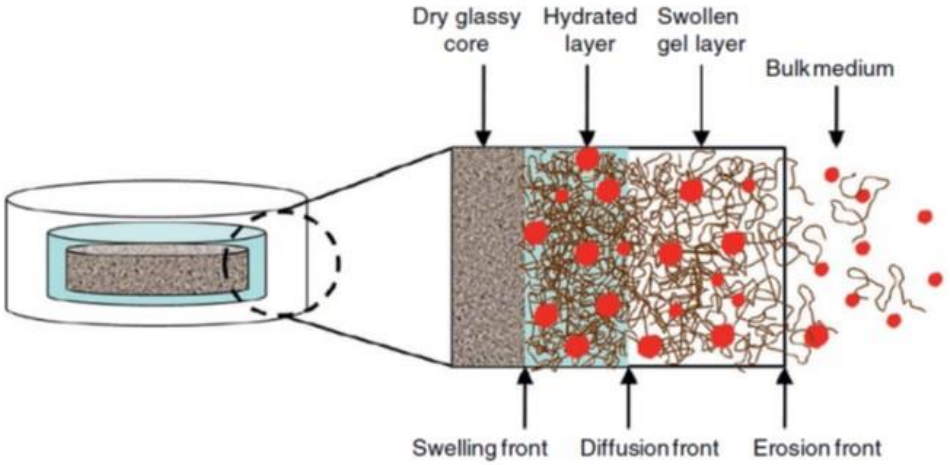

Figure 5. Illustration of drug release from hydrophilic matrix tablet by swelling mechanism [121]

Modeling release behavior is crucial for understanding the mechanisms in controlled release systems. Siepmann et al. (2002) applied the sequential layer model to analyze physicochemical effects on drug release, predicting how the initial tablet radius and height impact release rates for both highly and poorly water-soluble drugs [124]. Other works, like Lamberti et al. (2011), introduced a model explaining hydrogel morphology changes over time, considering water uptake, drug release, swelling, and erosion to predict parameters such as mass fraction of substitution, matrix radius, and released drug amount [125]. Caccavo et al. (2015) used Laplace smoothing to account for morphology alterations, and in 2017, Caccavo and colleagues demonstrated the poro-viscoelastic properties of polymer matrices influencing water uptake and release [126, 127]. Mathematical models also aid in estimating the impact of geometry and dimensions on release profiles, with surface area being a critical factor [128-130]. In fact, varying the initial tablet radius has a more significant effect on release profiles than changing the initial height due to the greater alteration in available surface area [131]. Colombo et al. (2009) illustrated how changes in geometry can assist in designing formulations for specific release profiles [132]. In summary, a comprehensive mathematical model that considers all dominant phenomena affecting release kinetics is a powerful tool for predicting how formulation factors like composition, initial size, and shape of tablets influence drug release rates. This allows for theoretically predicting the formulation needed to achieve a desired drug release profile [133, 134].

Melt granulation with high shear granulator (HSG)

Melt granulation is a method in which pharmaceutical powders are effectively agglomerated using a substance that melts at relatively low temperatures (50-80 ºC). This substance can be introduced to the powders either as a molten liquid (spray-on procedure) or as a solid that undergoes melting during the process (*in situ* melt granulation or melt-in procedure) [60]. In both scenarios, the molten substance functions as a liquid binder, forming dry granules as the molten binder solidifies through cooling. In recent years, interest in melt granulation has grown due to its numerous advantages over traditional wet granulation. Notably, melt granulation eliminates the need for organic or aqueous solvents. This absence of organic fluids eliminates the risk of residual solvents in the final dosage form and avoids issues related to environmental requirements for solvent capture and recycling. The process's water-free nature also streamlines operations, reducing time and energy consumption compared to wet granulation [60]. Another notable benefit of melt granulation is its versatility in preparing either controlled-release or immediate-release granules through the careful selection of meltable binders. Hydrophilic binders like polyethylene glycols (PEGs) and P are employed for enhanced-release formulations, while hydrophobic binders such as waxes, fatty acids, fatty alcohols, and glycerides can be applied for prolonged-release formulations [61]. Instruments suitable for melt granulation include

high shear granulator (HSG), fluidized bed granulator (FBG), and twin-screw granulator (TSG). The initial investigations into melt granulation using HSG date back to the early 1990s, where Shaefer and colleagues (1992) published a series of papers extensively exploring the impact of process and formulation variables on melt agglomeration and the mechanisms governing the growth of agglomerates [135-137]. Others researchers have examined the melt granulation process in HSG demonstrating that this process can be usefully employed both to enhance the dissolution rate of poorly water-soluble drugs [138-141] and to control the release of short half-life drugs [141, 142]. Passerini and colleagues (2010) developed melt granules of poorly water-soluble drugs, IBU and ketoprofen, utilizing PEG 6000 as the meltable binder. They conducted a comparative analysis of the physicochemical properties of melt granules produced with HSG and FBG. The findings indicated successful melt granulation in both granulators. Different equipment significantly influenced particle size distribution and morphology of the granules. Importantly, the solid-state characteristics and dissolution behavior of IBU and ketoprofen granules were essentially unaffected by the choice of equipment, with all granules exhibiting a noteworthy increase in drug dissolution rate under acidic conditions. [61]. In a study by Steffens et al. (2020), a comparison was made regarding the physicochemical properties of melt granules produced with different granulators, specifically TSG and HSG. Melt granules from HSG exhibited a more spherical shape, lower porosity, smaller mean particle size, and superior flowability compared to those from TSG. Conversely, TSG-produced granules showed a more elongated structure, higher porosity, larger mean particle size, and a smaller specific surface area (SSA). Regarding the compression process, granules from TSG displayed comparable compressibility to HSG granules [143]. Therefore, horizontal HSG is suitable for manufacture IBU incorporated effervescent monolithic matrix tablet in pilot scale due to good physical properties of melt granule can be obtained. In addition, P407 in formulation can be used as meltable binder during melt granulation with horizontal HSG. The outside and inside views of horizontal HSG are illustrated in Figure 6.

Figure 6. The outside (A, B) and inside views of horizontal HSG

Scope of research work

In this research work, poloxamer 407 served as a eutectic-forming agent to enhance the water solubility of ibuprofen. The study involved scrutinizing the physicochemical aspects, including thermal characteristics, crystallinity, and intermolecular interactions, to reveal the distinctive features of the ibuprofen-poloxamer 407 eutectic mixture. Effervescent matrix tablets incorporating ibuprofen-poloxamer 407 were formulated with HPMC K15M as the matrix-forming agent and a powder mixture of sodium bicarbonate and citric acid anhydrous (in a 1:1.3 ratio by weight) as effervescent agents. This investigation explored the impact of varying concentrations of HPMC K15M and effervescent agents on the physicochemical properties of matrices, employing a combination of conventional methods and advanced imaging techniques such as stereomicroscopy, synchrotron radiation X-ray tomographic microscopy, and UV-vis imaging. Additionally, numerical approximation based on developed mathematical model was employed to estimate diffusion parameters and comprehend the influence of HPMC K15M and effervescent agents. To capture the multi-scale characteristics, spanning microscopic to macroscopic levels, the study applied scaling up through high-shear melt granulation with various process parameters, providing a comprehensive understanding of effervescent matrix tablets containing the eutectic mixture of ibuprofen and poloxamer 407.

CHAPTER 3
MATERIALS AND METHODS

EQUIPMENT AND INSTRUMENT:

1. Aluminum pans and covers (Perkin Elmer, Shelton, USA)
2. Analytical balance (CP224S, Sartorius, Germany)
3. Analytical balance (PA4102, Ohaus, USA)
4. Circulator water bath (CWB-13L, Han Yang Scientific Equipment Co., Ltd, Seoul, Korea)
5. DDSolver software (Add-in program for Microsoft Excel (Redmond, WA, USA))
6. Desiccators (Biologix Research Company, USA)
7. Differential scanning calorimeter (DSC 8000, Perkin Elmer, USA)
8. Digital microscope (AM-413ZT, Dino-Lite Pro, Bangkok, Thailand)
9. Disintegration tester (ZT320, Erweka, Langen, Germany)
10. Dissolution apparatus equipped (DT 820, Erweka, Germany)
11. Drishti software (National Computational Infrastructure, Canberra, Australia)
12. Erlenmeyer flask
13. Fourier-transform infrared spectrophotometer (Nicolet 4700, Madison, USA)
14. Freeze dryer (Triad^{TM}, Labcondo, MO, USA)
15. Friability tester (Erweka GmbH, Langen, Germany)
16. Glass slide
17. GNU Octave 6.4.0 for Windows-64
18. Goniometer (FTA 1000, First Ten Angstroms, USA)
19. Hardness tester (TBH-325, Erweka, Langen, Germany)
20. High shear mixer/granulator (Pharmaceuticals and Medical Supply L.P., Samutsakorn, Thailand)
21. Hot stage microscope (Stage from Mettler Toledo, Bangkok, Thailand and microscopy from Olympus, Bangkok, Thailand)
22. Hydraulic press (Carver press, WI, USA)
23. Magnetic stirrer (C-MAG-HS7, IKA, Germany)
24. Octopus Reconstruction software (TESCAN, Gent, Belgium)
25. Octopus Analysis software (TESCAN, Gent, Belgium)
26. Oscillating granulator (Pharmaceuticals and Medical Supply L.P., Samutsakorn, Thailand)
27. OLYMPUS Stream Basic 2.2
28. Petri dish glass (diameter; 5.0 cm)
29. pH meter (Seven compact, Mettler Toledo, Japan)
30. Porcelain mortar and pestle
31. Powder X-ray diffractometer (Mini Flex II, Rigaku cop, Japan)
32. Quartz cuvette
33. Scanning electron microscope (Cam Scan MX-2000, UK)
34. SDi2 Analysis software (version 3.0.20, Sirius Analytical Ltd, Forest Row, UK)

35. SDi2 Collection software (version 1.2.0.0, Sirius Analytical Ltd, Forest Row, UK)
36. Shaking incubator (NB-205, N-Biotek, Korea)
37. Sirius SDi2 instrument (Forest Row, UK) equipped with a USP IV type flow cell
38. SPSS 11.5 for Windows (SPSS Inc., Chicago, IL, USA)
39. Stainless steel sieve No. 18 (1 mm), 20 (850 µm), 60 (250 µm)
40. Stereomicroscope (SZX10, Olympus corp., Japan)
41. Texture analyzer (TA.XT plus, Stable Micro Systems, UK)
42. Thickness tester (SM-112, Teclock, Nagano, Japan)
43. UV-vis spectrophotometer (Cary 60 UV-Vis G6860A, Agilent Technologies, Malaysia)
44. Vortex mixer (KMC-1300V, Vision scientific, Korea)
45. X-ray tomographic microscopy beamline (BL1.2W: XTM) of the Siam Photon Source (SPS), Synchrotron Light Research Institute (SLRI), Nakhon Ratchasima, Thailand.)

MATERIALS:

1. Aluminium monostearate (Lot no. 0001447128, Fluka, Sigma-aldrich Co., USA)
2. Brilliant blue FCF dye (Lot no. 000BC, PC Drug Co., Ltd, Bangkok, Thailand)
3. Citric acid anhydrous (Lot no. 90900209, Maxway Co., Ltd., Thailand)
4. Dibasic potassium phosphate (Lot no. 0711005, Ajax Finechem, Australia)
5. Glyceryl dibehenate (Lot no. 177179, Rama production Co., Ltd., Bangkok, Thailand)
6. Hydrochloric acid 37%, AR grade (Lot no. 07A300516, VWR Chemicals, UK)
7. Hydroxypropyl methyl cellulose K15M (HPMC K15M) (Lot no. PH26012N31, Dow Chemical, Michigan, USA)
8. Ibuprofen (Lot no. 4000/1101/18/A-0150B, PC Drug Co., Ltd, Bangkok, Thailand)
9. Lactose monohydrate (Lot no. 1009CON, Maxway Co., Ltd., Thailand)
10. Magnesium stearate (Lot no. MAF07, PC Drug Co., Ltd, Bangkok, Thailand)
11. Methanol AR grade (Lot no. 2040269, Fisher Chemical, UK)
12. Microcrystalline cellulose PH101 (Lot no. C1910113, Mingtai Chemical Co., Ltd., Taiwan)
13. Monobasic sodium phosphate (Lot no. 1310152834, Ajax Finechem, Australia)
14. Poloxamer 407 (Lot no. WPDF563B, BASF, Ludwigshafen, Germany)
15. Potassium bromide, For IR spectroscopy (Lot no. I297362002, Loba Chemie PVT, India)
16. Sodium bicarbonate (Lot no. AF310196, Ajax Finchem, Australia)
17. Sodium hydroxide (Lot no. AF310204, Ajax Finechem, Australia)
18. Stearic acid (Lot no. 3452018, PC Drug Co., Ltd, Bangkok, Thailand)

Experiment set-up:

3.1 The study of effervescent tablets containing eutectic mixture of IBU and P407

3.1.1 Sample preparation

3.1.1.1 Preparation of physical mixture (PM) between IBU and excipients

In this study, IBU was used as active pharmaceutical ingredient (API) whereas P407 was used as co-eutectic forming agent. Microcrystalline cellulose PH 101 (MCC PH101) and lactose monohydrate (L) were used as diluent. In addition, lubricants (stearic acid (SA), aluminium monostearate (AlSt), magnesium stearate (MgSt) and glyceryl dibehenate (Compritol®) and effervescent agents ($NaHCO_3$ and citric acid anhydrous in the ratio of 1:1.3 by weight) were also included in formulations. Each pure substance was sieved through a stainless-steel sieve No.60 mesh. PM was prepared by co-grinding of excipients and IBU in ratio of 1:1 by weight using porcelain mortar and pestle for 10 min. These PMs were kept in desiccator for further testing.

3.1.1.2 Preparation of IBU-P407 eutectic mixture

To achieve the suitable eutectic mixture between IBU and P407 as mentioned above, the binary mixture in the ratio of 1:1.5 was chosen to investigate in this study [20]. The preparation of IBU-P407 eutectic mixture with different methods including physical mixture (PM) and melting samples (MS) was also investigated in this study. PM was prepared by co-grinding of IBU and P407 in ratio of 1:1.5 by weight using porcelain mortar and pestle for 10 min. In case of MS, IBU and P407 were mixed together for 10 min using mortar and pestle then heated to 60 ºC in circulator water bath (Model: CWB-13L, Han Yang Scientific Equipment Co., Ltd, Seoul, Korea). Mixture was left to cooled down to room temperature, scrapped out and powdered with mortar and pestle. Both PM and MS were kept in desiccator for further analysis.

3.1.1.3 Preparation of effervescent tablets comprising IBU-P407 eutectic mixture

In this study, various tablets including plain IBU tablet, IBU-P407 eutectic tablet (IP) and five distinct eutectic effervescent tablets (5E to 30E) were produced using the direct compression method. Initially, IBU and P407 in the ratio of 1:1.5 were co-grinded in mortar and pestle for 10 min to induce eutectic formation. Subsequently, effervescent agents ($NaHCO_3$ and CA in ratio 1:1.3 by weight) and MCC PH101 were sieved through sieve no. 20 (opening: 850 µm) into the plastic bag and then mixed with the IBU-P407 eutectic mixture for 5 min. The resulting mixtures were compressed into 1000 mg eutectic effervescent tablets at a

compression force of 2 tons and dwell time of 10 sec using a hydraulic press (Carver press, WI, USA) with 12.7 mm round, flat and plain punch. The components of eutectic effervescent tablets are detailed in Table 2.

Table 2. Composition of eutectic effervescent tablets.

Compositions (% (w/w))	Formulation						
	IBU	IP	IP5E	IP10E	IP20E	IP25E	IP30E
IBU	100.00	40.00	34.00	32.00	28.00	26.00	24.00
P407	-	60.00	51.00	48.00	42.00	39.00	36.00
$NaHCO_3$	-	-	2.83	5.65	11.30	14.13	16.96
CA	-	-	2.17	4.35	8.70	10.87	13.04
MCC PH101	-	-	10.00	10.00	10.00	10.00	10.00
Total	100.00	100.00	100.00	100.00	100.00	100.00	100.00

Remarks: IBU = plain tablet consists of only IBU, IP = 40% by weight of ibuprofen in eutectic tablet, E = % by weight of effervescent agents (the mixture of $NaHCO_3$ and CA in the ratio of 1:1.3 by weight) in each formulation such as IP5E stands for formulation containing IP and 5% by weight of effervescent agents.

3.1.2 Physicochemical characterization of powder mixture

3.1.2.1 Differential scanning calorimeter (DSC)

Thermal analysis was conducted using individual pure compounds and their physical mixtures (PM) as samples. Each sample, weighing approximately 3-5 mg, was placed in a standard aluminum pan, sealed, and subjected to heating in a DSC chamber (DSC 8000, Perkin Elmer instruments, Japan). The heating rate employed was 10 ºC/min, and the temperature range was set between 40-140 ºC in a nitrogen atmosphere at a flow rate of 20 mL/min.

3.1.2.2 Hot stage microscopy (HSM)

HSM (stage from Mettler Toledo, Bangkok, Thailand and microscopy from Olympus, Bangkok, Thailand) was employed to examine the melting behavior of individual pure compounds and prepared PMs under heating conditions. The observations included the alterations in the morphology and crystallinity of each compound. The samples underwent heating at a rate of 10 ºC/min within the temperature range of 40-140 ºC. Photographs capturing the morphological changes of each sample were taken at room temperature (30 ºC), partial melting temperature (PMT), and complete melting temperature (CMT).

3.1.2.3 Powder X-ray diffractometry (PXRD)

The crystallinity of individual pure compounds and the changes in crystal behavior of the prepared PMs were assessed using PXRD (MiniFlex II, Rigaku Corp, Japan). All samples were finely ground using a mortar and pestle, then placed

into a PXRD disc. The evaluation involved scanning through the range of 5-55 for 2θº, with a resolution of 0.05º on 2θ.

3.1.2.4 Fourier-transformed infrared (FT-IR) spectroscopy

FT-IR was employed to examine the molecular interaction between IBU and excipients in PMs. Each pure compound and PMs were mixed with potassium bromide at a ratio of 1:100 and compressed into pellets using a plunger and die with hydraulic press (Carver Press, Carver Inc., IN, USA) at a compression force of 4 tons. The sample pellets were placed in IR chamber (Nicolet 4700, Madison, USA) and the %transmittance of sample was recorded. The spectra were acquired at a resolution of 4 cm^{-1}, covering the range of 400-4000 cm^{-1}.

3.1.2.5 Scanning electron microscopy (SEM)

To investigate surface morphology, SEM (Maxim 200 Camscan, Cambridge, UK) was utilized at an accelerated voltage of 15 kV and magnifications of 250X and 1000X. The observations focused on the surface morphology of IBU, P407, and eutectic mixtures prepared using various methods.

3.1.3 Physical properties characterization of tablets

Ten tablets from each formulation underwent examination for their diameter, thickness and hardness using a hardness tester (PHARMA TEST, USA). For weight variation evaluation, each eutectic effervescent tablet was individually weighed utilizing analytical balance (Sartorius model CP224S, Göttingen, Germany). The average weight and standard deviation were calculated based on sample size of 20 tablets (n=20). Furthermore, friability was determined as percent weight loss of 10 tablets after rotating for 100 revolutions in 4 mins using friability tester (Erweka GmbH, Langen, Germany).

3.1.4 Determination of wetting properties, swelling and erosion under stereomicroscope of tablets

The wetting properties of eutectic effervescent tablets were assessed using a stereomicroscope (Olympus model SZX10, Hamburg, Germany) at a magnification of 15x. Each eutectic effervescent tablet was submersed in 0.05% (w/v) of brilliant blue in distilled water or 0.1 N HCl buffer pH 1.2. The tablet was positioned in 5.0 cm diameter glass petri dish filled with the specified solution. The morphological changes in the eutectic effervescent tablet during immersion were captured under the stereomicroscope at one-minute intervals for 30 minutes. Image analysis was performed on a total of 31 images from each sequence using the OLYMPUS Stream Basic 2.2 program. In Figure 7A, the blue color penetration from the medium into the eutectic effervescent tablet was observed. The penetration distance (indicated by the white line) was calculated as the difference

between the initial border at 0 minutes (represented by the black line) and the wetting border at specific time intervals (red line). The wetting rate for each formulation was determined by calculating the slope of the profile depicting the relationship between penetration distance and time (n = 5).

For investigating the gel formation and erosion of the eutectic effervescent tablet, experiments were conducted under the same conditions as described in the wetting investigation above. Following immersion of the prepared tablet in the medium, swelling and gel formation occurred, and the tablet's gel formation was photographed. Gel thickness was measured as the difference between the tablet's initial boundary at 0 minutes (indicated by the black line) and the gel boundary at specific time intervals (represented by the red line) (Figure 7B). The gel formation rate for each formulation was calculated using the slope of the profile depicting the relationship between gel thickness and immersed time (n=5). For erosion rate calculation, the erosion of each formulation was determined as the difference between the tablet's initial border at 0 minutes (represented by the black line) and the erosion boundary at predetermined time intervals (represented by the red line) (Figure 7C). Subsequently, the erosion rate of each formulation was determined from the slope of the profile depicting the relationship between the erosion boundary diameter and the immersed time (n=5).

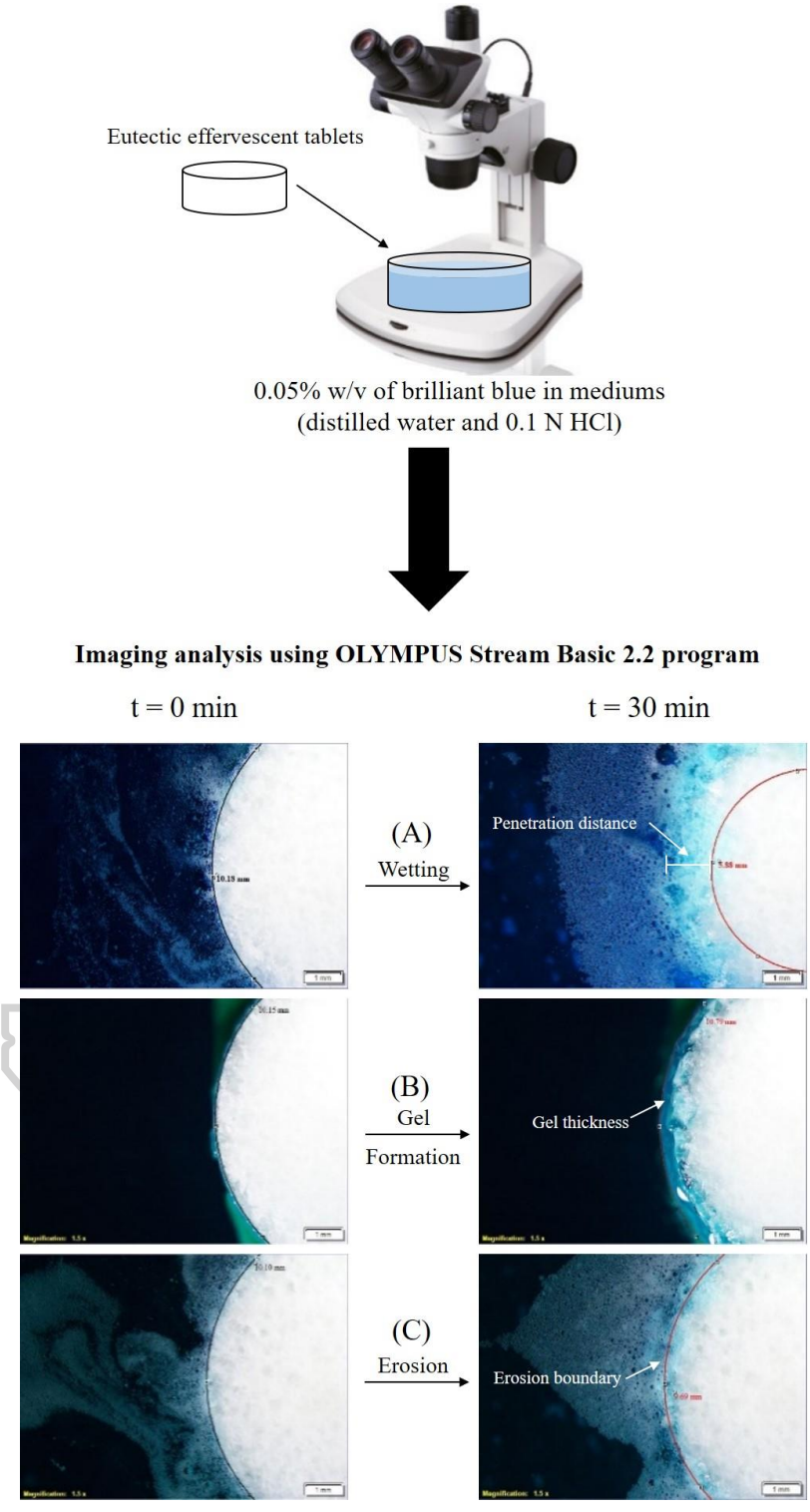

Figure 7. Wetting properties, gel formation and erosion investigation of eutectic effervescent tablet under stereomicroscope

3.1.5 *In vitro* disintegration studies of tablets

The disintegration time (DT) of eutectic effervescent tablets was determined using the disintegration tester (ZT 320, Erweka, Langen, Germany), following the procedures outlined in the US Pharmacopeia (USP) 43 <701>. The measurements were conducted with 900 mL of distilled water at 37 ± 2 ºC. Additionally, to explore the impact of the pH medium on the tablets' disintegration behavior and its correlation with observed parameters under the stereomicroscope, 0.1 N HCl buffer pH 1.2 was employed as the disintegration medium. Six tablets were placed in individual tubes of the basket-rack assembly, and the time at which each tablet completely disintegrated was recorded. The mean disintegration time (DT) ± standard deviation (S.D.) was then calculated (n = 6).

3.1.6 *In vitro* drug release studies of tablets

3.1.6.1 Calibration curve of drug

To create standard stock solutions, the drug was precisely weighed and dissolved in 0.1 N HCl buffer pH 1.2. These stock solutions were then diluted to various concentrations, encompassing the range of drug release samples. The optimal concentration range for UV detection was identified by establishing a correlation between concentration and absorbance using a UV-vis spectrophotometer (Cary 60 UV-Vis G6860A, Agilent Technologies, Malaysia). The resulting plot exhibited an r^2 value ranging between 0.9990 and 1.000, enabling the determination of the appropriate concentration range for UV detection.

3.1.6.2 Determination of *in vitro* drug release and release kinetics

According to USP43, the *in vitro* dissolution testing of IBU tablets should be conducted using phosphate buffer pH 7.2 as the dissolution medium. To evaluate the impact of eutectic formation on IBU dissolution, 0.1 N HCl buffer pH 1.2 was employed as discriminating medium owing to the low solubility of IBU in acidic medium [20]. The *in vitro* drug release was investigated in 0.1 N HCl buffer pH 1.2 using a dissolution apparatus (DT 820, Erweka, Germany) with the paddle method at 37ºC and rotational speed of 50 rpm, aligning with the USP43 <711> Dissolution procedure. At predetermined intervals, 5 mL aliquots were withdrawn from the dissolution media and replaced with 5 mL of fresh media. UV-vis spectrophotometer (Cary 60 UV-Vis G6860A, Agilent Technologies, Malaysia) at a wavelength of 220 nm was utilized to analyze the dissolved drug amount from tablets. The mean cumulative drug dissolution ± S.D. was then calculated (n=3).

3.1.6.3 Kinetic of drug release study

The *in vitro* drug release data were analyzed by DDSolver software which is a menu-driven add-in program for Microsoft Excel (Redmond, WA, USA) written in visual basic application [144]. To investigate the mechanism of drug release of formulations, cumulative drug release data were fitted with different mathematic release equations including modified Korsmeyer–Peppas and Peppas–Sahlin. The coefficient of determination (R^2), Akaike Information Criterion (AIC) and model selection criterion (MSC) were calculated and used to indicate the degree of curve fitting and appropriate modeling.

3.2 The study of effervescent matrix tablets comprising of IBU-P407 eutectic mixture

3.2.1 Preparation of IBU-P407 eutectic effervescent matrix tablets

For the combined mechanical and imaging characterization of effervescent matrix tablets, the melt granulation method was employed to fabricate effervescent matrix tablets (5E and 10E), along with a control tablet (IPM). Initially, IBU and P407 at the ratio of 1:1.5 by weight were co-grinded using a mortar and pestle for 10 min to induce the eutectic formation. Subsequently, effervescent agents ($NaHCO_3$ and CA at the ratio of 1.3:1 by weight), MCC PH101 and HPMC K15M were sieved through a no. 20 sieve (opening: 850 µm) and mixed with the IBU-P407 eutectic mixture for 5 min. For the control tablet, MCC PH101 was solely added and mixed with the IBU-P407 eutectic mixture. The resulting mixture was placed in a glass beaker in a circulating water bath (model: CWB-13L, Han Yang Scientific Equipment Co., Ltd., Seoul, Korea), stirred continuously, and maintained at 70 °C until melted granules were obtained. After 2 h of cooling down to room temperature, the granules were sieved through a no. 18 stainless steel sieve (1.0 mm of open diameter). Granules were then compressed into 1000 mg matrix tablets using 12.7 mm round, flat and plain punches with a hydraulic press (Carver press, Wabash, IA, USA), at a compression force of 2 tons and dwell time of 10 s. Table 3 shows the compositions of the effervescent matrix tablets.

Table 3. Compositions of IBU-P407 effervescent matrix tablets for characterization using combined mechanical and imaging techniques.

Formulation	Amount of substances (mg/tablet)						
	Ibuprofen (IBU)	Poloxamer 407 (P407)	Sodium bicarbonate	Citric acid anhydrous	HPMC K15M	MCC PH101	Total
IPM	200.00	300.00	-	-	-	500.00	1000.00
5E	200.00	300.00	28.26	21.74	200.00	250.00	1000.00
10E	200.00	300.00	56.52	43.48	200.00	200.00	1000.00

Remarks: E = % by weight of effervescent agents (the mixture of $NaHCO_3$ and CA at the ratio of 1.3:1 by weight) in each formulation.

For real-time characterization using UV-imaging technique, effervescent matrix tablets were fabricated as described above. However, the number of formulations was different due to the varying concentration of effervescent agents, and HPMC was also altered as shown in Table 4.

Table 4. Composition of IBU tablet and eutectic IBU effervescent matrix tablets for real-time characterization using UV-imaging technique

Formulation	Amount of substances (mg/tablet)						
	Ibuprofen (IBU)	Poloxamer 407 (P407)	Sodium bicarbonate	Citric acid anhydrous	HPMC K15M	MCC PH101	Total
IBU	1000.00	-	-	-	-	-	1000.00
EUTECTIC	200.00	300.00	-	-	-	500.00	1000.00
5E10HP	200.00	300.00	28.26	21.74	100.00	350.00	1000.00
5E20HP	200.00	300.00	28.26	21.74	200.00	250.00	1000.00
10E10HP	200.00	300.00	56.52	43.48	100.00	300.00	1000.00
10E20HP	200.00	300.00	56.52	43.48	200.00	200.00	1000.00

Remarks: E represents the amount of effervescent agents in percentage (%). HP represents the amount of HPMC K15M in percentage (%).

In the case of mechanistic characterization using numerical techniques, the similar preparation of eutectic effervescent matrix tablets was conducted and the different formulations are displayed in Table 5.

Table 5. Composition of eutectic tablets and effervescent matrix tablets for mechanistic characterization utilizing numerical technique

Formulation	Amount of substances (mg/tablet)						
	Ibuprofen (IBU)	Poloxamer 407 (P407)	Sodium bicarbonate	Citric acid anhydrous	HPMC K15M	MCC PH101	Total
EUTECTIC	200.00	300.00	-	-	-	500.00	1000.00
5E10HP	200.00	300.00	28.26	21.74	100.00	350.00	1000.00
5E20HP	200.00	300.00	28.26	21.74	200.00	250.00	1000.00
5E25HP	200.00	300.00	28.26	21.74	250.00	200.00	1000.00
10E10HP	200.00	300.00	56.52	43.48	100.00	300.00	1000.00
10E20HP	200.00	300.00	56.52	43.48	200.00	250.00	1000.00
10E25HP	200.00	300.00	56.52	43.48	250.00	200.00	1000.00

Remarks: E represents the amount of effervescent agents in percentage (%). HP represents the amount of HPMC K15M in percentage (%).

3.2.2 Physical properties characterization of effervescent matrix tablets comprising IBU-P407 eutectic mixture

The physical characteristics of effervescent matrices, including thickness, hardness, diameter, and weight of effervescent matrix tablets were evaluated. Ten tablets of each formulation underwent testing for diameter and hardness using a hardness tester (ERWEKA, model: TBH-325, Langen, Germany), while the thickness was measured with a thickness tester (Teclock, model: SM-112, Nagano, Japan). Tablet weights (n = 10) were determined with analytical balance (model: CP224S, Sartorius, Göttingen, Germany), and the average weight along with S.D. were calculated. Statistical significance of the data was analyzed using the independent t-test, with a significant level at $p < 0.05$. The analysis was conducted using SPSS for Windows (Version 11.5, SPSS Inc., Chicago, IL, USA.).

3.2.3 Determination of gel strength upon hydration using texture analysis

Each tablet of the effervescent matrix underwent testing with dissolution apparatus filled with 900 mL pH-shift dissolution medium, consisting of pH 1.2 HCl buffer (0.1 N) and phosphate buffer pH 6.8. Stirred with a paddle rotating at 50 rpm, the investigation occurred in pH 1.2 HCl buffer (0.1 N) for initial 1.5 h, followed by raising the pH of the medium to 6.8 until the completion of 4 h operation. At specified intervals of 15 and 30 minutes and 2 and 4 hours, five swollen tablets were delicately extracted, and the gel strength was individually assessed using a texture analyzer (TA.XT plus, Stable Micro Systems Ltd., Surrey, UK) equipped with a 2 mm diameter flat-tipped, round steel probe (Figure 8). The test conditions were set at 0.2 mm/s pre-test speed, 0.1 g trigger force, and 0.1 mm/s test speed. Gel strength was calculated as the ratio of the force to the penetration depth of the probe inside the gel, following the provided equation:

$$G = \frac{F}{x} \times \frac{1}{rp} \times 0.0098 \quad (5)$$

where G = gel strength (mPa), F = force (g) registered at the probe penetration, x = penetration depth (mm) and r_p = radius of the probe (1 mm). The gel strength at the gel–solution interface was considered as the first point after the probe came into full contact with the gel (trigger force reached), and the initial noise disappeared. The average gel strength was calculated as the mean of five consequent data [145].

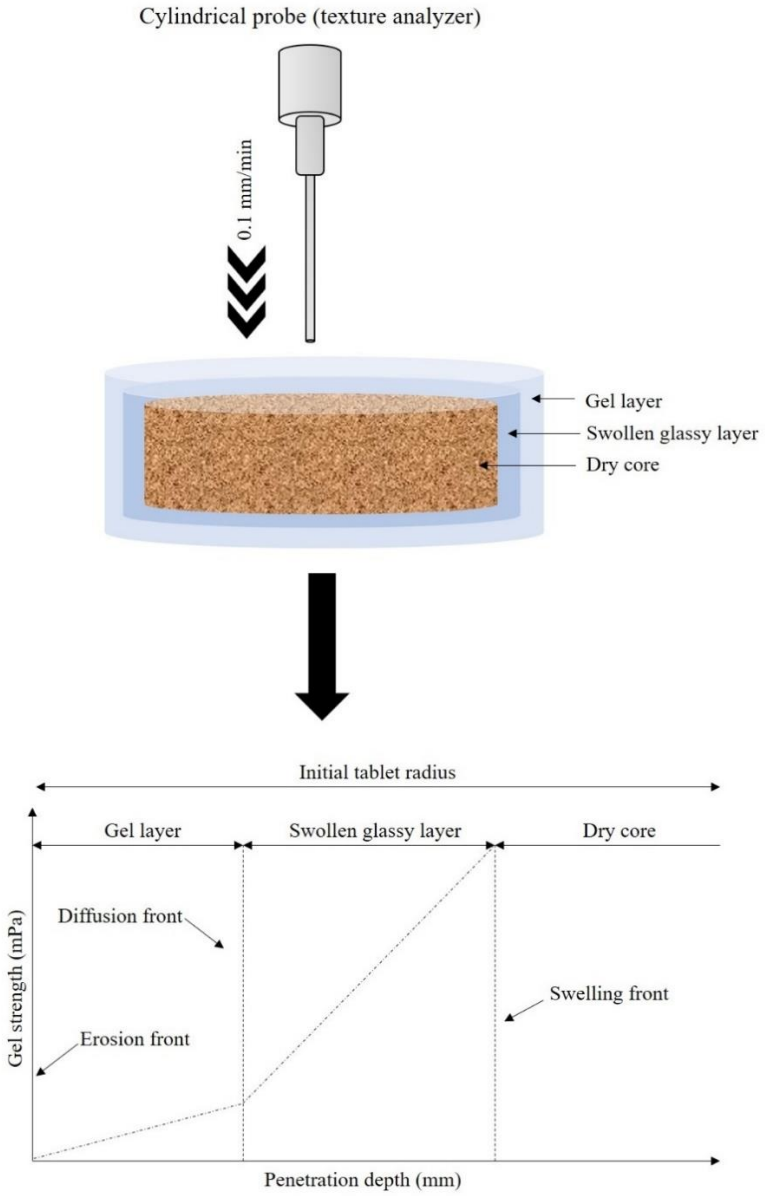

Figure 8. Schematic representation of gel strength determination upon hydration

3.2.4 Topological and microtomographic studies

3.2.4.1 Sample pretreatment using freeze-drying method

In line with previous findings suggesting that the freeze-drying technique preserves the microstructure of the hydration layer effectively due to its rapid cooling process [49, 146], standard dissolution test was conducted to assess the temporal alterations in the microstructure of the effervescent matrix tablets during hydration. At predetermined time intervals (0, 15 and 30 min; 2 and 4 h), the swollen tablets were delicately extracted along with 2 mL of the medium and individually placed in a glass Petri dish with a 5 cm diameter. Subsequently, the glass Petri dishes, containing the tablets at various stages of hydration and erosion, were promptly transferred to an ultra-low-temperature refrigerator (model: UF-V 500, BINDER GmbH, Tuttlingen, Germany) at −80 °C for 12 h. After this phase, the tablets underwent freeze-drying for 24 hours at −40 °C and 15 mbar vacuum conditions using a freeze dryer (Triad^{TM}, Labcondo, Kansas City, MO, USA). The tablets were stored in a desiccator under ambient temperature for further analysis.

3.2.4.2 Matrix morphological change under digital microscopy and SEM

Following freeze-drying, the alterations in the surface and cross-sectional morphology of effervescent matrix tablets, subsequent to hydration in the dissolution media, were documented using a digital microscope with a 26.8X magnification (model: AM-413ZT, Dino-Lite Pro, CHOSEN Technology Co., Ltd., Bangkok, Thailand). For the examination of surface morphology, SEM (Maxim 200 Camscan, Cambridge, UK) was employed to observe the dried tablet surfaces at an accelerated voltage of 15 kV and a magnification of 250X.

3.2.4.3 SRXTM and porosity determination

Microtomographic images of dried effervescent matrix tablets were acquired using an SRXTM beamline (BL1.2W: X-ray imaging and tomographic microscopy) at the Synchrotron Light Research Institute (SLRI), Nakhon Ratchasima, Thailand. The synchrotron X-ray radiation was generated by a 2.2-Tesla multipole wiggler at the Siam Photon Source operating at 1.2 GV. Employing a filtered polychromatic X-ray beam with a distance of 32 m from the source to the sample, experiments were conducted at a mean energy of 11.5 kV. Due to the formulations containing the IBU-P407 eutectic mixture, prone to melting at low temperatures, an extended exposure to the X-ray beam during testing could potentially liquefy the dried effervescent matrix tablet. To mitigate exposure time, the dried tablet was divided into eight parts, with one-eighth mounted on the stage. X-ray radiographs were then collected from 0° to 180° with an angular increment of 0.3°. Subsequently, Octopus Reconstruction software (TESCAN, Gent, Belgium) [147] was utilized to analyze the collected X-ray radiographs and

generate reconstruction images. A selection of 600 reconstruction images was processed, and Octopus Analysis software (TESCAN, Gent, Belgium) was employed to calculate porosity based on binary images. Drishti software (National Computational Infrastructure, Canberra, Australia) [148] was employed to compute the 3-D tomographic volume from the reconstruction images.

3.2.5 *In vitro* drug release study and release kinetics

To explore the influence of different media on the drug release profile of effervescent matrices, a volume of 900 mL of pH-shift media were employed in this investigation. The *in vitro* drug release in pH 1.2 HCl buffer was carried out for 1.5 h. Subsequently, the pH of the medium was adjusted to 6.8 by the addition of 1.09 g sodium hydroxide, 3.06 g monobasic potassium phosphate, and 5.02 g dibasic sodium phosphate, culminating in the completion of the operation at 24 h. *In vitro* drug release was examined using a dissolution apparatus (DT 820, Erweka, Langen, Germany) and the paddle method at 37 ± 0.5 °C with a rotational speed of 50 RPM, in accordance with the USP43 <711> dissolution procedure. At predefined intervals, 5 mL aliquots were withdrawn from the dissolution medium and replenished with an equivalent volume of fresh medium. The amount of dissolved drug was quantified using a UV-vis spectrophotometer (Cary 60 UV-vis, Agilent Technology, Santa Clara, CA, USA) at a wavelength of 220 nm. The mean cumulative drug dissolution ± S.D. was calculated (n = 3). The drug release mechanisms were assessed by fitting the release data to zero-order, first-order, Higuchi's, Korsmeyer–Peppas, Hixson–Crowell, Hopfenberg, and Peppas–Sahlin equations using DDSolver software, a menu-driven add-in program for Microsoft Excel (Redmond, WA, USA) designed in visual basic applications [144]. Furthermore, mathematical analysis included calculating the coefficient of determination (R^2), Akaike information criterion (AIC), and model selection criterion (MSC) for the drug release data with appropriate modeling.

3.2.6 UV-Vis imaging

For the imaging of the entire tablet, a Sirius SDi2 instrument from Forest Row, UK, equipped with a USP IV type flow cell, was employed. The cylindrical flow cell has a diameter of 28 mm and a volume of 60 ml, containing 12 g of 1 mm glass beads. The SDi2 system features LEDs with wavelengths of 255, 280, 300, 320, and 520 nm, capable of dual-wavelength imaging using an Actipix^{TM} phosphor-coated CMOS chip for detection. The effective imaging area of the system is 28 × 24 mm^2, with a nominal pixel size of 13.75 µm. In addition, the SDi2 is equipped with pumps for delivering the dissolution medium in open or closed-loop configurations, as well as heating elements to control the temperature of the dissolution medium. The operation of the instrument was carried out using

the Sirius SDi2 Collection software (version 1.2.0.0, Sirius Analytical Ltd, Forest Row, UK).

3.2.6.1 Dissolution imaging of eutectic ibuprofen effervescent matrices

The SDi2 system equipped with a whole dosage flow cell, illustrated in Figure 9A, was used to observe swelling, erosion, and drug release from IBU-loaded effervescent matrix tablets in open loop configuration. Dual wavelength imaging (255 nm and 520 nm) captured images at 1 image/sec, every fifth image was recorded. Dissolution studies were conducted in two setups: a) using 0.1 M phosphate buffer (pH 6.8) for 6 h, and b) a pH shift experiment, involving 0.1 N HCl buffer (pH 1.2) for 1.5 h, followed by 0.1 M phosphate buffer (pH 6.8) for 6 h. A stainless-steel wire held the tablet in place in the flow cell (see Figure 9A). The drug release mimicked the gastrointestinal environment at 37°C, and real-time absorbance images were generated using selected wavelengths. SDi2 Analysis software (version 3.0.20, Pion Inc., Billerica, MA, USA) was utilized to analyze the imaging data with analysis window at 255 nm and 520 nm shown in Figures 9B and 9C. At 255 nm, the absorbance of IBU was measured in the upper analysis window (Figure 9B). At 520 nm, light obscuration indicated tablet behavior during dissolution studies, including swelling, gel layer formation, or erosion (Figure 9C). A flow rate of 6.16 ml/min, corresponding to an average linear velocity of 1 cm/min, was used to mimic gastrointestinal transit [149]. The dissolution experiments were performed in triplicate.

3.2.6.2 Data analysis

The processing of the imaging data files was executed using SDi2 Analysis software (version 3.0.20, Pion Inc., Billerica, MA, USA). Tablet diameter changes during dissolution experiments were assessed by defining horizontal and vertical zones with a width of 1 mm. To define the edge of the dosage forms, a threshold absorbance value of 350 mAU at 520 nm was used, marking the boundary between the tablet and the dissolution medium. Tablet diameters were then expressed as a percentage of change relative to the initial measurement.

Dissolution studies involved imaging IBU release over 6 h in phosphate buffer (pH 6.8) and 7.5 h in the pH shift experiment, with measurements taken at various time points using 255 nm. The drug concentration, measured in mg/mL, was determined using a calibration curve (see Figure 64 in Appendix II). The dissolved drug amount and drug release rate were then calculated using equations 6 and 7. Cumulative percentage release profiles were calculated as the sum at each subsequent time point. The nominal IBU dose in the IBU tablet was 1000 mg, while in the eutectic tablet and effervescent matrix tablets, it was 200 mg, as described in below equations 6 to 8:

$$\text{Dissolved drug amount (mg)} = \text{Concentration (mg/mL)} \times \text{Flow rate (mL/min)} \times \text{Time interval (min)} \quad (6)$$

$$\text{Drug release rate (mg/min)} = \text{Concentration (mg/mL)} \times \text{Flow rate (mL/min)} \quad (7)$$

$$\text{Drug release (\%)} = \frac{\text{Dissolved drug amount (mg)}}{\text{Dose (mg)}} \times 100 \quad (8)$$

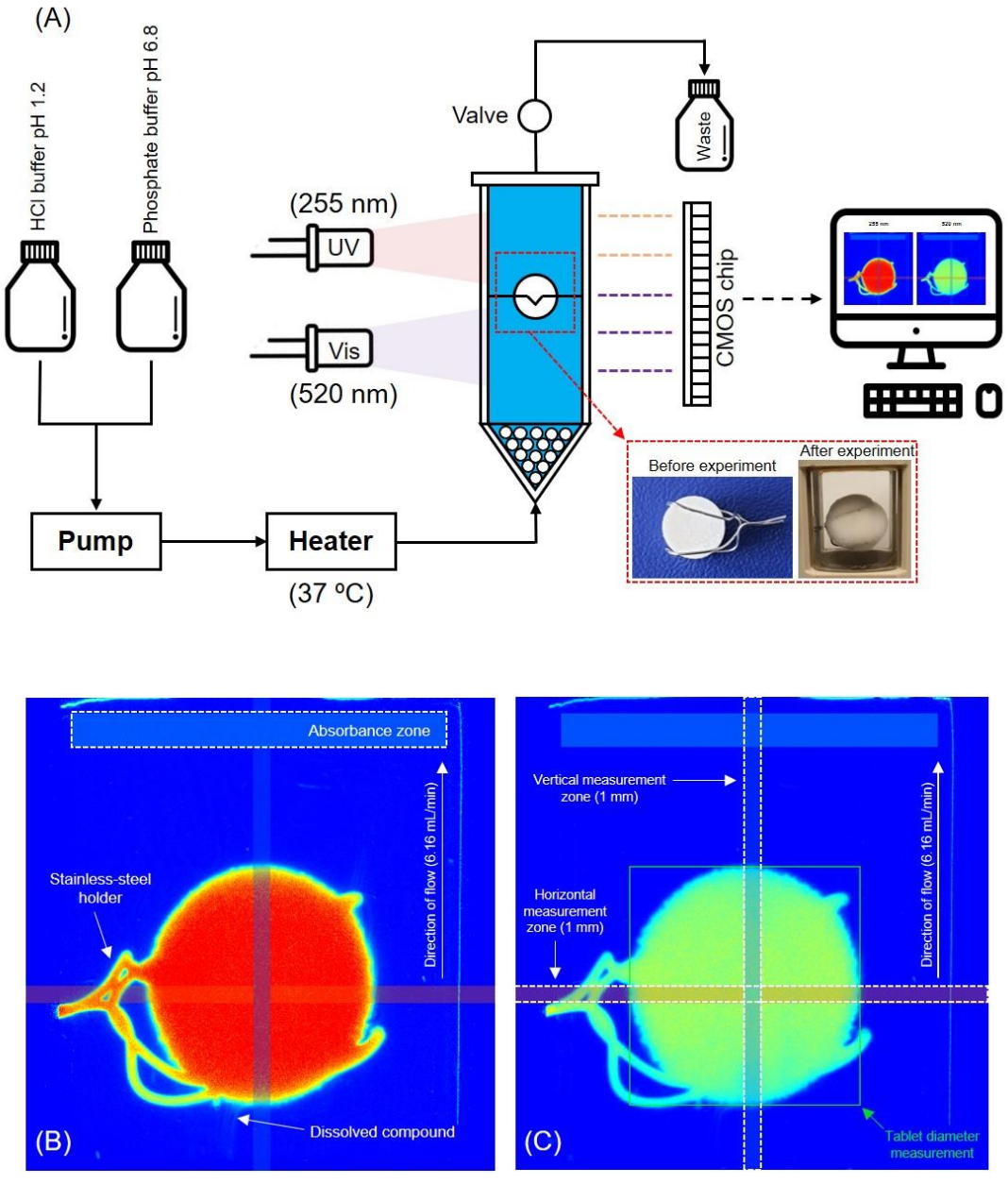

Figure 9. Set-up of SDi2 system equipped with whole dosage flow cell (A) for assessment of effervescent matrix tablets for measurement of IBU release (B) and tablet behaviors (C) in dissolution media.

3.2.7 Investigation of water sorption and erosion characteristics

To evaluate the water sorption and erosion of effervescent matrix tablets, the tablets were individually weighed before being immersed in medium as dry mass (*t=0*). Subsequently, the tablet was placed in a glass bottle containing 50 mL of HCl buffer pH 1.2 and phosphate buffer pH 6.8, rotating at 50 rpm at 37 ºC using a shaking incubator (Model SI4, Shel Lab, Cornelius, USA) for 12 h. At predetermined intervals, the tablets were withdrawn, excess water was removed by blotting with filter paper, and the wet mass (t) was documented. These tablets were then subjected to a hot air oven at 40 ºC for 72 h or until their weight stabilized, and the dry mass (*t*) was determined. Water sorption and erosion of effervescent matrix tablets were quantified in terms of water content and dry mass loss, respectively, using the following equations.

$$Water\ content\ (t) = \frac{wet\ mass\ (t) - dry\ mass\ (t)}{dry\ mass\ (t)} \quad (9)$$

$$Dry\ mass\ loss = \frac{dry\ mass\ (t{=}0) - dry\ mass\ (t)}{dry\ mass\ (t{=}0)} \quad (10)$$

3.2.8 The estimation of drug and water diffusivity using numerical approximation based on mathematical model

3.2.8.1 Model description

When HPMC-based matrix is exposed to the release medium, water penetrates into the matrix (water sorption), leading to swelling and polymer dissolution (erosion). As a result, the drug dissolves and diffuses out of matrix. These phenomena occur concurrently, adding complexity to the modeling. To develop an effective model, it is important to account for the changes in matrix dimensions over time.

Model is based on some assumptions as mentioned below:

I. The matrix had a cylindrical geometry, and the alteration in volume was described as an affine process, reflecting the changes in tablet dimensions.

II. Effervescent agent, MCC, HPMC and the drug were distributed homogeneously in the matrix [131].

III. Convective fluxes were neglected [150].

IV. Diffusion was considered in both axial and radial direction.

V. Drug dissolved continuously in the presence of solvent.

VI. Drug transport exclusively occurred within the solvent phase, therefore, non-dissolved drug could not diffuse [151].

VII. Although water diffuses more rapidly than the drug, the dissolved and non-dissolved drug existed at the same time [131].

VIII. The diffusion coefficient varied with the quantity of water within the matrix; typically, the diffusion coefficient rises as the water concentration increases. [124].

IX. Since the matrix was exposed to fluidic medium, MCC and HPMC started to swell which led to the increase in matrix dimensions.

X. Perfect sink conditions were maintained.

3.2.8.1.1 Diffusion

Water and drug transport in the matrix are described with Fick's second law [124] and expressed in Equation (11)

$$\frac{\partial C_k}{\partial t} = \frac{1}{r}\left[\frac{\partial}{\partial r}\left(rD_k\frac{\partial C_k}{\partial r}\right) + \frac{\partial}{\partial z}\left(rD_k\frac{\partial C_k}{\partial z}\right) + \frac{\partial}{\partial \theta}\left(\frac{D_k}{r}\frac{\partial C_k}{\partial \theta}\right)\right] \quad (11)$$

Here, C_k and D_k are the concentration and diffusion coefficient of the diffusing species (k = w: water; k = d: drug), respectively, r denotes the radial coordinate, z the axial coordinate, θ the angle perpendicular to both axis (Figure 10) and *t* represents time.

As there is no concentration gradient of any component with respect to θ owing to all components were homogeneously distributed in matrix, Equation (11) is written to be simplified as Equation (12) for cylindrical system

$$\frac{\partial C_k}{\partial t} = \frac{\partial}{\partial r}\left(D_k\frac{\partial C_k}{\partial r}\right) + \frac{D_k}{r}\frac{\partial C_k}{\partial r} + \frac{\partial}{\partial z}\left(D_k\frac{\partial C_k}{\partial z}\right). \quad (12)$$

As discussed above, diffusivity is sensible to the water concentration. This dependency is defined as the exponential equation of the diffusion coefficient according to the free volume theory [124] as expressed in Equation (13)

$$D_k = D_{k_{eq}} e^{-\beta_k\left(1-\frac{C_w}{C_{w_{eq}}}\right)} \quad (13)$$

where β_k is dimensionless constant, characterizing this concentration-dependence. Also, C_{weq} and D_{keq} are water concentration and diffusion coefficient in the equilibrium swollen state of the system, respectively. It is assumed that the concentration-dependence of diffusivities of two species on the water content of the system is time-invariant.

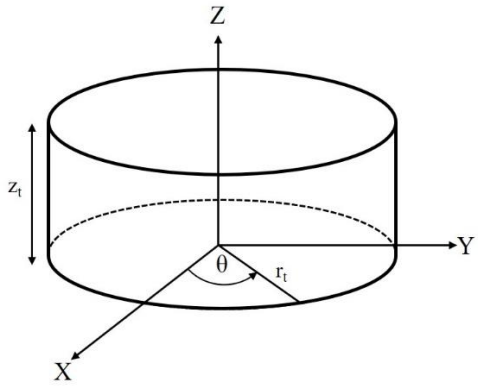

Figure 10. Schematic of the matrix in the cylindrical coordinate.

3.2.8.1.2 Swelling

The model considers two major impacts of polymer swelling due to water imbibition: (I) significant changes in the system's volume, resulting in dramatic changes in the concentrations of all species and (II) increased mobility of the macromolecules, which leads to increased diffusivity of water and drug (Equation (13)). Swelling is considered in both the axial and radial directions and is assumed to be ideal [124].

3.2.8.2 Model solving using numerical methods

In order to investigate the effect of effervescent agents on mass transport of HPMC matrix tablets, it is necessary to estimate the diffusion coefficient of both water and drug molecules based on experimental data of water sorption and drug release profiles. In addition, swelling behaviors of matrix tablets in dissolution medium were considered by monitoring the alteration of tablet dimension during drug release.

3.2.8.2.1 Estimation of water diffusivity based on experimental data of water contents

Firstly, we have some hypotheses in modeling this system which are necessary to be noted.

(I) The radius and height of matrix tablet changes linearly with time

define: $$r = a_r t + b_r \quad (14)$$

$$z = a_z t + b_z \quad (15)$$

where a_r and a_z are the rate of tablet radius change and tablet height change with time, respectively, t is time and b_r and b_z denote the radius and height of matrix tablet at $t=0$.

(II) The change in tablet radius and height over time affects water concentration, as described by the following equations:

$$\frac{\partial C_w}{\partial r} = \frac{\partial C_w}{\partial t}\frac{\partial t}{\partial r} \quad (16)$$

$$\frac{\partial C_w}{\partial z} = \frac{\partial C_w}{\partial t}\frac{\partial t}{\partial z} \quad (17)$$

The first and second derivatives of Equations (16) and (17) can be calculated as following:

$$\frac{\partial C_w}{\partial r} = \frac{1}{a_r}\frac{\partial C_w}{\partial t}, \quad (18)$$

$$\frac{\partial^2 C_w}{\partial r^2} = \left(\frac{1}{a_r}\right)^2 \frac{\partial^2 C_w}{\partial t^2}, \quad (19)$$

$$\frac{\partial C_w}{\partial z} = \frac{1}{a_z}\frac{\partial C_w}{\partial t}, \quad (20)$$

$$\frac{\partial^2 C_w}{\partial z^2} = \left(\frac{1}{a_z}\right)^2 \frac{\partial^2 C_w}{\partial t^2}. \quad (21)$$

Considering: $$D_w = D_{w_{eq}} e^{-\beta_w\left(1-\frac{C_w}{C_{w_{eq}}}\right)} \quad (22)$$

The differentiation process of D_w in Equation (22) with respect to r and z, we obtain:

$$\frac{\partial D_w}{\partial r} = D_{w_{eq}} e^{-\beta_w\left(1-\frac{C_w}{C_{w_{eq}}}\right)} \frac{\beta_w}{C_{w_{eq}}}\frac{\partial C_w}{\partial r} = \frac{\beta_w}{C_{w_{eq}}} D_w \frac{\partial C_w}{\partial r}, \quad (23)$$

$$\frac{\partial D_w}{\partial z} = D_{w_{eq}} e^{-\beta_w\left(1-\frac{C_w}{C_{w_{eq}}}\right)} \frac{\beta_w}{C_{w_{eq}}}\frac{\partial C_w}{\partial z} = \frac{\beta_w}{C_{w_{eq}}} D_w \frac{\partial C_w}{\partial z}. \quad (24)$$

Considering Fick's second law:

$$\frac{\partial C_w}{\partial t} = \frac{\partial}{\partial r}\left(D_w \frac{\partial C_w}{\partial r}\right) + \frac{D_w}{r}\frac{\partial C_w}{\partial r} + \frac{\partial}{\partial z}\left(D_w \frac{\partial C_w}{\partial z}\right)$$

The derivative of Fick's second law was calculated and the derivatives of C_w and D_w were then substituted. The obtained equation was rearranged and the resulting equation as expressed in Equation (25)

$$\frac{\partial C_w}{\partial t} = \frac{\tau}{C_{w_{eq}}}\left(\frac{\partial C_w}{\partial t}\right)^2 \beta_w D_{w_{eq}} e^{-\beta_w\left(1-\frac{C_w}{C_{w_{eq}}}\right)} + \left(\tau\frac{\partial^2 C_w}{\partial t^2} + \frac{1}{r a_r}\frac{\partial C_w}{\partial t}\right) D_{w_{eq}} e^{-\beta_w\left(1-\frac{C_w}{C_{w_{eq}}}\right)} \quad (25)$$

where:

$$\tau = \left(\frac{1}{a_r}\right)^2 + \left(\frac{1}{a_z}\right)^2.$$

The details of differentiation process and parameter substitution are shown in Appendix III. In order to work with Equation (25), it is necessary to discretize. This means creating a set of cut points that span the range of values for the variable. To do this, we assumed time, t between $[t_1, t_7]$, divided into equivalently interval which was defined as h. Thus, time point is $t_1, t_1, t_2, .., t_7$ for $i = 1,2,\ldots,7$, $C_{w,i}$ denotes $C_w(t_i)$ and $r_i = r(t_i)$. The first and second derivatives are then estimated using a central-difference formula of order $O(h^2)$, as follows:

$$\frac{\partial C_w}{\partial t} \approx \frac{C_{w,i+1} - C_{w,i-1}}{2h}$$

$$\frac{\partial^2 C_w}{\partial t^2} \approx \frac{C_{w,i+1} - C_{w,i} + C_{w,i-1}}{h^2}$$

After applying central-difference formula into Equation (25), we obtain:

$$\frac{1}{D_{w_{eq}}} e^{\beta_w\left(1-\frac{C_{w,i}}{C_{w_{eq}}}\right)} - \frac{\tau}{C_{w_{eq}}}\frac{C_{w,i+1} - C_{w,i-1}}{2h}\beta_w = \frac{2h}{C_{w,i+1} - C_{w,i-1}}\left(\tau\frac{C_{w,i+1} - C_{w,i} + C_{w,i-1}}{h^2} + \frac{1}{r_i a_r}\frac{C_{w,i+1} - C_{w,i-1}}{2h}\right)$$

for $i = 2,3,\ldots,6$

define:

$$y_i = \frac{2h}{C_{w,i+1} - C_{w,i-1}}\left(\tau\frac{C_{w,i+1} - C_{w,i} + C_{w,i-1}}{h^2} + \frac{1}{r_i a_r}\frac{C_{w,i+1} - C_{w,i-1}}{2h}\right)$$

and $d = \frac{1}{D_{w_{eq}}}$.

According to the objective of this research is to calculate the diffusion coefficient of diffusing species which is water in this case, it is necessary to estimate D_{weq} and β_w, as displayed in Equation (12). Now, the equation can be expressed as follows:

$$g_i(d,\beta_w) = de^{\beta_w\left(1-\frac{C_{w,i}}{C_{w_{eq}}}\right)} - \frac{\tau}{C_{w_{eq}}}\frac{C_{w,i+1}-C_{w,i-1}}{2h}\beta_w - y_i$$

for $i = 2,3,\ldots,6$

As discuss above, the obtained equation is non-linear equation and if let $g_i(d,\beta_w)$ for $i = 2,3,\ldots,6$ equals to zero, these equations system would have five equations with two unknowns which is considered as overdetermined system of non-linear equation. The overdetermined systems present a computationally difficult problem to solve because they have either infinitely many solutions or no solutions at all. A least squares method can find the best approximation to a system of equations. The best approximation is the solution of the minimization problem that provides a minimum error. If

$$E(d,\beta_w) = \frac{1}{2}\sum_{i=2}^{6}\left(g_i(d,\beta_w)\right)^2 = \frac{1}{2}\|G\|^2$$

when $\|G\|^2 = g_2^2(d,\beta_w) + g_3^2(d,\beta_w) + \ldots + g_6^2(d,\beta_w)$, then the best approximation yields a minimal value for $E(d,\beta_w)$

In previous work [152], it was discussed that the iterative algorithm of the Gauss-Newton method was used to solve the nonlinear least squares problem and proposed approximates closely to the actual data, indicating the efficacy of the Gauss-Newton algorithm. In this study, we used the Gauss-Newton method to determine the unknown parameters by minimizing the sum of squared errors (SSE). According to Gauss-Newton method, it is important to calculate the gradient and Jacobian matrix as expressed below.

The gradient of g_i is

$$\nabla g_i(d,\beta_w) = \left[\frac{\partial g_i}{\partial d}, \quad \frac{\partial g_i}{\partial \beta_w}\right] = \left[e^{\beta_w\left(1-\frac{C_{w,i}}{C_{w_{eq}}}\right)}, \quad de^{\beta_w\left(1-\frac{C_{w,i}}{C_{w_{eq}}}\right)}\left(1-\frac{C_{w,i}}{C_{w_{eq}}}\right) - \frac{\tau}{C_{w_{eq}}}\frac{C_{w,i+1}-C_{w,i-1}}{2h}\right]$$

Jacobian matrix is

$$J(d,\beta_w) = \begin{bmatrix}\nabla g_2(d,\beta_w)\\ \vdots \\ \nabla g_6(d,\beta_w)\end{bmatrix} = \begin{bmatrix} e^{\beta_w\left(1-\frac{C_{w,2}}{C_{w_{eq}}}\right)}, & de^{\beta_w\left(1-\frac{C_{w,2}}{C_{w_{eq}}}\right)}\left(1-\frac{C_{w,2}}{C_{w_{eq}}}\right) - \frac{\tau}{C_{w_{eq}}}\frac{C_{w,3}-C_{w,1}}{2h} \\ \vdots & \\ e^{\beta_w\left(1-\frac{C_{w,n-1}}{C_{w_{eq}}}\right)}, & de^{\beta_w\left(1-\frac{C_{w,n-1}}{C_{w_{eq}}}\right)}\left(1-\frac{C_{w,n-1}}{C_{w_{eq}}}\right) - \frac{\tau}{C_{w_{eq}}}\frac{C_{w,n}-C_{w,n-2}}{2h}\end{bmatrix}_{(n-2)x2}.$$

When we define $n = 7$ based on the sampling time points of water content determination and drug release profile in experimental testing and $x = (d, \beta_w)$

Computation procedure:

(I) Set the initial value of x_0 when $x_0 = (d_0, \beta_{w,0})$

(II) For $k = 0,1,2,\ldots$

(1) Construct R_k when $R_k = [g_2,\ g_3,\ g_4,\ g_5\ , g_6]_k^T$ and

$$g_i(x_k) = de^{\beta_w\left(1-\frac{C_{w,i}}{C_{weq}}\right)} - \frac{\tau}{C_{w_{eq}}}\frac{C_{w,i+1} - C_{w,i-1}}{2h}\beta_w - y_i$$

(2) Construct the Jacobian matrix; J_k

(3) Find the solution; $J_k(x_k)\Delta x = -R_k$

(4) Calculate $x_{k+1} = x_k + \Delta x$

To find the solution of linear equation $J_k(x_k)\Delta x = -R_k$ using least square method, it is necessary to multiply both side of equation with $J_k^T(x_k)$, we acquire:

$$J_k^T(x_k)J_k(x_k)\Delta x = -J_k^T(x_k)R_k\ . \qquad (26)$$

Owing to the ill-posedness of Equation (26), a solution cannot achieve by using the inverse matrix of $J_k^T(x_k)J_k(x_k)$. In addition, the divergence of x_k can be observed. To solve this problem, truncated singular value decomposition was used and the solution of Equation (26) can be calculated as following [153]:

$$\Delta x = -vSu^T J_{x_k}^T(x_k)R_k$$

where the matrix u and v are the left and right singular matrix, respectively and the diagonal matrix S consists of the inverse of singular value.

Using this solution, the D_w, D_{weq} and β_w can be estimated when water content at the given time ($C_{w,i}$) from water sorption and erosion studies are given. The octave script used for estimating water diffusivity in this study is illustrated below.

```
clc
clear all
clf
h = 2; % Time interval
t = 0:12; % Time range
ar = 0.2; % Rate of dimension change in radius
az = 0.3; % Rate of dimension change in height
r = ar*t+6.12; % 6.12 is initial radius of tablet at t=0
Tau = (1/ar)^2+(1/az)^2;
Cw = [0.00; 0.4707; 0.4958; 0.4967; 0.5068; 0.5134; 0.5151]; % Experimental data of water contents


% Vector Y construction
for i = 2:6
  C1 = (2*h)/(Cw (i+1) – Cw (i-1));
  C2 = (Cw (i+1) – Cw (i) + Cw (i-1))/(h^2);
  C3 = (Cw (i+1) – Cw (i-1))/(2*h);
  y (i) = C1*(Tau*C2+C3/(ar*r(i)));
end

Cweq=0.93; % Water content at equilibrium swollen state
x=[5; 1]; % Initial value for Gauss-Newton iterative algorithm
for k=1:2000 % Iteration number
  K = water (x, Cw, Cweq, Tau, h, y) ;
  R = -K (2 : end) ;
  G = jacobian (x, Cw, Cweq, Tau, h);
  J = G (2 : end,:);
  b (k) = cond (J'*J);
  [u, D, v] = svd (J'*J);
  S = [1/D (1,1), 0; 0,0];
  dx = v*S*u'*(J'*R); %TSVD Truncated Singular Value Decomposition
  x = x + dx;
  x;
end
x
1/x (1)
Dw = (1/(x (1)))*exp(-x (2)*(1-(Cw/Cweq)))
```

```
function output = jacobian (x, Cw, Cweq, Tau, h)
  for i = 2:6
    Z (i,1) = exp (x (2)*(1-(Cw (i) / Cweq)));
    Z (i,2) = x (1)*exp (x (2)*(1-(Cw (i) / Cweq)))*(1- (Cw (i) / Cweq))-(Tau / Cweq)*(Cw (i+1)-Cw (i-1)/(2*h));
  endfor
output = Z;
```

```
function output = water (x, Cw, Cweq, Tau, h, y)
  for i = 2:6
    D1 = x (1)*exp (x (2)*(1- (Cw (i)/Cweq)));
    D2 = (Tau/Cweq)*(Cw (i+1) – Cw (i-1))/(2*h);
    Z (i,1) = D1-D2*x (2) – y (i);
  endfor
output=Z;
```

3.2.8.2.2 Estimation of drug diffusivity based on experimental data of water contents and drug release profiles

Continuing in a similar manner as elucidated in estimation of water diffusivity, the resulting equation for drug diffusivity estimation is expressed in Equation (27). The details of differentiation process and parameter substitution are illustrated in Appendix III.

$$\frac{\partial C_d}{\partial t} = \frac{\tau}{C_{w_{eq}}}\left(\frac{\partial C_d}{\partial t}\right)^2 \beta_d D_{d_{eq}} e^{-\beta_d\left(1-\frac{C_w}{C_{w_{eq}}}\right)} + \left(\tau\frac{\partial^2 C_d}{\partial t^2} + \frac{1}{r a_r}\frac{\partial C_d}{\partial t}\right) D_{d_{eq}} e^{-\beta_d\left(1-\frac{C_w}{C_{w_{eq}}}\right)}. \quad (27)$$

After applying central-difference formula into Equation (27), we acquire:

$$\frac{1}{D_{d_{eq}}} e^{\beta_d\left(1-\frac{C_{w,i}}{C_{w_{eq}}}\right)} - \frac{\tau}{C_{w_{eq}}}\frac{C_{d,i+1}-C_{d,i-1}}{2h}\beta_d = \frac{2h}{C_{d,i+1}-C_{d,i-1}}\left(\tau\frac{C_{d,i+1}-C_{d,i}+C_{d,i-1}}{h^2} + \frac{1}{r_i a_r}\frac{C_{d,i+1}-C_{d,i-1}}{2h}\right) \quad (28)$$

for $i = 2,3,\ldots,6$

Then, least square method with Gauss-Newton iterative algorithm was employed to solve non-linear overdetermined system. In addition, truncate singular value decomposition was additionally implemented as discussed above. The water content at given time ($C_{w,i}$) from water sorption and erosion studies and drug release profile were used as input data to approximate the drug diffusion parameters. The octave script for drug diffusion parameters estimation employed in this study are given in next page.

```
clc
clear all
clf
h = 2; % Time interval
t = 0:12; % Time range
ar = 0.2; % Rate of dimension change in radius
az = 0.3; % Rate of dimension change in height
r = ar*t+6.12; % 6.12 is initial radius of tablet at t=0
Tau = (1/ar)^2+(1/az)^2;
Cw = [0.00; 0.4707; 0.4958; 0.4967; 0.5068; 0.5134; 0.5151]; % Experimental data of water contents
Cd = [0.00; 6.2851; 11.3732; 14.5809; 18.1652; 20.2922; 22.7921] % Experimental data of drug release profiles

% Vector Y construction
for i = 2:6
  C1 = (2*h)/(Cd (i+1) – Cd (i-1));
  C2 = (Cd (i+1) – Cd (i) + Cd (i-1))/(h^2);
  C3 = (Cd (i+1) – Cd (i-1))/(2*h);
  y (i) = C1*(Tau*C2+C3/(ar*r(i)));
end

Cweq=0.93; % Water content at equilibrium swollen state
x=[5; 1]; % Initial value for Gauss-Newton iterative algorithm
for k=1:2000 % Iteration number
  K = drug (x, Cw, Cweq, Tau, h, y) ;
  R = -K (2 : end) ;
  G = jacobian (x, Cw, Cweq, Tau, h);
  J = G (2 : end,:);
  b (k) = cond (J'*J);
  [u, D, v] = svd (J'*J);
  S = [1/D (1,1), 0; 0,0];
  dx = v*S*u'*(J'*R); %TSVD Truncated Singular Value Decomposition
  x = x + dx;
  x;
end
x
1/x (1)
Dd = (1/(x (1)))*exp(-x (2)*(1-(Cw/Cweq)))
```

```
function output = jacobian (x, Cw, Cweq, Tau, h)
  for i = 2:6
    Z (i,1) = exp (x (2)*(1-(Cw (i) / Cweq)));
    Z (i,2) = x (1)*exp (x (2)*(1-(Cw (i) / Cweq)))*(1- (Cw (i) / Cweq))-(Tau / Cweq)*(Cw (i+1)-Cw (i-1)/(2*h));
  endfor
output = Z;
```

```
function output = drug (x, Cw, Cweq, Tau, h, y)
  for i = 2:6
    D1 = x (1)*exp (x (2)*(1- (Cw (i)/Cweq)));
    D2 = (Tau/Cweq)*(Cw (i+1) – Cw (i-1))/(2*h);
    Z (i,1) = D1-D2*x (2) – y (i);
  endfor
output = Z;
```

3.2.8.3 Model verification

The objective of model verification in this study is to assess the accuracy of the numerical solution of the developed mathematical model by quantifying the errors, with a specific emphasis on calculation verification. Verification provides mathematical evidence regarding the accuracy of a numerical solution [154]. Equation (28) was selected for utilization in model verification and the experimental data of water contents of each tablet at the given time and drug release profiles were substituted to compute the concentration of the released drug at each time point. Subsequently, the calculated concentration was compared to experimental data and coefficient of determination (R^2), as denoted by Equation (29), was calculated to evaluate the degree of correspondence between calculated and experimental data. This assessment serves to ascertain the accuracy of the numerical solution of developed mathematical model

$$R^2 = 1 - \frac{Sum\ squared\ regression\ (SSR)}{Total\ sum\ of\ squares\ (SST)} \qquad (29)$$

where SSR is the sum of the residuals squared and SST is calculated by summing the squared distances of each data point from the mean.

3.3 Scaling up of high-shear melt granulation using HSG

3.3.1 Granule preparation using high-shear melt granulation

The granules were prepared in a laboratory-scale high-shear mixer (MG 15, Pharmaceutical and Medical Supply Co., Ltd., Samut Sakhon, Thailand), equipped with a heated water jacket, three-bladed agitator and a side chopper. The mixing chamber had a volume of 13L and the batch size was 3000 g, which was about 60% of maximum volume. To avoid confounding factors from product and achieve the possibility of melt granulation scale-up using HSG, the eutectic tablet, composed of IBU (20 % (w/w)), P407 (30% (w/w)) and MCC (50% (w/w)) was selected for use in this experiment. Several research works have shown that the process variables such as agitator speed, mixing time and jacket temperature can affect the characteristics of the granules obtained by melt granulation [138, 140, 155]. In this study, the jacket temperature, chopper and agitator speed were varied during granulation process based on preliminary trials. These process parameter variations are illustrated in Table 6. The granulation process began with heating the jacket to 70 ºC and manually filling the mixing chamber with MCC. The agitator was then operated at 125 RPM for 15 min without a chopper. After that, the mixture of IBU and P407 was added to the mixing chamber and mixed for 5 min using the desired speed of the agitator and chopper. The granules were then cooled to room temperature by spreading them out on trays, collected and sieved to remove lumps. Finally, the granules were stored in a desiccator for further analysis.

Table 6. process parameters used in high-shear melt granulation

Samples	Jacket temperature (ºC)	Agitator speed (RPM)	Chopper speed (RPM)
50T170A1500C	50	170	1500
50T170A1750C			1750
50T200A1500C		200	1500
50T200A1750C			1750
70T170A1500C	70	170	1500
70T170A1750C			1750
70T200A1500C		200	1500
70T200A1500C			1750

Remarks: T = temperature, A = agitator speed and C = chopper speed

3.3.2 Characterization of the physical properties of granules

3.3.2.1 Bulk density, tapped density and compressibility

Prior to testing, the acquired granules underwent sieving through sieve no. 16 (opening of 1.18 mm) to break up agglomerates that may have formed during storage. The bulk volume (V_0) was determined by filling approximately 100 g of each sample into a 250 mL volumetric cylinder. Tapped volume (V_{tapped}) was measured after subjecting the samples to 1250 taps using a tap density apparatus (Erweka SVM 12, Erweka GmbH, Germany). The bulk (ρ_0) and tapped density (ρ_{tapped}) were then calculated, respectively. All measurements were conducted in triplicate. The compressibility index (CI) and Hausner's ratio (HR) were calculated by employing the equations 30 and 31, respectively:

$$CI = \left(\frac{\rho_{tapped} - \rho_0}{\rho_{tapped}}\right) \times 100 \quad (30)$$

$$HR = \left(\frac{V_0}{V_{tapped}}\right) \quad (31)$$

3.3.2.2 Particle size distribution (PSD)

The size distribution of granules was evaluated by sieve analysis, utilizing a vibrating shaker (Retsch GmbH, Germany) and five standard sieves ranging from 75 to 425 µm. The mass of the granules used for the analysis was approximately 100 g and the sieving time was 10 min at an amplitude of 2 mm. The retained amount on each sieve was determined by weighing.

3.3.3 Characterization of thermal properties of granules

To study the thermal properties of granules produced using high-shear melt granulation, it is necessary to perform DSC analysis. DSC can be employed to determine the effect of process parameters on the thermal properties of the prepared

granules. More information on the methodology was provided above (3.1.2.1 Differential scanning calorimeter (DSC)).

3.3.4 Characterization of crystallinity of granules

PXRD was conducted to investigate the crystallinity of granules produced by high-shear melt granulation. The methods used for PXRD analysis were mentioned in section 3.1.2.3 Powder X-ray diffractometry (PXRD).

3.3.5 Tableting

The granules of each sample were compressed into 1000 mg matrix tablets using 12.7 mm round, flat, and plain punches with a hydraulic press (Carver press, Wabash, IA, USA) at a compression force of 2 tons and a dwell time of 10 sec.

3.3.6 Characterization of tablets

3.3.6.1 Physical properties of tablets

The tests were conducted according to the methods as mentioned above (3.2.2 Physical properties characterization of effervescent matrix tablets comprising IBU-P407 eutectic mixture).

3.3.6.2 Dissolution performance of tablets

In order to study how process parameters affect dissolution characteristics, the *in vitro* dissolution was conducted in 900 mL phosphate buffer pH 6.8 using a dissolution apparatus (DT 820, Erweka, Germany) utilizing paddle method at 37ºC and rotational speed of 50 rpm that followed the USP43 <711> Dissolution procedure. At predetermined intervals, each 5 mL aliquot was withdrawn from the dissolution media and replenished with 5 mL of fresh media. the UV-vis spectrophotometer (Cary 60 UV-Vis G6860A, Agilent Technologies, Malaysia) was used to determine the amount of dissolved drug from tablets at a wavelength of 220 nm. The mean cumulative drug dissolution ± S.D. was calculated (n=3). In addition, eutectic tablets were included to investigate the performance of scaling up using high-shear melt granulation by comparison with the dissolution profile of eutectic tablets prepared using a beaker in a circulating water bath. The details as described in topic 3.2.1 (preparation of effervescent matrix tablets comprising IBU-P407 eutectic mixture). For dissolution profile comparison, similarity factor (f_2) and dissolution efficiency (DE) were calculated by the equations 32 and 33, respectively.

$$f_2 = 50\ log\ \left\{100\left[1 + \frac{1}{N}\sum_{i=1}^{N}(x_{ti} - x_{ri})^2\right]^{-1/2}\right\} \quad (32)$$

where N is the number of time points, x_{ti} is the mean percentage of drug dissolved for the test product, and x_{ri} is the mean percentage of drug dissolved for the reference product.

$$DE = 100\left(\frac{\int_0^t d\ dt}{d_{100}t}\right) \quad (33)$$

where d is a function of the percentage of drug dissolved at time t.

CHAPTER 4
RESULTS AND DISCUSSIONS

4.1 Study of effervescent tablets containing eutectic mixture of IBU and P407

4.1.1 Compatibility study between IBU and excipients in formulation

4.1.1.1 Thermal properties investigation using DSC and HSM

DSC thermograms and thermal parameters, encompassing onset temperature, peak of melting point temperature and enthalpy, were examined for IBU, lubricants (SA, AlSt, MgSt and Compritol®) and their corresponding PM, as illustrated in Figure 11 and summarized in Table 7. IBU displayed a distinctive endothermic peak at 80.1 ºC, indicating complete drug melting [156]. SA exhibited a single sharp endothermic peak at 57.8 ºC, similar to Compritol®, which showed a melting endothermic peak at 75.3 ºC. Bose et al. (2013) noted that the melting point of Compritol® varied between 69 and 74 ºC, depending on its polymorphic form [157]. MgSt revealed two endothermic peaks at 98.7 ºC and 122.6 ºC. The initial endothermic peak of MgSt originated from the dehydration of bound water in its crystalline structure, while the second one represented the melting temperature [158]. All lubricants exhibited endothermic peaks within the range of 40-140 ºC, except for AlSt, which did not display any endothermic peak in this interval. Typically, the melting temperature of AlSt falls within the range of 200 to 225 ºC [159].

The thermograms of all PMs of IBU and lubricants at ratio of 1:1 (w/w) revealed significant changes in endothermic peaks, indicating incompatibility between IBU and lubricants. The PM of IBU and SA displayed two endothermic peaks. The first endothermic peak appeared at 56.4 ºC, a lower temperature than that of each individual compound, suggesting the occurrence of the eutectic phenomenon resulting from the interaction between SA and IBU, as reported previously [156]. Another endothermic peak at 71.6 ºC might be an intermediate substance resulting from incomplete interaction between IBU and SA. Similar results were observed for the PM of IBU with stearate lubricants (AlSt and MgSt). The thermogram exhibited one endothermic peak at 75.2 ºC for the PM of IBU and AlSt and 64.3 ºC for the PM of IBU and MgSt, indicating the eutectic phenomenon. This was evident as a new endothermic peak occurred at a lower temperature than the melting endothermic peak of IBU, AlSt, and MgSt. The observed eutectic formation between IBU and stearate lubricants in this study aligns with a previous report by Gordon et al. (1984) [160]. The eutectic phenomenon is entropy-driven, occurring when at least two compounds come into intimate contact in the solid state and are mutually soluble in each other in the molten state. A key characteristic

of eutectic mixtures is the lower melting temperature of the binary mixture compared to that of each pure compound [85]. The decrease in the melting temperature of the eutectic mixture is explained by thermodynamic theory, suggesting an increase in the total entropy of the system [161]. Bi et al. (2003) emphasized that essential criteria for eutectic formation include intimate contact in the solid state and mutual solubility in the liquid state. Without such contact, there would be no increase in the total entropy of the system, and a decrease in eutectic melting temperature would not be evident [85].

Numerous previous studies have explored the interactions within eutectic mixtures. For instance, Yue et al. (2012) investigated the eutectic mixture of choline chloride and urea using FT-IR and identified a hydrogen bond between the components [162]. Perkin et al. (2013) conducted vibrational analysis and molecular dynamic simulations on the same eutectic mixture, revealing interactions between amine (NH_2) and carbonyl (C=O) groups of urea with chloride (Cl-) and hydroxyl (-OH) groups of choline, forming hydrogen bonds [163]. Phaechamud et al. (2016) explored the evaporation behavior and basic characterization of eutectic solvents between menthol, camphor, and IBU. The IR spectra suggested hydrogen bonding between the hydroxyl group (-OH) in menthol and the carbonyl group (C=O) of camphor at various ratios of the menthol-camphor mixture [164]. Considering the chemical structure of the substances in this study, the proposed interaction between compounds may involve hydrogen bonding between the hydroxyl group (-OH) of ibuprofen and the carbonyl group (C=O) of SA, which is liberated from stearate lubricants. Surprisingly, the PM of IBU and Compritol® exhibited a new endothermic peak at 68.05 ºC, possibly indicating the formation of a eutectic mixture through the interaction between the hydroxyl group (-OH) of IBU and the hydroxyl group (-OH) of the glyceryl part in the Compritol® structure. The proposed interactions between compounds are illustrated in Figure 12. Compritol® is a versatile excipient in the pharmaceutical field, commonly used as a lubricating agent in tablets and capsules and as a hot-melt coating agent for controlled-release granules. Its inert properties have led to successful applications in various pharmaceutical dosage forms, and there have been no previous reports of incompatibility between Compritol® and APIs/excipients in the pharmaceutical field [165]. However, our investigation, as revealed by the DSC thermogram, indicated an incompatibility between the PM of Compritol® and IBU.

Table 7. Summary of thermal parameters; onset temperature, peak of melting point (T_{peak}) and enthalpy (ΔH) of individual substance and physical mixture

Substances	Onset temperature (ºC)		T_{peak} (ºC)		ΔH (J/g)	
	Peak 1	Peak 2	Peak 1	Peak 2	Peak 1	Peak 2
IBU	77.0	-	80.1	-	100.5	-
SA	55.2	-	57.8	-	166.9	-
AlSt	-	-	-	-	-	-
MgSt	95.0	115.7	98.7	122.6	22.9	326.6
Compritol®	70.9	-	75.3	-	117.4	-
IBU-SA	49.6	64.7	56.4	71.6	127.1	18.6
IBU-AlSt	68.1	-	75.2	-	81.9	-
IBU-MgSt	57.1	-	64.3	-	98.9	-
IBU-Compritol®	62.8	-	68.1	-	127.6	-

Remark: - means there is no endothermic peak in DSC thermograms

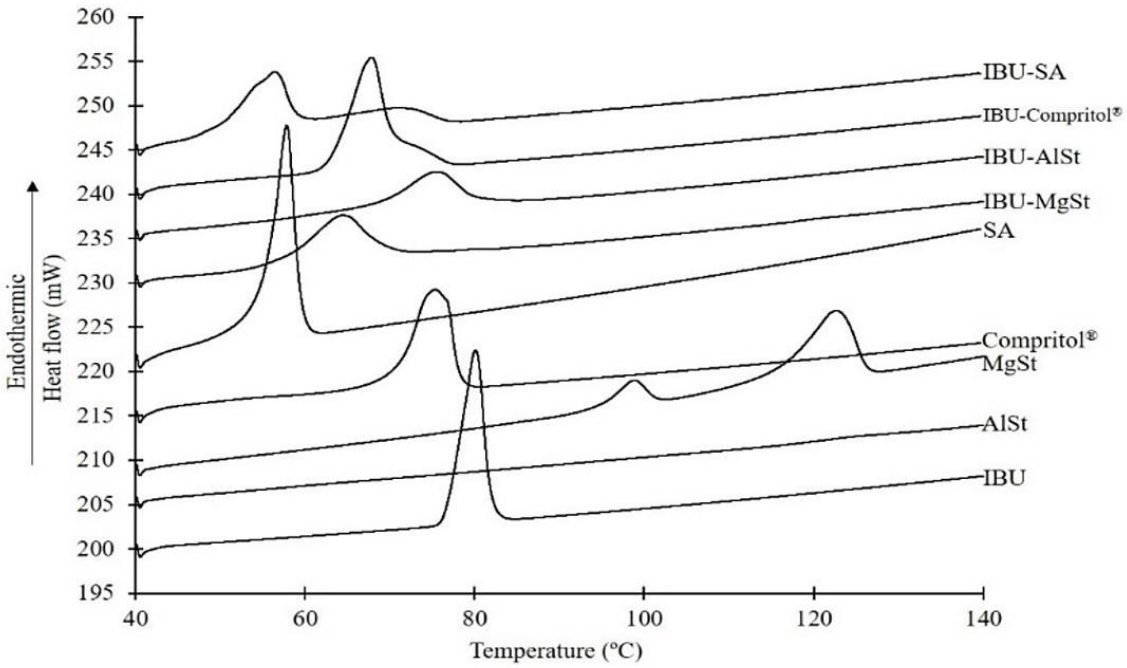

Figure 11. DSC thermograms of individual substance and PM between IBU and lubricants (SA, AlSt, MgSt and Compritol®)

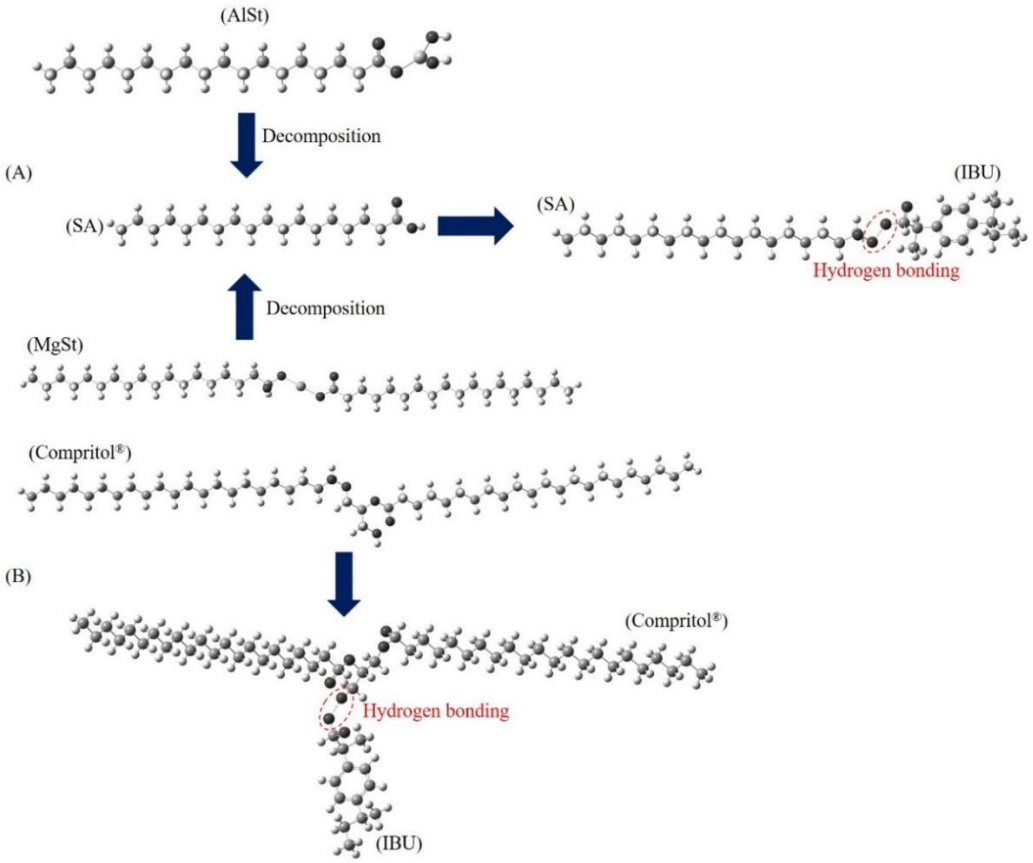

Figure 12. Proposed interaction diagram between (A) IBU and SA, Alst, MgSt (B) IBU and Compritol®

The melting behaviors and crystal morphologies observed under a hot stage microscope for IBU, SA, AlSt, MgSt, and Compritol are illustrated in Figure 13. At room temperature, grain-like IBU crystals were observed, which began melting at 75 ºC and completed melting at 78 ºC, corresponding to the endothermic peak at around 80 ºC in the DSC thermogram. AlSt and MgSt exhibited polyhedral-like crystals at room temperature, with MgSt initiating melting at 113 ºC and completing melting at 122 ºC. AlSt, on the other hand, displayed no change in crystal morphology throughout the temperature range of 30-100 ºC, as this range was below the melting point of AlSt. SA and Compritol displayed rectangle and spherical-like crystals, respectively, and completely melted at temperatures corresponding to the endothermic peaks in their DSC thermograms. Figure 14 depicts the melting behaviors and crystal morphologies of the PMs between IBU and lubricants (SA, AlSt, MgSt, and Compritol). At room temperature, conglomeration between IBU and lubricant was observed in all PMs, marked with a white arrow. This characteristic resulted from the typical property of boundary lubricants, which readily adsorb onto the surface of IBU crystals, forming a thin film to reduce friction at the particle-particle interface. The interface between IBU and lubricant melted initially, occurring at a lower temperature than the pure

compound, especially in the PMs between IBU and SA and between IBU and stearate lubricants (AlSt and MgSt). The observed completely melting temperature in HSM micrographs aligned with the melting temperature from the DSC analysis. This phenomenon was consistent with the study by Setyawan et al. (2016), who investigated the physical characteristics of IBU-SA after compression force application and identified solid-state interactions between these compounds using a polarizing microscope with a hot stage. Their micrographs showed a single blank line, indicating eutectic formation at the interface between IBU and SA [166]. Notably, there is no previous report on the application of HSM in compatibility studies of IBU and these lubricants of interest.

Moreover, HSM serves as a thermal analysis technique that combines the favorable attributes of thermal analysis and microscopy. It facilitates the observation of DSC and thermogravimetric analysis (TGA) and detects subtle changes in the sample that may escape notice in DSC and TGA during thermal experiments [167]. Table 8 presents a comparison between the thermal parameters derived from DSC (onset temperature and T_{peak}) and the partial melting temperature (PMT) and complete melting temperature (CMT) observed using HSM. PMT and CMT observed through HSM closely aligned with the thermal parameters obtained from DSC. Consequently, the thermal properties of individual substances and all PMs between IBU and lubricants from DSC analysis were validated using the HSM technique. Furthermore, HSM could be utilized as a screening testing method for observing the thermal behavior of substances.

Table 8. Comparison of thermal parameters from DSC with observed temperature of alteration from HSM

Substances	Observed thermal parameters from DSC				Observed temperature from HSM	
	Onset temperature (°C)		T_{peak} (°C)		PMT (°C)	CMT (°C)
	Peak 1	Peak 2	Peak 1	Peak 2		
IBU	77.0	-	80.1	-	75.0	78.0
SA	55.2	-	57.8	-	54.0	57.0
AlSt	-	-	-	-	-	-
MgSt	95.0	115.7	98.7	122.6	113.0	122.0
Compritol®	70.9	-	75.3	-	71.0	75.0
IBU-SA	49.6	64.7	56.4	71.6	48.0	57.0
IBU-AlSt	68.1	-	75.2	-	68.0	74.0
IBU-MgSt	57.1	-	64.3	-	58.0	63.0
IBU-Compritol®	62.8	-	68.1	-	61.0	68.0

Remarks: - means there is no endothermic peak in DSC thermograms/ there is no change of micrograph under HSM, T_{peak} means endothermic peak in DSC thermograms, PMT means partial melting temperature and CMT means complete melting temperature.

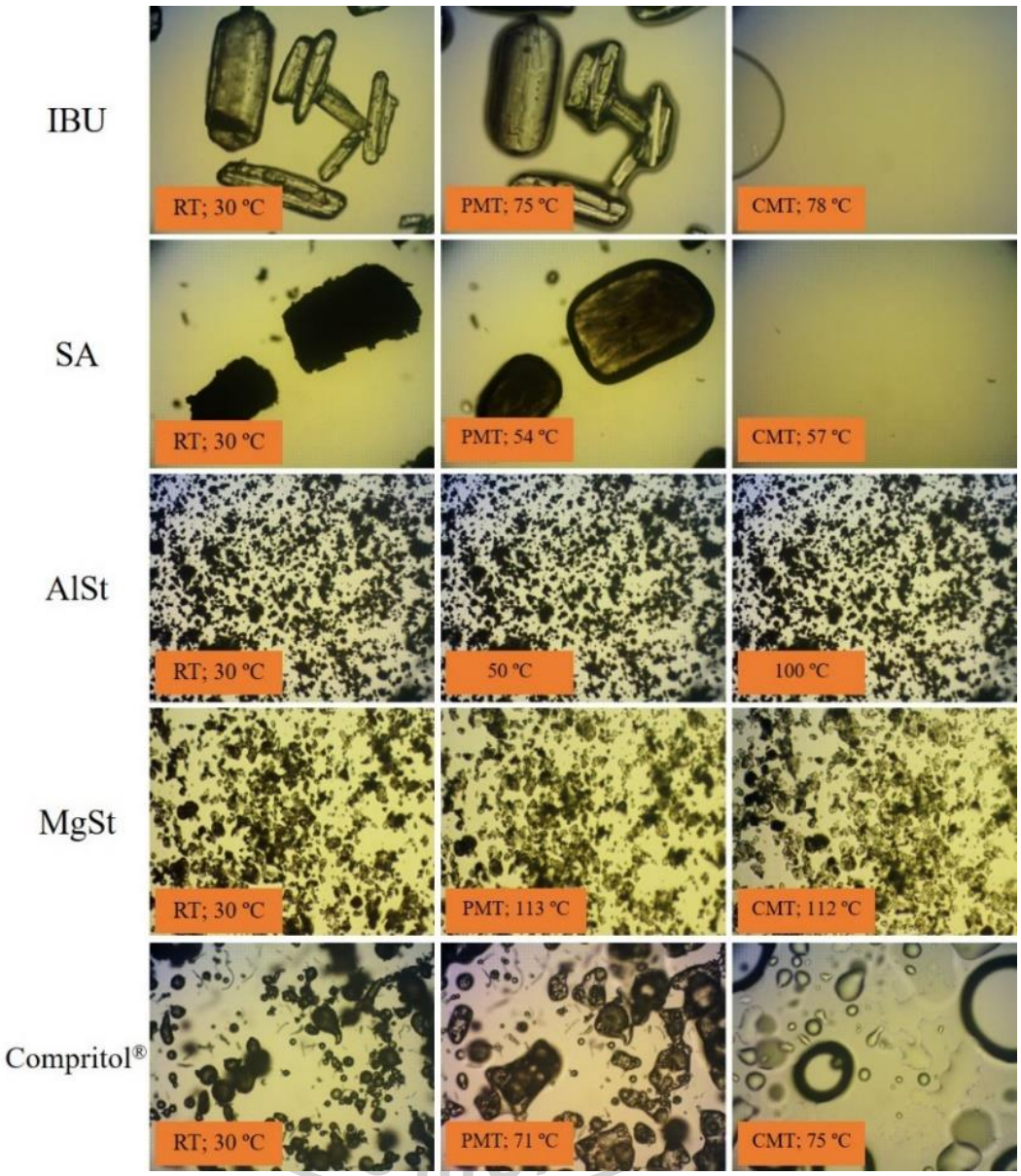

Figure 13. HSM micrograph of IBU, SA, AlSt, MgSt and Compritol at room temperature (RT), partial melting temperature (PMT) and complete melting temperature (CMT) (Magnification of 100X)

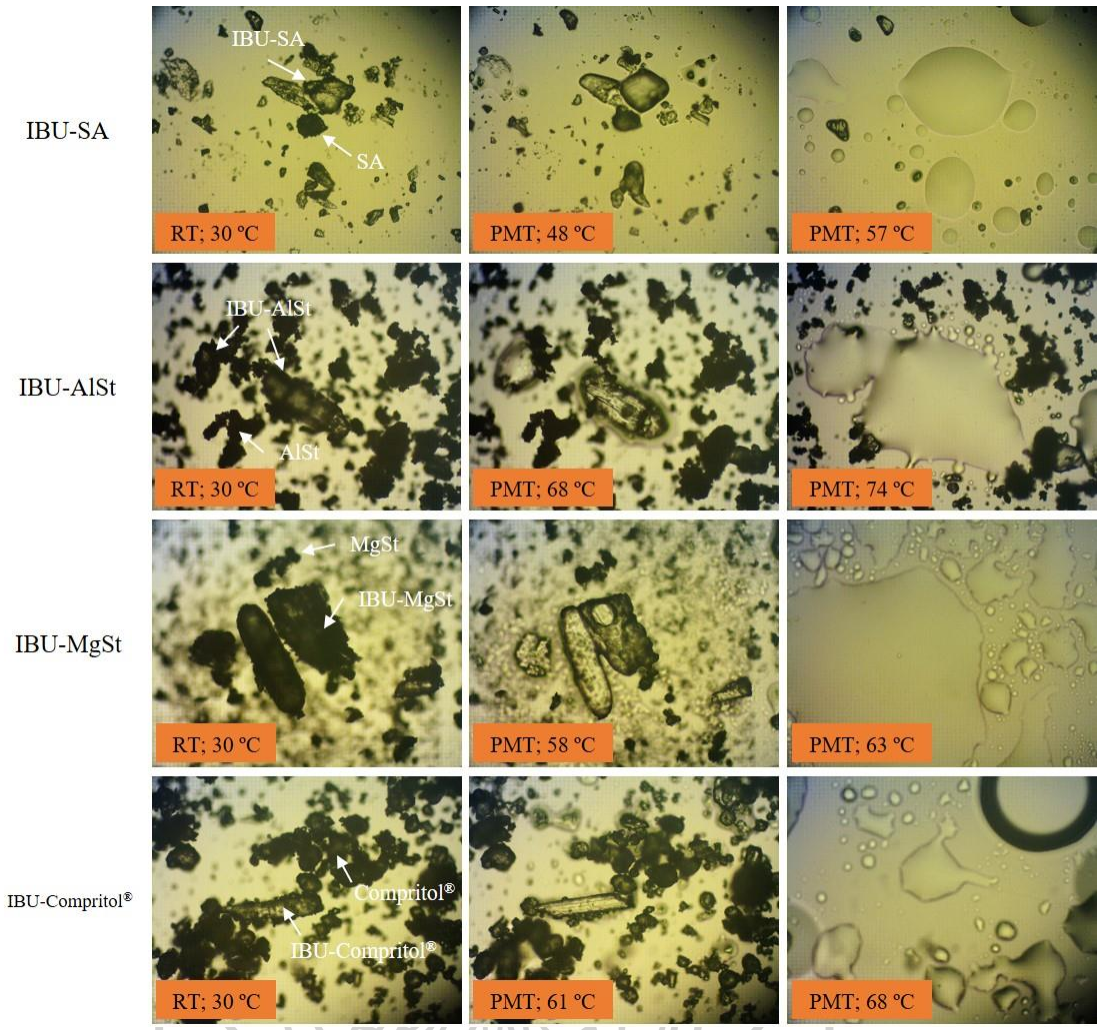

Figure 14. HSM micrographs of physical mixture between IBU and lubricants (SA, AlSt, MgSt and Compritol) at room temperature (RT), partial melting temperature (PMT) and complete melting temperature (CMT) (Magnification of 100X)

4.1.1.2 Crystallinity investigation using PXRD

The diffractograms for each individual compound and the PMs between IBU and lubricants are illustrated in Figure 15. IBU exhibited robust diffraction peaks at 6.2, 12.3, 16.7, 18.7, 20.1, and 22.4 2θº, consistent with the positions reported by Mallick et al. (2008) [168]. SA displayed a few prominent diffraction peaks at 7.0, 20.5, 23.8, and 36.2 2θº. In the PM between IBU and SA, the diffraction peaks aligned with those of SA but showed a significant reduction in peak intensity, particularly around 12 and 20 2θº. This reduction indicated eutectic formation between IBU and SA, which may not alter IBU's crystal habit but could impact its crystallinity. The HSM micrograph of this PM also revealed conglomeration between IBU and SA particles in the solid state. A similar phenomenon was observed in the PMs between IBU and stearate lubricants (AlSt

and MgSt), particularly the disappearance of two main diffraction peaks (around 12 and 20 2θº) of IBU in the PM between IBU and AlSt. MgSt displayed various strong diffraction peaks at 5.5, 8.9, 21.7, 22.3, and 23.4 2θº, indicative of its monohydrate form, as reported previously [169]. The PM between IBU and MgSt exhibited a similar diffraction pattern to the PM between IBU and AlSt but with a slight decrease in the intensity of IBU's characteristic diffraction peak. Compritol exhibited a high intensity peak at 21.2 2θº and a small peak at 23.4 2θº, consistent with previous findings by Fini et al. (2011) [170]. In the PM between IBU and Compritol, the diffractogram showed the same diffraction peaks but with a slight decrease in peak intensity. The PXRD results corroborated the DSC and HSM findings, indicating eutectic formation upon contact of SA, stearate lubricants (AlSt and MgSt), or Compritol with IBU.

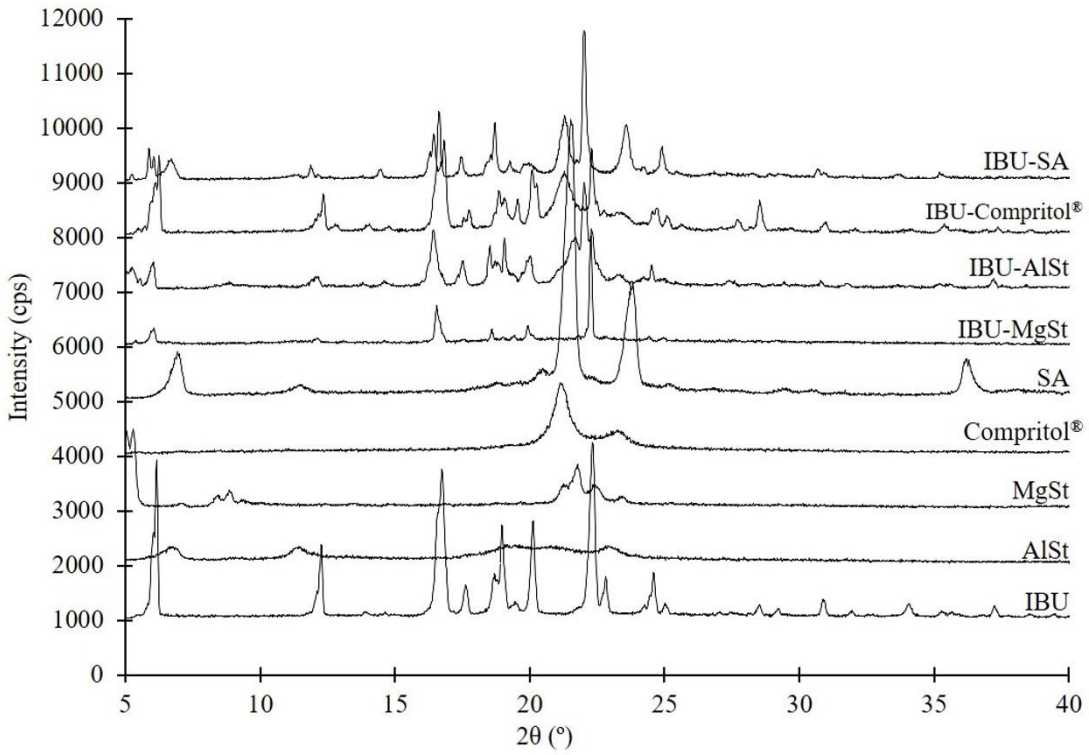

Figure 15. PXRD patterns of individual substances and PM between IBU and lubricants (SA, AlSt, MgSt and Compritol®)

4.1.1.3 Molecular interaction evaluation using FT-IR

The FT-IR spectra for each individual compound and the PMs between IBU and lubricants are depicted in Figure 16. The IBU spectra displayed a distinctive peak at 1721 cm^{-1}, representing the stretching vibration of the carboxylic group (C=O) in its chemical structure. In the spectral region of 3000-2500 cm^{-1}, IBU exhibited bands corresponding to the stretching vibrations of the methylene and

methyl groups at 2956, 2922, and 2869 cm^{-1}. The C-C stretching vibrations of the aromatic ring were evident at 1508 cm^{-1}, and the region of 1400-1300 cm^{-1} showed bands corresponding to the symmetric and asymmetric bending vibrations of the methyl group ($-CH_3$) [171]. The FT-IR spectra of SA, AlSt, MgSt, and Compritol showed a similar pattern in the 3000-2500 cm^{-1} region, indicating strong C-H vibrations of long-chain fatty acids. Significant bands corresponding to the symmetric and asymmetric stretching vibrations of -COO- and the bending vibration of aliphatic C-H bonds appeared in the 1700-1400 cm^{-1} region. PMs between IBU and lubricants exhibited strong C-H vibrations in the 3000-2500 cm^{-1} region and C=O vibrational frequencies. The -COO- vibration was shifted to lower values, indicating the formation of hydrogen bonds, as previously described [162-164, 171]. Thus, the FT-IR results also support and reinforce the eutectic formation between IBU and lubricants (SA, AlSt, MgSt, and Compritol®).

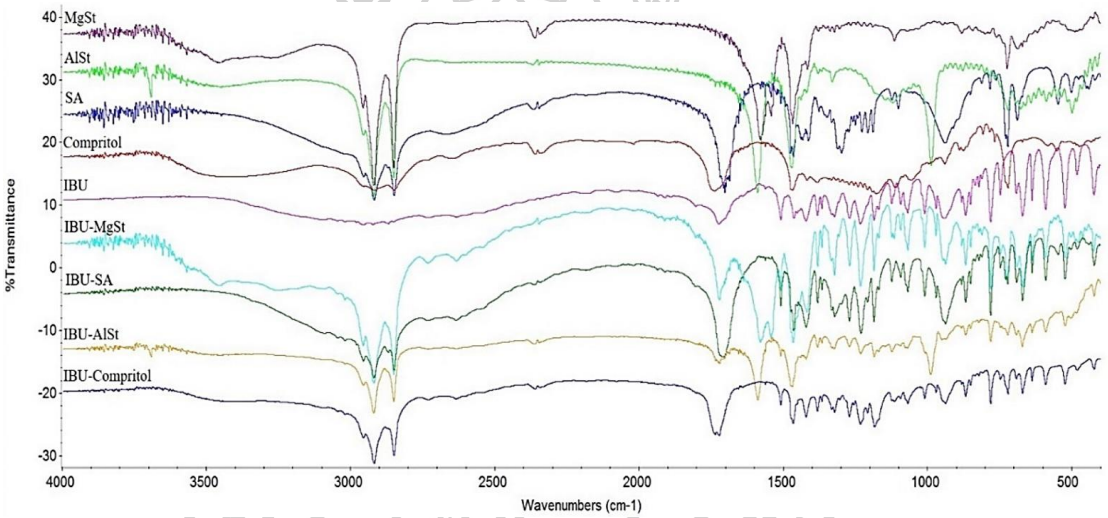

Figure 16. FT-IR Spectra of individual substance and PM between IBU and lubricants (SA, AlSt, MgSt and Compritol®)

4.1.1.4 Summary

The thermal characteristics of PMs formed between IBU and lubricants (SA, AlSt, MgSt, and Compritol) were examined using DSC and HSM. The DSC thermograms clearly indicated incompatibility between IBU and all lubricants, as evidenced by the appearance of a new endothermic peak at a noticeably lower temperature than that of each individual compound, indicative of eutectic formation. HSM micrographs supported the DSC findings, revealing conglomeration in the solid state between IBU and all boundary lubricants employed in this study. The PXRD technique further substantiated the DSC and HSM results, confirming the eutectic formation in PMs between IBU and all lubricants by assessing their crystallinity behavior. Moreover, FT-IR analysis demonstrated intermolecular interactions between IBU and all lubricants, as

indicated by shifts in vibrational frequencies in the 1700-1400 cm^{-1} region, suggesting molecular hydrogen bonding. Incompatibilities between drugs and excipients pose significant challenges in formulation development. Understanding the alterations in crystallinity and thermal properties resulting from the incompatibility between IBU and certain excipients, such as boundary lubricants, is valuable for selecting suitable excipients during preformulation studies and can avoid the instability problem of pharmaceutical formulation.

4.1.2 Physicochemical characterization of IBU-P407 eutectic mixture

4.1.2.1 Morphology investigation using SEM

The eutectic mixtures between IBU and P407 were successfully fabricated using different method. In SEM micrographs (Figure 17), IBU was observed in the form of a crystal that had a smooth surface and a needle-like shape. The size of IBU crystals ranged between 100-200 µm. P407 appeared as smooth-surfaced spherical particles as previously reported [172]. SEM images revealed that eutectic mixtures produced by the melting method (MS) had uniform particle sizes of around 50 µm, but irregular shapes. On the other hand, particles produced by grinding (PM) had different shapes, including irregular and needle-like shapes with rough surfaces, indicating the impact of the preparation method. The co-grinding of IBU and P407 appeared to induce eutectic formation when intimate contact between the two occurred. This was depicted in Figure 17C, where the needle-like particle resembled an IBU particle and the rough surface was caused by melting or softening of P407, which adhered to the surface of the IBU particle. In contrast, heating at 60 ºC can facilitate P407 melting, which cause powder aggregation resulting in rough, irregularly shaped particles once cooled down to room temperature (Figure 17D).

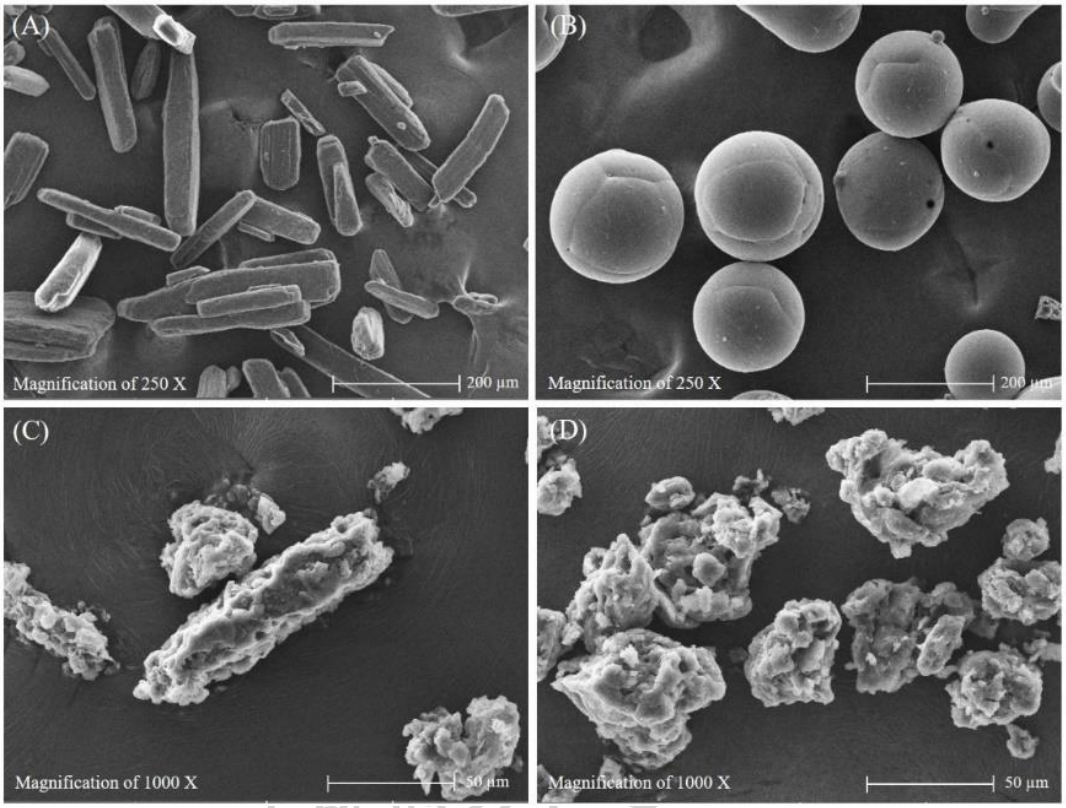

Figure 17. SEM micrographs of IBU (A), P407 (B) and eutectic mixtures prepared with different methods; physical mixture (C) and melting sample (D).

4.1.2.2 Thermal properties investigation of IBU-P407 eutectic mixture using DSC and HSM

Thermal analysis revealed distinct behaviors for the drug and polymeric carrier. In Figure 18, thermograms for IBU, P407, and eutectic mixtures prepared using different methods are displayed. IBU exhibited a singular endothermic peak at approximately 80 ºC, consistent with prior studies, indicating complete drug melting [173, 174]. P407 displayed a melting point around 60 ºC, as reported by Dugar et al. (2016) [20]. The DSC curves of PM and MS demonstrated a significant shift in the endothermic peak to about 53 and 47 ºC, respectively, lower than that of IBU and P407, suggesting eutectic formation between IBU and P407, as previously noted [20]. Eutectic phenomenon is characterized by increased entropy, occurring when two compounds in solid state intimately contact each other and are mutually soluble in molten state. Eutectic mixtures possess the unique property of a lower melting temperature than each pure compound [85]. The reduction in melting temperature is explained by thermodynamic theory, indicating an overall increase in the total entropy of the system [161]. Bi et al. (2003) emphasized that essential criteria for eutectic formation involve intimate contact in solid state and mutual solubility in liquid state. Without such contact, there would be no increase

in total entropy, and a decrease in eutectic melting temperature would not be apparent [85]. However, these phenomena in both solid and liquid states are not observable in the DSC experiment alone. Therefore, to elucidate the thermal behavior indicative of eutectic formation between IBU and P407, a complementary technique, HSM, was employed.

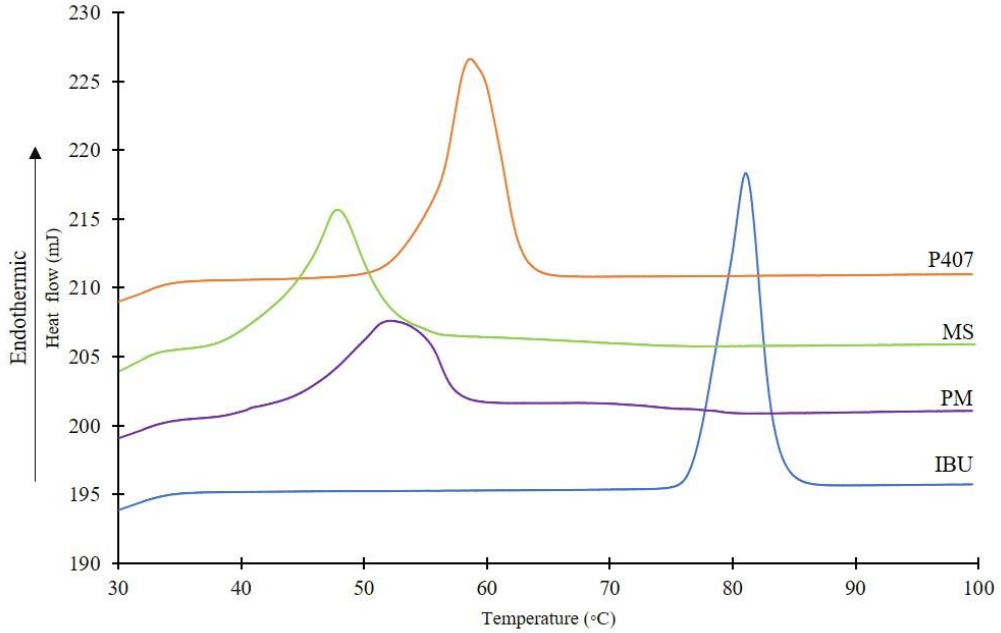

Figure 18. DSC thermograms of IBU, P407 and eutectic mixtures prepared with different preparation methods (PM = physical mixture, MS = melting sample)

Figure 19 illustrated HSM micrographs of IBU, P407, and eutectic mixtures at a magnification of 100X. The HSM examination revealed that IBU and P407 completely melted at approximately 78°C and 58°C, respectively, as shown in the DSC curves in Figure 18. IBU exhibited a needle-like crystal structure while P407 had a spherical crystal shape. In PM samples, most of the observed particles were IBU particles that were adhered with melted or softened P407. In contrast, MS samples showed irregularly shaped particles (Figure 20). This observation was consistent with the SEM photographs in Figure 17. Both the PM and MS samples displayed similar thermal behaviors, but the MS completely melted at a lower temperature than the PM, as shown in Figure 18. Upon melting of P407, a residual solid particle attributed to IBU was left behind, which slowly underwent phase transition to the liquid state at 53°C and 49°C for PM and MS, respectively. This indicated that IBU is dispersed as a solid solution, as commonly observed in solid dispersion [172]. HSM micrographs confirmed the difference in melting point of the eutectic mixture influenced by the preparation method, also observed in DSC thermograms. Furthermore, HSM visualization can provide the insight of eutectic formation between IBU and P407.

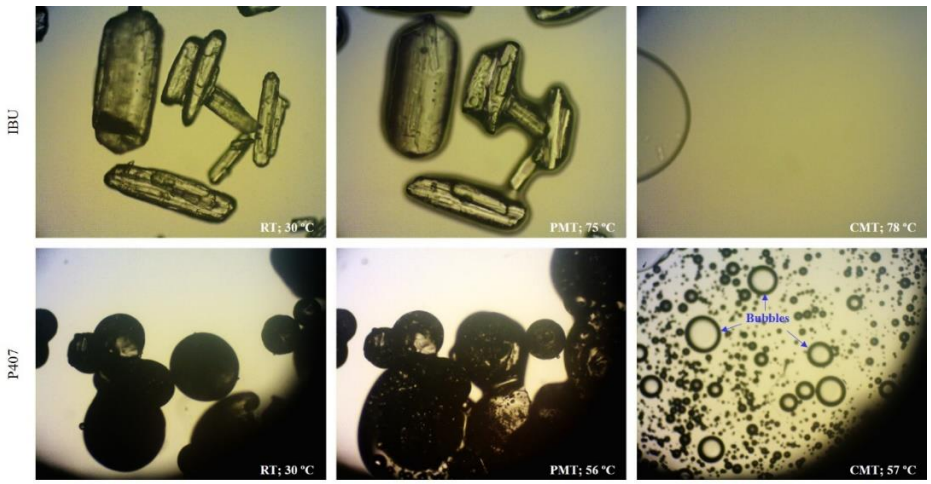

Figure 19. HSM micrographs of IBU and P407 at room temperature (RT), partial melting temperature (PMT) and complete melting temperature (CMT) (Magnification of 100X)

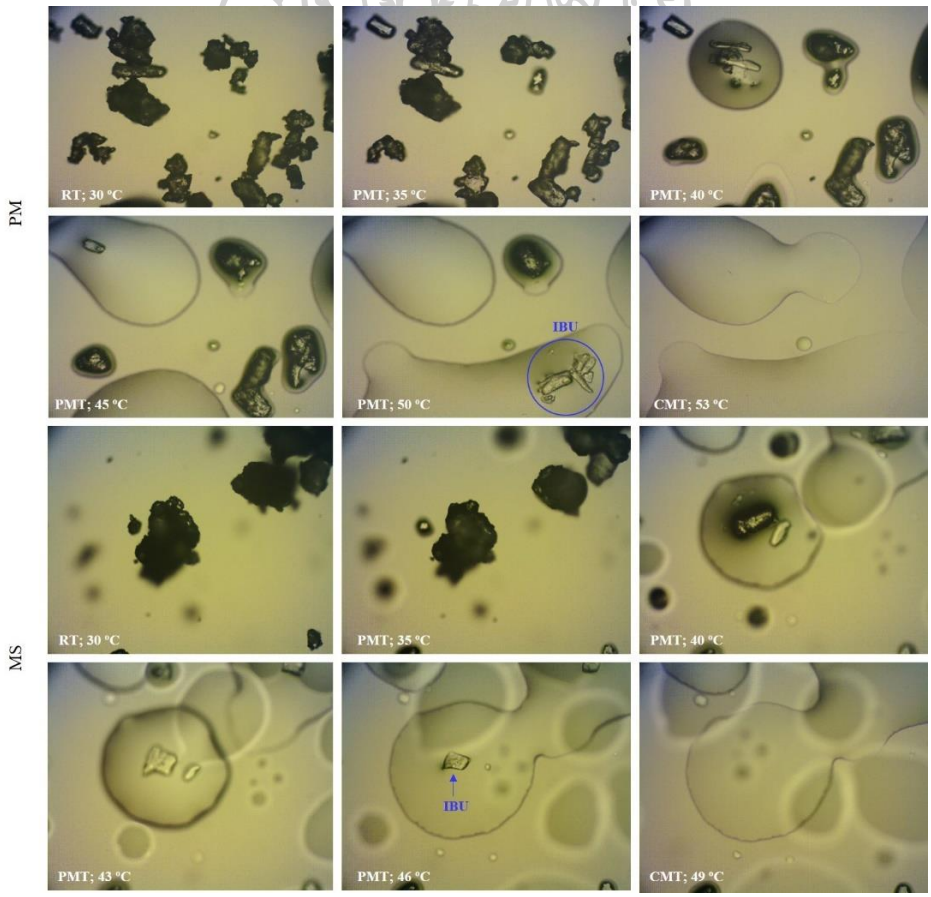

Figure 20. HSM micrographs of IBU-P407 eutectic mixtures prepared using different preparation methods (PM = physical mixture, MS = melting sample).

4.1.2.3 Crystallinity investigation of IBU-P407 eutectic mixture using PXRD

In order to evaluate whether the eutectic preparation method resulted in a crystalline change of IBU, PXRD analysis was conducted. The diffractograms of each pure compound and eutectic mixtures fabricated using different preparation methods are shown in Figure 21. IBU exhibited numerous distinct peaks, with the most prominent being 6.2, 12.3, 16.7 and 22.3 2θº, indicating that IBU was present in a highly crystalline form, which was in accordance with the previously described by Mallick, et al. (2008) [168]. P407 showed only two prominent peaks at about 19 and 23 2θº, with additionally a broad halo indicative of crystalline domains within the amorphous polymeric material [17, 175]. The diffractograms of both PM and MS displayed the same diffraction peak but dramatically decreased in peak intensity especially at about 6, 12 and 20 2θº which attributed to IBU crystalline in particular system. Moreover, the diffractogram of MS showed a more pronounced reduction in peak intensity when compared to PM. These findings suggested the eutectic formation between IBU and P407, which might not affect the crystal habit of IBU but decrease the crystallinity degree of IBU. The PXRD diffractograms supported eutectic formation between IBU and P407, consistent with DSC and HSM observations.

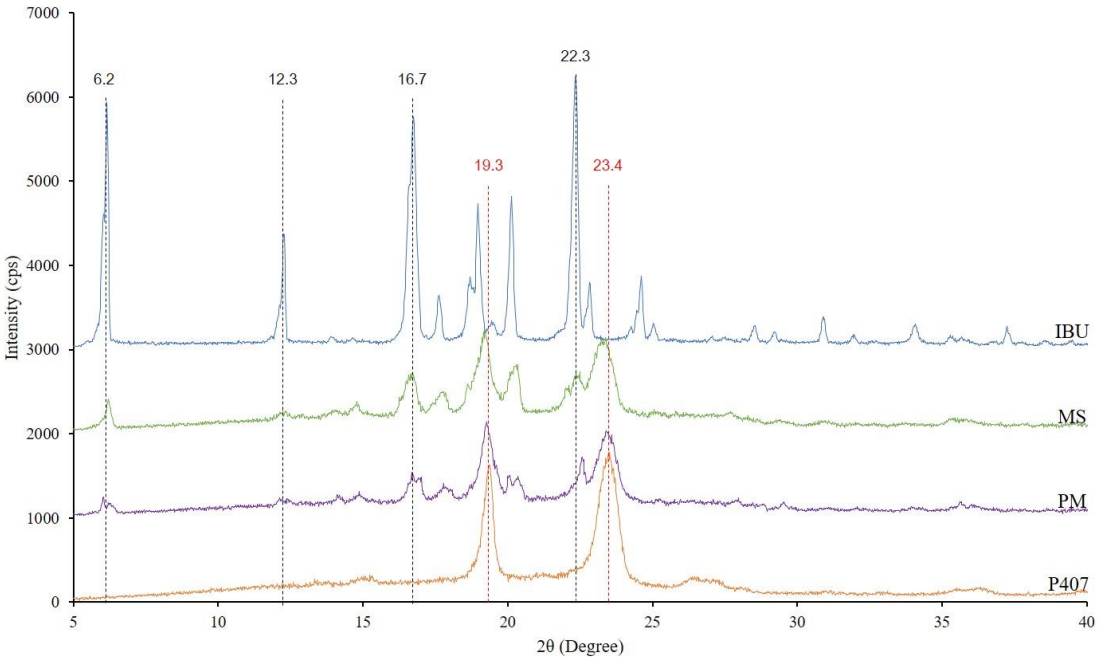

Figure 21. X-ray diffractograms of IBU, P407 and eutectic mixtures fabricated using different preparation methods (PM = physical mixture, MS = melting sample).

4.1.2.4 Evaluation of molecular interaction between IBU and P407 in eutectic mixture using FTIR

In this study, the interaction between the drug and carrier systems was investigated using infrared spectroscopy. Figure 22 illustrates the FTIR spectra of IBU, P407, and their eutectic mixtures. The pure drug showed a characteristic absorption band at 1720 cm^{-1}, which was identified as the stretching vibration of the carboxylic group (C=O) of dimerized IBU, resulting from the hydrogen bonding between two IBU molecules [17]. Moreover, the C-C stretching vibrations of the aromatic ring were observed at 1500 cm^{-1}, while the absorption band at 1420 cm^{-1} corresponded to the symmetric and asymmetric bending vibrations of the methyl group ($-CH_3$). [171]. For FTIR spectra of P407, a characteristic absorption band was observed at approximately of 1110 cm^{-1} from C-O stretching vibration in chemical structure [17]. The characteristic peaks of IBU and P407 were observed for both PM and MS, indicating that the crystalline structures of IBU and P407 were preserved in this system. Interestingly, new peak at 1734 cm^{-1} (as a shoulder on the band of 1720 cm^{-1}) was observed. This new feature strengthened in eutectic mixture prepared with melting method (MS) and the intensity of the 1720 cm^{-1} IBU dimer peak decreased, suggesting the hydrogen bonding between IBU and P407. Since P407 possesses two terminal -OH groups, it is expected that two molecules of IBU would form a hydrogen bond with one P407 molecule. This explanation has already been observed for solid dispersion of IBU and P407 in the study of Ali, et al. (2010) [17]. The obtained spectra from FTIR analysis supported the results of thermal analysis and crystallinity and indicated the eutectic formation of IBU and P407 *via* hydrogen bonding between carboxylic group of IBU and hydroxyl group of P407.

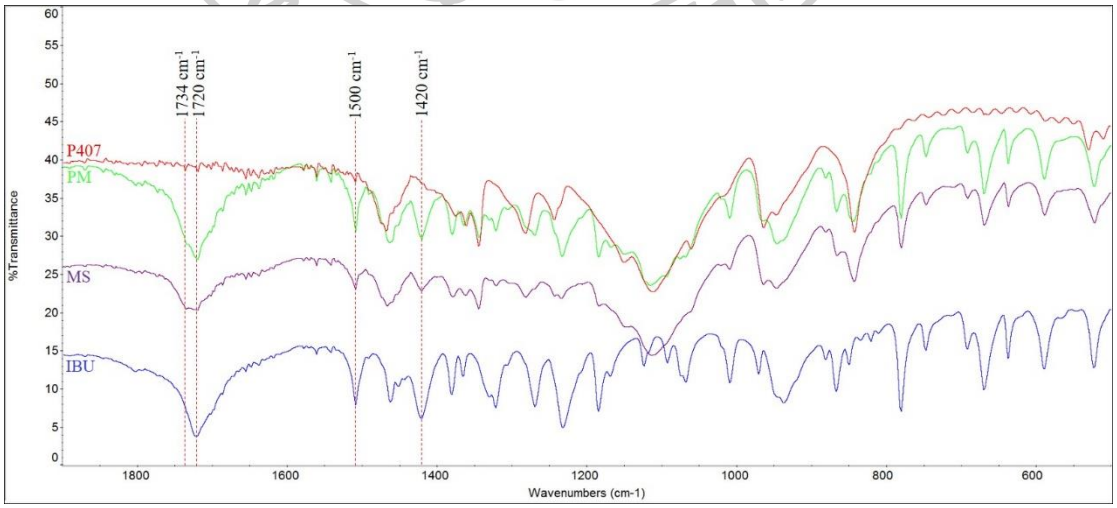

Figure 22. FTIR spectra for IBU, P407 and eutectic mixtures fabricated using different preparation methods (PM = physical mixture, MS = melting sample).

4.1.2.5 Summary

Successful fabrication of the eutectic mixture of IBU and P407 in the ratio of 1:1.5 was achieved using various preparation techniques including grinding and heating methods. The eutectic formation was confirmed by thermal analysis and PXRD. The HSM technique provided additional insight, revealing that IBU was dispersed as a solid solution in the eutectic system. Moreover, the formation of the IBU-P407 eutectic was indicated by a new absorption band in the FTIR spectra at 1734 cm^{-1}, which suggested hydrogen bonding. Nevertheless, different preparation methods have negligible impact on the characteristics of the IBU-P407 eutectic mixture.

4.1.3 Tablet behaviors of effervescent tablets comprising IBU-P407 eutectic mixture

4.1.3.1 Wetting, swelling and erosion characteristics of eutectic effervescent tablets under stereomicroscope

Under a stereomicroscope at a 1.5X magnification, alterations in the morphology of eutectic effervescent tablets were documented after immersion in distilled water and 0.1 N HCl buffer pH 1.2 at specified intervals, as depicted in Figures 23A and 23B, respectively. Following a 30-minute immersion in distilled water, a minimal penetration of blue color into the tablet was observed, indicating the limited wetting properties of the IBU tablet in deionized water (Figure 23A). In contrast, there was no discernible change in 0.1 N HCl buffer pH 1.2 (Figure 23B). This observation might be attributed to the pH-dependent solubility of IBU, consistent with findings by Potthast et al. IBU exhibits a solubility of 3.44 mg/mL in medium pH 7.4 at 37 ºC, and its solubility significantly decreases to 0.038 mg/mL in medium pH 1.0 [13]. The lower solubility in acidic medium, coupled with lower wetting properties, prevented the penetration of blue color into the IBU tablet in 0.1 N HCl buffer pH 1.2. To address the hydrophobicity and pH-dependent solubility of IBU, P407 was employed as a eutectic co-forming agent to enhance IBU solubility and wetting properties. After immersion in both testing media solutions, the penetration of blue color into the IP tablet was more prolonged than that into a plain IBU tablet. This outcome supports the notion that P407 could enhance the wettability and solubility of IBU, consistent with previous reports [17, 20]. The presence of intermolecular interaction between IBU and P407 during eutectic formation led to a reduction in the melting point (T_m) and enthalpy (ΔH_f). The decrease in ΔH_f signified a thermodynamically increased solubility according to the van't Hoff reaction. Additionally, as T_m decreased, the logarithmic value of the molar fraction of solute, in this case, IBU, approached zero and increased substantially [79, 176]. The higher solubility of the IBU-P407 eutectic mixture resulted in a more extended penetration of blue color into the IP formulation.

Furthermore, under the stereomicroscope, swelling and gel formation of the IP tablet were observable due to the gelling ability of P407 [29]. For formulations ranging from IP5E to IP30E, incorporating 5-30% (w/w) of effervescent agents in the IP tablet, their penetration distances in both testing media exhibited similar trends, with a higher content of effervescent agents promoting a greater penetration distance. Upon contact with the testing medium, the effervescent tablets generated CO_2 gas (Figures 23A and 23B). A higher loading of effervescent agents produced more CO_2, enhancing the rough surface of eutectic effervescent tablets, which facilitated deeper penetration of the medium into the tablets [31]. In comparison with traditional wetting testing methods, such as contact angle measurement using a goniometer, these stereomicroscope results offered a clearer understanding of the wetting behavior of eutectic effervescent tablets in both immersion media through visual observation.

Wetting properties were evaluated using a stereomicroscope, employing imaging analysis to measure the penetration distance of a blue-colored medium into eutectic effervescent tablets. The wetting rate was then determined from the slope of the penetration distance versus time profile. The penetration distance capacity of effervescent tablets in both distilled water and 0.1 N HCl buffer pH 1.2 is depicted in Figure 24. The wetting rate for each formulation was calculated from the slope of the penetration distance versus time profile, as detailed in Table 9. In distilled water, the wetting rate of eutectic effervescent tablets increased from 0.201 to 1.459 mm/min with the addition of more effervescent agents, ranging from 5 to 30% (w/w), respectively. Notably, P407 demonstrated the ability to improve the wetting rate by more than double when compared to the plain IBU tablet. This enhancement can be attributed to the high thermodynamic functions discussed earlier. When tested in 0.1 N HCl buffer pH 1.2, the wetting rate of eutectic effervescent tablets exhibited a similar trend to distilled water but was slightly lower. In the case of the plain IBU tablet, there was no penetration of the blue-colored medium into the tablet after immersion in the medium for 30 minutes, as illustrated in Figures 23A and 23B. Consequently, the wetting rate of IBU was reported as zero in Table 9 due to the high hydrophobicity and low solubility of IBU in 0.1 N HCl buffer pH 1.2, as previously reported by Cristofoletti et al. [177]. These results align with the morphological changes observed in eutectic effervescent tablets under a stereomicroscope, as mentioned earlier. The incorporation of more effervescent agents in the formulation enhanced surface roughness, allowing the medium to penetrate deeper into the tablet and resulting in a higher wetting rate in formulations with a higher effervescent agent content. Additionally, the inclusion of P407 in the IBU tablet significantly improved its wetting properties, evident from the higher wetting rate compared to the plain IBU tablet.

Table 9. Rate of wetting, gel formation, erosion and dissolution parameters of eutectic effervescent tablets in various testing media.

Formulation	Wetting rate (n=5) (mm/min)		Gel formation Rate (n=5) (mm/min)		Erosion rate (n=5) (mm/min)	
	Distilled water	0.1 N HCl buffer	Distilled water	0.1 N HCl buffer	Distilled water	0.1 N HCl buffer
IBU	0.201 ± 0.025	0.000 ± 0.000	0.000 ± 0.000	0.000 ± 0.000	0.000 ± 0.000	0.000 ± 0.000
IP	0.515 ± 0.017	0.084 ± 0.005	0.184 ± 0.008	0.171 ± 0.004	0.000 ± 0.000	0.000 ± 0.000
IP5E	0.682 ± 0.122	0.159 ± 0.083	0.053 ± 0.004	0.049 ± 0.004	0.072 ± 0.011	0.058 ± 0.009
IP10E	0.823 ± 0.164	0.236 ± 0.091	0.035 ± 0.002	0.025 ± 0.007	0.153 ± 0.063	0.118 ± 0.044
IP20E	1.407 ± 0.201	0.388 ± 0.143	ND	ND	0.216 ± 0.070	0.194 ± 0.068
IP25E	1.420 ± 0.332	0.485 ± 0.148	ND	ND	0.242 ± 0.069	0.283 ± 0.055
IP30E	1.459 ± 0.311	0.516 ± 0.187	ND	ND	0.301 ± 0.084	0.375 ± 0.092

Remarks: DI = distilled water, ND = not determined

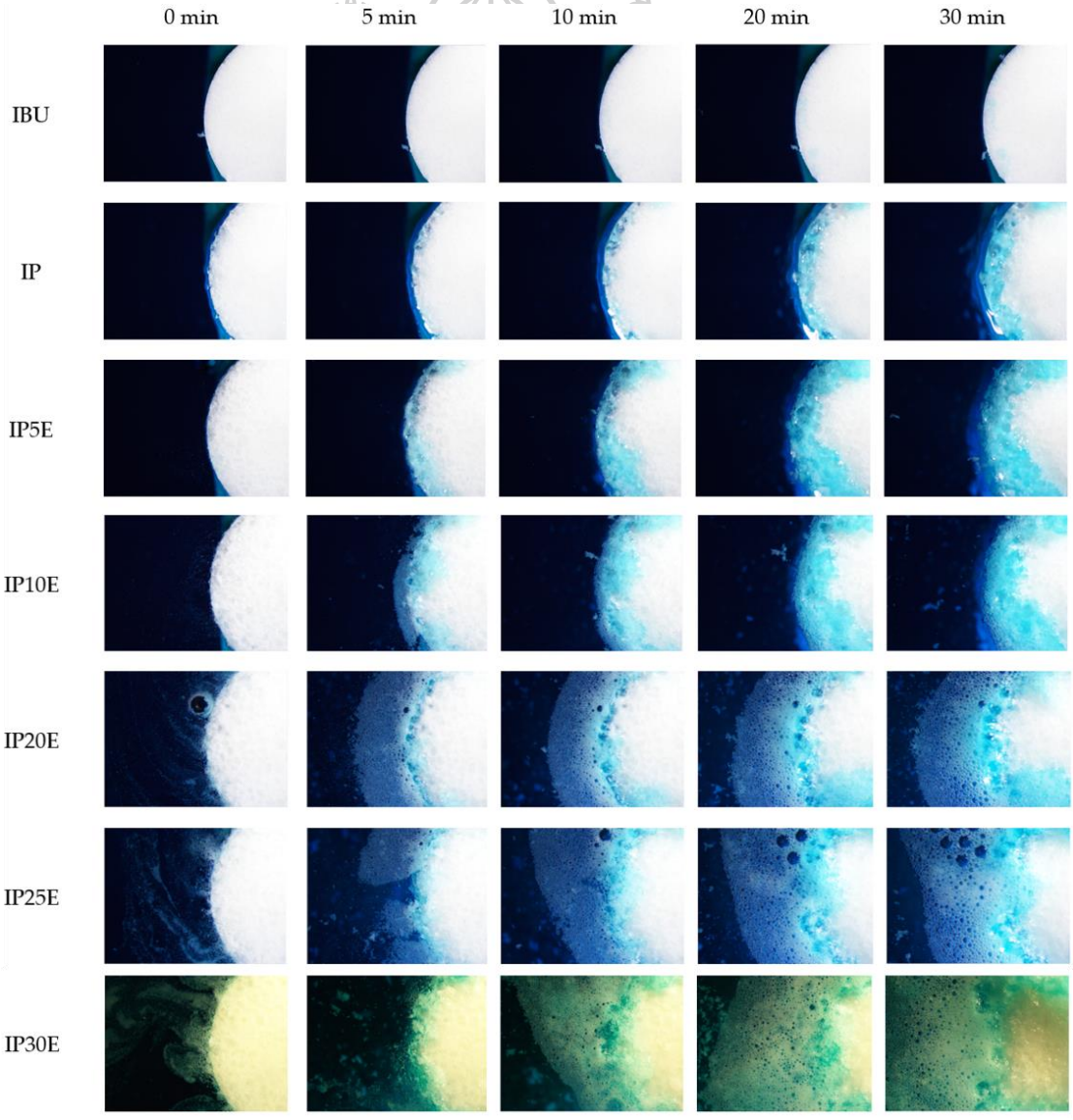

(A)

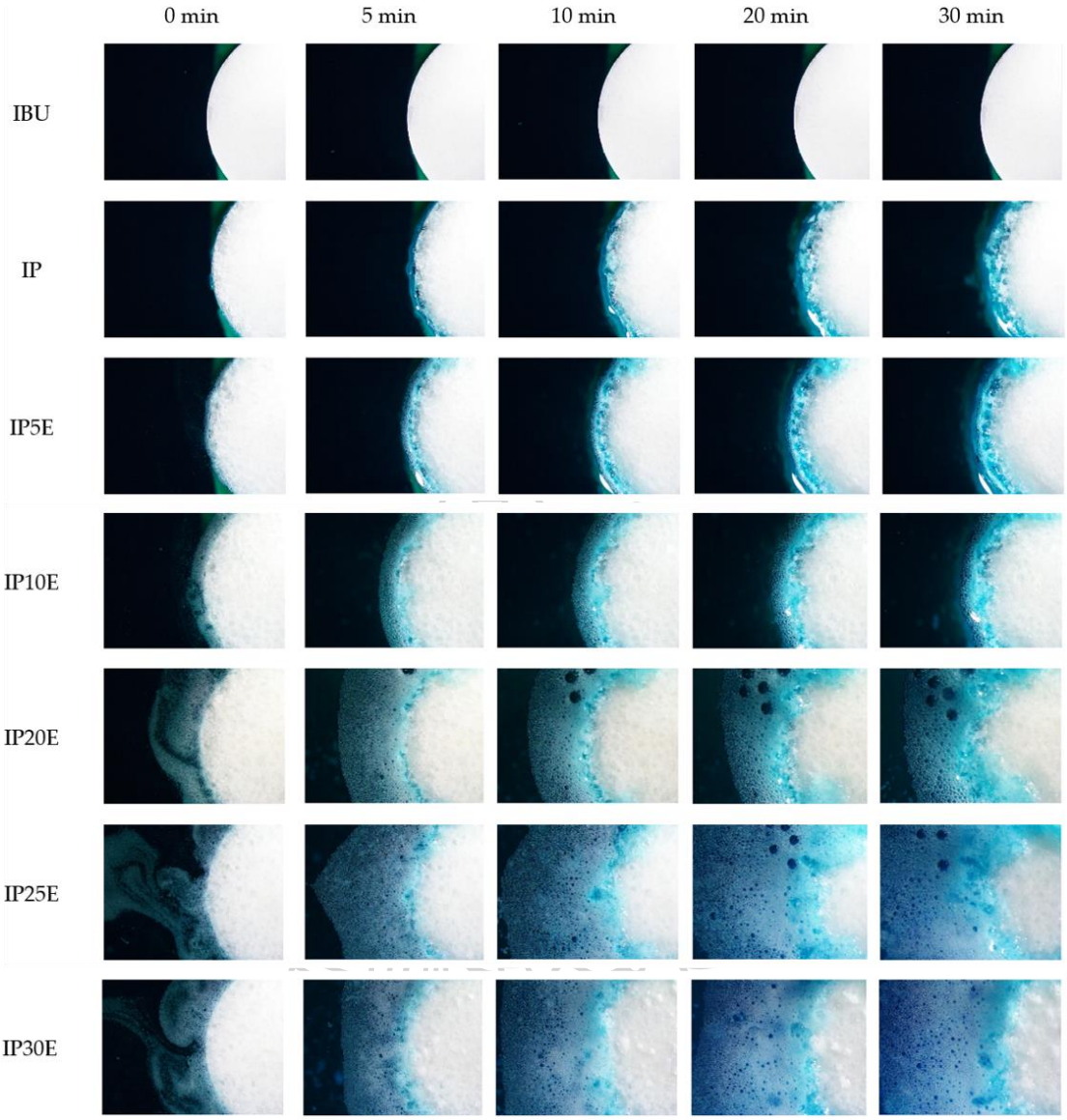

(B)

Figure 23. Photomicrographs of eutectic effervescent tablets in distilled water (A) and 0.1 N HCl buffer pH 1.2 (B) under stereomicroscope at magnification of 15X.

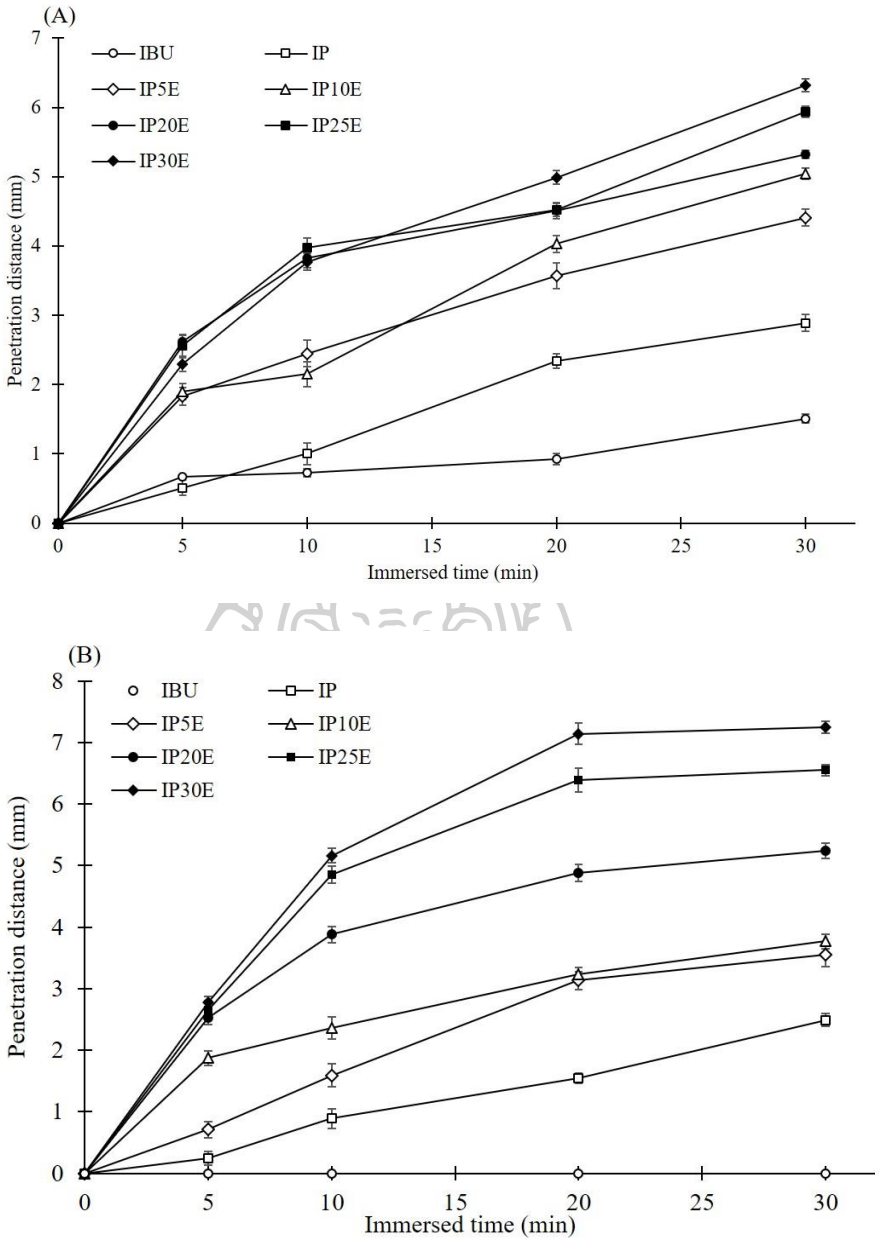

Figure 24. The penetration distance capacity of eutectic effervescent tablets in distilled water (A) and 0.1 N HCl buffer pH 1.2 (B)

Enhancing wetting is a crucial mechanism for improving the dissolution of solid dispersions, recognized for its efficacy in enhancing the oral bioavailability of poorly water-soluble drugs by incorporating them into inert hydrophilic polymer matrix carriers [178, 179]. The sessile drop method, also known as contact angle measurement, is commonly employed to assess wettability by examining the interfacial interaction between solid and liquid systems. Prabhu et al. utilized the co-grinding method to create a solid dispersion of atorvastatin calcium and P407, evaluating its wetting properties with the sessile drop method. Pure atorvastatin

calcium exhibited a high contact angle due to its hydrophobic nature. However, when dispersed in P407 as a solid dispersion, it displayed an extremely low contact angle, confirming the substantial improvement in drug solubility facilitated by P407 [180]. In another study, Łyszczarz et al. developed orodispersible films (ODFs) incorporating aripiprazole-P407 solid dispersion. The contact angle values of ODFs containing aripiprazole-P407 solid dispersion were lower than those of placebo films, indicating improved wettability of ODFs due to the surface activity of P407 [181]. Clearly, P407 proves to be an excellent choice as a hydrophilic carrier in solid dispersion, as well as a co-eutectic forming agent with IBU in this study. Under a stereomicroscope, the higher penetration distance of the IP tablet signifies its superior wetting properties compared to a plain IBU tablet. This observation aligns with wetting measurements obtained using the sessile drop method. Moreover, the wetting rate, calculated from the slope of the penetration distance versus time profile, yields results consistent with contact angle measurements reported in previous research studies [182, 183]. Consequently, measurements of penetration distance and wetting rate using stereomicroscopy with imaging analysis serve as a viable alternative for investigating the wetting properties of pharmaceutical solid dosage forms.

After immersed in medium, swelling, gel formation and erosion of eutectic effervescent tablet subsequently occurred. Stereomicroscopy, coupled with imaging analysis techniques, was applied to explore the gel thickness and erosion boundary. The gel thickness for each formulation was plotted against the immersion time and depicted in Figure 25. The rate of gel formation, calculated from the slope of the gel thickness versus time profile, is presented in Table 9. The determination of gel thickness under the stereomicroscope was focused on three formulations, namely IP, IP5E, and IP10E, because higher erosion rates of formulation containing more than 10% (w/w) of effervescent agents interfered the determination of gel thick-ness under stereomicroscope. As illustrated in Figure 25, all three eutectic effervescent formulations exhibited greater gel formation in distilled water than in 0.1 N HCl buffer, with IP formulation demonstrating the highest gel formation in both media due to the superior gelling ability of P407 in distilled water, consistent with previous findings by Jannin et al. [29]. The gel formation behavior of P407 observed under stereomicroscopy aligns with the results obtained in wetting rate determination. Poloxamers, being nonionic surfactants, are widely employed as emulsifiers, wetting agents, and solubilizers in pharmaceutical formulations. Incorporating them into solid dispersions aims to enhance the solubility and dissolution profiles of poorly water-soluble drugs, attributed to the formation of self-assembly nanoaggregates and surface activity [182]. Furthermore, increasing the concentration of effervescent agents in formulations led to a reduction in the gel formation of P407 in eutectic effervescent tablets. The introduction of effervescent agents into the tablet generated CO2 gas,

promoting tablet erosion and subsequently decreasing the gel formation of P407 in the eutectic effervescent formulation. Gel formation rates exhibited a similar trend in both distilled water and 0.1 N HCl buffer. P407 in the formulation contributed to the creation of a gel layer around the tablet surface, with the highest gel formation rate in distilled water recorded as 0.184 mm/min, as illustrated in Table 9. With the addition of effervescent agents, the gel formation rate gradually decreased, reaching 0.035 mm/min for the formulation containing 10% (w/w) of effervescent agents immersed in distilled water.

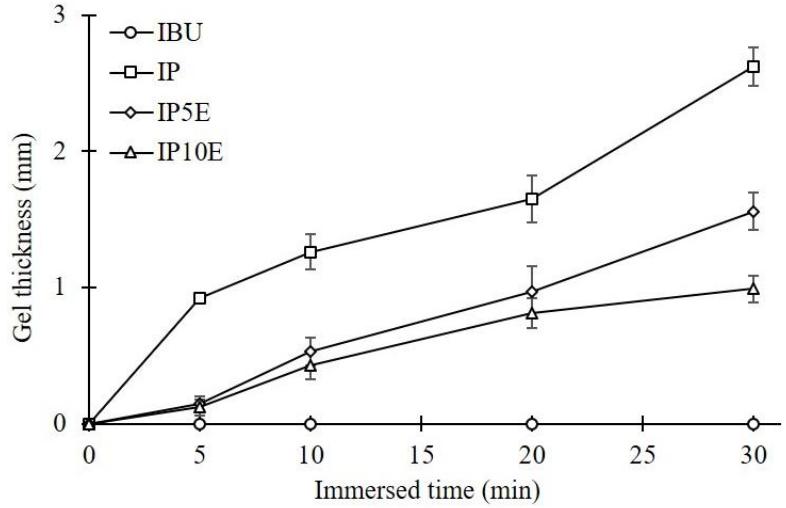

(A)

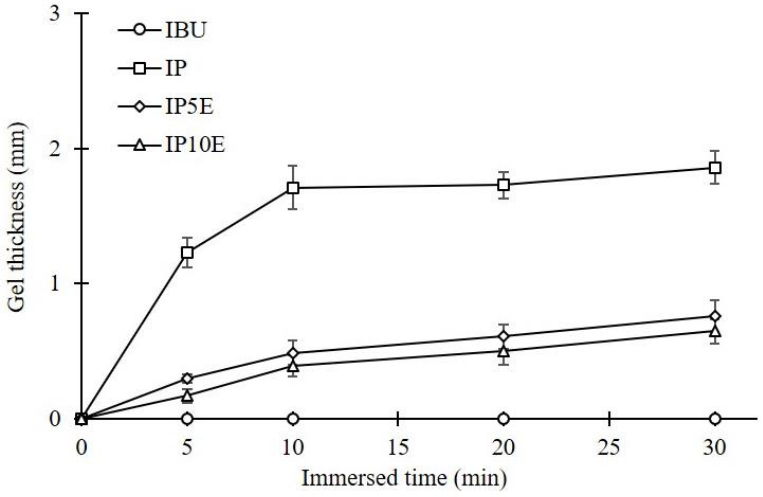

(B)

Figure 25. The gel formation capacity of eutectic effervescent tablets in distilled water (A) and 0.1 N HCl buffer pH 1.2 (B).

The erosive capability of eutectic effervescent tablets in different medium solutions is illustrated in Figure 26. The formulation containing 5% (w/w) of effervescent agents demonstrated an erosion distance of approximately 1 mm after immersion in distilled water for 30 minutes, and an increase in the incorporation of effervescent agents further enhanced the erosion of the formulations. Additionally, the erosion capacity in 0.1 N HCl buffer displayed a similar pattern, with slightly higher erosion compared to that in distilled water. The acidic environment of 0.1 N HCl buffer triggered more effervescence reactions, consequently leading to increased erosion. Subsequently, the erosion rate of each formulation was calculated from the slope of the profile depicting the relationship between erosion boundary and immersion time, as illustrated in Table 9. Concerning erosion rate, there was no erosion observed in the IP formulation after immersion in both different medium solutions for 30 minutes. The erosion rate increased with the introduction of more effervescent agents into the tablets, reaching a maximum of 0.375 mm/min when the formulation containing 30% (w/w) of effervescent agents was immersed in 0.1 N HCl buffer. In the study conducted by Desai et al., effervescent agents were regarded as tablet disintegrant. The volumetric air expansion resulting from the combination of an organic acid with inorganic carbonate or bicarbonate facilitated the disintegration of effervescent tablets after wetting [183]. Comparing with traditional and advanced techniques for investigating erosion behavior, the erosion boundary diameter and erosion rate obtained from stereomicroscopy with imaging analysis serve as an alternative tool in pharmaceutical product development. These techniques yield corresponding results, indicating that a higher amount of disintegrant addition promotes greater tablet disintegration [184-186].

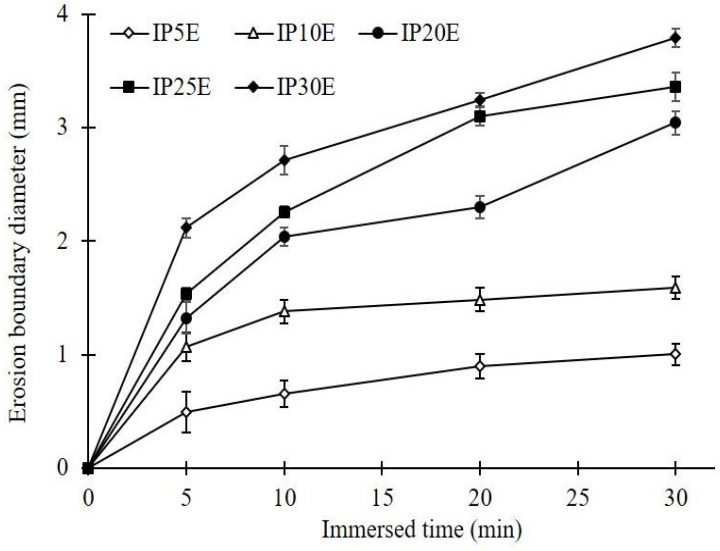

(A)

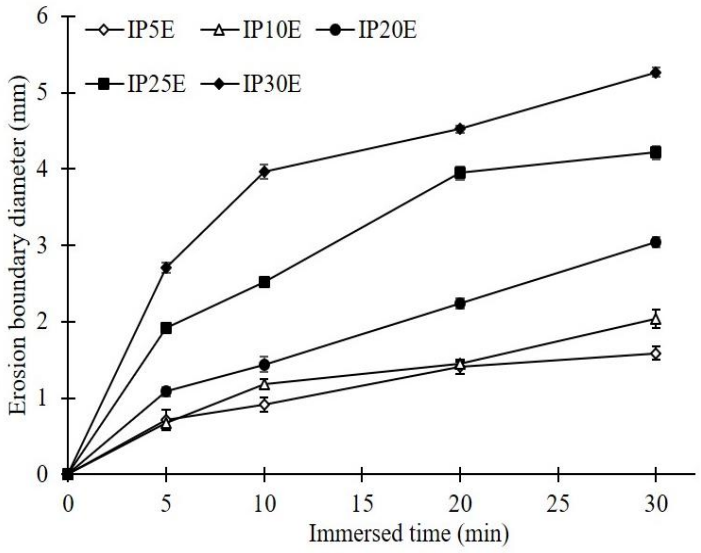

(B)

Figure 26. The erosion capacity of eutectic effervescent tablets in distilled water (A) and 0.1 N HCl buffer pH 1.2 (B)

4.1.3.2 *In vitro* disintegration of eutectic effervescent tablets

To explore the impact of pH on the disintegration behavior of eutectic effervescent tablets, the *in vitro* DT was examined in both distilled water and 0.1 N HCl buffer pH 1.2, as depicted in Figure 27. No alteration was observed in the IBU tablet in both media even after immersion for more than 6 hours (data not shown in Figure 27). With the incorporation of P407 into the IBU tablet, the DT of the IP tablet significantly decreased to 67.90 minutes in distilled water and 94.56 minutes in 0.1 N HCl buffer. This reduction can be attributed to the improved solubility resulting from eutectic formation, which was evident in the increased wetting rate and erosion rate discussed earlier. All formulations exhibited similar trends in DT in both media, with slightly shorter times in distilled water. Consequently, solubility emerges as a crucial factor influencing the formulation's disintegration behavior, leading to enhanced dissolution [187, 188]. The carbonation reaction induced by effervescent agents triggered surface erosion, facilitating deeper penetration of the medium and hastening the disintegration of the eutectic effervescent tablet [183, 185, 186]. As the effervescent agent content increased from 5% to 30% (w/w), DT in distilled water decreased from 57.13 minutes to 11.15 minutes. In the case of 0.1 N HCl buffer pH 1.2, it was reduced to approximately 30 minutes when 30% (w/w) effervescent agents were used in the IP formulation. These results align with the observed trends in wetting rate and erosion rate, as discussed earlier.

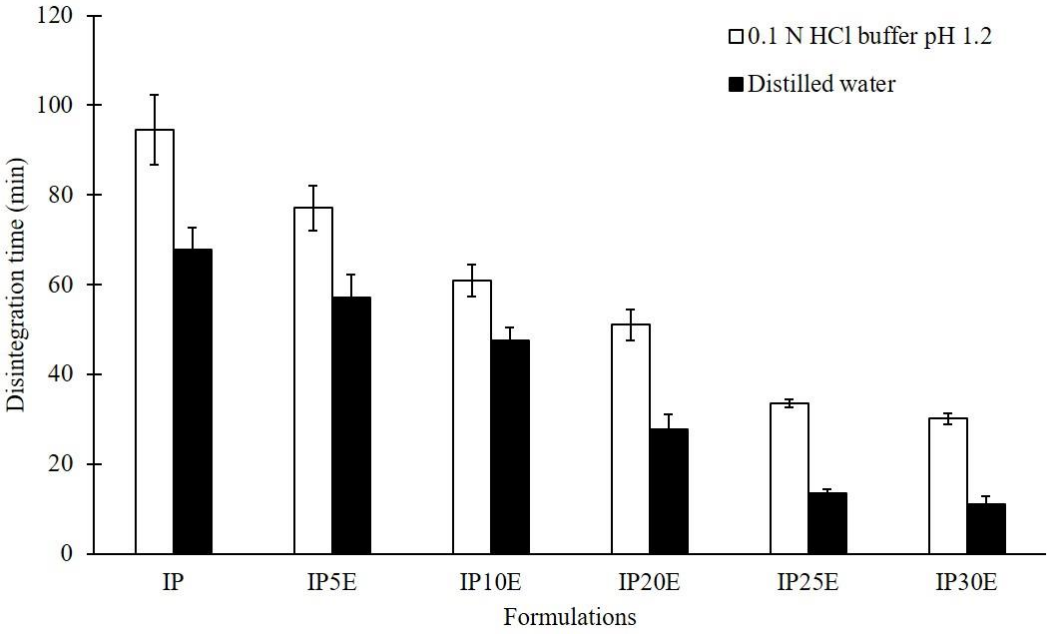

Figure 27. *In vitro* disintegration of eutectic effervescent tablets in distilled water and 0.1 N HCl buffer pH 1.2

4.1.3.3 *In vitro* drug release of eutectic effervescent tablet in 0.1 N HCl buffer and kinetic parameters

The *in vitro* drug release profiles of eutectic effervescent tablets, examined in 0.1 N HCl buffer pH 1.2, are presented in Figure 28. In formulations containing effervescent agents, there might be an initial burst release (F_0) resulting from carbonation upon contact with the dissolution medium. The Modified Korsmeyer-Peppas model, incorporating F_0, was applied to assess the mechanism of IBU release from the tablets. However, F_0 cannot be treated as an independent variable in the Peppas-Sahlin model. [144]. Therefore, cumulative drug dissolution versus time profiles were fitted using both the F_0-modified Korsmeyer-Peppas and Peppas-Sahlin models. Table 10 provides the mathematical modeling of IBU release from eutectic effervescent tablets, with R^2, AIC, and MSC values serving as criteria for model selection. The best model is indicated by the highest R^2 value closest to 1.0, the highest MSC value, and the lowest AIC [144]. From the results, F_0 obtained from the modified Korsmeyer-Peppas modeling for all formulations exhibited a zero value, indicating no initial burst release. This seems inconsistent with the dissolution profile, especially in formulations with higher effervescent agent content. For instance, the eutectic tablet containing 30% effervescent agents showed approximately 25% dissolved drug within 30 minutes. In comparison with the study of Andhariya et al., this suggests a slight initial burst release of IBU from eutectic tablets with higher effervescent agent amounts [189]. Normally, carbonation reaction should occur immediately upon contact with the medium,

resulting in a higher initial burst release for effervescent tablets. In this study, as observed under the stereomicroscope, the carbonation reaction of eutectic effervescent tablets gradually occurred upon immersion in the medium. This can be attributed to the gelling capabilities of P407, which can delay the breakdown of eutectic effervescent tablets [190].

Regarding the mathematical model fitting results, all formulations exhibited tendencies toward the Peppas-Sahlin model, with R^2 values close to 1.0. The dissolution rate, obtained from the positive k value in the Peppas-Sahlin model, is an indicator of the release mechanism [191]. The plain IBU tablet showed the lowest dissolution rate at 0.3694% dissolved drug/h, with heterogeneous erosion as the predominant drug release mechanism, as indicated by the positive k_2 value in Table 10. In comparison, the incorporation of IP enhanced the dissolution rate to 5.1761% dissolved drug/h, achieving a maximum dissolution of about 28% at 24 h. The addition of effervescent agents to IP formulation increased the dissolution rate from about 8% dissolved drug/h for 5% (w/w) effervescent agents to 32% for 30% (w/w) effervescent agents. Furthermore, 30% (w/w) effervescent agents promoted the maximum dissolution to up to 38% (Figure 28). Kinetic parameters, estimated using the Peppas-Sahlin model fitting, indicate the release mechanism, with a higher value suggesting dominance when comparing k_1 and k_2 values. A higher k_1 value suggests that the diffusion process is the predominant drug release mechanism, while a higher k_2 indicates that poloxamer relaxation or heterogeneous erosion is the main drug release mechanism [191]. Except for the IBU tablet, all formulations indicated a positive k_1 value, suggesting that IBU release could be explained by the diffusion process. Additionally, the addition of effervescent agents to the IP tablet did not affect the IBU release mechanism. These findings support the slightly observed initial burst release in eutectic effervescent tablets mentioned earlier. Upon contact with the medium, effervescent agents could promote tablet breakdown, with small granules suspended in the medium. Some fractions of granules would disintegrate and release as an initial burst drug release, while remaining fractions could swell due to the gelling properties of P407, facilitating drug release through diffusion [192, 193].

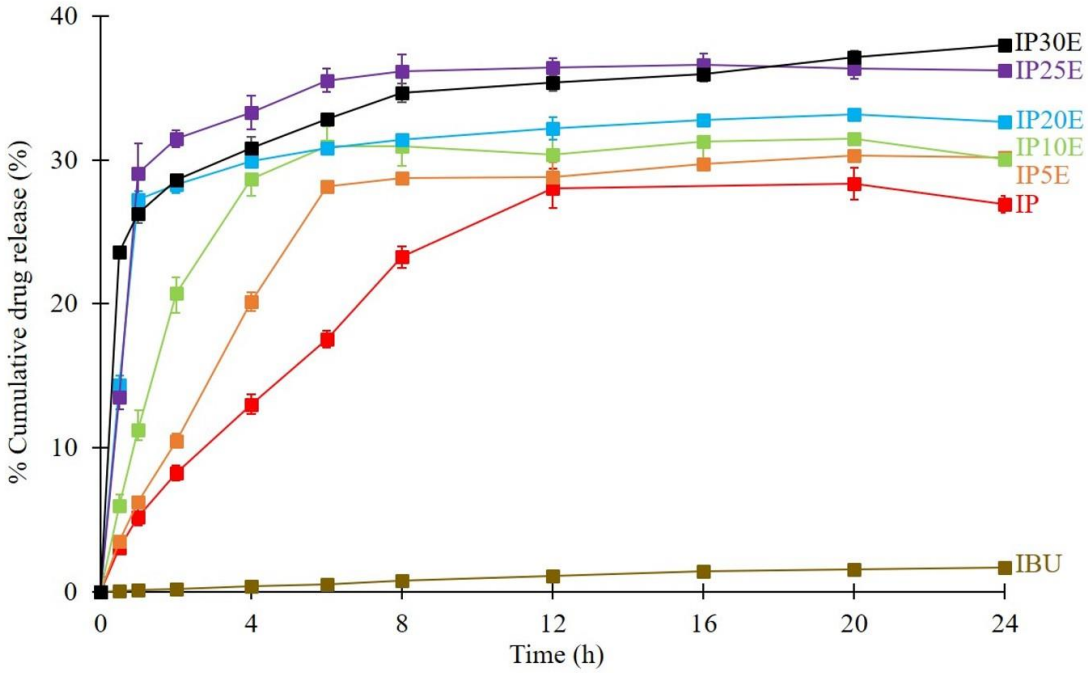

Figure 28. *In vitro* drug release profiles of eutectic effervescent tablets in 0.1 N HCl buffer pH 1.2.

Table 10. Mathematic modeling of eutectic effervescent tablets in 0.1 N HCl buffer pH 1.2

Formulation	Kinetic modeling	Criteria for model selection			Kinetic parameters		
		R^2	AIC	MSC			
IBU	F_0 modified KP	0.9883	-30.5054	4.0201	K_{KP} = 0.1326	n = 0.8168	F_0 = 0.0000
	PS	0.9926	-35.5699	4.4805	k_1 = -0.2924	k_2 = 0.3694	m = 0.3023
IP	F_0 modified KP	0.9137	54.3542	1.8752	K_{KP} = 7.5186	n = 0.4476	F_0 = 0.0000
	PS	0.9841	35.4159	3.5978	k_1 = 5.1761	k_2 = -0.2349	m = 0.8300
IP5E	F_0 modified KP	0.8517	62.8388	1.2833	K_{KP} = 10.8410	n = 0.3659	F_0 = 0.0000
	PS	0.9593	48.5215	2.5848	k_1 = 8.5832	k_2 = -0.5887	m = 0.7207
IP10E	F_0 modified KP	0.8072	64.8453	0.8465	K_{KP} = 16.0896	n = 0.2479	F_0 = 0.0000
	PS	0.9472	50.4698	2.1534	k_1 = 15.3681	k_2 = -1.7729	m = 0.5647
IP20E	F_0 modified KP	0.8979	55.0850	0.8593	K_{KP} = 23.6146	n = 0.1225	F_0 = 0.0000
	PS	0.9385	49.5094	1.3662	k_1 = 29.2022	k_2 = -6.4220	m = 0.3129
IP25E	F_0 modified KP	0.8609	61.5988	0.7086	K_{KP} = 25.5091	n = 0.1369	F_0 = 0.0000
	PS	0.9299	53.6240	1.4336	k_1 = 30.1941	k_2 = -6.0546	m = 0.3633
IP30E	F_0 modified KP	0.9956	20.4575	3.8429	K_{KP} = 26.2569	n = 0.1183	F_0 = 0.0000
	PS	0.9973	16.1655	4.2330	k_1 = 31.4441	k_2 = -5.3375	m = 0.1751

Remarks: KP = Korsmeyer-Peppas; PS = Peppas—Sahlin; R^2 = coefficient of determination; k = rate constant; F_0 = initial fraction of the drug in the solution resulting from a burst release, AIC = Akaike information criterion; MSC = Model selection criterion

4.1.3.4 Correlation between rate of wetting, gel formation and erosion with disintegration and dissolution parameters

To elucidate the primary mechanism behind the enhancement of dissolution rate in effervescent formulations, the wetting rate, gel formation rate, and erosion rate were correlated with the dissolution rate and disintegration time, as depicted in Figures 29 and 30, respectively. A positive linear relationship between the wetting rate and dissolution rate was observed with a high coefficient of correlation (R^2 = 0.9641), indicating that the increase in drug dissolution rate could be attributed to the improvement in the wetting rate (Figure 28A). Regarding the erosion rate, the dissolution rate showed an initial increase with the elevation of the erosion rate. However, no substantial change in the dissolution rate occurred once the erosion rate exceeded approximately 0.16 mm/min (Figure 28C). These findings align with the investigation of the drug release mechanism using mathematical model fitting, as discussed earlier. After tablet breakdown, residual granules containing P407 can form a gel layer that surrounds and facilitates drug diffusion across the gel layer [194]. Typically, the solubility of a soluble ingredient is affected by both wicking and the disintegration of the tablet, especially in tablets containing a high concentration of soluble ingredients [186]. Wicking refers to the penetration of liquid by capillary action between the pores of the tablet [195], and this can be likened to the wetting parameter in this study. The penetration of liquid surrounding the tablet into the target tablet could be stimulated by the eutectic mixture between IBU and P407, as evident in the morphological changes observed under the stereomicroscope. Increased liquid penetration promoted a higher rate of effervescence reaction in the formulation and a higher rate of erosion of IBU-P407 eutectic effervescent tablets, resulting in increased drug release, as illustrated in Figure 28 [31, 195, 196]. Regarding the gel formation rate, there was no discernible relationship between the dissolution rate and gel formation rate. This result can be explained as follows: the gel formation of P407 in the formulation was interrupted by surface erosion from the CO_2 gas generated by the effervescence reaction, as observed in the morphological changes under the stereomicroscope (Figure 23B).

The relationship between the rates of wetting, gel formation, and erosion with DT is depicted in Figure 30. The rate of tablet wetting demonstrated a negative correlation with DT, described by a linear equation with a high R^2 of 0.9992, as shown in Figure 30A. In 0.1 N HCl buffer, DT decreased from 94.56 min to 77.13 min when 5% effervescent agents were incorporated into the IP formulation and gradually declined with a decrease in the wetting rate. In terms of the rate of gel formation, DT gradually increased with an increasing gel formation rate, as illustrated in Figure 30B. The erosion rate exhibited a negative relationship with DT, described by a linear equation, as shown in Figure 30C. These findings can be explained by observing the morphological changes under the stereomicroscope.

The effervescent reaction rapidly occurred when effervescent tablets came into contact with the dissolution medium. The rough surface of the tablet was evident from erosion, promoting a larger surface area of the tablet, resulting in a decrease in DT and an increase in drug dissolution [31]. The effervescent reaction of the effervescent tablet occurred faster than the gel formation of P407, and DT rapidly decreased with the addition of effervescent agents. This explanation is evident, as shown in Figure 30C. However, there was no relationship between the gel formation rate and dissolution rate, but a positive relationship was found in the initial period of the graph plotted between the erosion rate and dissolution rate (Figure 29C). This could be described by the drug release mechanism obtained from mathematical modeling, as discussed previously, and is consistent with the previous study by Zuo et al. [197]. Therefore, monitoring tablet behaviors under the stereomicroscope with imaging analysis could explain the mechanism of the dissolution rate improvement of IBU-P407 eutectic effervescent tablets. Wetting enhancement through eutectic formation between IBU and P407 could promote the penetration of surrounding liquid into eutectic effervescent tablets, leading to a greater effervescence reaction. Furthermore, stereomicroscope imaging analysis was employed to describe the main mechanisms of tablet dissolution and revealed that tablet disintegration and erosion caused by the carbonation of the effervescent agent and the gel formation of P407 in formulations had a potential influence on drug dissolution enhancement.

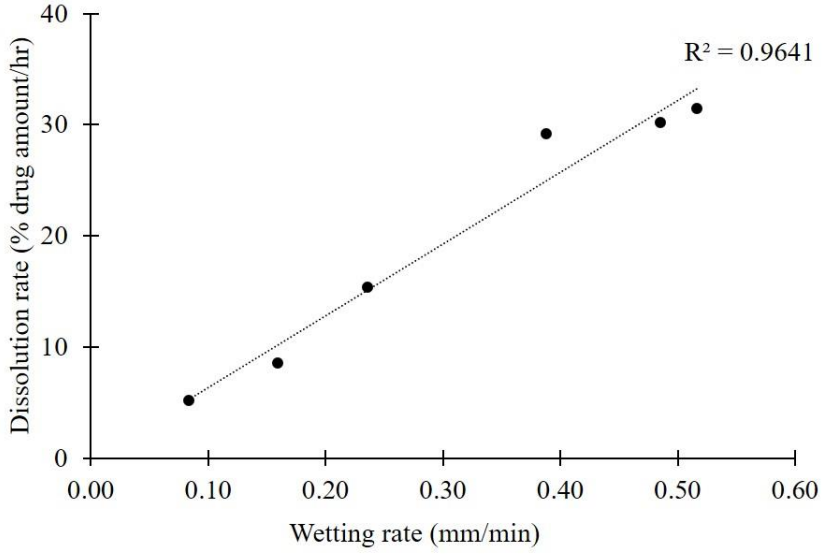

(A)

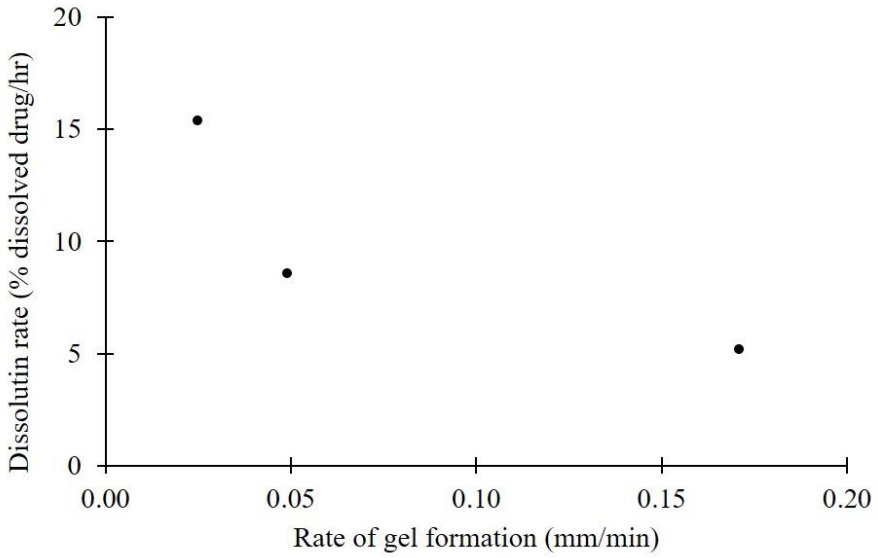

(B)

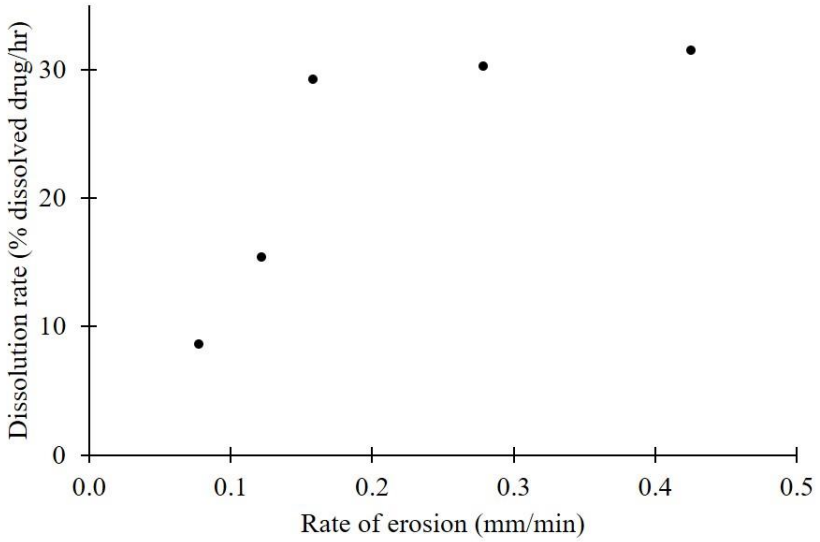

(C)

Figure 29. Correlation between rate of wetting (A), gel formation (B) and erosion (C) with dissolution rate of eutectic effervescent tablets in 0.1 N HCl buffer pH 1.2.

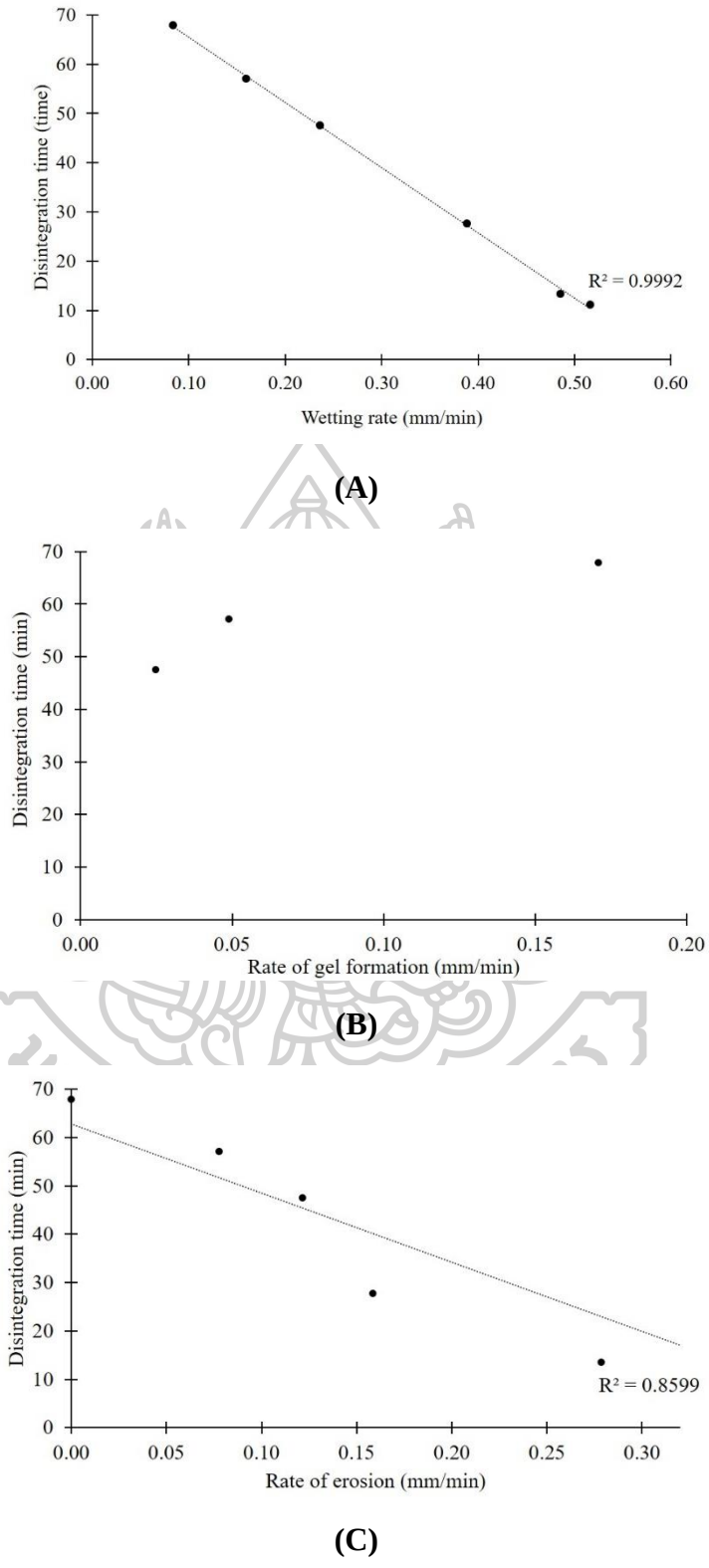

Figure 30. Correlation between rate of wetting (A), gel formation (B) and erosion (C) with disintegration time of eutectic effervescent tablets in 0.1 N HCl buffer pH 1.2.

4.1.3.5 Summary

Stereomicroscope with imaging analysis has proven to be a versatile tool for the measurement and comprehension of the wetting properties, gel formation, and erosion behaviors of eutectic effervescent tablets. By monitoring the penetration of the immersion medium into the tablet, valuable information regarding penetration distance and the determination of gel thickness/erosion boundary diameter was obtained. These values served as indicators of gel formation and erosion behaviors, respectively. The wetting enhancement observed in IBU-P407 eutectic mixture-incorporated effervescent tablets was characterized by a greater liquid penetration distance. Effervescent agents within the tablet contributed to heightened erosion behavior due to CO_2 generation and increased surface roughness. This, in turn, led to deeper liquid penetration into the eutectic effervescent tablet, resulting in enhanced disintegration and drug dissolution rates, as evidenced in in vitro disintegration and drug release studies. The formation of P407 gel surrounding the tablet decreased with an increase in the content of effervescent agents. Stereomicroscope observation revealed a rapid effervescence reaction disrupting the gel formation of tablet containing IBU-P407 eutectic mixture. Various behaviors of eutectic effervescent tablets after immersion in different media were effectively described using this technique. Moreover, this approach provided a better understanding of the primary dissolution mechanism of eutectic effervescent tablets through visual observation. The correlation between several parameters observed under the stereomicroscope and disintegration/dissolution parameters suggested that a combination of erosion due to the carbonation of the effervescent agent and P407 gel formation promotes drug dissolution enhancement. Therefore, the stereomicroscope with imaging analysis technique demonstrates potential as a versatile tool for determining the wetting properties, gel formation, and erosion behaviors of solid dosage forms. Further investigation and evaluation of these behaviors with this technique should be conducted on other solid dosage forms.

4.2 Study of effervescent matrix tablets comprising IBU-P407 eutectic mixture

4.2.1 Microscopic and macroscopic characterization of effervescent matrix tablets using combined mechanical and imaging techniques

4.2.1.1 Physical properties of effervescent matrix tablets

Effervescent matrix tablets were successfully produced through melt granulation, utilizing a circulator water bath at 70 °C. The composition of these tablets involved a eutectic mixture between IBU and P407, with both components capable of melting at approximately 50 °C [20]. This mixture served as a meltable binder, facilitating the agglomeration of powder particles into granules. All resulting effervescent matrix tablets exhibited satisfactory physical appearance. The investigation of physical properties, including thickness, hardness, diameter, and tablet weight, is presented in Figure 31. No significant differences were noted in the thickness, diameter, and average tablet weight across all formulations. Regarding tablet hardness, IPM demonstrated the highest hardness at 170.40 ± 2.79 N. The hardness values for 5E and 10E decreased significantly to 126.20 ± 7.79 N and 132.80 ± 6.14 N, respectively, due to the inclusion of effervescent agents. However, there was no significant difference in hardness between 5E and 10E. The hygroscopic nature of effervescent agents, particularly CA, had a softening effect on tablet texture, leading to a reduction in tablet hardness [198, 199]. The lower quantity of MCC PH101 in the effervescent matrix tablets (5E and 10E) compared to the IPM tablet contributed to a decrease in tablet hardness. MCC possesses a remarkably low coefficient of friction and residual die wall pressure, providing binding properties to tablets [200, 201]. Additionally, MCC can induce adhesion between particle agglomerates, resulting in higher hardness and less friability of tablets [202].

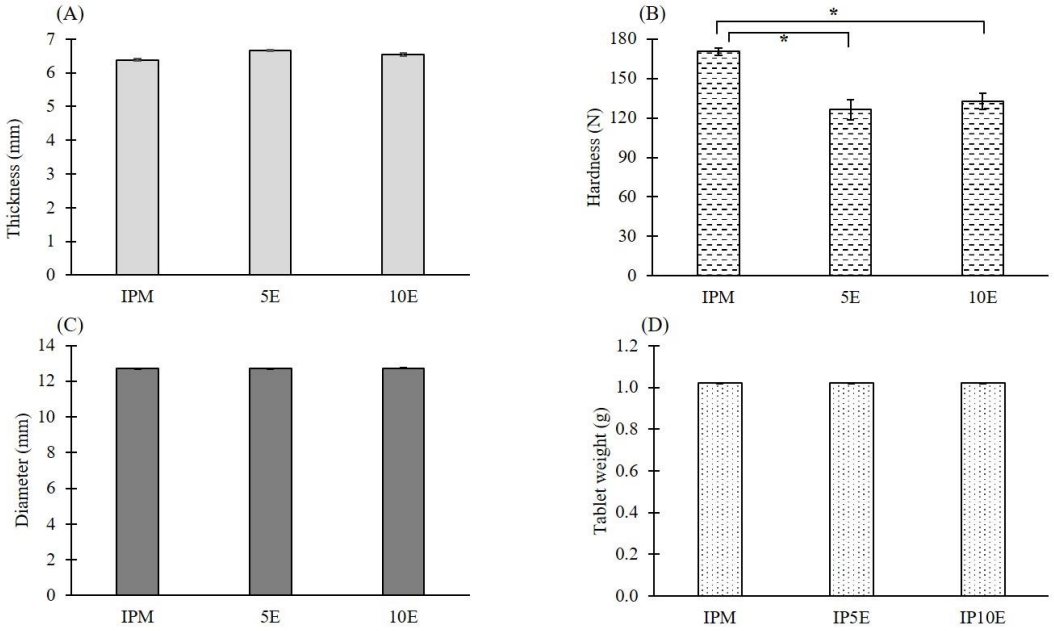

Figure 31. Thickness (A), hardness (B), diameter (C) and tablet weight (D) of IBU-P407 effervescent matrix tablets (n=10) (the asterisk (*) represents a significant difference ($p < 0.05$))

4.2.1.2 Gel strength of effervescent matrix tablets after immersion in pH-changed media

The impact of effervescent agents on the formation of a gel layer surrounding matrix tablets has not been previously explored. In this investigation, the gel strength of hydrated matrix tablets was assessed using a texture analyzer at various dissolution times. Typically, three regions within a swollen matrix tablet were distinguished based on the degree of hydration: the gel layer (highest hydration), swollen glassy layer (low hydration), and dry core (no hydration), as illustrated in Figure 8. Consequently, the mechanical properties were evaluated using a texture analyzer [145]. At the gel-solution boundary, the gel strength was minimal and gradually increased toward the tablet's center. The swollen glassy layer, representing a partially hydrated region, exhibited a continuously increasing gel strength until reaching the dry core (Figure 8). Figure 32 illustrates the gel strength profiles of different effervescent matrix tablets. All formulations were immersed in pH 1.2 HCl buffer (0.1 N) for 1.5 h before the pH medium was adjusted to 6.8 for the next 4 h. Thus, the gel strength profiles at 15 and 30 min reflected conditions in acidic medium, while those at 2 and 4 h represented the profiles in pH 6.8 phosphate buffer. IPM tablet, comprising a eutectic mixture of IBU, P407, and MCC PH101, was employed as the control. The gel strength profiles for all formulations exhibited a similar pattern, starting with a plateau before a linear increase in gel strength. Upon raising the medium pH to 6.8, the

profiles dramatically declined. Lower gel strength of the matrix tablets typically indicated the presence of a gel layer around them [145]. In the case of matrix tablets containing 5% (w/w) (Figure 32B) and 10% (w/w) (Figure 32C) effervescent agents by weight, in comparison to the IPM tablet (Figure 32A), both formulations displayed a significant reduction in gel strength. Similar patterns were observed in both gel strength profiles, with a slightly lower gel strength found in tablets incorporating higher amounts of effervescent agents. When considering the same HPMC concentration in the matrix tablets (20% (w/w)), a higher quantity of effervescent agents (10E) promoted a gel layer with lower strength (Figure 32C).

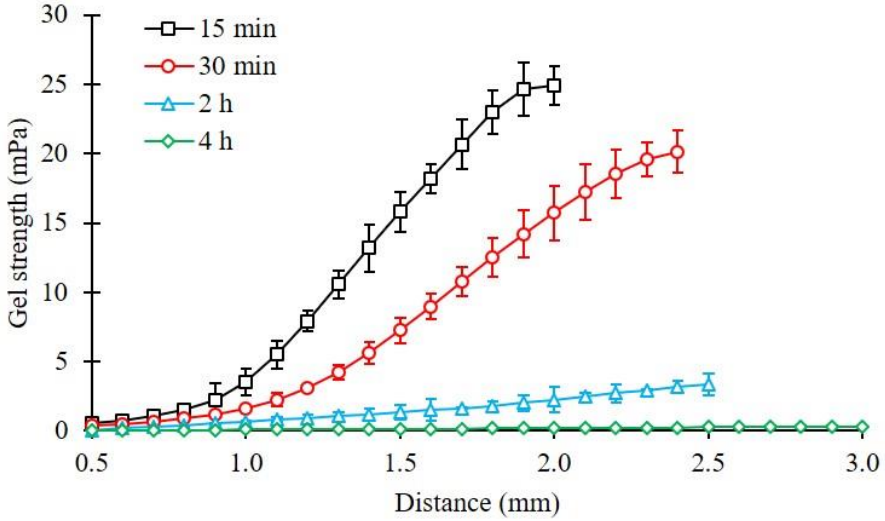

(A)

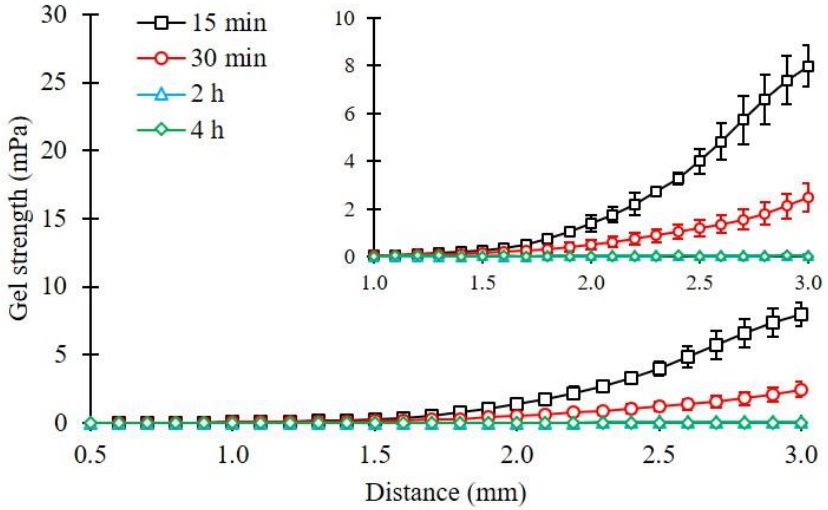

(B)

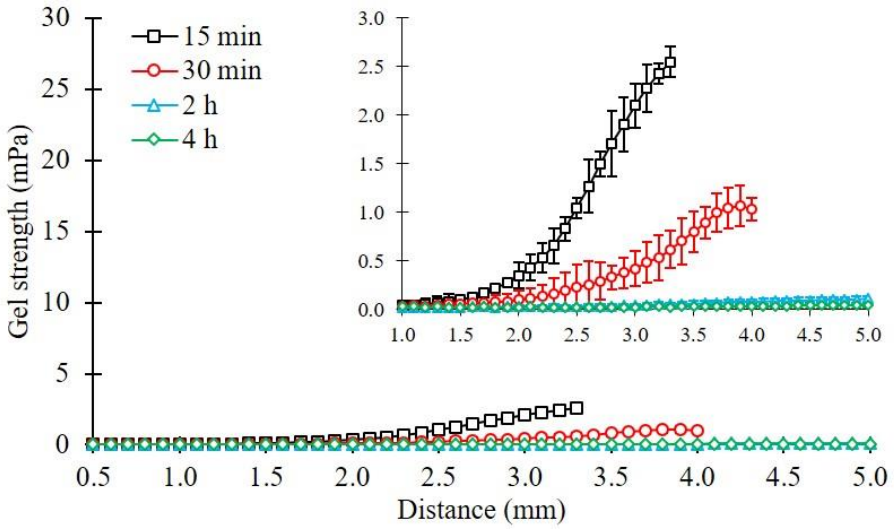

(C)

Figure 32. Gel strength profiles of IBU-P407 effervescent matrix tablets (n=5); IPM (A), 5E (B) and 10E (C).

As depicted in Figure 33, the gel strength profiles of all formulations were compared at various immersion times, and the impact of different types of media on gel strength was investigated. In the acidic medium, the gel strengths at 15 and 30 min (Figures 33A and 33B) were higher than those at 2 and 4 h in pH 6.8 phosphate buffer (Figures 33C and 33D). This observation can be attributed to the higher solubility of IBU-P407 [20, 202] and the gel-forming capability of HPMC [203, 204] upon contact with the medium. There was a notable reduction in gel strength after the incorporation of HPMC into formulations (5E and 10E) following immersion for 30 min and 2 h. This decrease in gel strength resulted from continued hydration and partial dispersion of the gel layer matrix between 30 min and 2 h. Practically, the height of the gel layer surrounding the matrix tablet can be gauged by estimating the inflection point, which marks the change in the slope of gel strength profiles. Table 11 presents the estimated gel layer height, gel strength at the gel-solution interface, and the rate of gel layer formation. In pH 1.2 HCl buffer (0.1 N) for 30 min, the 10E formulation exhibited the highest gel layer height of 2.70 ± 0.28 mm, followed by 5E and IPM tablets (1.90 ± 0.10 and 1.17 ± 0.15 mm, respectively). After raising the medium pH to 6.8, a higher gel layer height was observed in the 5E and 10E formulations. Consequently, the formation of the gel layer around the tablet occurred more rapidly due to the inclusion of effervescent agents. Typically, surface roughness increased with the rise in effervescent agents, facilitating inward medium penetration, i.e., deeper into the tablet, and boosting the tablet wetting rate. The high wetting rate promoted the swift formation of the gel layer in the matrix tablet [203-206]. Regarding the gel-solution interface, the IPM tablet exhibited the maximum gel strength of 0.213 ± 0.075 mPa at 15 min.

Over the immersion period, the gel strength significantly decreased, reaching 0.041 ± 0.023 mPa at 4 h due to the enhanced dissolution of the IBU-P407 eutectic mixture. Matrices containing effervescent agents (5E and 10E) displayed similar gel strength patterns compared to the IPM tablet. The gel strength of the 5E formulation surpassed that of the 10E formulation. Increased porosity in the formulation containing more effervescent agents can reduce gel strength. Therefore, the observed gel strength profiles and gel layer heights, analyzed using a texture analyzer, can be deemed crucial factors in comprehending the influence of effervescent agents on gel layer formation in matrix tablets.

Table 11. Estimated gel layer height and strength at the gel-solution interface tested in pH-changed media (n=5)

Immersed time	Estimated gel layer height (mm) (Mean ± SD)			Gel strength at gel-solution interface (mPa) (Mean ± SD)		
	IPM	5E	10E	IPM	5E	10E
15 min	0.93 ± 0.15	1.73 ± 0.06	2.17 ± 0.32	0.213 ± 0.075	0.034 ± 0.002	0.029 ± 0.017
30 min	1.17 ± 0.15	1.90 ± 0.10	2.70 ± 0.28	0.147 ± 0.034	0.023 ± 0.005	0.011 ± 0.004
2 h	0.60 ± 0.20	4.03 ± 0.25	4.63 ± 0.35	0.047 ± 0.022	0.015 ± 0.003	0.006 ± 0.001
4 h	0.70 ± 0.28	5.00 ± 0.00	5.00 ± 0.00	0.041 ± 0.023	0.015 ± 0.003	0.006 ± 0.003

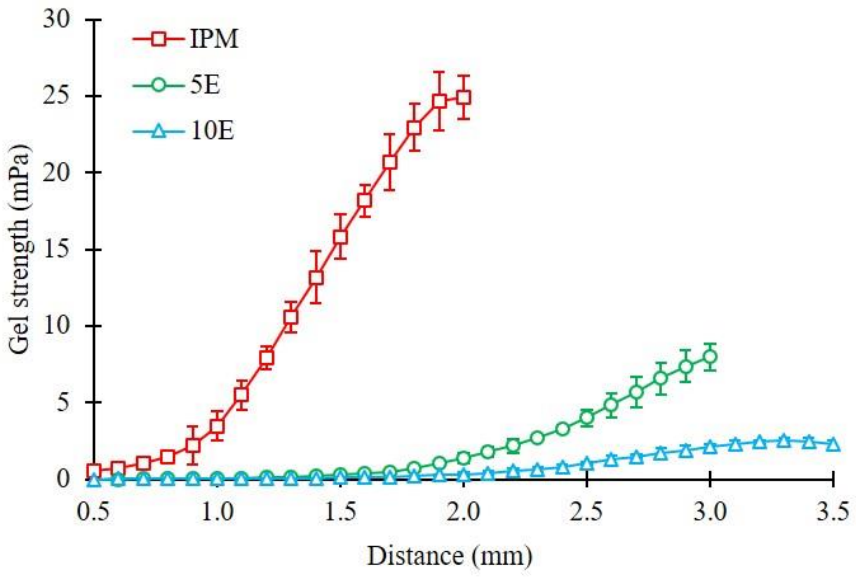

(A)

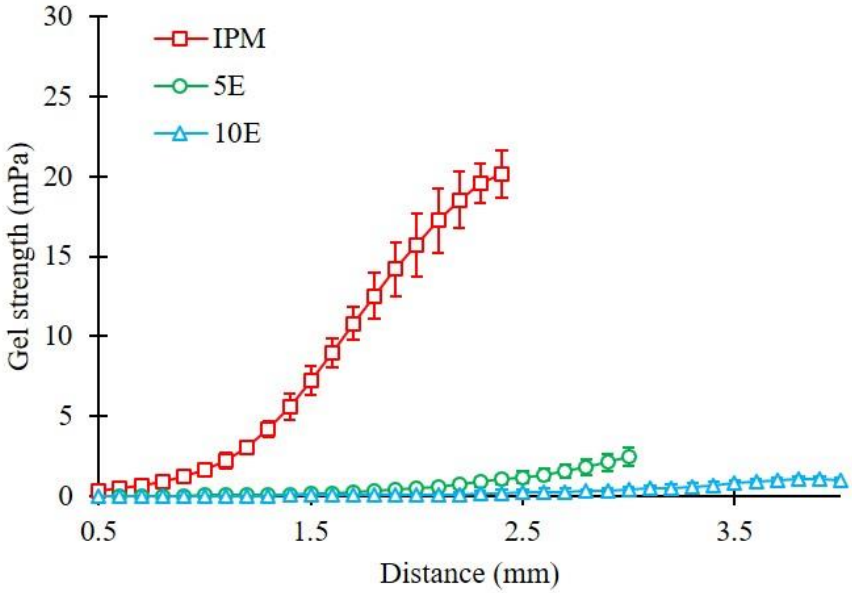
IPM
5E
10E
Gel strength (mPa)
Distance (mm)
0
5
10
15
20
25
30
0.5
1.5
2.5
3.5

(B)

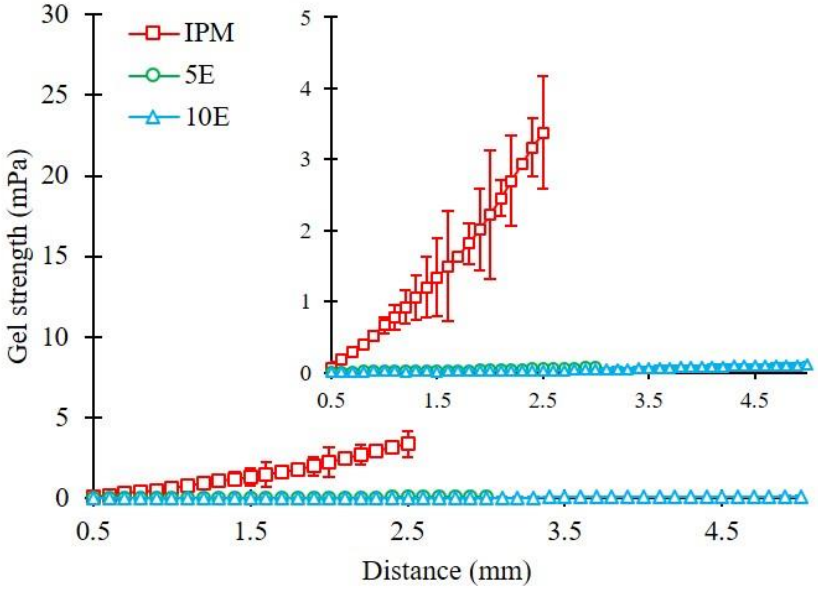
IPM
5E
10E
Gel strength (mPa)
Distance (mm)
0
5
10
15
20
25
30
0.5
1.5
2.5
3.5
4.5
1
2
3
4

(C)

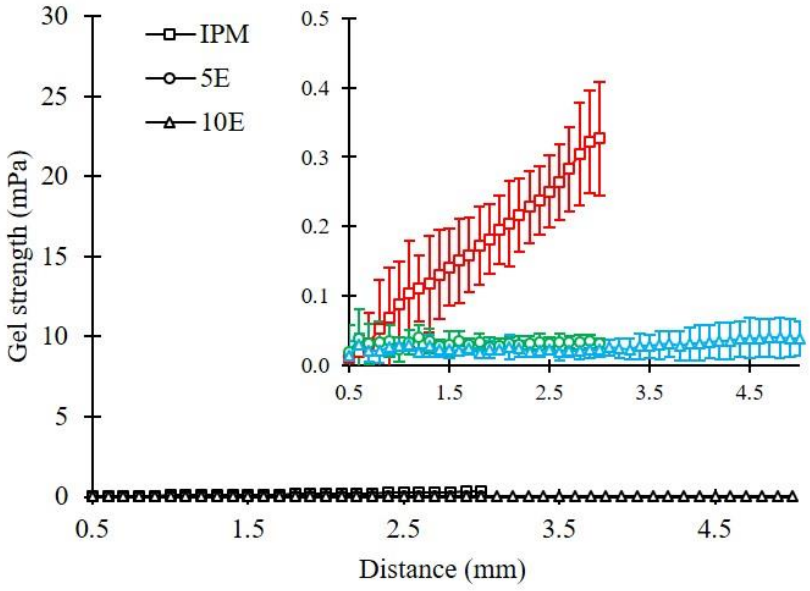

(D)

Figure 33. Gel strength profiles of IBU-P407 effervescent matrix tablets at different immersion times (n = 5); 15 (A) and 30 min (B); 2 (C) and 4 h (D).

4.2.1.3 Morphological Changes Observed under Digital Microscopy and SEM

Following immersion in pH-shift media, a freeze-drying technique was employed to dry the effervescent matrix tablets, and the resulting dried tablets underwent further examination using imaging techniques. While the freeze-drying method preserves the microstructure of the tablets in a dried state, it is essential to acknowledge the potential lack of correlation between the dried state and the hydrated state of the matrix tablets. However, the combination of tracking temporal changes in tablet microstructure in the dried state through imaging techniques and characterizing mechanical properties in the hydrated state could prove beneficial in elucidating the impact of effervescent agents on tablet microstructure.

Figures 34A and 34B display the micrographs of the surface and cross-sections of effervescent matrix tablets after immersion in pH-shift media, respectively. The tablet size of the IPM formulation reduced during the immersion periods. The heightened roughness observed on the IPM tablet surface after prolonged immersion in the media indicated heterogeneous erosion on the tablet surface (Figure 34A). In the cross-sectional micrographs of IPM, a dry core was clearly identified, surrounded by a thin gel layer. Additionally, the cylindrical shape of IPM at the initial time point transformed into a small sphere after immersion in media for 4 hours (Figure 34B). This observation aligns with the previous explanation for the gel strength profiles of IPM tablets. The improvement in dissolution due to IBU-P407 eutectic formation facilitated erosion and a reduction in tablet size as the immersion time progressed [203]. Moreover, the thin

gel layer surrounding the IPM tablet could not maintain the tablet shape due to its low viscosity and high solubility in the aqueous system of P407 [207]. In the case of 5E and 10E formulations, the tablet size gradually increased due to the swelling and the high gel layer formation of HPMC K15M in the formulations. High porosity and roughness were evident in the 5E and 10E formulations compared to those of the IPM, but these characteristics were more pronounced in the 10E tablet (Figure 34A). The cross-sectional micrographs of 5E and 10E (Figure 34B) revealed the progressively more apparent surrounding gel layer, while the dry core steadily diminished over time. A high porosity was observed in the 10E tablet, especially at the immersion time of 4 h. Some space was noted between the dry core and the surrounding gel layer, which did not appear in the IPM and 5E formulations (yellow arrows in Figure 34B). Moreover, the 10E tablets exhibited the lowest gel strength of 0.006 ± 0.003 mPa at 4 h after immersion in the dissolution media. Therefore, the high concentration of effervescent agents promoted increased carbonation reaction, resulting in a high CO_2 gas level. This, in turn, enhanced the porosity and low-strength microstructure of the matrix tablets, especially the gel layer. Additionally, a large porosity can typically augment the wetting rate and increase the rate of gel layer formation.

The surface morphology of all formulations was analyzed by SEM (Figure 35). The SEM micrographs of 5E and 10E revealed macropores of various sizes and interconnected channels on the tablet surface at 15 and 30 min after immersion in the medium. These pores and channels resulted from CO_2 generated by the carbonation reaction of effervescent excipients in the formulation, and their porosity characteristics facilitated the absorption of a significant amount of water, leading to swelling or gel layer formation. The microporous structure, indicated by brown arrows in Figure 35, pointed to the generation of the gel layer [208-210]. The pore size decreased, and a microporous network surrounded the pores and channels after the medium pH was raised to 6.8 at sampling time periods of 2 and 4 h (yellow arrows in Figure 35). Furthermore, the pore size of the 10E tablet (diameter > 200 µm) was larger than that of the 5E tablet (diameter < 200 µm), resulting in a higher rate of gel layer formation, evident in the microporous network of 10E tablets. This observation aligned with the earlier findings on gel strength and morphological changes under digital microscopy, confirming the previous explanation regarding the effect of effervescence on the microstructure of matrix tablets. For the IPM formulation, a small microporous network was unevenly distributed. Additionally, surface erosion was observed in the first 30 min in the acidic medium, and it was more pronounced in the medium with a high pH. This observation confirmed the heterogeneous erosion at the surface of the IPM tablet, consistent with the previous results in the gel strength study.

Immersion time	IPM	5E	10E
Initial			
15 min			
30 min			
2 h			
4 h			

(A)

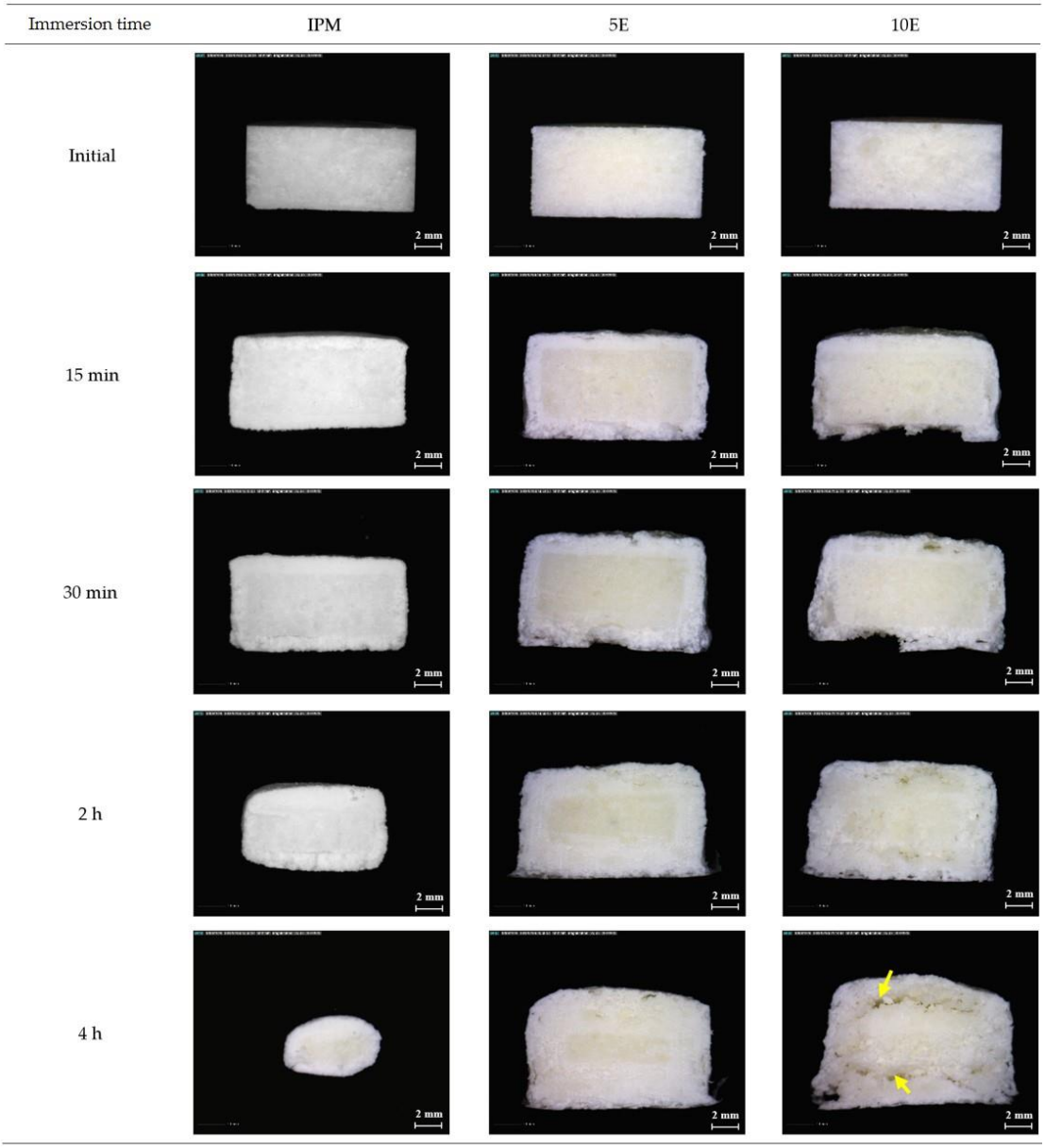

(B)

Figure 34. Surface (A) and cross-sectional (B) micrographs of IBU-P407 effervescent matrix tablets in pH-changed media at various immersion times (magnification of 26.8X)

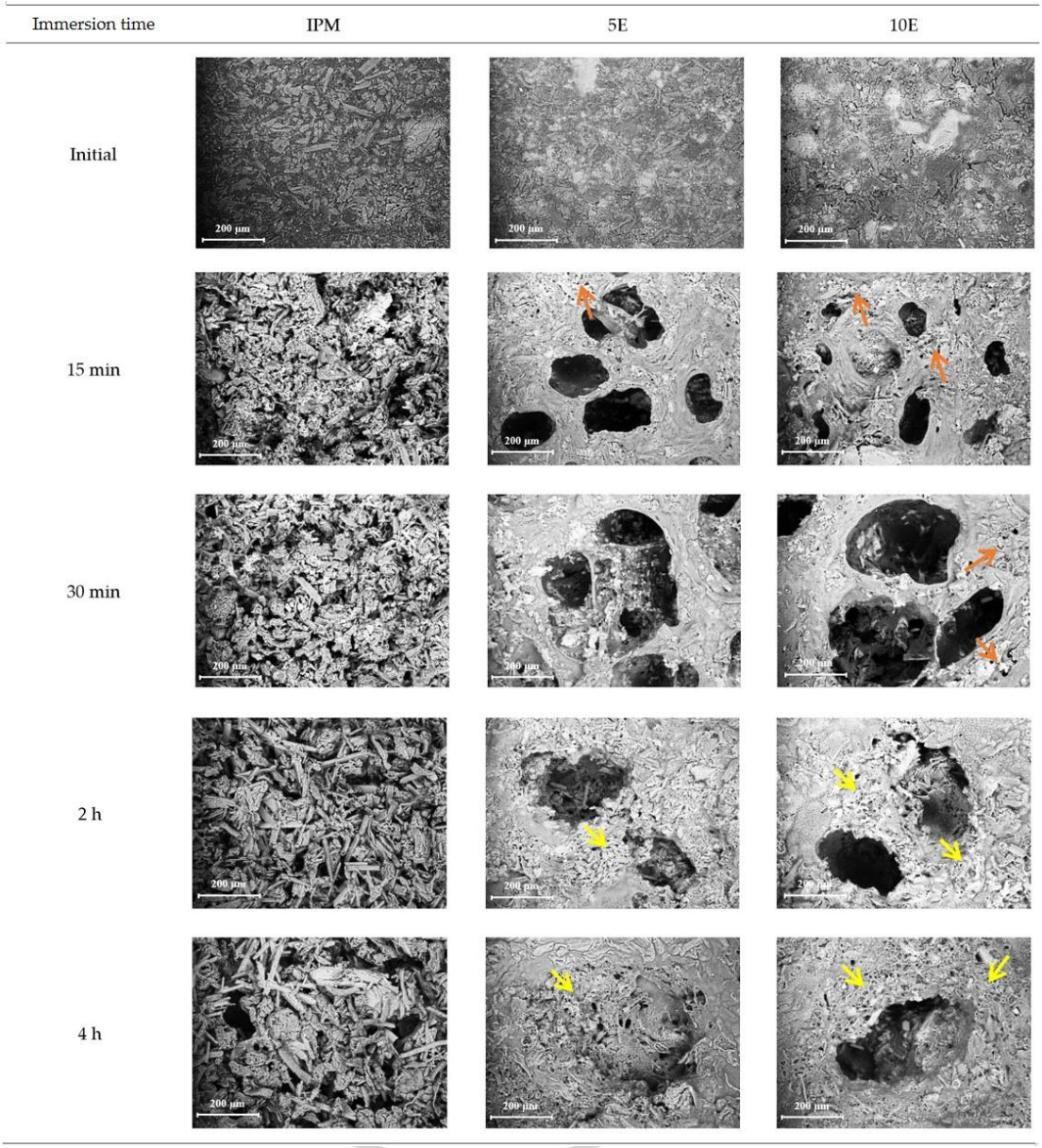

Figure 35. SEM micrographs of IBU-P407 effervescent matrix tablets in pH-changed media at various immersion times (magnification of 250X)

4.2.1.4 SRXTM and porosity determination

Figures 36A and 36B depict the reconstructed 3D images of the surface and cross-sections of effervescent matrix tablets in pH-shift media at different immersion times, respectively. In the first 15 min after immersion in the acidic medium, the 5E and 10E formulations displayed pores and channels on their surfaces. The presence of pores and channels was more pronounced in matrix tablets containing higher amounts of effervescent agents, particularly in the 10E formulation. The microporous structure became clearly evident and exhibited inhomogeneity in terms of pore size and shape after immersion in nearly neutral

medium at the 4-h time point, indicating the coverage of the surface by the gel layer. In contrast, surface roughness was observed in the IPM formulation at both time points in both acidic and neutral media. These reconstructed 3D images of the surface and cross-sections align with the findings from the gel strength study and the previously discussed morphological changes.

As shown in Figure 36B, the color gradient from light brown to dark brown represents low to high X-ray absorption, where higher absorption, indicating higher density, is depicted as white. Well-distributed and organized white spots were observed in the cross-sectional reconstructed 3D images of 5E and 10E (highlighted by white circles), with a particularly greater presence in the 10E formulation. These white spots gradually diminished over time and were absent in the porous structure at the 4-h time point after immersion. These detected white spots, representing bicarbonate salts, were specific to the 5E and 10E formulations, based on the X-ray absorption behavior of the metal salt [211, 212]. Given its density-based contrast, SRXTM is well-suited for detecting voids or pores in the matrix, providing high-resolution images [213-215]. In the case of IPM tablets, differences in density were observed and identified in the outer and inner layers of the tablets. Following immersion in the media, the surrounding water ingress led to the gradual expansion and erosion of the tablets. Internal cracks formed in the hydrated tablet after immersion for 2 and 4 h (indicated by white arrows in Figure 36B). Water-soluble components, such as P407 and IBU-P407 eutectic mixtures in the tablets, dissolved and were released into the medium, resulting in heterogeneous surface roughness on the tablet surface depending on their distribution. [214]. For the 5E and 10E formulations, interconnected pores of various sizes and shapes were observed at the outer layer of tablets in the initial stage (15 and 30 min). The surrounding gel layer appeared as the pore size diminished, and the microporous structure increased steadily when the formulations were immersed in a medium with a higher pH at 2 and 4 h. These characteristics were consistent with the morphological changes observed during digital microscopy and SEM.

Immersion time	IPM	5E	10E
Initial		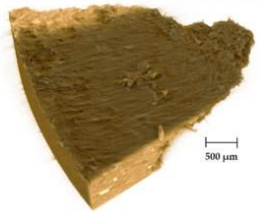	
15 min			
4 h			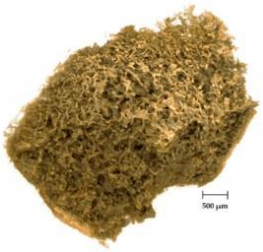

(A)

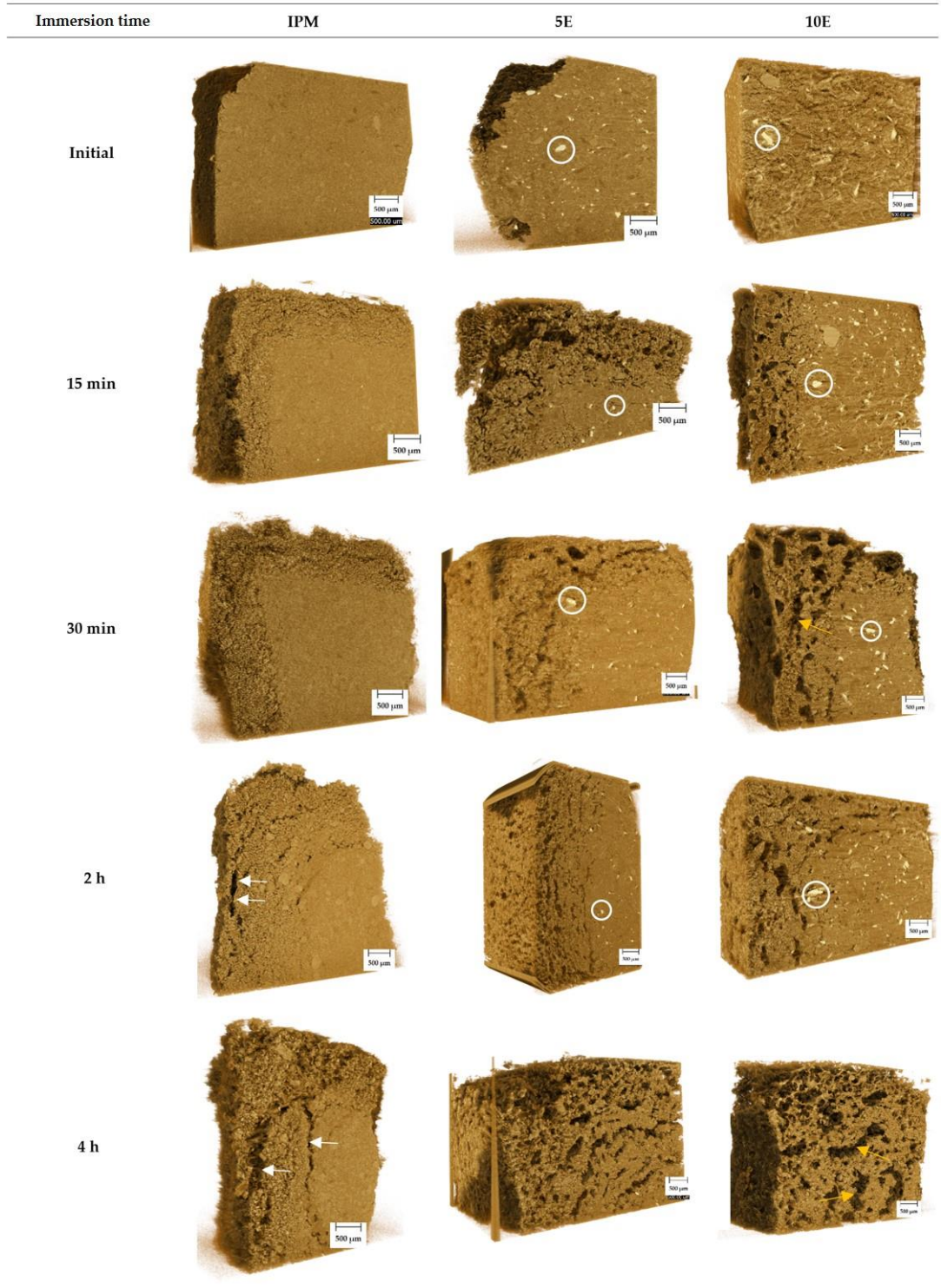

(B)

Figure 36. Surface (A) and cross-sectional (B) reconstructed 3D images of IBU-P407 effervescent matrix tablets in pH-changed media at various immersion times.

The porosity parameter, a crucial feature obtained from SRXTM, was calculated from 600 reconstruction images using Octopus Analysis software. Figure 37 presents the opened, closed, and total porosities for all formulations. In line with the findings of de Terris and colleagues, closed porosities are entirely isolated within a dense material, while opened porosities are pores near the surface that is not completely enclosed [216]. The 10E formulation showed the highest values for opened (57.62%) and total (57.69%) porosities after being immersed in dissolution media for 4 h (Figures 37A and 37C, respectively), while 5E exhibited lower values of 55.42% and 55.52%, respectively (Figure 37B). Therefore, the carbonation reaction facilitated the development of interconnected pores, as indicated in Figure 36B (highlighted by orange arrows), with closed porosities being present in less than 1% of cases. This observation aligns with the study by Hesaraki et al. [217], where they created a macroporous calcium phosphate cement matrix using a mixture of $NaHCO_3$ and CA as effervescent agents. The abundance of effervescent agents led to an increase in total porosity and the formation of interconnected pores in the cement, subsequently altering its physicochemical properties, especially compressive strength. In the case of IPM tablets, closed porosities were more prominent than opened and total porosities due to the dissolution of water-soluble components from the formulation, as previously explained [214]. Therefore, the impact of effervescent agents on the microstructure of matrices was effectively elucidated using imaging techniques, including morphological studies under digital microscopy, SEM, and tomographic analysis with SRXTM investigations. Effervescent agents played a role in promoting interconnected pore structures or opened porosities in the microstructure of matrix tablets, particularly in the surrounding gel layer. Subsequently, they influenced the gel strength of matrices and the drug release behavior of the formulation, as discussed.

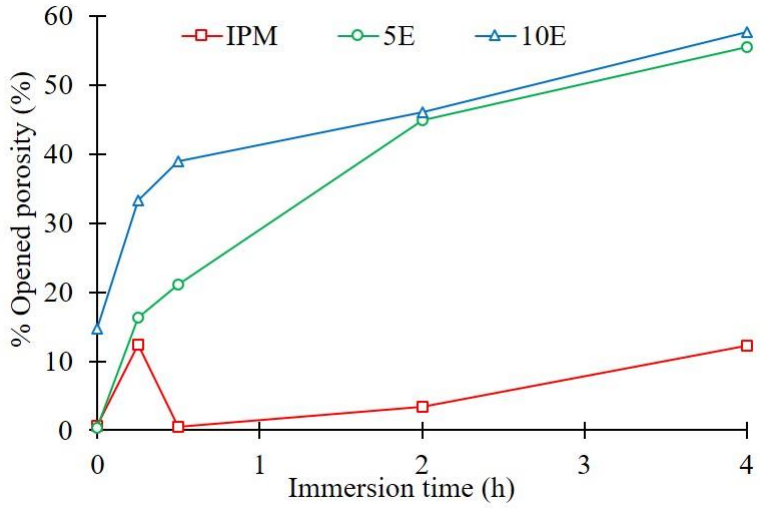

(A)

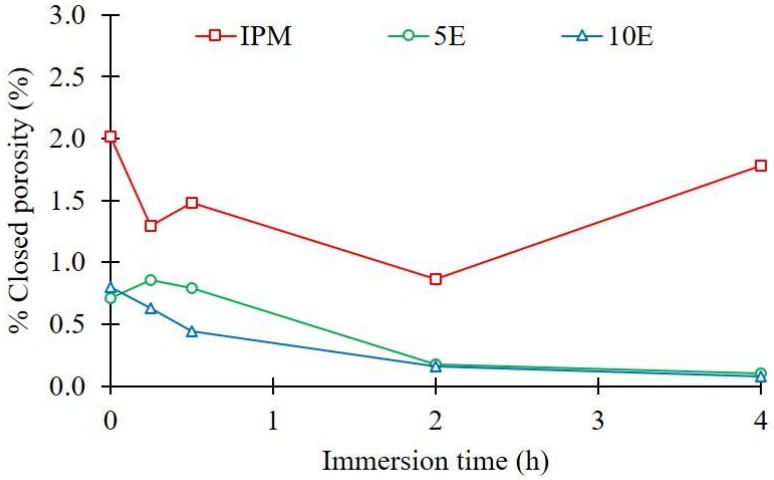

(B)

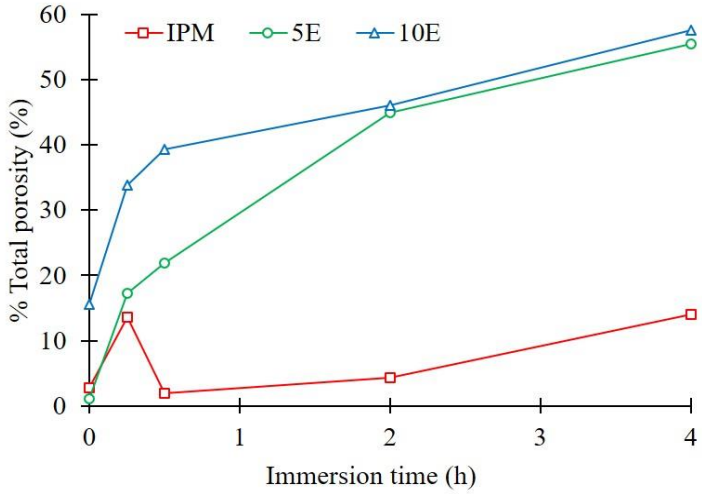

(C)

Figure 37. Opened (A), closed (B) and total porosities (C) of IBU-P407 effervescent tablets in pH-changed media at various immersion time

4.2.1.5 *In vitro* drug release and release kinetics

Figure 38 presents the drug release profiles of effervescent matrix tablets in both pH 1.2 HCl buffer (0.1 N) and pH-shift media. To evaluate the influence of the medium on the drug release behavior of the formulations, cumulative drug dissolution in pH 1.2 HCl buffer (0.1 N) and pH 6.8 phosphate buffer were separately fitted and are depicted in Tables 12 and 13, respectively. The selection of the best model was based on criteria such as the highest and closest value to 1.0 for R^2, the maximum MSC value, and the minimum AIC value [198]. In pH 1.2 HCl buffer (0.1 N), the IPM tablets demonstrated the highest drug release, reaching

6.4% within 1.5 h. The 5E and 10E formulations exhibited drug releases of 3.8% and 2.4%, respectively (Figure 38A). Subsequently, when all formulations were immersed in a medium with a pH of 6.8, the drug release pattern of IPM notably increased to approximately 25% after 2 h and continued to rise steadily, reaching 100% within 12 h. Interestingly, the drug release patterns from 5E and 10E tablets steadily increased, reaching 50.8% and 57.5%, respectively, at 24 h (Figure 38B).

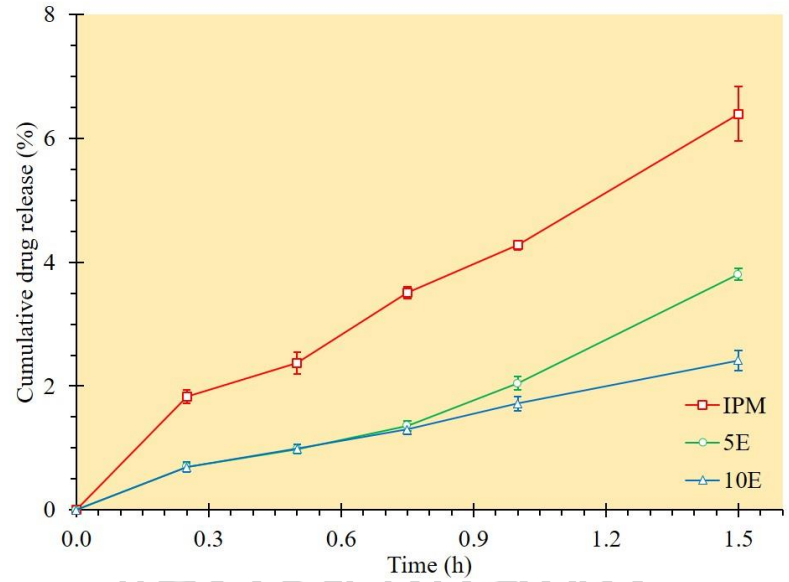

(A)

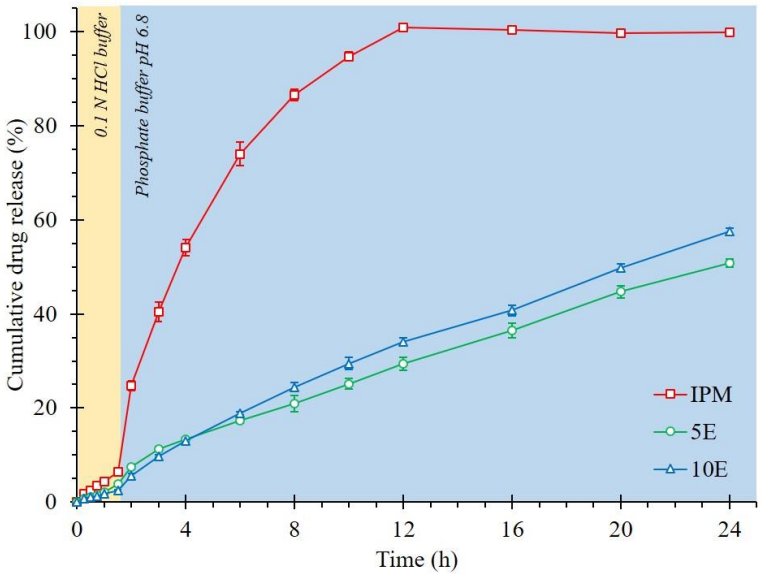

(B)

Figure 38. *In vitro* drug release of IBU-P407 effervescent matrix tablets in pH 1.2 HCl buffer (0.1 N) (A) and pH-changed media (B).

For the mathematical model fitting, the release of IBU from the IPM formulation in both media exhibited a Peppas–Sahlin trend, with an R^2 close to 1.0. The estimation of kinetic parameters using Peppas–Sahlin model fitting indicated the release mechanism, with a higher value comparison between the k_1 and k_2 values. A higher k_1 value suggested that the diffusion process was the primary drug release mechanism, while a higher k_2 indicated that poloxamer relaxation or heterogeneous erosion was the main mechanism [191]. Negative k values were typically observed as one term in the model for compensation to achieve the best fit to the data; however, it should not be included in the interpretation of the release mechanism based on the comparison of k values [191]. IPM tablets exhibited the highest dissolution rate of 2.7052% dissolved drug/h in pH 1.2 HCl buffer (0.1 N), with Fickian diffusion as the predominant drug release mechanism, as indicated by the higher k_1 value shown in Table 12. When the medium pH was increased to 6.8, the positive k_2 value (Table 13) indicated that heterogeneous erosion was the main drug release mechanism, and the dissolution rate dramatically increased to 284.2489% dissolved drug/h [191]. This observation suggested that the medium pH influenced the drug release pattern of IPM tablets due to the solubility of the IBU-P407 eutectic mixture, which depended on the medium pH. This result aligned with the findings of Dugar et al., who developed various ratios of eutectic mixtures between IBU and P407 using the fusion method and observed that the drug release pattern of this eutectic mixture could increase to around 60% within 1 h, reaching 100% in pH 7.2 phosphate buffer within 10 min [20]. For the 5E tablets, cumulative drug release profiles in pH 1.2 HCl buffer (0.1 N) were fitted using the Hopfenberg model with the highest R^2 value of 0.9855. Thus, heterogeneous erosion was the predominant release mechanism of 5E tablets in pH 1.2 HCl buffer (0.1 N). After adjusting the medium pH to 6.8, the Peppas–Sahlin model displayed a strong tendency with an R^2 close to 1.0. Fickian diffusion was the main release mechanism for the drug release pattern of the 5E formulation in pH 6.8 phosphate buffer, as indicated by the higher k1 value in Table 13. Regarding the 10E formulation, drug release patterns in pH 1.2 HCl buffer (0.1 N) and pH 6.8 phosphate buffer showed the best fit with the Peppas–Sahlin model, with R^2 values of 0.9891 and 0.9986, respectively. However, the main release mechanism changed from Fickian diffusion in pH 1.2 HCl buffer (0.1 N) to polymer relaxation in pH 6.8 phosphate buffer. Consequently, the medium pH likely influenced the release mechanism of effervescent matrices but had a minor impact on the amount of drug dissolved in the dissolution medium.

Table 12. Mathematical modeling of IBU release from effervescent matrix tablets in pH 1.2 HCl buffer (0.1 N)

Modeling	Formulation	Parameters			R^2 Adjusted	AIC	MSC
Zero-order	IPM	k_0 = 4.3977			0.9685	0.0607	2.6787
	5E	k_0 = 2.2858			0.9566	-3.8335	2.5255
	10E	k_0 = 1.6920			0.9624	-11.1238	2.5833
First-order	IPM	k_1 = 0.0452			0.9714	-0.5353	2.7781
	5E	k_1 = 0.0232			0.9544	-3.5304	2.4749
	10E	k_1 = 0.0171			0.9640	-11.4244	2.6334
Higuchi's	IPM	k_H = 4.4344			0.9245	5.2908	1.8070
	5E	k_H = 2.2293			0.7662	6.3148	0.8341
	10E	k_H = 1.7110			0.9373	-7.2374	1.9356
Korsmeyer-Peppas	IPM	k_{KP} = 4.4822	n = 0.8128		0.9860	-5.1810	3.5523
	5E	k_{KP} = 2.1939	n = 1.2903		0.9736	-6.1534	2.9121
	10E	k_{KP} = 1.7299	n = 0.7760		0.9892	-20.2020	4.0963
Hixson-Crowell	IPM	k_{HC} = 0.0149			0.9705	-0.3396	2.7454
	5E	k_{HC} = 0.0077			0.9551	-3.6304	2.4916
	10E	k_{HC} = 0.0057			0.9635	-11.3240	2.6167
Hopfenberg	IPM	k_{HB} = 0.0023	n = 93.2625		0.9642	1.4792	2.4423
	5E	**k_{HB} = 0.4191**	**n = 0.0390**		**0.9855**	**-9.8755**	**3.5325**
	10E	k_{HB} = 0.0014	n = 20.3999		0.9548	-9.4031	2.2965
Peppas-Sahlin	**IPM**	**k_1 = 2.7052**	k_2 = 1.7390	m = 0.5990	**0.9862**	**-5.4580**	**3.5985**
	5E	k_1 = 1.2791	k_2 = 0.8772	m = 0.9303	0.9752	-6.3063	2.9376
	10E	**k_1 = 1.1047**	k_2 = 0.6117	m = 0.5863	**0.9891**	**-20.2437**	**4.1033**

Remark: The significance of bold indicates the estimated parameters from the best-fitted mathematic model.

Table 13. Mathematical modelling of IBU release from effervescent matrix tablets in pH 6.8 phosphate buffer.

Modeling	Formulation	Parameters			R^2 Adjusted	AIC	MSC
Zero-order	IPM	k_0 = 9.8725			0.8070	50.0124	1.3762
	5E	k_0 = 2.2892			0.9509	47.3542	2.8195
	10E	k_0 = 2.5741			0.9692	46.1229	3.2903
First-order	IPM	k_1 = 0.2126			0.9549	59.7612	2.9031
	5E	k_1 = 0.0296			0.9894	31.9786	4.3571
	10E	k_1 = 0.0345			0.9977	19.7189	5.9307
Higuchi's	IPM	k_H = 25.0070			0.7664	76.2141	1.2578
	5E	k_H = 8.8980			0.8997	54.5326	2.1017
	10E	k_H = 9.9457			0.8774	60.0271	1.8998
Korsmeyer-Peppas	IPM	k_{KP} = 14.2673	n = 0.9289		0.9833	14.5716	3.5403
	5E	k_{KP} = 4.3409	n = 0.7735		0.9968	19.1651	5.6385
	10E	k_{KP} = 4.3089	n = 0.8179		0.9960	26.1915	5.2834
Hixson-Crowell	IPM	k_{HC} = 0.0564			0.9846	49.0139	3.9778
	5E	k_{HC} = 0.0091			0.9830	36.8165	3.8733
	10E	k_{HC} = 0.0105			0.9960	25.6593	5.3366
Hopfenberg	IPM	k_{HB} = 0.0836	n = 1.8288		0.9957	36.9415	5.1851
	5E	k_{HB} = 0.0001	n = 828.0660		0.9880	33.9938	4.1556
	10E	k_{HB} = 0.0027	n = 22.3850		0.9977	20.8258	5.8200
Peppas-Sahlin	**IPM**	k_1 = -282.7329	**k_2 = 284.2489**	m = 0.1229	**0.9990**	**-2.8625**	**7.8988**
	5E	**k_1 = 3.3267**	k_2 = 1.5962	m = 0.5233	**0.9976**	**17.8431**	**5.7707**
	10E	k_1 = -12.5306	**k_2 = 14.2621**	m = 0.2888	**0.9986**	**15.9478**	**6.3078**

When comparing with IPM tablets, the presence of effervescent agents in 5E and 10E tablets promotes the carbonation reaction at the initial stage of immersion in the acidic medium. This reaction generates CO2 gases, fostering porosity in the surrounding gel layer and on the tablet surface. The heightened porosity leads to increased water ingress into the tablet, facilitating the rapid formation of the surrounding gel layer and impeding drug release from matrices containing effervescent agents. This observation elucidates how 5E and 10E formulations can delay and regulate drug release from effervescent matrices. In contrast to effervescent matrices in pH 1.2 HCl buffer (0.1 N), the higher concentration of effervescent agents in the 10E formulation supports the creation of highly porous structures. This phenomenon accelerates the water penetration rate, resulting in a rapid hydration and swelling rate of HPMC K15M, the gel-forming agent, followed by the swift formation of a gel layer that acts as a barrier to drug release. This result characterizes the diffusion process as the primary release mechanism of 10E in pH 1.2 HCl buffer (0.1 N) [56, 218, 219]. On the other hand, the lower concentration of effervescent agents in the 5E formulation implies that the rate of gel layer formation is slower than the rate of the carbonation reaction of effervescent agents, leading to more pronounced surface erosion. Consequently, heterogeneous erosion becomes the predominant release mechanism of 5E in pH 1.2 HCl buffer (0.1 N). As a sufficiently strong gel layer forms in the pH 6.8 phosphate buffer with progressing immersion time, the amount of drug released from the effervescent matrices decreases based on the rate of drug diffusion, gel layer disruption, and system erosion [220, 221]. This transition makes the diffusion process the primary release mechanism of 5E in pH 6.8 phosphate buffer. Throughout the drug release process, the erosion front occurs at the external interface between the surrounding medium and effervescent matrices [219]. Due to the higher porosity of the gel layer in 10E, the surface area significantly increases compared to that of the 5E formulation [206], leading to enhanced surface erosion. Therefore, polymer relaxation emerges as the predominant release mechanism of 10E in pH 6.8 phosphate buffer.

In comparison with the study of Xu et al. [222], who formulated extended-release tacrolimus matrix tablets using HPMC as a matrix-forming agent, involved the incorporation of tacrolimus into a solid dispersion with Compritol® ATO888 and Pluronic F127. The drug release data demonstrated a good fit to the Kosmeyer–Peppas model with an n value of 0.85, indicating an anomalous transport mechanism for tacrolimus release. This mechanism combined both diffusion and erosion-controlled release, aligning with the observed matrix erosion and swelling behavior of the formulation [222]. Furthermore, the composition of matrix materials, including the type and content of HPMCs and the preparation methods, can be pivotal in tailoring the drug release pattern. Viridén and colleagues explored the impact of the chemical heterogeneity of HPMC on the release of model drug

substances from hydrophilic matrix tablets. Notably, the interaction between the hydrophobic segment of HPMC and butylparaben altered the hydration and fragility of the gel, making it more susceptible to erosional stresses [223]. This discovery highlights the potential variability in drug release based on the substituent heterogeneity of the utilized HPMC. Additionally, the solubility of additives in the HPMC matrix tablet can influence the drug release mechanism, as demonstrated by a novel NMR microimaging method [224]. The rate of solvent transport into the tablet, influenced by the solubility of the additive, affects the release mechanism of matrix tablets [224]. In this study, the incorporation of effervescent agents modified the drug release pattern of the matrix tablets. The morphological and topological changes in the gel layer microstructures, observed through digital microscopy, SEM, and SRXTM, elucidate the alteration in drug release patterns and gel strength of effervescent matrices, as discussed earlier. Consequently, the combination of mechanical and imaging characterization serves as alternative methods to explore the temporal changes in tablet microstructure and clarify drug release mechanisms. Moreover, these combined techniques could be applied to investigate the microstructure and drug release mechanism of various dosage forms, such as polymer membranes for wound healing [225], hydrogels for tissue engineering applications [226] and carbohydrate-based hydrogel for substitute as articular cartilages [227].

4.2.1.6 Summary

Effervescent matrix tablets were successfully fabricated by melt granulation using a circulating water bath at 70 °C. The IBU-P407 eutectic mixture, acting as a meltable binder, facilitated particle agglomeration into granules, which were subsequently compressed into tablets using a hydraulic press. The hygroscopic nature of effervescent agents had a notable impact on the physical properties of matrix tablets, particularly on tablet hardness. In media with varying pH levels, the presence of high concentrations of effervescent agents led to a swift carbonation reaction upon tablet immersion. This reaction resulted in the formation of a gel layer with low strength, as determined by a texture analyser. This outcome was corroborated by surface roughness and porosity observed under digital microscopy, along with the detection of a microporous structure within the gel layer through SEM. It is essential to note that, from certain perspectives, there might not be a direct correlation between the mechanical attributes in the hydrated state and the imaging characterization in the dried state. Moreover, SRXTM was employed to scrutinize the microstructure and porosity of the tablets. The reconstructed 3D images revealed interconnected pores of various sizes resulting from the effervescent-induced carbonation reaction, forming a microporous network indicative of the presence of a gel layer on the tablet surface. Significantly, CO_2 gases generated during the carbonation reaction of effervescent agents played

a crucial role in augmenting opened or interconnected porosities. These porosities, in turn, influenced the strength of the gel layer microstructure, as well as the drug release patterns and release mechanism of the effervescent matrix tablet. Consequently, the integration of mechanical characterisation and imaging techniques provides novel insights into the impact of effervescent agents on the microstructure of the gel layer. This understanding contributes to elucidating the relationship with drug release patterns and release mechanisms in matrix tablets. Furthermore, exploring the application of these combined techniques in diverse dosage forms such as polymer membranes and hydrogels presents an intriguing avenue for future research.

4.2.2 Real-time characterization of effervescent matrix tablets using UV-imaging technique

4.2.2.1 Dissolution imaging of IBU tablet, eutectic tablet and effervescent matrices in phosphate buffer pH 6.8

4.2.2.1.1 Swelling and erosion behavior of tablets

Figure 39A illustrates Vis images recorded at 520 nm during the release studies conducted on IBU tablets, eutectic tablets and effervescent matrices in phosphate buffer pH 6.8. The changes in tablet diameter over time is shown in Figure 39B. The diameter of the IBU tablets slightly decreased ~ 5% over time. Additionally, a roughened (orange-peel) surface was noticed after the release studies, which aligns with previous findings regarding surface erosion of IBU tablets during dissolution in neutral and alkaline pH dissolution fluids [228]. Regarding the eutectic tablet, composed of an IBU-P407 eutectic mixture and MCC PH101, the tablet initially experienced a 6-7% increase in diameter within the first hour (Figure 39B). However, after 3 h of exposure to phosphate buffer (pH 6.8), the tablet's diameter gradually decreased, ultimately sliding off a metal wire at 6 h (Figure 39A). This behavior can be attributed to the special characteristics of the eutectic mixture, which include enhanced wettability and solubility. These characteristics facilitate medium penetration into the eutectic tablets and subsequent swelling due to the gel-forming capability of P407 upon contact with the medium [29, 206].

This aligns with our prior studies using digital microscopy to investigate morphology, which found that the size of the eutectic tablets decreased over time in phosphate buffer (pH 6.8) [229]. In contrast, the effervescent matrix tablets exhibited significant increases in diameter during drug release, especially the 10E10HP tablets, which rapidly expanded by 30% within the first hour. Subsequently, the diameter

continued to increase, reaching approximately 40% at 5.5 h before experiencing a slight decrease due to the release of particles from the swollen tablet, as shown in Figure 39A. The 10E20HP tablets displayed similar patterns but with a smaller change, reaching a maximum diameter increase of about 23% (Figure 39B). The tablets comprising 10% (w/w) effervescent agents exhibited an irregular matrix shape (Figure 39A), leading to higher standard deviation (S.D.) values in their diameter change profiles (Figure 39B). In contrast, tablets containing 5% (w/w) of effervescent agents showed no significant difference in diameter change or tablet shape when compared to those with 10% (w/w) and 20% (w/w) of HPMC (Figure 39A). These tablets gradually increased in size by approximately 25% over 6 h dissolution experiment (Figure 39B). Therefore, effervescent agents indeed influenced tablet behavior in phosphate buffer (pH 6.8), promoting either swelling or erosion.

In Figure 40, further insights into the behavior of IBU tablets, eutectic tablets, and effervescent matrix tablets in 0.1 M phosphate buffer (pH 6.8) are presented. Unlike eutectic tablets and effervescent matrix tablets, IBU tablets did not display a multilayer structure. Additionally, particles were observed escaping from the surface of IBU tablets (indicated by the yellow arrow), suggesting a surface erosion-based drug release profile, which is consistent with findings by Xiong et al. (2023) [228]. In the early stages of testing (15 min), finger-like structures were evident in the eutectic tablets, marked by a black arrow, confirming water penetration into the formulation, as previously mentioned [116]. The tablets gradually expanded while the finger-like structures disappeared. Moreover, particle dissipation was observed from the swollen eutectic tablet (indicated by red arrows) due to its weak mechanical strength and high solubility in the aqueous medium of P407 gel, as reported by Fakhari et al. (2017) [207]. During swelling, the eutectic tablets experienced the packing and entanglements of P407 micelles. In higher concentrations of P407, such as the 30% (w/w) used in this study, the spherical P407 micelles could transform into rod-like micelles packed in a hexagonal system, decreasing micellar interaction as the temperature increases, especially at body temperature (~37 ºC).

As a result, the gelation of P407 promoted lower mechanical strength in the tablet and accelerated drug dissolution, as observed by He et al. (2008) [230]. When compared to eutectic tablets, effervescent matrix tablets displayed more pronounced finger-like structures (indicated by black arrows at 15 minutes in Figure 40). Moreover, numerous void spaces were present in the gel layer on the surface of effervescent matrix

tablets (marked by white arrows), likely caused by the release of CO_2 gas bubbles upon contact between effervescent agents and the aqueous medium. Gel layer structures became apparent in HPMC matrix tablets containing 5% (w/w) effervescent agents after 1 h due to water ingress. However, different results were observed for HPMC matrix tablets containing 10% (w/w) of effervescent agents. After 1 h in phosphate buffer (pH 6.8), irregularly shaped tablets emerged, which became more pronounced at 2 h. Some particles escaped from the swollen tablets, possibly due to the release of CO_2, promoting the disintegration of swollen matrices. Detailed insights into the role of effervescent agents in swelling and erosion behaviors of effervescent matrices were provided by Vis images captured at 520 nm. The liberation of CO_2 gas facilitated water penetration, leading to increased gel layer formation and tablet swelling.

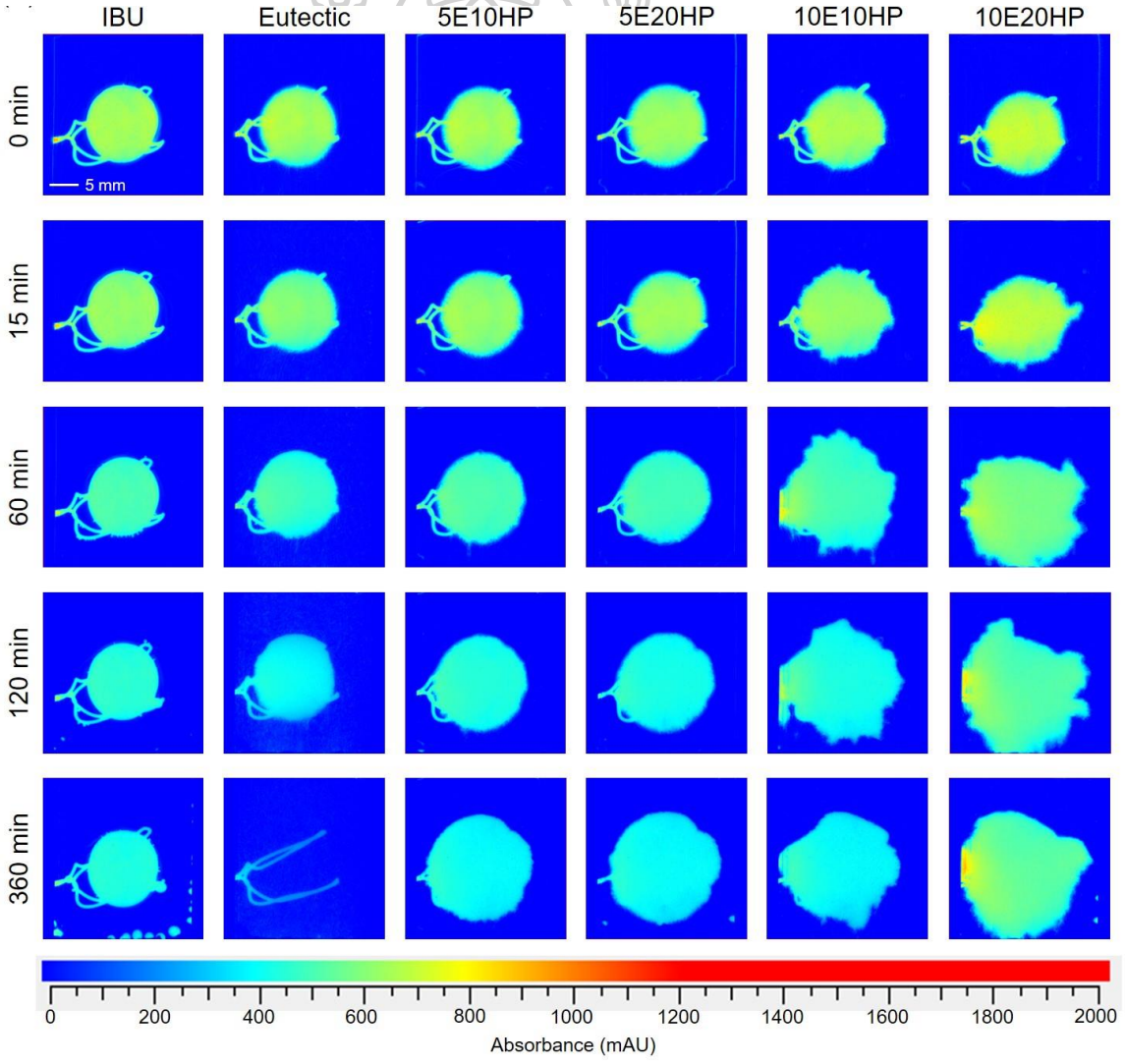

(A)

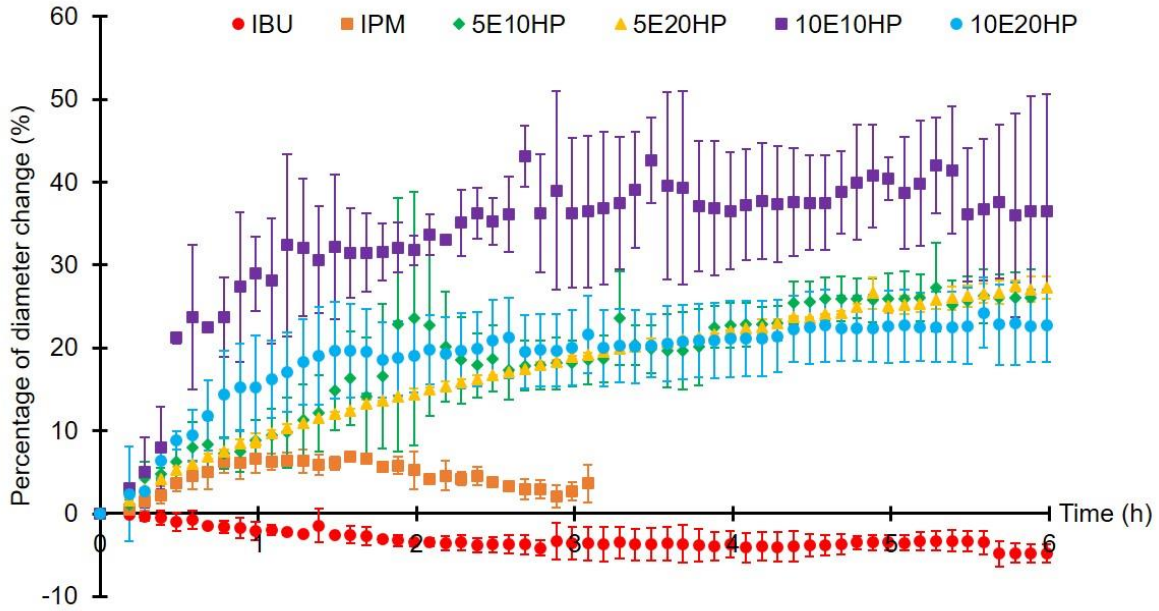

(B)

Figure 39. Vis images (A) and diameter change profiles (B) of IBU tablets, eutectic tablets and effervescent matrix tablets in 0.1 M phosphate buffer, pH 6.8 obtained by imaging at 520 nm (n=3). Imaging area: 28 × 24 mm^2. Intense red color indicates high absorbance.

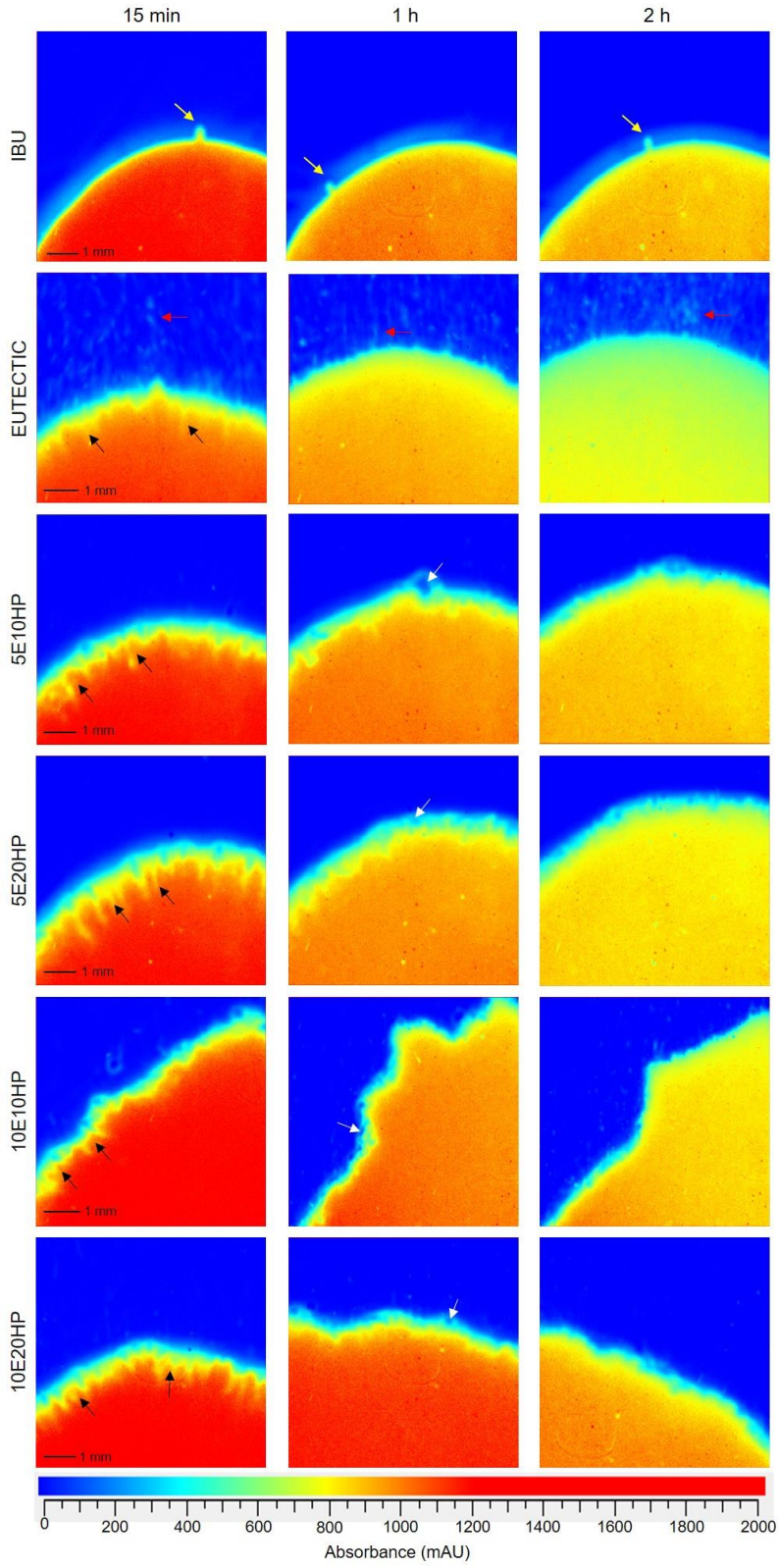

Figure 40. Enlarged Vis images of IBU tablet, eutectic tablet and effervescent matrix tables in 0.1 M phosphate buffer pH 6.8 at different time points obtained by imaging at 520 nm. Intense red color indicates high absorbance.

4.2.2.1.2 The release of ibuprofen from tablets in phosphate buffer pH 6.8

UV images of IBU tablets, eutectic tablets and effervescent matrix tablets during IBU liberation in 0.1 M phosphate buffer, pH 6.8, at 255 nm are shown in Figure 41A. The drug release is visually evident from the UV images, as indicated by increased absorbance (false coloration) in the vicinity of the tablets. Intense red color signifies high UV absorbance, indicating a substantial release of IBU from the tablets. Both IBU tablets and eutectic tablets exhibited a high release of IBU after 15 min in phosphate buffer (pH 6.8). The absorbance observed around both types of tablets remained in the range of 400-600 mAU throughout the drug release study, suggesting that IBU release occurred primarily through surface erosion. However, there was an uneven release pattern in the case of IBU tablets, whereas eutectic tablets demonstrated a more consistent release pattern.

Furthermore, after 6 h in phosphate buffer at pH 6.8 for eutectic tablets, the observed absorbance exceeded 800 mAU, which was above the range defined by the calibration curve (see Figure 64 in the Appendix II). This was likely due to a combination of IBU dissolution and the release of MCC particles from the tablet (indicated by the red arrow in Figure 40), which obscured the UV light from reaching the detector, resulting in an increase in absorbance. As a solution, the apparent absorbance of these particles was determined and defined as the solid particle threshold, which should not exceed 600 mAU. This threshold was used to ignore absorbance values above it during data processing. It is important to note that this could potentially introduce errors in quantitative analysis.

The release of IBU from HPMC matrix tablets containing 5% (w/w) effervescent agents, namely the 5E10HP and 5E20HP tablets, was found to be comparable. In comparison to eutectic tablets, the absorbance surrounding 5E10HP and 5E20HP tablets was lower, typically ranging between 100-200 mAU. This difference was attributed to the swelling and gelation of HPMC, which slowed down the release of IBU from the matrix tablets. For HPMC matrix tablets containing 10% (w/w) effervescent agents, 10E10HP tablets exhibited higher absorbance (~400-500 mAU) around the tablets at 1 and 2 h, while the drug release profile of the 10E20HP tablets resembled that of HPMC matrix tablets containing 5% (w/w) effervescent agents. This variation can be attributed to the presence of void spaces or porosities in the gel layer on the tablet surface and the release of particles, as observed in Figure 40. Cumulative IBU release

profiles and release rates of IBU over time are shown in Figures 41B and 41C, respectively. Among all the tablets, 10E10HP tablets displayed the highest absorbance value of approximately 530 mAU after first hour release experiment in phosphate buffer at pH 6.8. This value fell within the range of the calibration curve, allowing measurements up to 650 mAU (as shown in Figure 64 in the supplementary data). The cumulative amount of dissolved IBU for the IBU tablets was measured at 23.3 ± 1.2 mg, while the eutectic tablets showed a slightly higher value of 24.2 ± 0.6 mg.

The cumulative release profile of ibuprofen was presented as a percentage relative to the formulation dose, which was 1000 mg in IBU tablets and 200 mg in eutectic tablets and effervescent matrix tablets, as shown in Figure 41B. Notably, eutectic tablets exhibited a higher percentage of drug release compared to IBU tablets (Figure 41B). After 1 h in phosphate buffer at pH 6.8, the release rate of IBU from IBU tablets fluctuated between 0.11 ± 0.02 and 0.45 ± 0.05 mg/min (Figure 41C), with the observed drug concentration surrounding the tablets ranging from 0.02 to 0.08 mg/mL. In the case of eutectic tablets, the highest release rate was observed after 6 h in phosphate buffer at pH 6.8, indicated by the highest absorbance across the entire imaging area of the flow cell, as presented in Figure 41A. This can be attributed to the dissipation of MCC particles and dissolved IBU. To quantify only dissolved IBU, a solid particle threshold, as discussed earlier, is necessary. The IBU release rate from eutectic tablets remained in the range of 0.45 ± 0.03 to 0.52 ± 0.03 mg/mL, which was more consistent than that of IBU tablets (Figure 41C).

Consequently, the drug release from eutectic tablets was approximately 1.5 times higher than that from IBU tablets (170.9 ± 3.8 mg for eutectic tablets against 117.3 ± 3.5 mg for IBU tablets). This indicates that using P407 to form a eutectic mixture with IBU in tablets enhanced the release rate and dissolution of IBU compared to pure IBU in phosphate buffer at pH 6.8. Poloxamer has been reported to form eutectic mixtures with hydrophobic drugs, which facilitates the drug dissolution rate by enabling molecular dispersion of the drug within the eutectic mixture [17]. Additionally, eutectic mixtures can enhance wetting through intimate contact between poloxamer and the drug, as suggested by Ahuja et al. (2007) [231] and Dugar et al. (2016) [20]. The release profiles of IBU from effervescent matrix tablets containing 5% (w/w) effervescent agents (5E10HP and 5E20HP) were similar.

The release rate of IBU from both formulations was approximately 0.1 mg/min, resulting in cumulative drug release percentages of 23% for 5E10HP and 20% for 5E20HP (as shown in Figures 41B and 41C). In contrast, 10E10HP exhibited the highest release rate of around 0.9 mg/min at 1 h (Figure 41C) and a rapid release of IBU, going from 9% at 1 h to 30% after 2 h (Figure 41B). Subsequently, the release rate fluctuated, ranging from 0.11 ± 0.02 to 0.64 ± 0.03 mg/min, with the drug release amounting to nearly 60% after 6 h. This pattern was evident from the high absorbance around the tablet at 1 and 2 h, as depicted in Figure 41A. In comparison, 10E20HP tablets exhibited a drug release profile similar to that of HPMC matrix tablets containing 5% (w/w) effervescent agents. However, 10E20HP had a notably higher release rate, as illustrated in Figure 41C. Therefore, the modification of swelling and erosion behaviors by incorporating effervescent agents into HPMC matrix tablets significantly affected the release of IBU, as evidenced by the UV images captured at 255 nm.

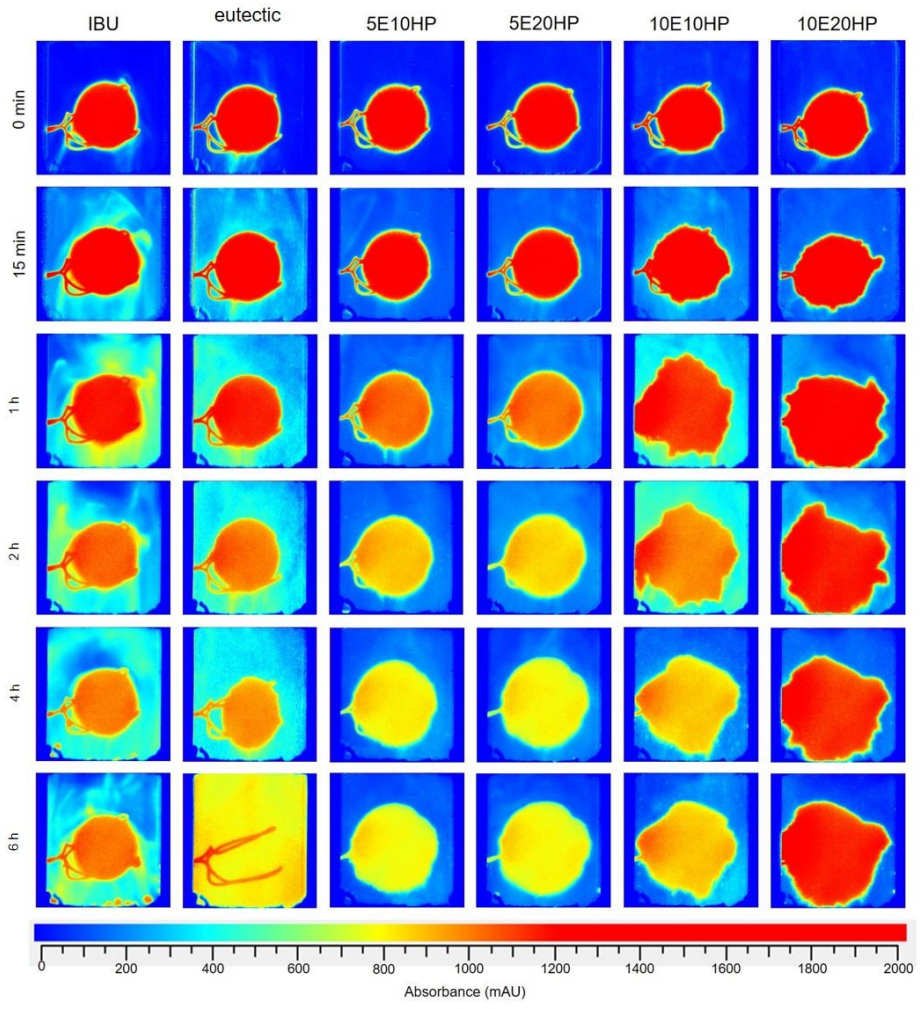

(A)

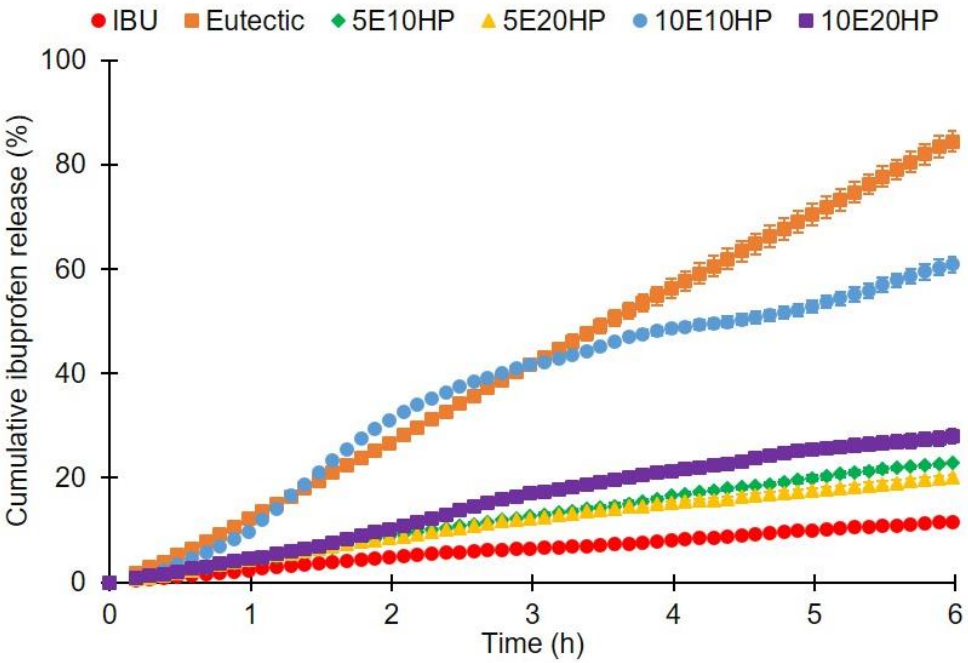

(B)

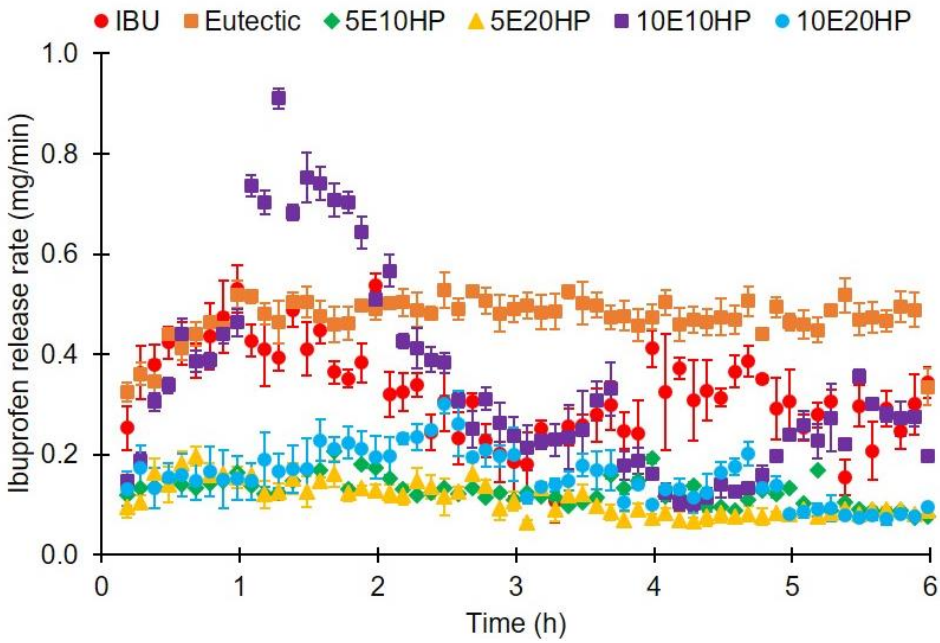

(C)

Figure 41. Representative UV -images (A), cumulative release profile (B) and release rate (C) of IBU from IBU tablets, eutectic tablets and effervescent matrix tablets in 0.1 M phosphate buffer pH, 6.8 obtained by imaging at 255 nm (n=3). Imaging area: 28 × 24 mm^2. Intense red color indicates high absorbance.

4.2.2.2. Dissolution imaging of IBU tablet, eutectic tablet and effervescent matrices in pH shift experiment

4.2.2.2.1 Swelling and erosion behavior of tablets

In this experiment, a shift in pH was introduced to simulate the change in environmental pH by a dosage form travelling from highly acidic in the stomach to the duodenum with a pH ~6 [232]. The dosage form spends approximately 2.8-8.8 h at pH > 6.0 in the small intestines [233]. The tablets were first exposed to 0.1 N HCl buffer, pH 1.2, for 1.5 h to simulate acidic stomach conditions. Afterwards, they were exposed to 0.1 M phosphate buffer pH 6.8 for 6 h to simulate the transit through the duodenum and upper small intestine. Figure 42A illustrates Vis images of test samples recorded at 520 nm during the pH shift experiment. IBU tablets exhibited a slight expansion of tablet size after 1 h in HCl buffer. This observation was surprising and there has not been reported previously. After switching the medium to phosphate buffer, pH 6.8, the diameter of IBU tablets gradually decreased. This might be described by the pH-dependent solubility of IBU [234]. IBU is more soluble in phosphate buffer pH 7.4 than in phosphate buffer pH 5.4 or deionized water [235]. Hence, water penetration caused IBU tablets to expand in HCl buffer, while surface erosion in phosphate buffer (pH 6.8) led to a reduction in tablet size. These observations were further confirmed by changes in tablet diameter over time, as shown in Figure 42B. The diameter of IBU tablets increased, reaching 2.7 ± 4.4% at 1.5 h in HCl buffer and then slightly decreased to -3.81 ± 3.13% after completing the pH shift experiment. Additionally, the escape of IBU particles observed in phosphate buffer at pH 6.8 (at 2 h and 6 h, marked by yellow arrows in Figure 43) confirmed this tablet erosion. Eutectic tablets exhibited behavior similar to that of IBU tablets but with a greater tablet expansion of 5.9 ± 0.1% after 1.5 h in HCl buffer (Figure 42B). Subsequently, the tablet diameter gradually decreased, eventually becoming soft and slipping out from the sample holder at 6 h, as depicted in Figure 42A. Additionally, an enlarged Vis image at 6 h revealed erosion of the eutectic tablets due to the release of MCC particles (red arrow in Figure 43).

Tablet expansion was also observed in the effervescent matrix tablets containing 5% (w/w) and 10% (w/w) effervescent agents. HPMC matrix tablets containing 10% (w/w) effervescent agents exhibited the highest change, approximately 15%, with a roughened surface observed on swollen tablets after an hour in HCl buffer. An irregular tablet shape was found after switching the medium to phosphate buffer at pH 6.8

(Figure 42A), leading to a high deviation in the diameter change of 10E10HP and 10E20HP tablets (Figure 42B).

In comparison to the tablet behavior in phosphate buffer at pH 6.8 without prior exposure to HCl buffer, 10E10HP tablets displayed the highest swelling, with a diameter change of around 40%. However, in the pH shift experiment, the highest swelling was found in 10E20HP, with a tablet diameter change of approximately 30%. This suggests that the tablet behaviors of effervescent matrix tablets were influenced by the type of dissolution medium. Moreover, finger-like structures also appeared at 15 min in the pH shift experiment for the eutectic tablets and effervescent matrices (indicated by black arrows at 15 min in Figure 43), signifying water penetration into the tablets.

Interestingly, after 15 min in HCl buffer, a more profound water penetration occurred, particularly in 10E10HP tablets (Figure 43), when compared to phosphate buffer at pH 6.8 in Figure 40. The release of carbon dioxide (CO_2) is influenced by the quantity and ratios of organic acids and bicarbonate salts in the mixture of effervescent agents, as well as the acidity of the solution as noted by Zhang and Huang (2013) [236]. CO_2 release is faster in highly acidic solutions (low pH) compared to neutral or basic solutions (high pH). Over time, this deeper water penetration promoted tablet expansion and the formation of a gel layer on the tablet surface.

After the medium was changed to phosphate buffer at pH 6.8, water rapidly penetrated the partially swollen tablets, leading to the swift release of water-soluble particles. As a result, a porous surface with a finger-like structure facilitated the disintegration of particles from the tablet surface (black arrows at 2 h in Figure 43). This finding directly correlated with the decrease in tablet diameter for effervescent matrices during the earlier stages after exposure to phosphate buffer, which gradually enlarged after 2 h of the release study (Figure 42B). Furthermore, the rapid release of water-soluble particles resulted in higher porosity in the gel layer after 2 h of dissolution in the pH shift experiment (white arrows in Figure 43). The porous morphology of dried effervescent matrix tablets, as observed through synchrotron radiation X-ray tomographic microscopy (SRXTM) [229], supports the findings from UV-Vis imaging. The presence of effervescent agents resulted in the formation of interconnected pores or open porosity in the matrix tablets [229]. As a result, the behavior of effervescent matrix tablets was strongly influenced by the type of dissolution medium. In HCl buffer, these tablets exhibited swelling because the effervescent agents facilitated water

penetration into the matrix tablets, whereas the release of water-soluble particles and the development of porosities in the gel layer occurred in phosphate buffer, as observed in the Vis imaging at 520 nm.

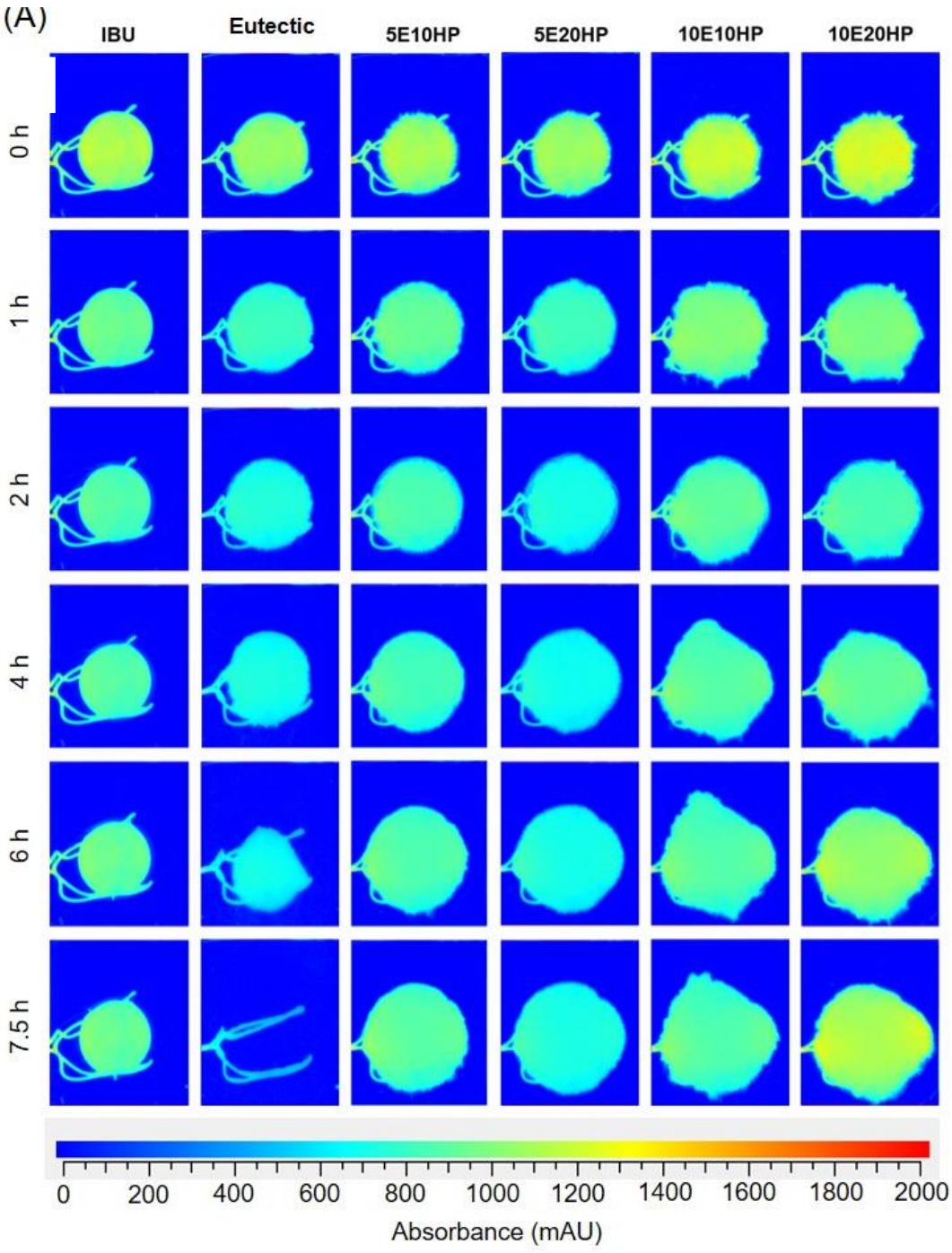

(A)

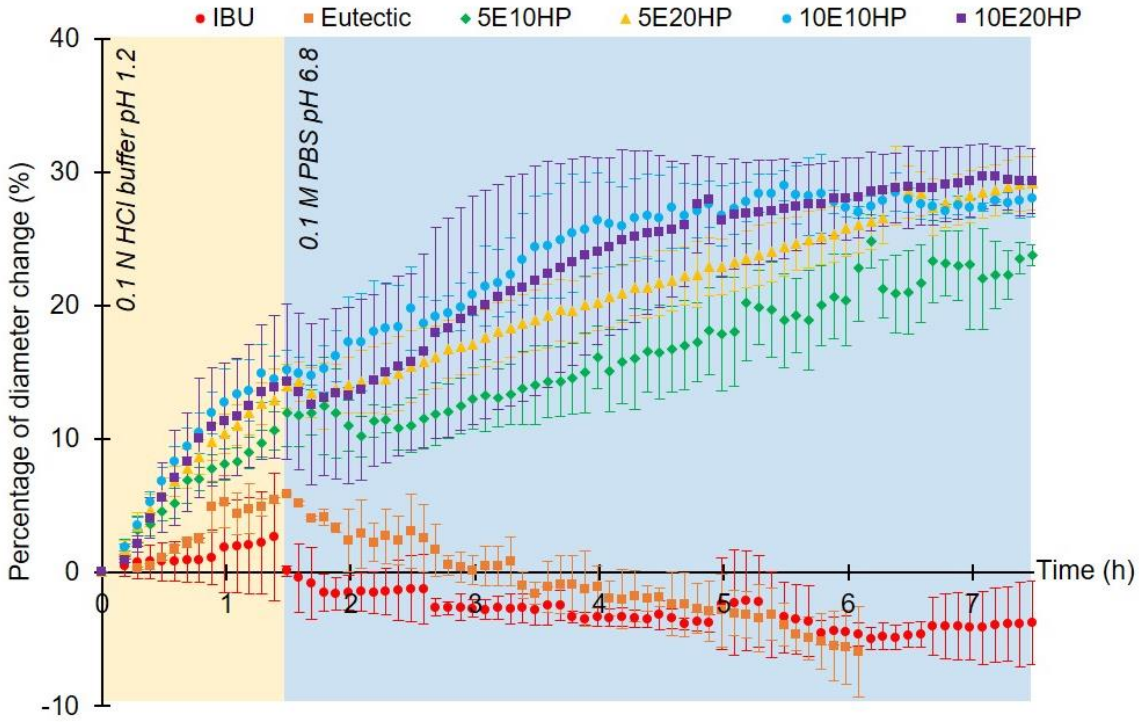

(B)

Figure 42. Vis images (A) and diameter change profiles (B) of IBU tablets, eutectic tablets and effervescent matrix tablets in pH-shift experiment obtained by imaging at 520 nm (n=3). Imaging area: 28 × 24 mm^2. Intense red color indicates high absorbance.

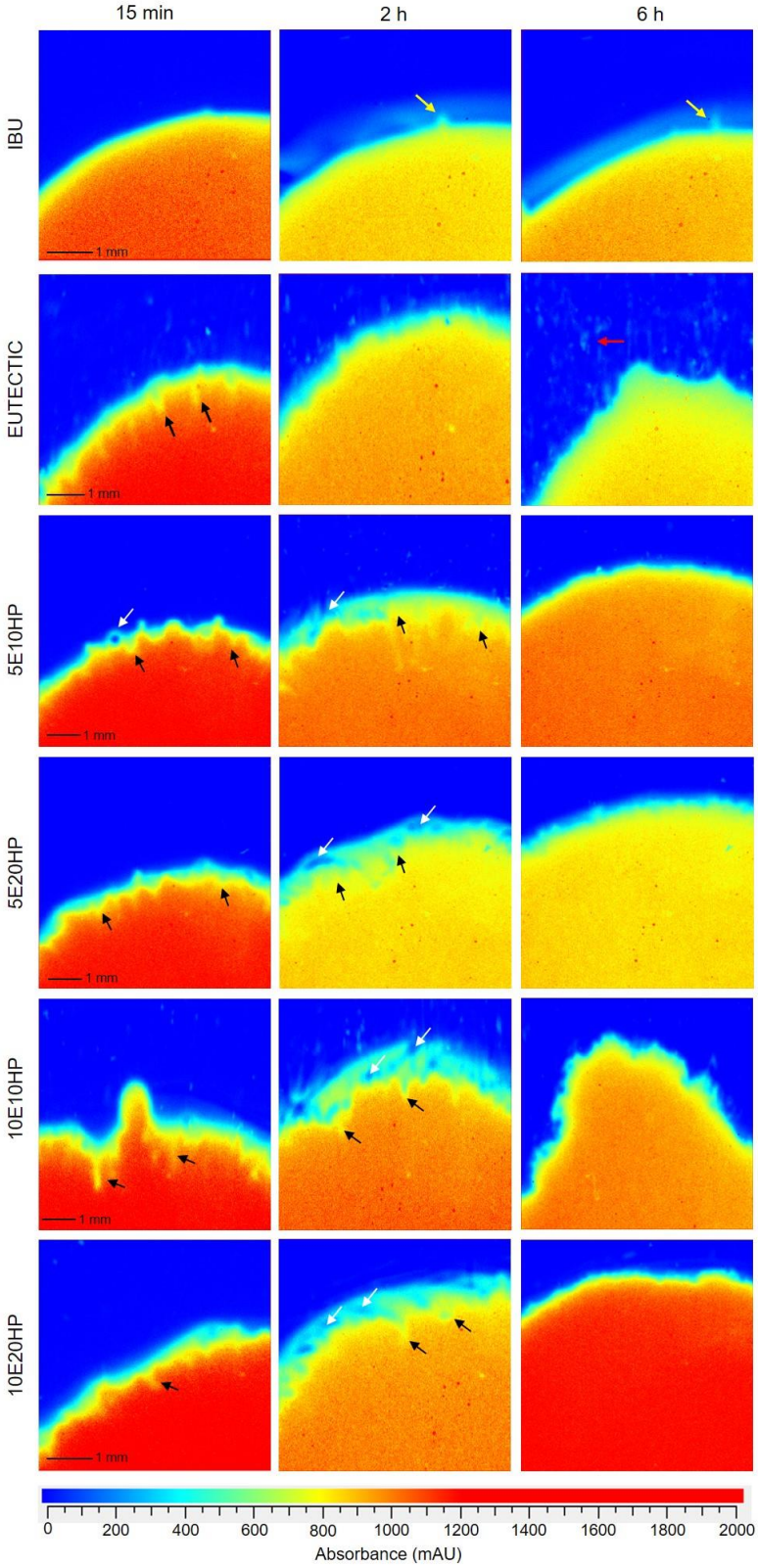

Figure 43. Enlarged Vis images of IBU tablet, eutectic tablet and effervescent matrix tablets in pH-shift experiment at different time points obtained by imaging at 520 nm. Intense red color indicates high absorbance

4.2.2.2.2 The release of ibuprofen from tablets in pH shift experiment

To investigate the impact of effervescent agents on drug release from effervescent matrix tablets during dissolution, particularly in response to a pH change from 1.2 to 6.8, UV images at 255 nm were captured, as presented in Figure 44. After 1 h in HCl buffer, all tablets, except for the eutectic tablet, exhibited extremely low absorbance (approximately 25-40 mAU), which fell within the range of the calibration curve. This suggests limited or negligible IBU releases due to the low solubility of ibuprofen in an acidic environment [234]. Higher absorbance around the eutectic tablets indicated more IBU release. When the medium was switched to phosphate buffer, the absorbance surrounding IBU tablets fluctuated between 200-600 mAU until the completion of the experiment. Eutectic tablets displayed a consistent release pattern, with absorbance in the range of 400-600 mAU. Furthermore, the dissipation of MCC particles occurred around the tablets concurrently with a reduction in the size of the eutectic tablets. Hence, it is important to exclude the apparent absorbance of MCC particles in quantitative analysis, as previously mentioned. For HPMC matrix tablets containing 5% (w/w) effervescent agents (5E10HP and 5E20HP), a lower release of IBU was observed compared to eutectic tablets, primarily due to the swelling and gelation of HPMC, as shown in Figures 42 and 43. In contrast, 10E10HP and 10E20HP tablets exhibited a slightly higher IBU release compared to those with 5% (w/w) effervescent agents incorporated in HPMC matrices. This result differed from the drug release behavior of both types of tablets in phosphate buffer without prior exposure to HCl (Figure 41A), emphasizing that the dissolution medium significantly influenced the drug release from effervescent matrix tablets.

The calculated cumulative drug release and release rates are presented in Figures 45A and 45B, respectively. The limited release of IBU in HCl buffer, as evident in the UV images (Figure 44), was confirmed by cumulative IBU release values of <1% and extremely low release rates of IBU for all tablets, except for the eutectic tablets. The IBU tablet in HCl buffer had a cumulative release value of 0.65 ± 0.21 mg, while the eutectic tablets exhibited a relatively higher value of approximately 5 mg of ibuprofen, representing an increase of approximately 7.6-fold (Figure 45A). The formation of eutectic mixtures and micellar solubilization of the acidic drug using poloxamer P407 can enhance local solubility and dissolution rates in both acidic and neutral media [20].

When the dissolution medium was changed to phosphate buffer, the UV images of the IBU tablet revealed a non-uniform release pattern, characterized by an increase in the cumulative release profile. This profile eventually reached around 76 mg, which corresponds to 7.6% of the initial dose. The release rate promptly increased to approximately ~0.2 mg/min at 30 minutes after the medium was changed (2 h into the release study). Subsequently, the release rate fluctuated between ~0.15-0.25 mg/min with high S.D. values throughout the testing period (Figure 45B).

For eutectic tablets, the cumulative drug release exhibited a gradual increase, reaching approximately 70% after the completion of the experiment, during which the tablet size steadily decreased with particle disintegration (Figure 42). In the case of HPMC matrix tablets containing 5% (w/w) effervescent agents, the release rates were nearly similar, hovering around 0.1 mg/min, and similar drug release profiles were obtained. Considering the tablet behavior observed at 520 nm, the 0.1 N HCl buffer induced tablet swelling for both 5E10HP and 5E20HP (Figures 42 and 43), resulting in a delayed release of IBU. The release rate and IBU release of 10E20HP were comparable to HPMC matrix tablets containing 5% (w/w) effervescent agents, with a slightly elevated release observed at ~16%. The 10E10HP tablets in the pH shift experiment exhibited the highest swelling behavior with irregularly shaped tablets, as evidenced by Vis images (Figure 42). Surprisingly, when first exposed to HCl buffer, it exhibited an even more sustained release, with a cumulative drug release of ~18%, compared to dissolution in phosphate buffer alone, which achieved a drug release of ~60%.

Thus, effervescent agents could promote water penetration into HPMC matrix tablets when exposed to HCl buffer. This was demonstrated by the development of finger-like structures and gel layer structures with high porosities, as shown in Figure 43. The microstructure of effervescent matrix tablets underwent modification due to the release of CO_2 resulting from the effervescent agents upon contact with an acidic buffer. Upon changing the medium to phosphate buffer at pH 6.8, the tablets exhibited a modified gel layer structure and a significant decrease in the drug release rate, resulting in a more prolonged release compared to dissolution in phosphate buffer alone, especially for 10E10HP tablets. Therefore, the inclusion of 5-10% (w/w) effervescent agents within HPMC matrix tablets demonstrated the potential to induce changes in the microstructure of the tablets, thereby influencing their performance and the drug release profile.

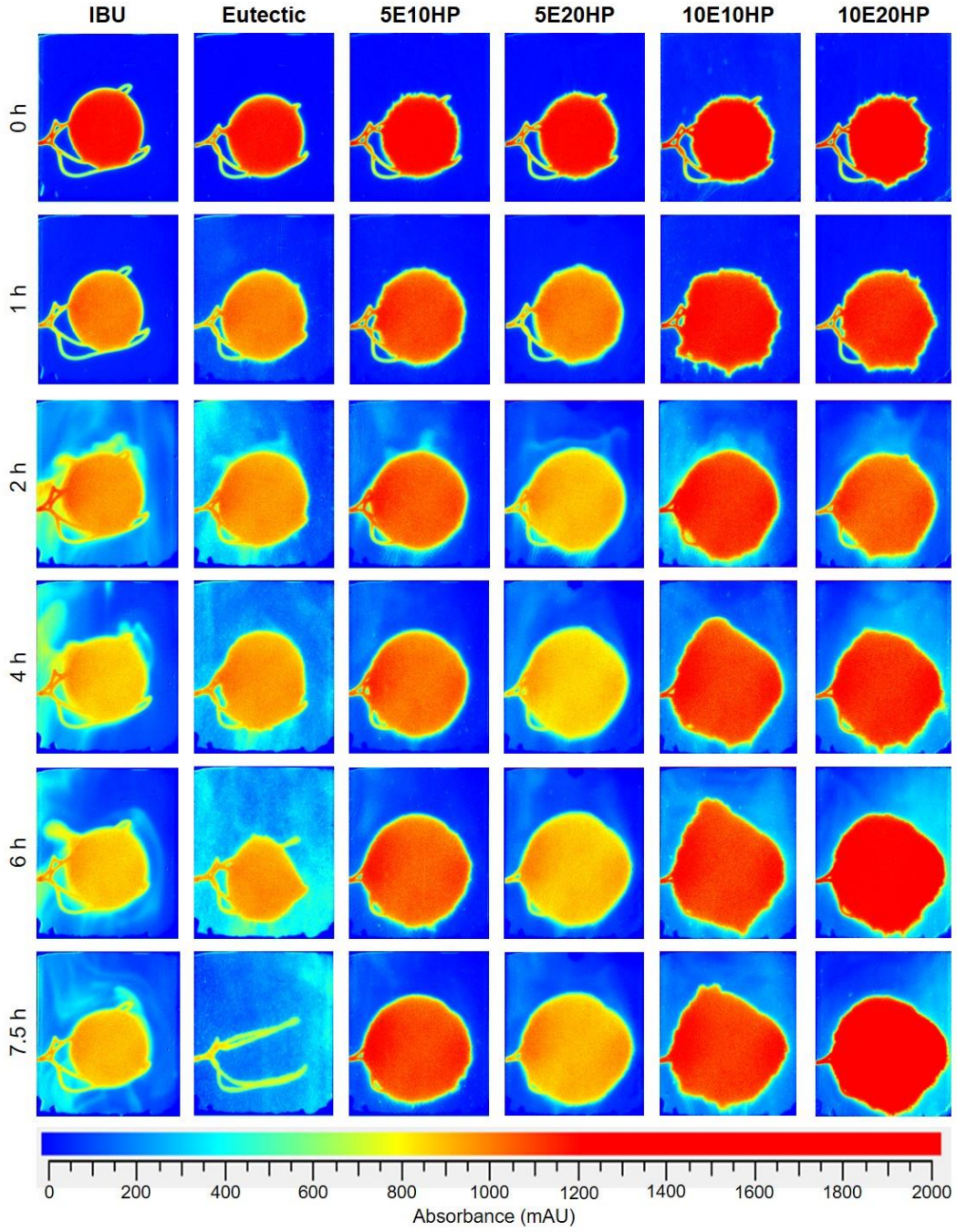

Figure 44. Representative UV imaging during drug release in pH-shift experiment of IBU tablet, eutectic tablet and effervescent matrix tablets at different time points obtained by imaging at 255 nm. Imaging area: 28 × 24 mm^2. Intense red color indicates high absorbance

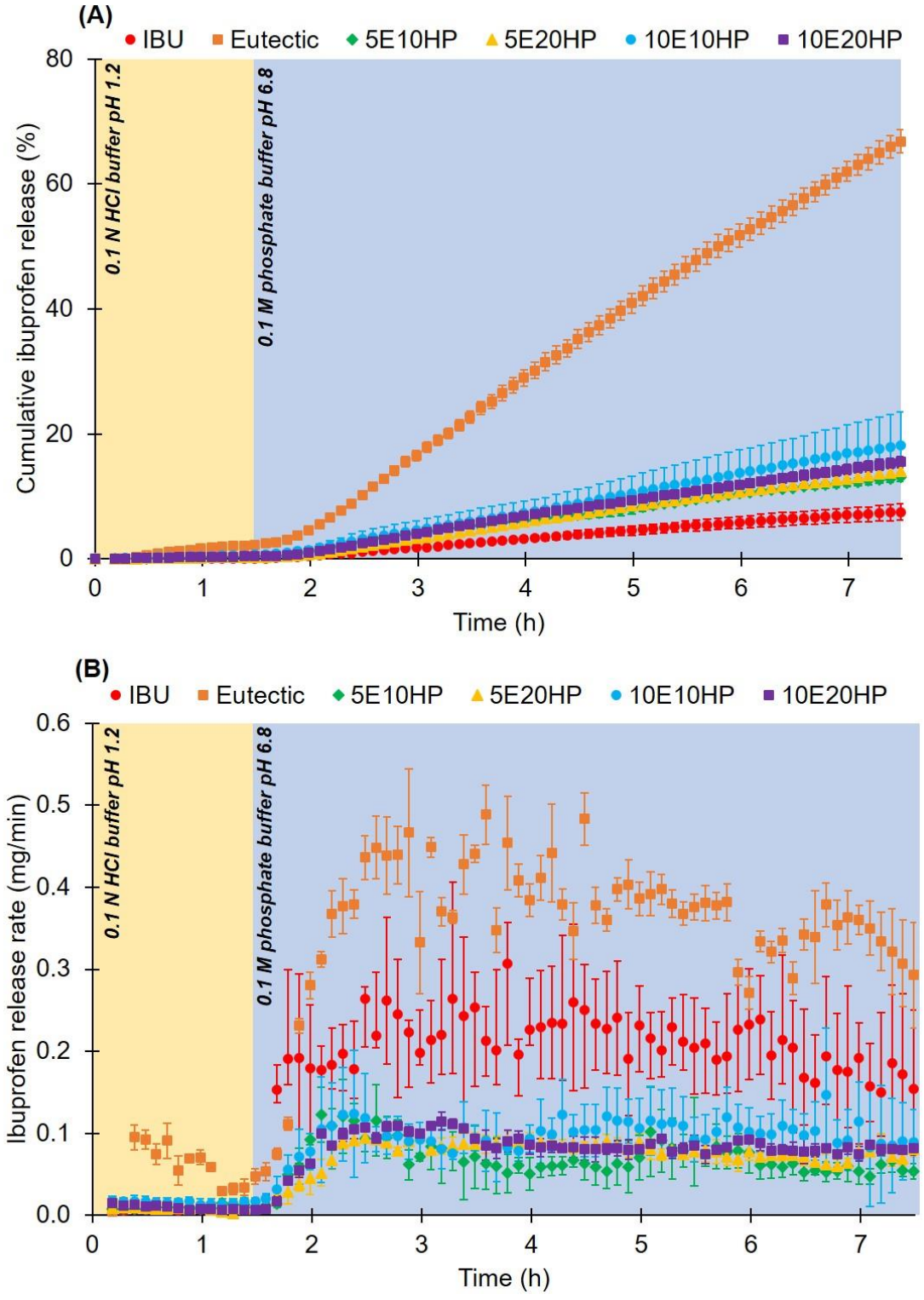

Figure 45. Cumulative release profiles (A) and release rate of IBU from IBU tablets, eutectic tablets and effervescent matrix tablets in pH-shift experiment obtained by imaging at 255 nm (n=3).

4.2.2.3 Summary

A novel UV imaging technique, utilizing the SDi2 system with a USP IV type flow cell, was devised to monitor in real-time the swelling, erosion characteristics, and drug release profiles of effervescent matrix tablets in phosphate buffer at pH 6.8, both with and without prior exposure to HCl buffer at pH 1.2. The behavior of the tablets was observed at 520 nm, and the concentration of dissolved ibuprofen was measured at 255 nm. The images obtained at both wavelengths were analyzed to determine the impact of effervescent agents on tablet behavior and drug release. In phosphate buffer without prior exposure to HCl buffer, the incorporation of 5-10% (w/w) effervescent agents into HPMC matrices promoted water penetration, gel layer formation, and swelling due to CO_2 release upon contact with the medium. This affected the release of ibuprofen from the tablets. However, in phosphate buffer with prior exposure to HCl buffer, HPMC matrix tablets containing effervescent agents exhibited increased water penetration when exposed to HCl buffer, as indicated by the development of finger-like structures and gel layer structures with high porosities. When the medium was changed to phosphate buffer at pH 6.8, the tablets with the modified gel layer structure showed a significant decrease in the drug release rate, resulting in a more prolonged release compared to dissolution in phosphate buffer alone. Therefore, the addition of 5-10% (w/w) effervescent agents within HPMC matrix tablets demonstrated the potential to induce changes in the microstructure of the tablets, thereby influencing their performance and the drug release profile.

4.2.3 Mechanistic characterization of effervescent matrix tablets using numerical techniques based on mathematical modeling of water sorption, erosion and drug release behaviors

4.2.3.1 Water sorption and erosion behaviors of effervescent matrix tablets in 0.1 N HCl buffer and phosphate buffer pH 6.8

Water sorption and erosion behaviors of effervescent matrix tablet in 0.1 N HCl buffer pH 1.2 are illustrated in Figures 46A and 46B. Water content and dry mass loss were determined to represent the water sorption and erosion behaviors of tablet in medium, respectively. After being immersed in HCl buffer for 2 h, water content of eutectic tablets increased rapidly to 0.47 ± 0.06 and remained in the range of 0.50 - 0.52 until the completion of the study. For erosion property, dry mass loss decreased to 0.77 ± 0.02 at 2h and continuously decreased until remained constant at about 0.5 after 6 h. This might be attributed to the special properties of IBU-P407 eutectic mixture, which enhanced wetting and dissolution [86]. Moreover, previous research has shown that the hydrophilicity of P407 can increase water sorption and erosion of matrix tablets. [29, 237]. Upon adding

effervescent agents to HPMC matrix tablets, both tablets containing 5 and 10% (w/w) agents showed increased water uptake compared to eutectic tablets, as demonstrated by the increasing water content in Figure 46A. Matrix tablets containing 10% effervescent agents had a higher water content compared to those containing 5% effervescent agents. Among all the tablets, 10E10HP tablets had the highest water content of approximately 0.8 at 4 h. This suggests that the effervescent agent increased the water uptake of HPMC matrix tablets. In contrast, HPMC tablets containing 5% (w/w) effervescent agents showed different patterns compared to water sorption characteristics. With the exception of 10E10HP, effervescent matrix tablets exhibited a lower erosion rate compared to the eutectic tablets, as indicated by the larger dry mass loss value depicted in Figure 46B. Furthermore, it was observed that the dry mass loss values exhibited a tendency to increase when the concentrations of HPMC in effervescent matrices increased. A higher concentration of HPMC resulted in increased strength to the gel layer that formed upon hydration. This made the gel layer more resistant to erosion [238]. The 10E10HP tablets underwent a significant reduction in dry mass loss. After 2 hours in HCl buffer, it reached a value of 0.56 ± 0.02. This was due to the low HPMC content of the matrix tablets, which cannot be resistant to erosion caused by the release of carbon dioxide (CO_2) when effervescent matrices came in contact with the medium.

Figure 47 illustrates the water sorption and erosion of effervescent matrix tablets in phosphate buffer pH 6.8. In comparison to tablet characteristics in 0.1 N HCl pH 1.2, it was seen that all tablets had increased water sorption and erosion, as demonstrated by higher water content and lower dry mass loss in Figures 46A and 46B, respectively. The water uptake and erosion of eutectic tablets in phosphate buffer pH 6.8 was about twice as high as in HCl buffer. This disparity can be attributed to the pH-dependent solubility of IBU. For effervescent matrix tablets, the incorporation of 5 and 10% (w/w) effervescent agents has been seen to enhance water sorption as well as erosion of tablets when immersed in phosphate buffer. Among all effervescent matrix tablets, 10E10HP tablets exhibited the highest water content, around 1.0, and the lowest dry mass loss, close to 0.0 after being immersed for 12 h. The findings suggest that the presence of effervescent agents has the potential to increase the water uptake and erosion of HPMC matrix tablets in acidic and neutral media. Upon contact with the medium, carbon dioxide (CO_2) was produced and released, causing the surface of the HPMC tablet to become rough and porous. This facilitates water penetration into the tablets, hence facilitating tablet erosion. However, tablet erosion was also influenced by the quantity of HPMC.

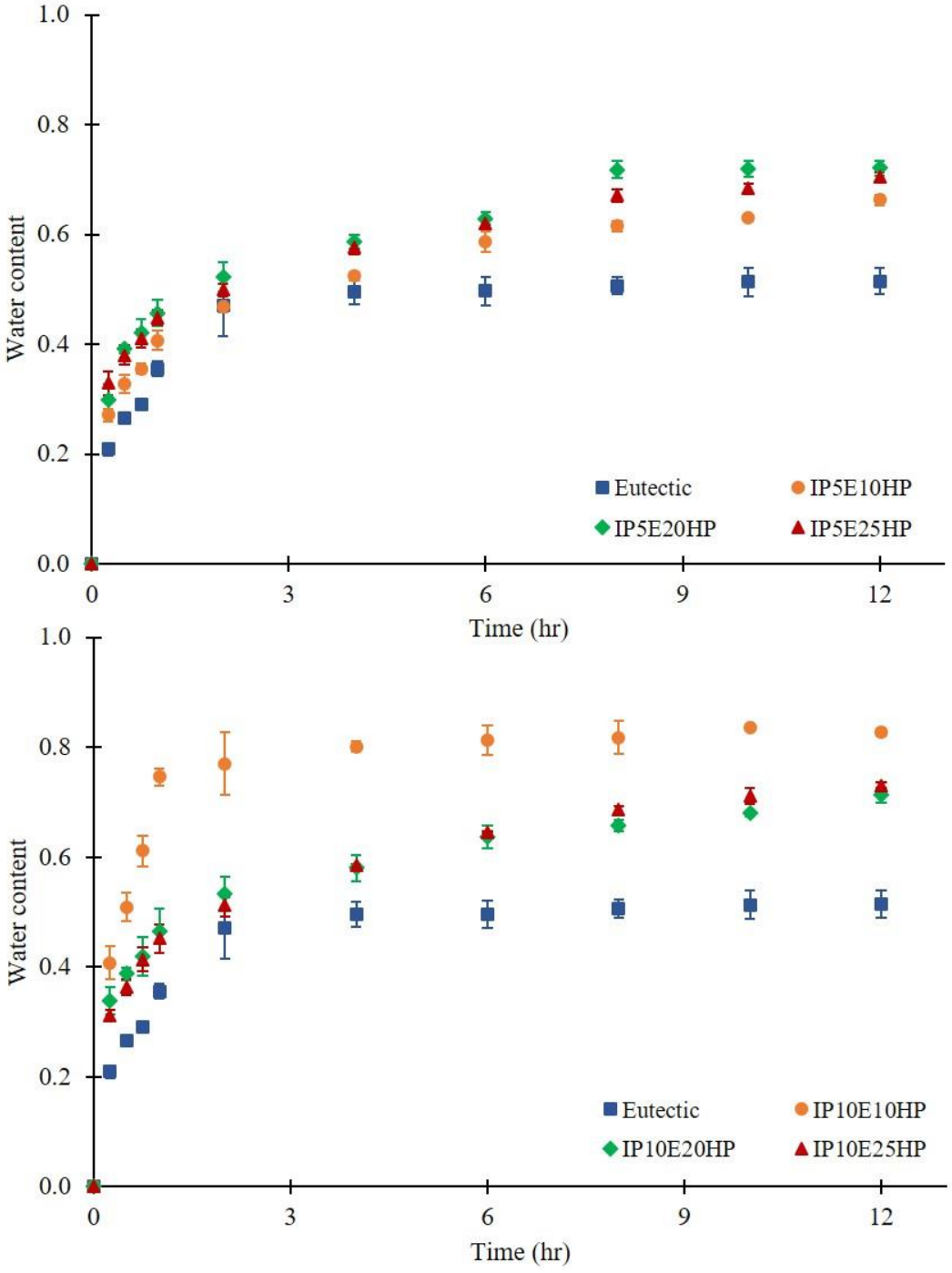
1.0
0.8
0.6
0.4
0.2
0.0
Water content
0
3
6
9
12
Time (hr)
Eutectic
IP5E10HP
IP5E20HP
IP5E25HP
1.0
0.8
0.6
0.4
0.2
0.0
Water content
0
3
6
9
12
Time (hr)
Eutectic
IP10E10HP
IP10E20HP
IP10E25HP

(A)

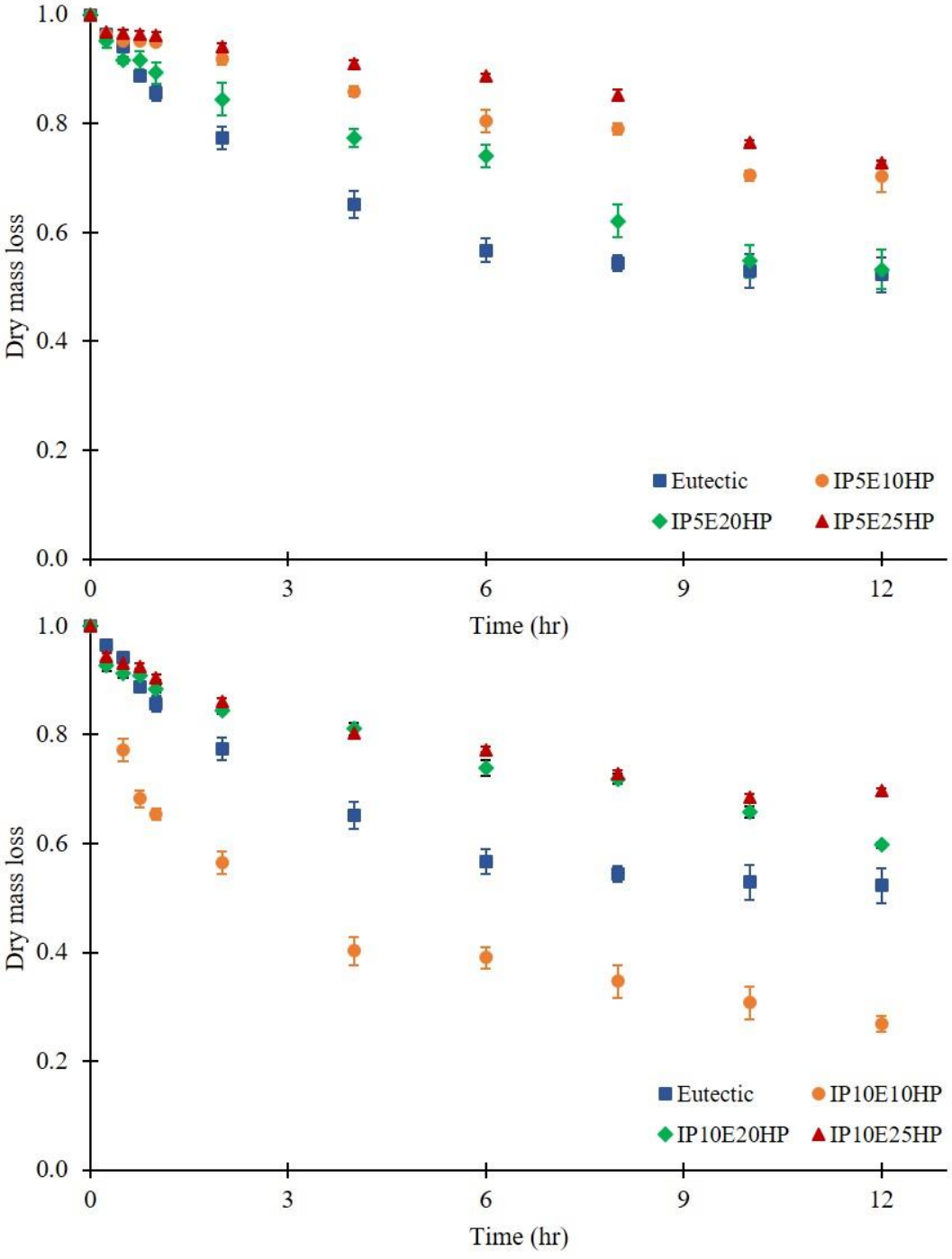

(B)

Figure 46. Water sorption (A) and erosion (B) behaviors of effervescent matrix tablets in 0.1 N HCl buffer pH 1.2

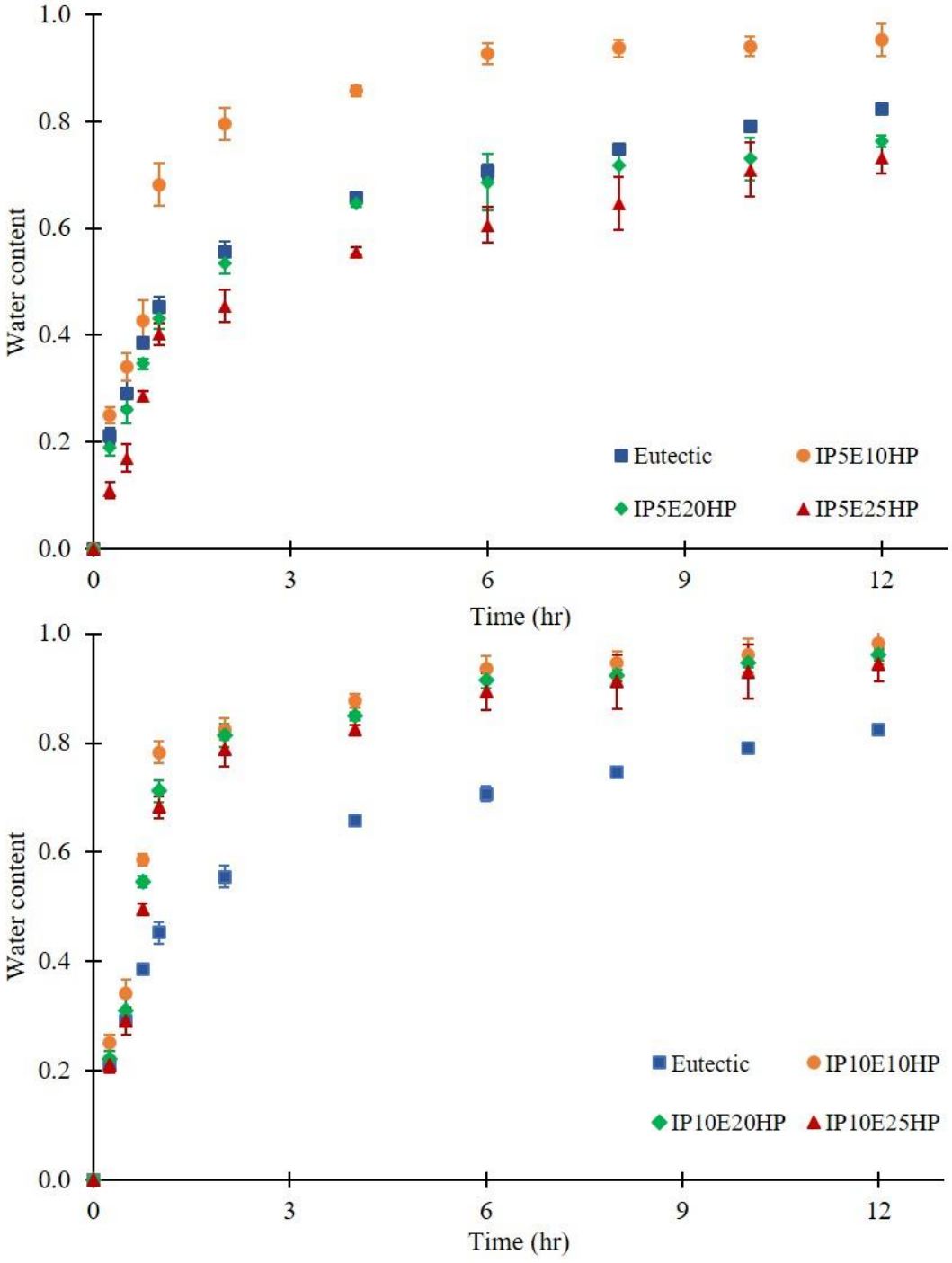
Water content
Time (hr)
Eutectic
IP5E10HP
IP5E20HP
IP5E25HP
Water content
Time (hr)
Eutectic
IP10E10HP
IP10E20HP
IP10E25HP

(A)

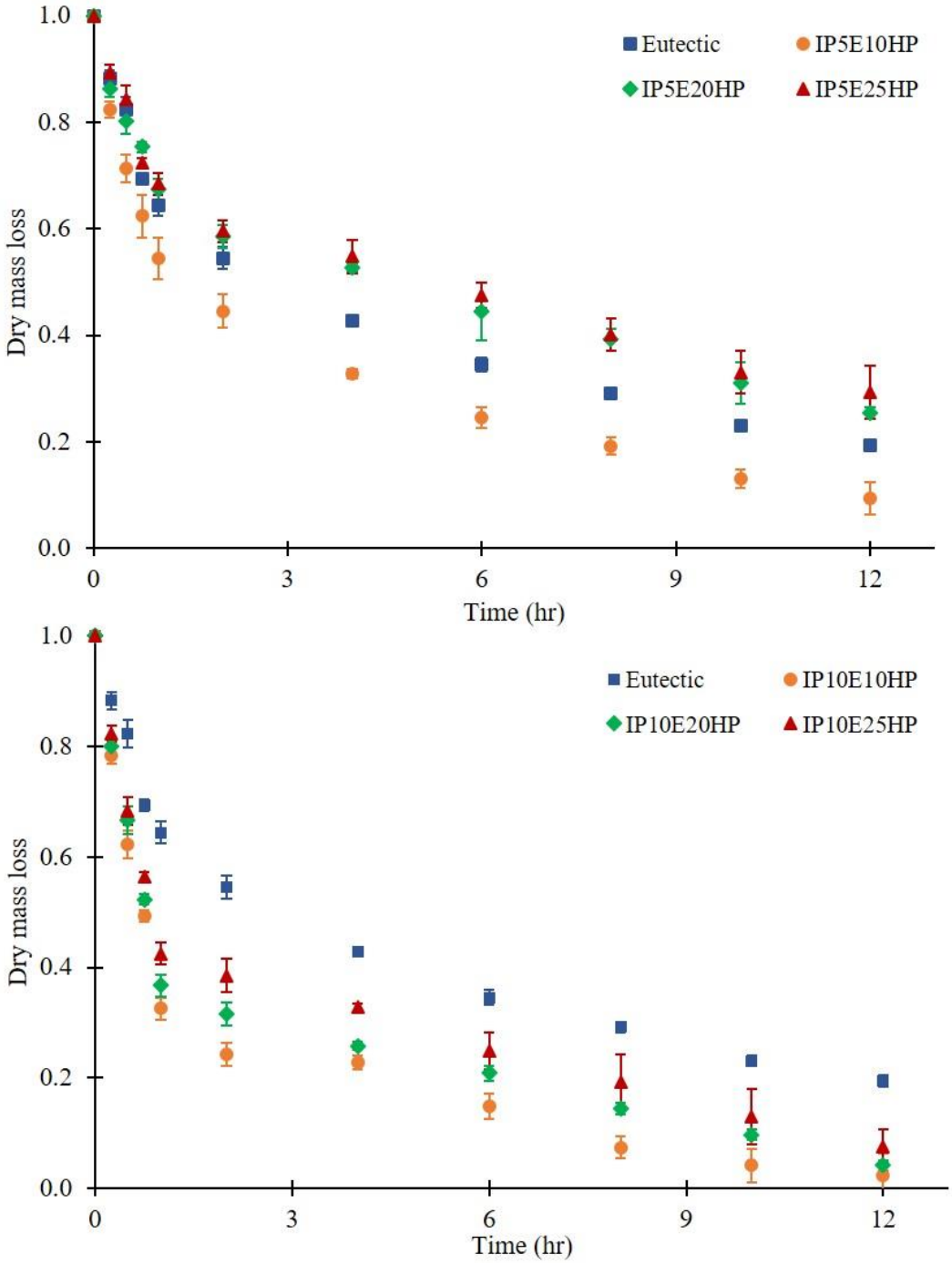

(B)

Figure 47. Water sorption (A) and erosion (B) behaviors of effervescent matrix tablets in phosphate buffer pH 6.8

4.2.3.2 *In vitro* drug release study of effervescent matrix tablets in 0.1 N HCl buffer

Effervescent matrix tablets were tested for drug release in two different buffers - HCl buffer (pH 1.2) and phosphate buffer (pH 6.8). The cumulative drug release profiles are shown in Figure 48. The drug release from eutectic tablets showed a gradual increase to about 23% after 12 h in HCl buffer. In comparison, matrix tablets containing 5% (w/w) effervescent agents released the drug at a lower rate than the eutectic tablets. In contrast, most tablets with 10% (w/w) effervescent agents showed a rapid increase to 20-25% at 2 h, followed by a gradual increase to about 30% after 12 h in HCl buffer. For drug release study in phosphate buffer pH 6.8, In the drug release study conducted in phosphate buffer pH 6.8, all tablets showed a higher drug release rate compared to testing in HCl buffer. Most of the tablets displayed a 100% drug release pattern with initial high release rate, except for 5E20HP and 5E25HP tablets. This could be due to the combined effect of effervescent agents and HPMC on drug release. As the concentration of HPMC increased, the drug release rate decreased, whereas the release rate increased with an increase in the effervescent agent. These patterns could be attributed to erosion more than water sorption characteristic of the tablets, as shown in Figures 46 and 47.

Furthermore, DE and MDT could be calculated from obtained cumulative drug release and displayed in Figure 49. DE represents the area under the dissolution curve up to a certain time, expressed as a percentage or ratio of the area of the rectangle described by 100% dissolution in the same period [239]. MDT, on the other hand, indicates the time it takes for 63.2% of the drug to dissolve and can be calculated using statistical moment's theory [240]. Previous studies have suggested that MDT ranges from 62-64% [241]. DE values for all tablets in phosphate buffer (pH 6.8) ranged from 0.17-0.92, which was higher than that observed in HCl buffer (0.08-0.25). HPMC matrix tablets containing 5% (w/w) effervescent agents had lower DE than those containing 10% (w/w) in both media. DE values decreased with an increase in HPMC concentration except for tablets containing 10% effervescent agents in pH 6.8 buffer, which showed no significant difference in DE values. These findings suggested that concentrations of HPMC and effervescent agents influence on drug release behaviors. However, wetting or solubility properties can also impact drug release, as evidenced by higher DE values in phosphate buffer (pH 6.8) compared to HCl buffer. In case of MDT, a lower MDT value indicates a higher drug release rate of tablets. The effervescent matrices in phosphate buffer showed promising results, as it produced lower MDT values than HCl buffer. In the case of MDT, a lower MDT value indicates a higher drug release rate of tablets. The immersion of effervescent matrices in phosphate buffer has shown promising results, as it produced lower MDT values than HCl

buffer. When the content of HPMC increased, the MDT values also increased. On the other hand, the increment of effervescent agents resulted in lower MDT values. Therefore, the results obtained for MDT were consistent with the observations made in the drug release profiles and DE.

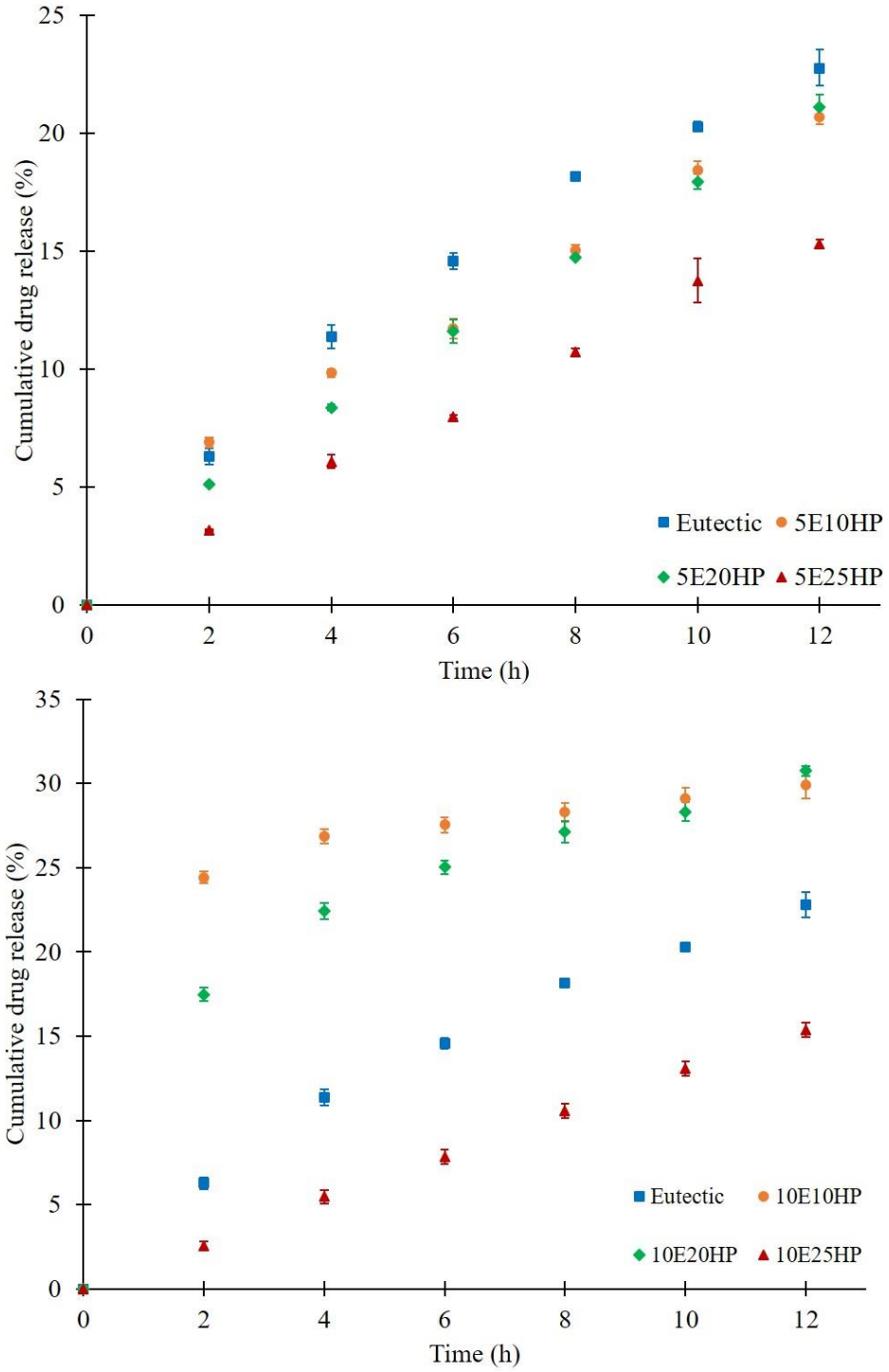

(A)

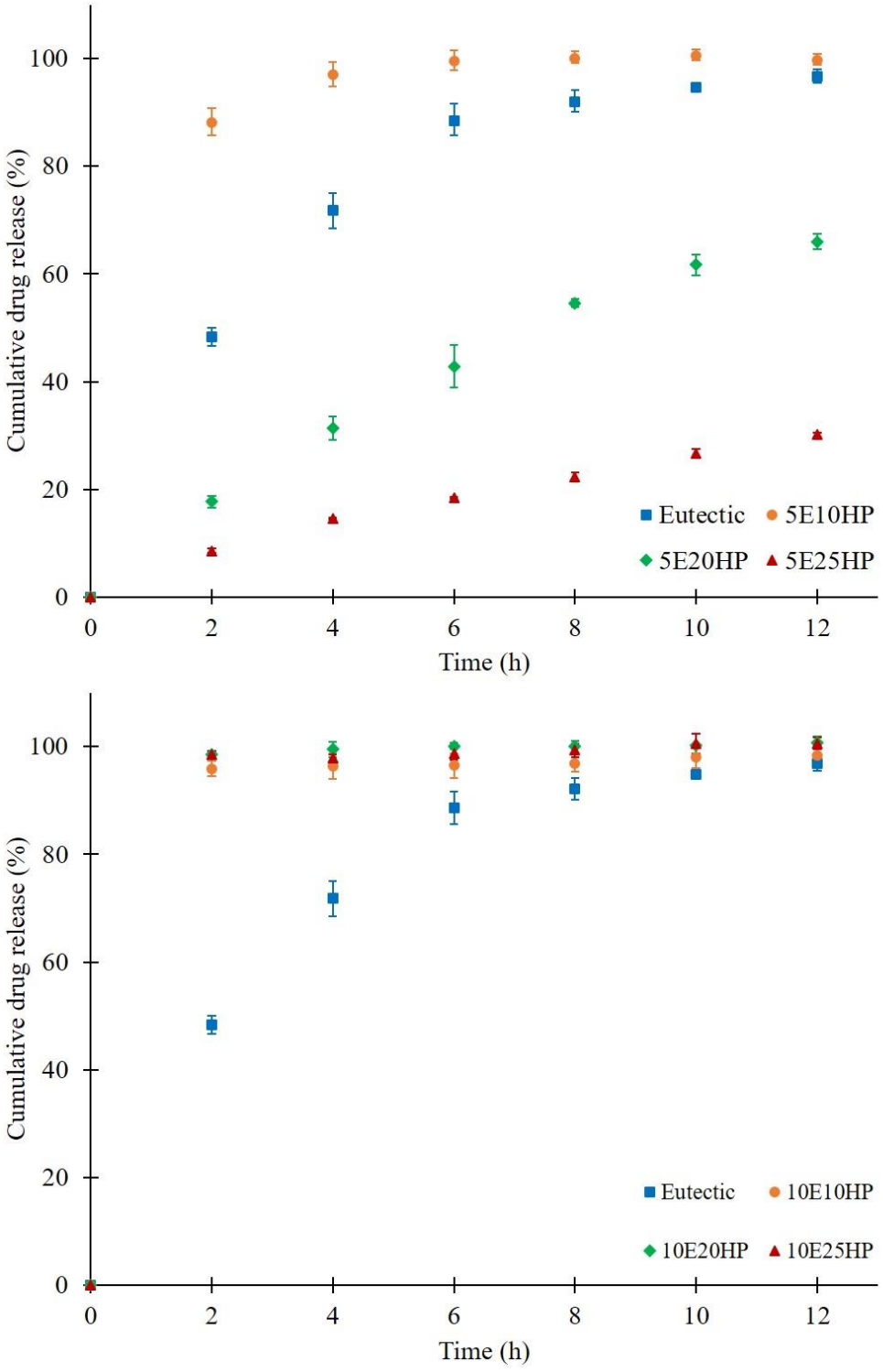

(B)

Figure 48. *In vitro* drug release profiles of effervescent matrix tablets in 0.1 N HCl buffer pH 1.2 (A) and phosphate buffer pH 6.8 (B)

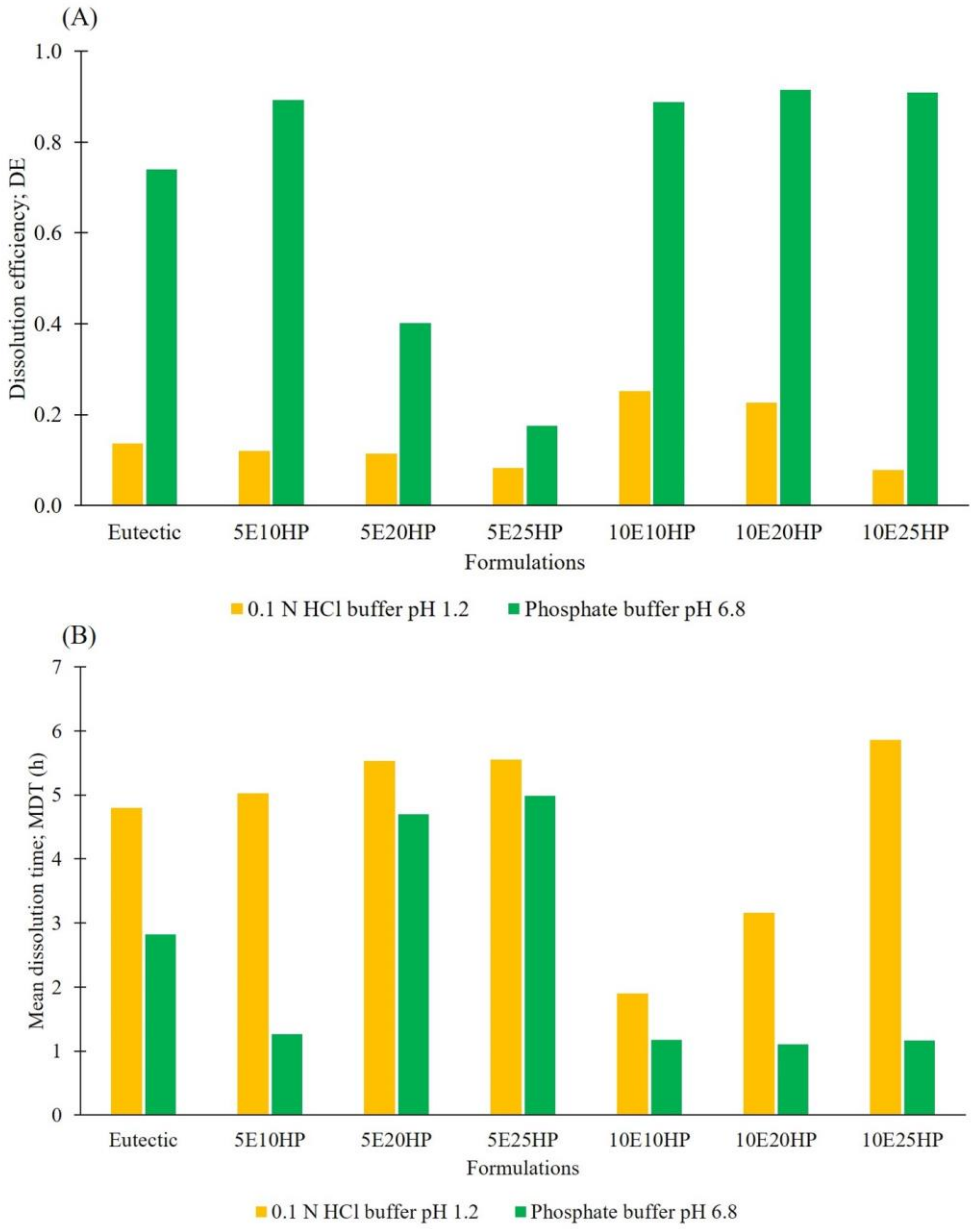

Figure 49. Dissolution efficiency (A) and mean dissolution time (B) obtained from cumulative dissolution profiles of effervescent matrix tablets in 0.1 N HCl buffer pH 1.2 and phosphate buffer pH 6.8.

4.2.3.3 Mass transport characterization of effervescent matric tablets in 0.1 M HCl buffer using numerical techniques

To assess the impact of effervescent agents on the mass transport of effervescent matrix tablets, it is essential to estimate the diffusivities of both the drug and water. A mathematical model was successfully developed by integrating Fick's second law, describing diffusion, with the free volume theory, defining the exponential relationship between diffusivity and water concentration. Swelling

was also considered by monitoring changes in the tablet's radius and height during immersion, directly influencing water content and swelling behavior. The model was fitted to experimental data, including water content and drug release profiles, to calculate diffusivity over time, as well as the diffusion coefficient at the equilibrium swollen state (D_{keq}) and β_k. Accuracy was ensured by considering data solely from the 0.1 N HCl buffer pH 1.2, where tablet exhibited least erosion during drug liberation studies, minimizing the combined effects of other factors that can occur during immersion, such as erosion.

The water and drug diffusion parameters (D_{weq}, D_{deq}, β_w, β_d) were determined through a numerical approximation. The model was solved using the least square approach with an iterative Gauss-Newton algorithm and truncated singular value decomposition. The estimated diffusion parameters are presented in Table 14. To assess the validity of the developed model, a verification process involved calculating the released drug concentration and comparing it to the experimental data. Figure 50 depicts the comparison between calculated and experimental drug release data for eutectic tablets, matrix tablets with 5% (w/w) effervescent agents and those with 10% (w/w) effervescent agents.

Table 14. Estimated diffusion parameter of water and drug using numerical approximation.

Formulations	Water diffusion parameters		Drug diffusion parameters	
	D_{weq} ($\times 10^4$ cm^2/min)	β_w	D_{deq} ($\times 10^4$ cm^2/min)	β_d
Eutectic	25.95	3.0350	7.11	4.7002
5E10HP	136.93	5.0822	6.44	4.7358
5E20HP	23.60	4.6519	5.94	4.7954
5E25HP	112.18	5.1422	6.74	4.7677
10E10HP	5.23	3.9570	0.29	4.3599
10E20HP	91.67	5.1967	2.55	4.8995
10E25HP	35.80	4.6556	6.54	4.7827

Remark: D_{weq} and D_{deq} are diffusion coefficient of water and drug at equilibrium swollen state, respectively. β_w and β_d are degree of dependency of diffusion coefficient on water and drug concentration, respectively.

After verifying the model, as depicted in Figure 50, it can be inferred that there is a strong agreement between the experimental data and the model approximation. The R^2 values, ranging from 0.9935 to 0.9998, suggest that the model accurately determines the diffusion parameters with a high level of precision. Furthermore, the validity of the model can be assessed by comparing the estimated parameters with those from prior studies. The parameter β_w, representing the dependence of the diffusion coefficient on water concentration and reliant solely on the type and molecular weight of the polymer, serves as a valuable point

of comparison [242]. Lamberti et al. found β to be 3 for an HPMC K15M-based matrix [150], while Chirico and colleagues reported a value of 2.5 for β [243]. This suggests a likelihood that β decreases with an increase in the molecular weight of the polymer. In this investigation, the calculated β_w, presented in Table 14, ranged from 3.0350 to 5.1967, surpassing values reported in prior research. This discrepancy could be attributed to variations in tablet composition, specifically the presence of effervescent agents. As outlined in our earlier research, these agents have the potential to alter the microstructure and surface of the matrix tablets. Upon contact with the medium, the effervescence reaction occurs rapidly, releasing CO_2 and inducing roughness and porosity in the matrix tablets [229]. The rate of water penetration into matrix tablets was observed to be contingent on their porosity [244]. Consequently, the elevated β_w observed in this study appears justifiable.

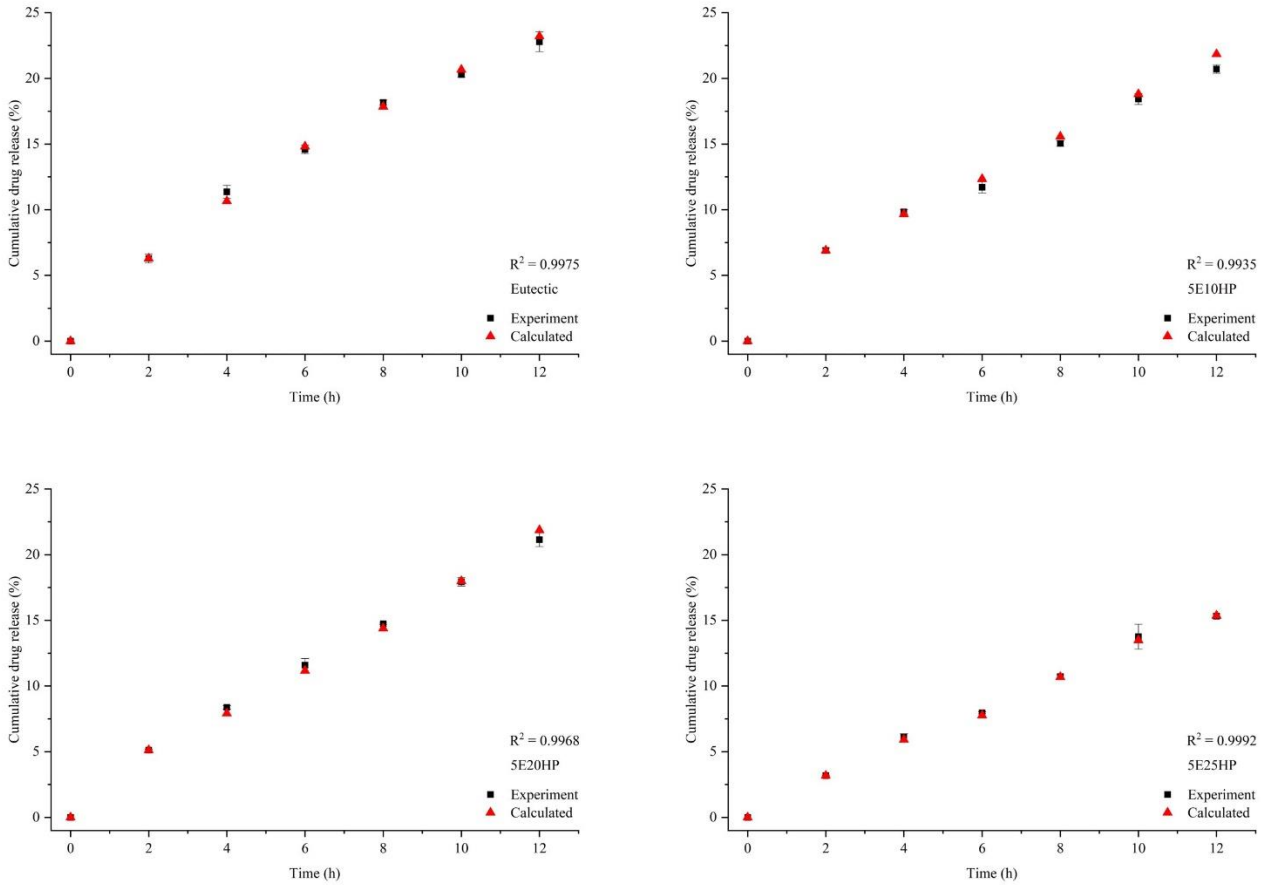

(A)

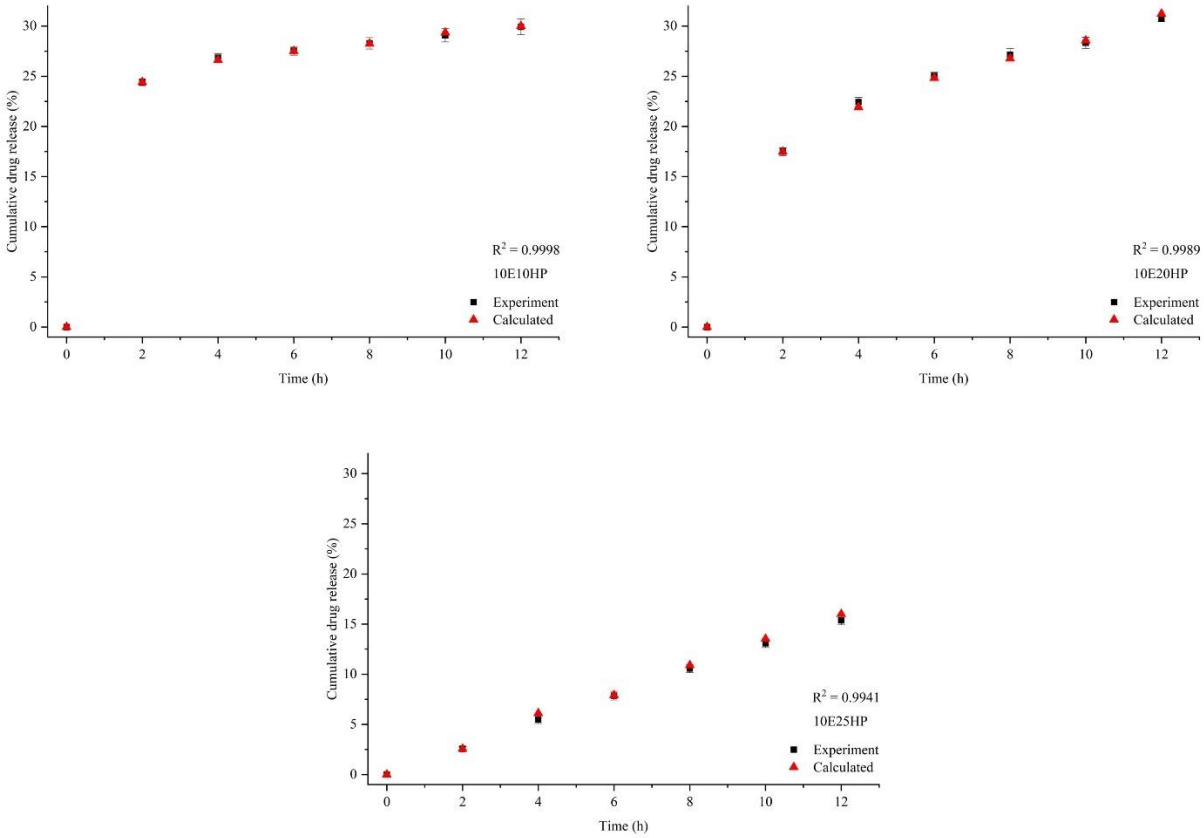

(B)

Figure 50. Comparison of experiment data (symbols) of drug release with model calculation (dash line) during exposure to HCl buffer of eutectic tablets and effervescent matrix tablets containing 5% (w/w) effervescent agents (A) and those with 10% (w/w) effervescent agents (B).

From the approximation of D_{keq} and β_k of water and drug, as outlined in Table 14, these parameters serve to calculating the diffusion coefficient over time for both water and drug. Figure 51A and 51B depict the relationship between water diffusivity and drug diffusivity in matrix tablets containing 5% (w/w) effervescent agents and those with 10% (w/w) effervescent agents, respectively. All effervescent matrices displayed a linear relation between water and drug diffusivity, with the exception of the 10E25HP tablets. Interestingly, an increase in HPMC concentration was associated with a rise in water diffusivity. When compared to eutectic tablets without effervescent agents and HPMC, effervescent matrices exhibited greater water diffusion but a lower diffusion coefficient for the drug. In contrast, eutectic tablets demonstrated comparable diffusion rates between drug and water, with a notably lower diffusion coefficient for water compared to effervescent matrix tablets. This observation implies potential differences in mass

transport mechanisms between eutectic tablets and effervescent matrices, highlighting the distinct influences of effervescent agents and HPMC on water and drug diffusion.

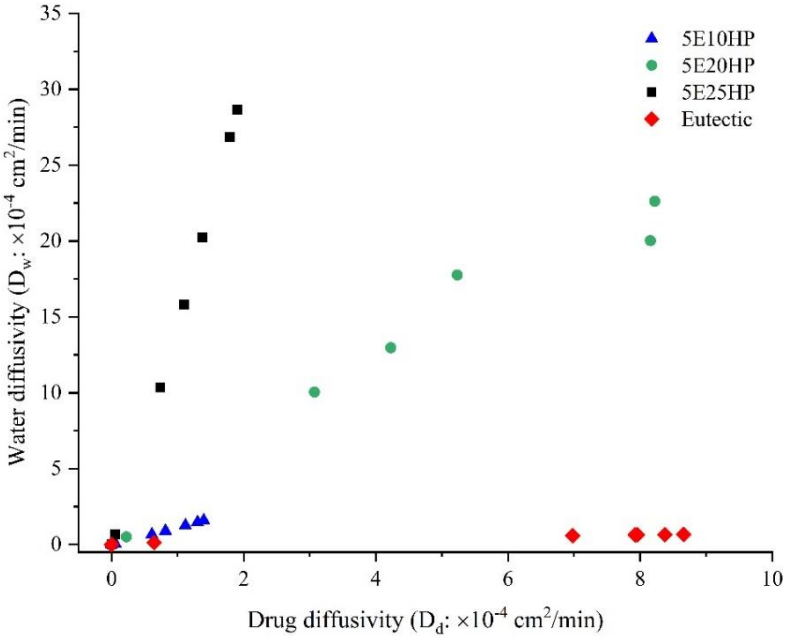

(A)

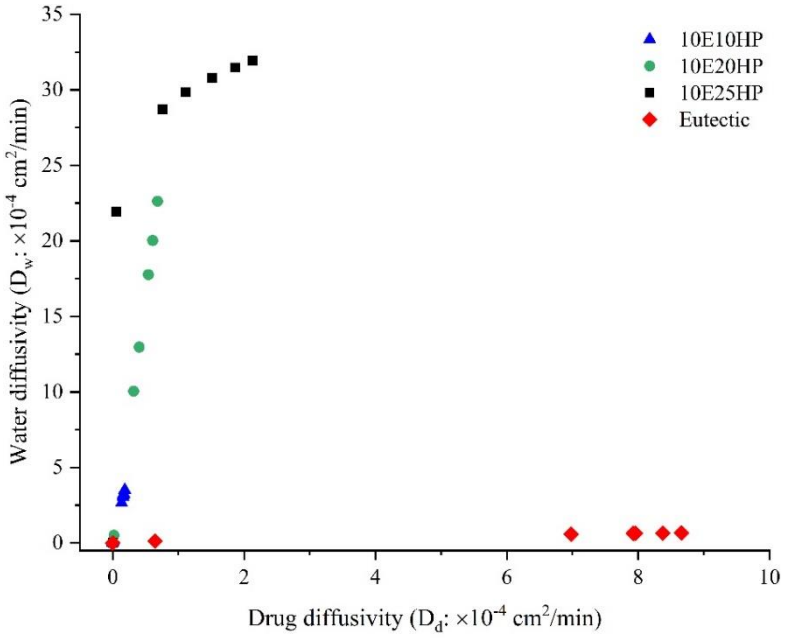

(B)

Figure 51. The relationship between water and drug diffusivity in matrix tablets containing 5% (w/w) effervescent agents (A) and those with 10% (w/w) effervescent agents (B)

Moreover, when comparing matrix tablets containing 5% and 10% (w/w) effervescent agents, the relationship between water and drug diffusivity exhibited a significantly steeper slope in tablets with 10% (w/w) effervescent agents than in those with 5% (Figure 51B), indicating that effervescent agents play a role in enhancing water penetration into the matrix. Typically, the movement of liquids through porous materials occurs in open pores *via* concentration-driven transport and capillary absorption [245]. In the research work of Chaiya et al. (2022), SRXTM clearly demonstrated that effervescent agents induce open porosity in matrix tablets following immersion in a medium [229], facilitating increased water penetration. The increased water diffusivity, in turn, leads to rapid gel layer formation, resulting in a subsequent decrease in drug diffusion and the manifestation of a sustained drug release pattern in matrix tablets incorporating 10% (w/w) effervescent agents, especially 10E20HP and 10E25HP tablets. In effervescent matrices with a 10% (w/w) HPMC concentration, the least water and drug diffusivities were observed at both 5% and 10% (w/w) effervescent agent levels. This can be attributed to increased erosion, leading to shorter diffusion paths and consequently reduced diffusion.

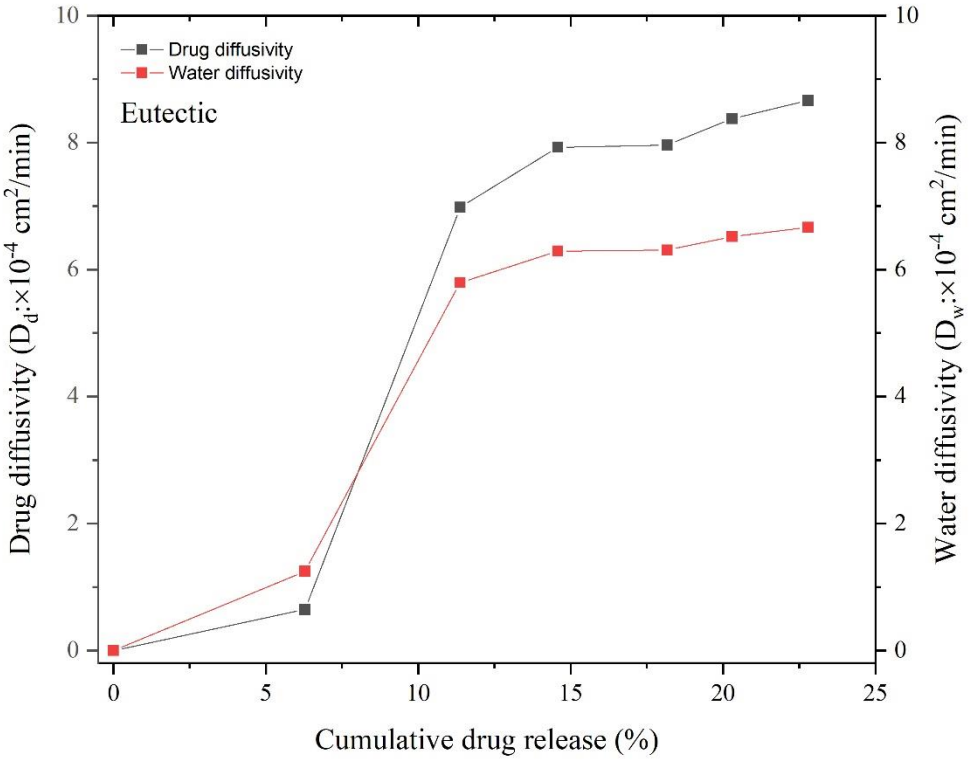

Figure 52. The relationship between diffusivity and cumulative drug release profile of eutectic tablets in 0.1 N HCl buffer.

Figure 52 illustrate the relationship between diffusivity and cumulative drug release profile of eutectic tablets in 0.1 N HCl buffer. Similar trends were observed in the diffusion patterns of both water and the drug. Initially, during the early stage of drug release (~ 5% initial drug release), water ingress into the tablet surpassed drug effusion from the tablet. Subsequently, both water and drug diffusivities experienced a substantial increase, reaching values of around 6×10^{-4} cm^2/min and 7×10^{-4} cm^2/min, respectively. These rates then gradually rose until they stabilized at approximately 6.5×10^{-4} cm^2/min for water diffusivity and 8.5×10^{-4} cm^2/min for drug diffusivity. This clearly illustrated the influence of eutectic mixture properties, such as improved wetting and dissolution. [79, 86]. Moreover, this was substantiated through real-time monitoring of tablet behavior of eutectic tablets in HCl buffer using UV-vis imaging, as elaborated in section 4.2.2.2 on dissolution imaging in pH shift experiments. The observation revealed concurrent surface erosion and drug release in eutectic tablets during immersion in the dissolution medium, suggesting that the release mechanism could potentially involve anomalous transport, a combination of diffusion and polymer relaxation.

Figure 53 displays the relationship between diffusivity and the cumulative drug release profile of effervescent matrix tablets in 0.1 N HCl buffer. When comparing water and drug diffusivities, it was consistently observed that drug diffusivity remained lower than water diffusivity across all effervescent matrices. The observed relationship between diffusivity of water and drug and cumulative drug release profiles can be categorized into three phases based on diffusivity pattern; (I) drug release characterized by low diffusivity, (II) drug release accompanied by an increase in diffusivities and (III) drug release exhibiting a plateau pattern of diffusivities. For matrix tablets with 5% (w/w) effervescent agents, phase I of relationship was found at the early stage of drug release ((~ 5% initial drug release) of all effervescent matrix tablet comprising 5% (w/w) effervescent agents. This could be ascribed to the dissolution of the drug substance on the tablet surface [116], facilitated by effervescent agents promoting the release of particles from the tablet during the initial immersion period in the medium. Then, the ingress of water was continuously increased during drug liberation while drug was slowly diffused out from tablet. Following the alteration of the tablet surface upon contact with the medium due to effervescent agents, there was an enhancement in water ingress (phase II of relationship), leading to the accelerated formation of a porous gel layer. This structural change resulted in the gradual release of the drug from the tablets, as depicted in Figure 48A. Moreover, the water diffusivity increased with an increase in HPMC concentration.

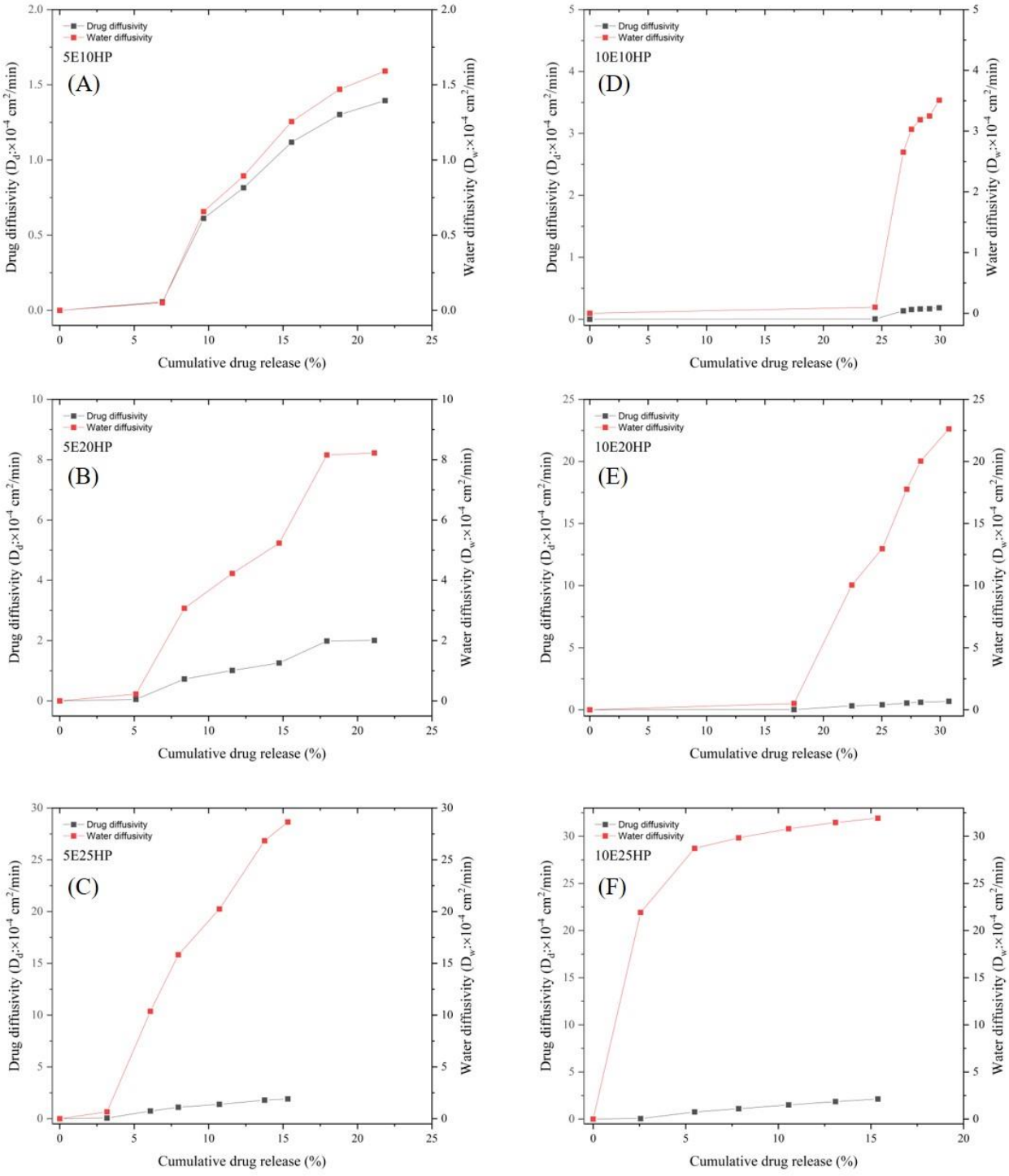

Figure 53. Relationship between diffusion coefficient and cumulative drug release of effervescent matrix tablets containing 5% (w/w) effervescent agents (A-C) and those with 10% (w/w) effervescent agents (D-F)

For matrix tablets comprising 10% (w/w) effervescent agents, phase I of correlation was found in almost drug release pattern, indicating initial burst drug release, particularly 10E10HP tablets. This observation aligns with the erosion patterns observed in the tablets (Figure 46B). Owing to the low HPMC concentration in effervescent matrices, these tablets lack resistance to erosion induced by the effervescence reaction upon contact with the medium. In 10E20HP tablets, phase I of the relationship was still present but at a lower level compared to 10E10HP, while a different pattern emerged in 10E25HP tablets. In the relationship between diffusivity and drug release of 10E25HP in HCl buffer, only phases II and III were observed. The effervescence reaction facilitated water ingress, but the tablets demonstrated resistance to erosion due to the high HPMC concentration. This led to the production of a porous gel structure surrounding the tablets, resulting in sustained drug release, as depicted in Figure 48A. This clearly highlights the synergistic impact of effervescent agents and HPMC on the behavior of tablets in effervescent matrix tablets.

Ordinarily, when HPMC matrix tablets are immersed in a medium, they exhibit swelling and the formation of a gel layer. This gel layer serves as a diffusion barrier, impeding additional water uptake and consequently influencing the swelling kinetics of the tablets [40]. The study of Kikuchi, et al. (2012) substantiated that the movement of water molecules in hydrating HPMC tablet was more tightly restricted than that in bulk water [246]. Unexpectedly, nearly all effervescent matrix tablets displayed a consistent rise in both water and drug diffusivity. This phenomenon is likely attributed to the influence of effervescent agents, which enhance the surface roughness and the formation of a porous gel layer structure in HPMC tablets. The heightened surface roughness facilitates rapid water ingress during the initial time intervals, followed by continuous ingress through the porous structure of the gel layer in later stages. Simultaneously, the drug steadily diffuses out from the tablet through the porous gel layer, resulting in the sustained release pattern observed in effervescent matrix tablets.

4.2.3.4 Summary

Numerical techniques were effectively employed to estimate water and drug diffusivity in the context of drug release investigations involving effervescent matrices in 0.1 N HCl buffer. The mathematical model, constructed using Fick's second law and the free volume theory, successfully accommodated these considerations. The model's accuracy was validated through a high coefficient of determination, and the estimated diffusion parameters were consistent with prior research findings. The approximation of water and drug diffusivities yielded valuable data, contributing to the understanding of how effervescent agents impact the mass transport of effervescent matrix tablets, aligning well with observations made in the laboratory experiment.

4.3 Study of high-shear melt granulation scale-up using HSG

4.3.1 Physical properties of granules prepared by high-shear melt granulation

4.3.1.1 Bulk density, tapped density and compressibility

The granules comprising IBU, P407 and MCC were successfully fabricated using high-shear melt granulation at various level of process parameters. The physical properties of prepared granules including bulk density, tapped density and compressibility (CI and HR) are outlined in Table 15. Furthermore, flow character of prepared granules can be predicted by CI and HR and also displayed in Table 15. In this investigation, high-shear melt granulation involved the variation of process parameters, specifically processing temperature, agitator impeller speed, and chopper speed. There was a similar trend observed in bulk density and tapped density alterations with changes in these parameters. Notably, both bulk and tapped densities exhibited a substantial increase, transitioning from approximately 0.4 g/mL to around 0.5 g/mL as the processing temperature was adjusted from 50 ºC to 70 ºC. In contrast, modifications in agitator and chopper speeds at the same processing temperature resulted in negligible changes in both bulk and tapped densities. CI and HR are indicators used to assess the powder or granule flow properties based on bulk and tapped densities. These parameters provide valuable information about the powder's compressibility and flowability. The CI and HR values of all prepared granules were classified as moderate, suggesting passible or fair flow properties [247].

Table 15. Bulk density, tapped density, compressibility and flow character of granules prepared using high-shear melt granulation with variation of process parameters

Samples	Bulk density (g/mL)	Tapped density (g/mL)	CI	HR	Flow character
50T170A1500C	0.424	0.538	21.186	1.269	Passible
50T170A1750C	0.409	0.528	22.449	1.286	Passible
50T200A1500C	0.419	0.515	18.750	1.231	Fair
50T200A1750C	0.432	0.534	19.149	1.237	Fair
70T170A1500C	0.528	0.659	19.753	1.246	Fair
70T170A1750C	0.544	0.657	17.284	1.209	Fair
70T200A1500C	0.497	0.629	20.930	1.265	Passible
70T200A1750C	0.523	0.668	21.795	1.279	Passible

Remark: T = processing temperature, A = agitator speed in unit of RPM, C = chopper speed in the unit of RPM, CI = compressibility index, HR = Hausner's ratio

4.3.1.2 Particle size distribution

The particle size distribution of prepared granule using sieve shaker are shown in Figure 54. The majority of the prepared granules exhibited a particle size larger than 425 µm, falling within the specified size fraction for melt granulation, as discussed in a previous study [143]. When adjusting the processing temperature from 50 ºC to 70 ºC, the larger particle size fraction (> 425 µm) showed a significant increase, reaching up to approximately 70%. This trend aligned with the higher values of bulk and tapped densities, indicating the influence of temperature on the agglomeration process in melt granulation. At 70 ºC, the meltable binder, P407, likely completely melted, assuming the role of a binder and contributing to the growth of granules. In contrast, granulation at 50 ºC might involve partial melting of P407, resulting in some powder portions failing to agglomerate into granules, as evidenced by a lower percentage of retained weight in the greater particle size fraction (> 425 µm). Furthermore, the particle size of prepared granules is influenced by the speed of the agitator and chopper, depending on the processing temperature. At 70 ºC, higher speeds reduced granule size, while at 50 ºC, higher speeds increased granule size. In high-shear melt granulation, the energy induced by increased agitator speed transforms into heat in the powder mass, raising the product temperature [248]. Consequently, a higher agitator speed may lead to an increase in the larger particle fraction (> 425 µm) at 50 ºC, indicating partial melting of P407.

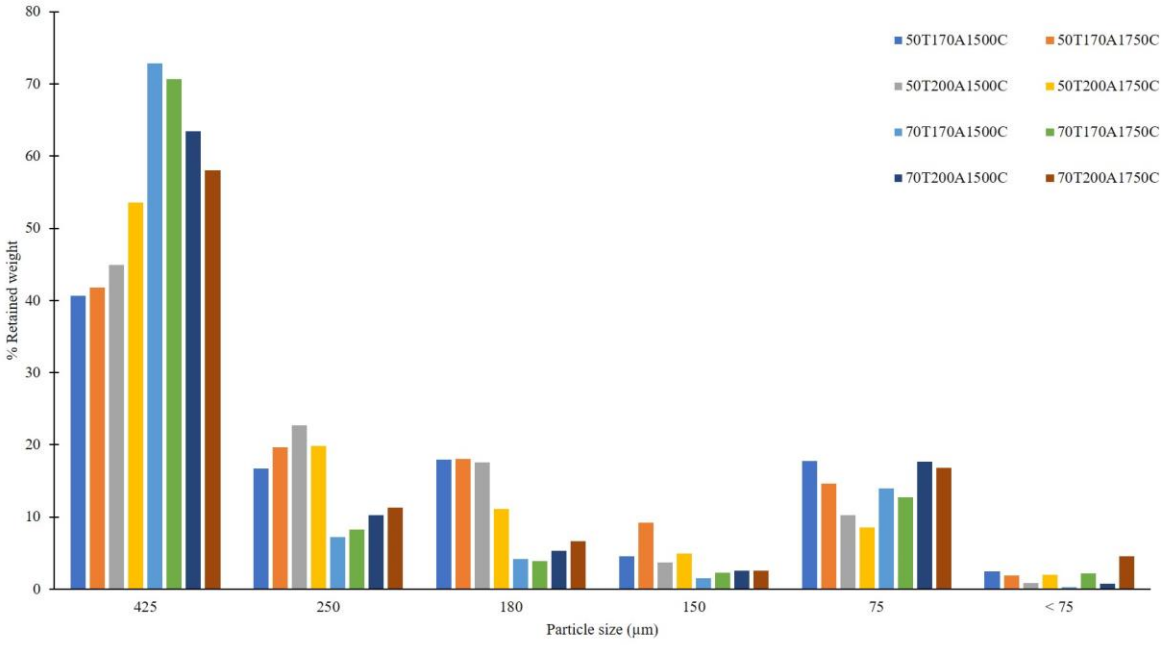

Figure 54. Particle size distribution of granules prepared using high-shear melt granulation with variation of process parameters (T = processing temperature, A = agitator speed in the unit of RPM and C = chopper speed in the unit of RPM)

4.3.2 Thermal properties of prepared granules using high-shear melt granulation

Figure 55 depicts thermograms of individual substances and granules produced using high-shear melt granulation at various processing temperatures. IBU displayed a single endothermic peak around 80 ºC, consistent with prior research, indicating complete drug melting [173, 174]. P407 exhibited a melting point at approximately 60 ºC, as reported in the research work of Dugar and co-worker [20]. The DSC curves of the physical mixture (PM), prepared by blending IBU and P407 in the same ratio employed in melt granulation, revealed two endothermic peaks at approximately 58 ºC and 78 ºC, corresponding to the melting points of P407 and IBU, respectively (Figure 55A).

Regarding granules produced at 50 ºC with different agitator and chopper speeds, as depicted in Figure 55B, comparable thermogram patterns were observed, revealing three endothermic peaks around 40 ºC, 55 ºC, and 75 ºC. The peak at 40 ºC could be attributed to the eutectic mixture formed by certain portions of IBU and P407, while the peaks at 55 ºC and 70 ºC could be identified as excess P407 and IBU, respectively. This finding aligns with the physical characteristics of granules at 50 ºC (Table 15 and Figure 54), indicating partial melting of P407. At this temperature, specific portions of P407 underwent partial melting and interacted with IBU, resulting in the formation of the eutectic mixture in some part of powder bed in high-shear melt granulation.

For granules fabricated at 70 ºC with variations in agitator and chopper speeds, as shown in Figure 55C, they exhibited consistent thermogram patterns featuring a single endothermic peak around 45 ºC, indicating the formation of the IBU and P407 eutectic in the prepared granules [20]. The eutectic phenomenon is driven by entropy and occurs when at least two compounds come into close contact in the solid state, demonstrating mutual solubility in the molten state. A distinctive characteristic of eutectic mixtures is their lower melting temperature compared to that of each individual pure compound [85]. Hence, the processing temperature is deemed a critical process parameter in high-shear melt granulation, exerting influence over both the physical and physicochemical attributes of the granules.

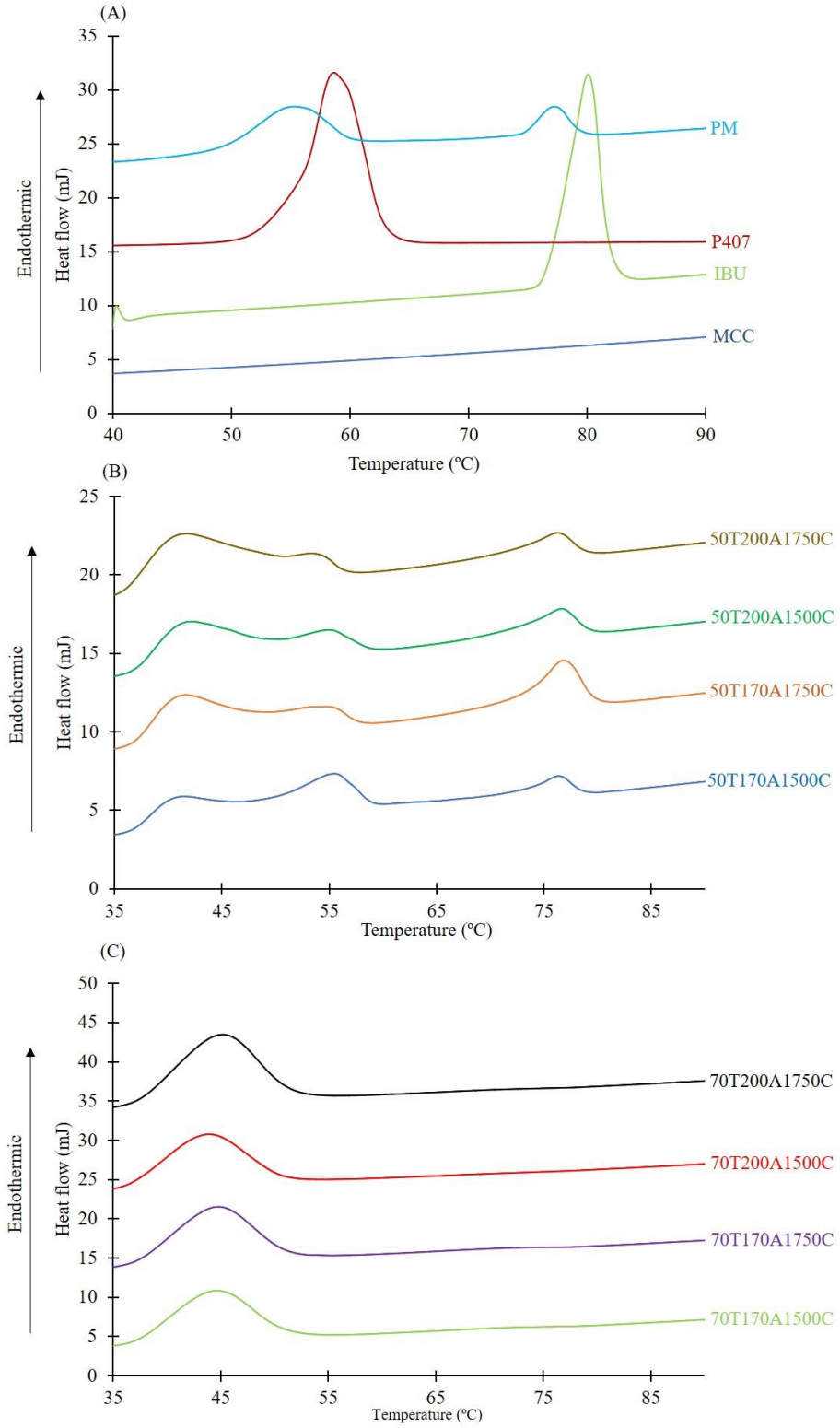

Figure 55. Thermogram of pure substance (A) and granule prepared using high-shear melt granulation at processing of 50 ºC (B) and 70 ºC (C) (T = processing temperature, A = agitator speed in the unit of RPM and C = chopper speed in the unit of RPM)

4.3.3 Crystallinity of prepared granules using high-shear melt granulation

In order to evaluate the impact of process parameters on the crystallinity or granules fabricated using high-shear melt granulation, PXRD analysis was performed and obtained diffractograms are depicted in Figure 56. IBU displayed several distinctive peaks, notably at 6.2, 12.3, 16.7, and 22.3 2θº, as depicted in Figure 56A. This pattern suggests that IBU was in a highly crystalline state, aligning with findings described by Mallick et al. (2008) [168]. In contrast, P407 exhibited only two prominent peaks around 19 and 23 2θº, as shown in Figure 56A, along with a broad halo indicative of crystalline domains within the amorphous polymeric material [17, 175]. The diffractograms of PM displayed the same diffraction peaks, with a significant decrease in peak intensity, particularly at around 6, 12, and 20 2θº, attributed to the crystalline nature of IBU within the specific system. In the case of granules produced using high-shear melt granulation with various process parameters, the diffractograms of all granules showcased analogous diffraction peaks, notably with a notable reduction in peak intensity, especially around 6 and 12 2θº. These results imply the occurrence of eutectic formation between IBU and P407. While this eutectic formation may not impact the crystal habit of IBU, it contributes to a decrease in the crystallinity degree of IBU. The PXRD diffractograms provide support for the observed eutectic formation between IBU and P407, aligning with the findings from DSC observations.

4.3.4 Physical properties of tablets fabricated from the granules prepared by high-shear melt granulation.

Following the fabrication of granules using high-shear melt granulation employing various process parameters, these granules were subsequently compressed into tablets. All manufactured tablets exhibited favorable physical appearance and physical properties, including tablet weight, thickness, diameter, hardness, and friability were investigated as detailed in Figure 57. Noteworthy variations were not observed in the average tablet weight, thickness, and diameter across all tablets. However, in terms of hardness, tablets fabricated from granules prepared at 70 ºC exhibited higher hardness values, ranging from 140.40 ± 3.78 N to 146.80 ± 5.22 N when compared to tablets made from high-shear melt granulation at 50 ºC. This disparity can be attributed to the physical properties of the granules, where higher tapped and bulk densities and lower CI contributed to the increased hardness of the tablets, as elucidated in previous research by Macho and colleagues [249].

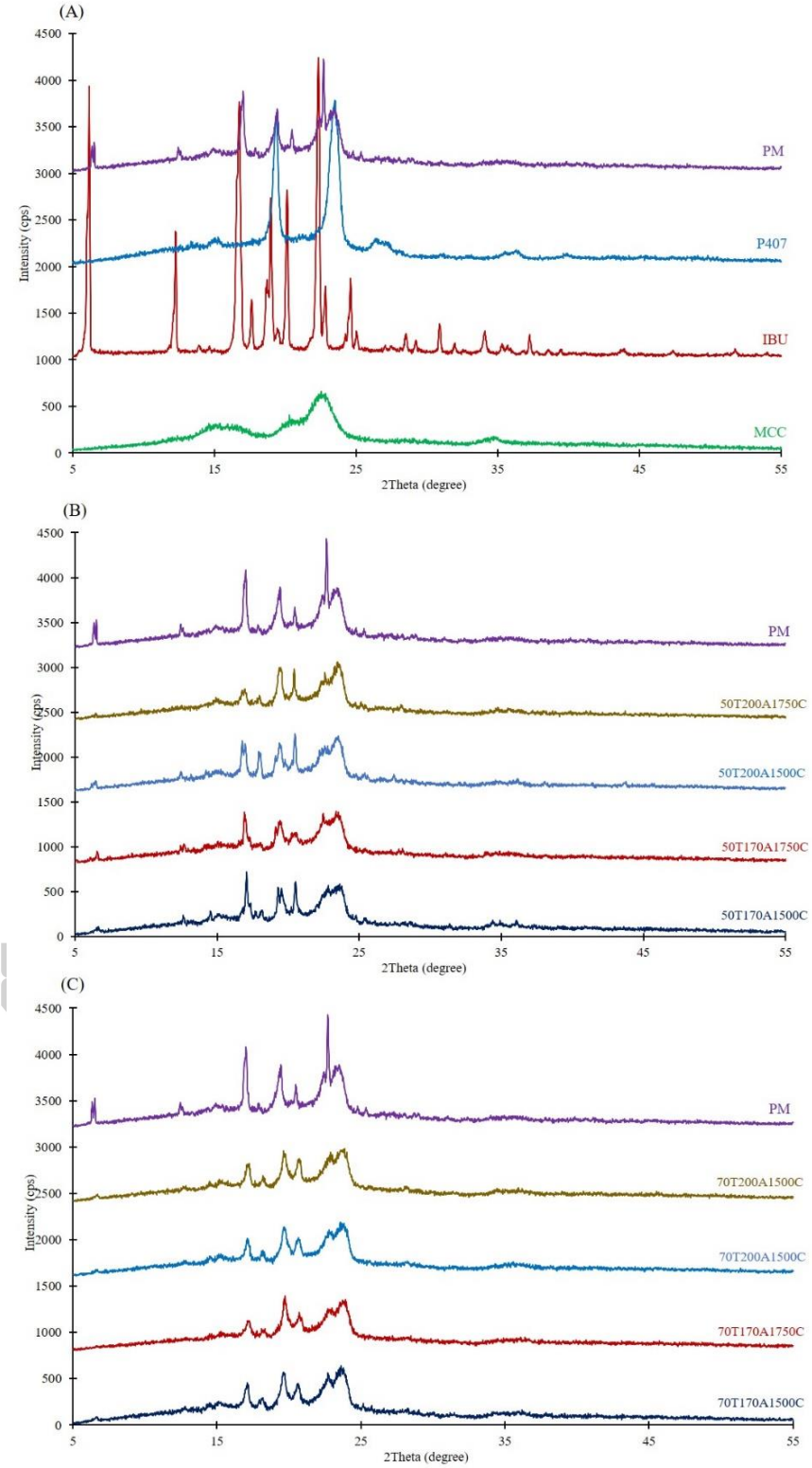

Figure 56. Diffractogram of pure substance (A) and granule prepared using high-shear melt granulation at processing of 50 ºC (B) and 70 ºC (C) (T = processing temperature, A = agitator speed in the unit of RPM and C = chopper speed in the unit of RPM)

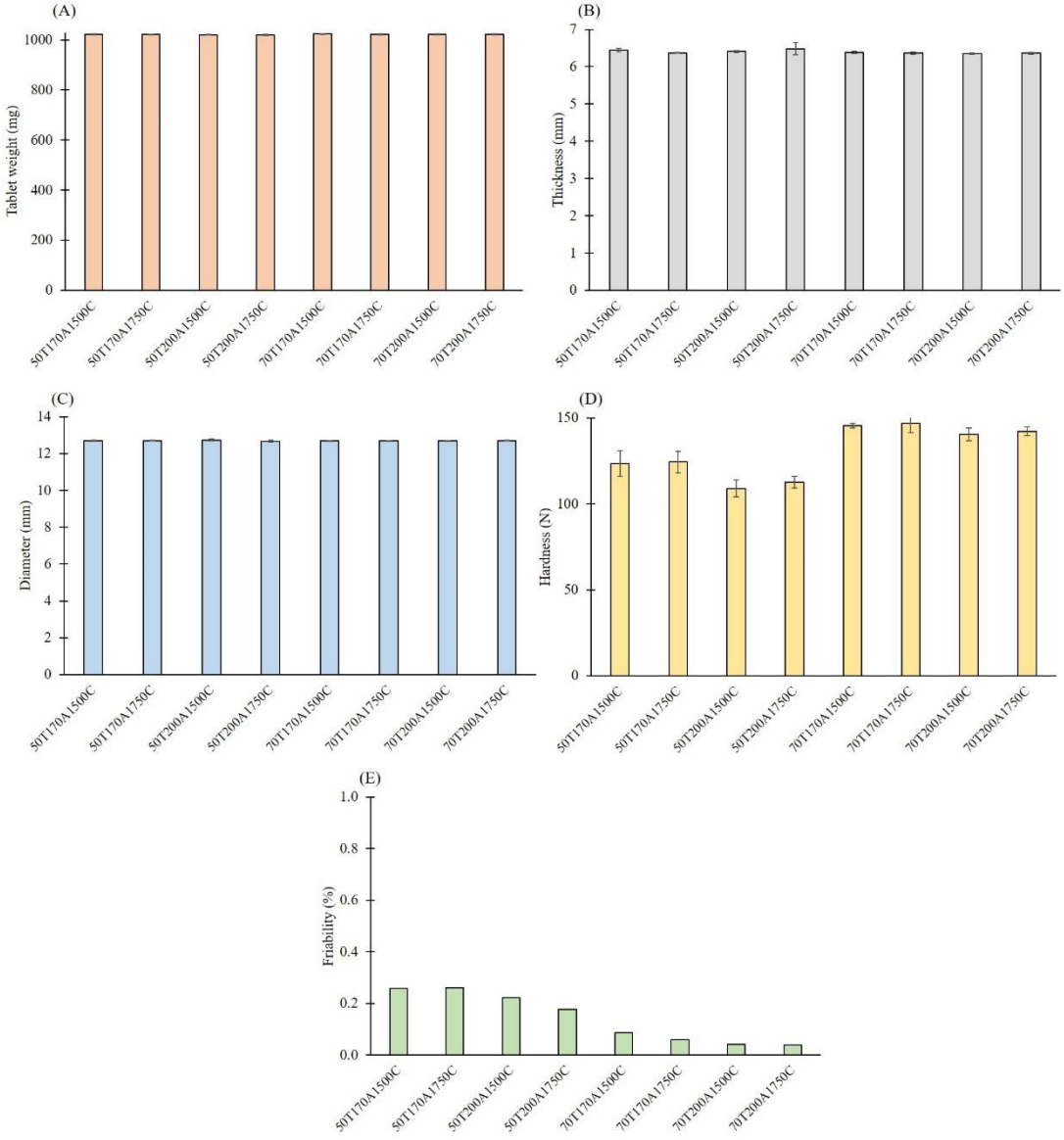

Figure 57. Tablet weight (A), thickness (B), diameter (C), hardness (D) and friability of tablets fabricated from the granules prepared by high-shear melt granulation (T = processing temperature, A = agitator speed in the unit of RPM and C = chopper speed in the unit of RPM)

4.3.5 *In vitro* drug release studies and dissolution performance

4.3.5.1 *In vitro* drug release studies

To explore the impact of process parameters, such as processing temperature and agitator and chopper speeds, on the dissolution properties of the manufactured tablets, *in vitro* dissolution tests were carried out in phosphate buffer pH 6.8. The cumulative drug release profiles are presented in Figure 58. Additionally, to assess the performance of scaling up using high-shear melt granulation, eutectic tablets produced in a beaker within a circulating water bath were utilized for comparative analysis. The eutectic tablet fabricated using beaker in circulating water bath exhibited drug release of about 50% within the initial 2 h, followed by s sustained release until reaching approximately 97% release at 12 h. In contrast, IBU tablets exhibited a rapid release of about 15% at 0.5 h, maintaining constant throughout the dissolution study. All tablets made from the granules prepared using melt granulation with various process parameters consistently demonstrated the highest drug release, ranging from approximately 90% to 100% with negligible differences between formulations, indicating a notable enhancement in IBU release, approximately 7-fold compared to IBU tablets. This observation was in accordance with the previous studies [20, 86]. Nonetheless, a distinctive pattern in drug release profiles is evident in tablets produced from granules prepared using melt granulation at 50 ºC. These tablets exhibited lower drug release in the early phase (initial 6 h), followed by an increase in release after 7 h compared to tablets made using beaker in circulating water bath. This distinction was further supported by the comparison of dissolution parameter, including $t_{50\%}$ and $t_{90\%}$, as depicted in Figure 59. The $t_{50\%}$ and $t_{90\%}$ represent the time required for 50% and 90% drug release from tablets, respectively. Tablets prepared using melt granulation at 50 ºC exhibited higher $t_{50\%}$ and lower $t_{90\%}$ compared to tablets made using melt granulation at 70 ºC and tablets prepared with a beaker in circulating water bath. This observation can be attributed to the physicals and physicochemical properties of the granules. Complete eutectic formation occurred when granules were prepared at 70 ºC, enhancing the wettability of tablets compared to tablets made from granule prepared at 50 ºC due to their eutectic characteristics. This contributes to the lower $t_{50\%}$ observed in tablet prepared using melt granulation at 70 ºC. Moreover, at this processing temperature, the higher bulk and tapped densities of the granules lead to increased tablet hardness, resulting in lower disintegration and dissolution [250].

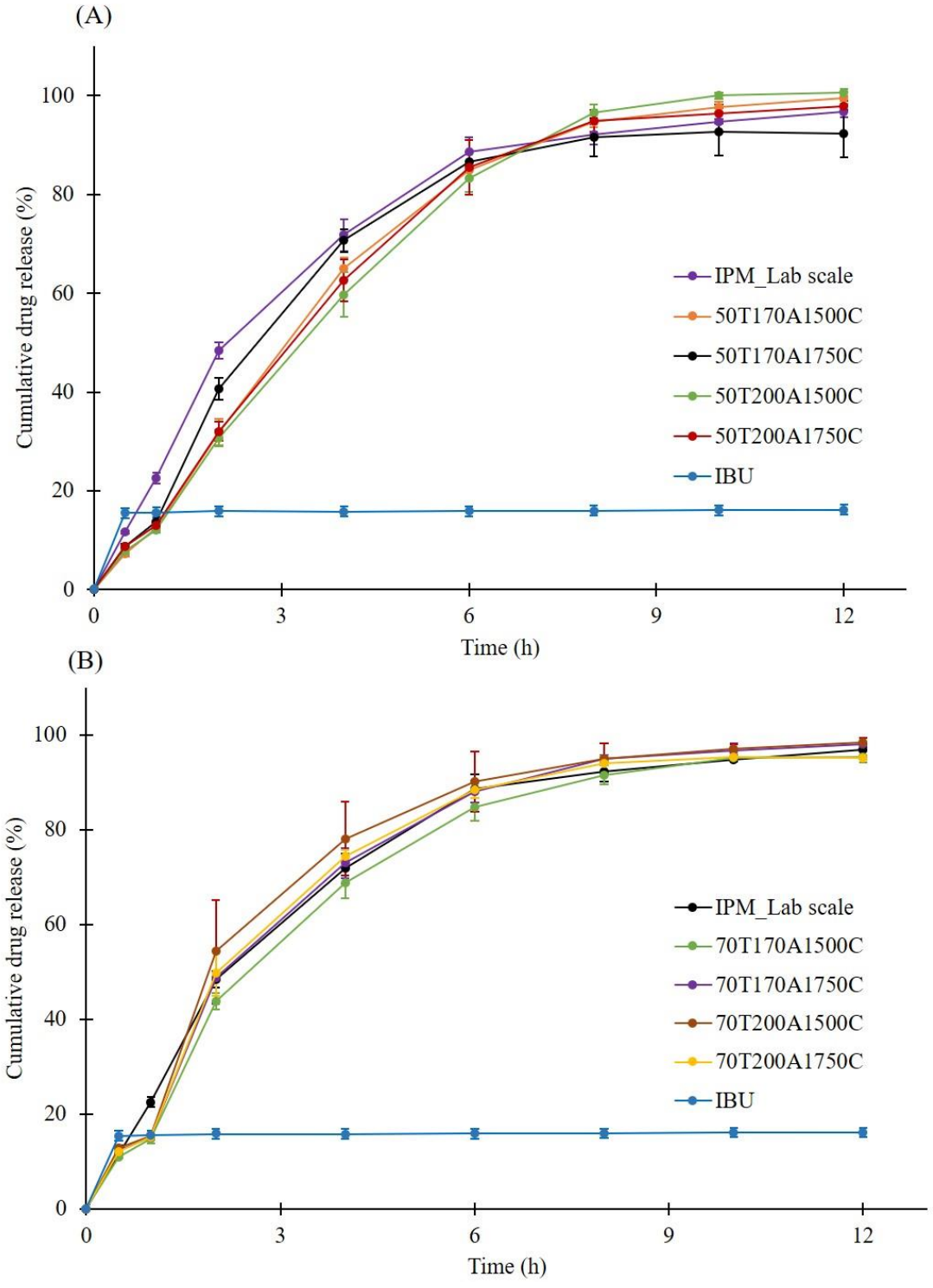

Figure 58. Dissolution profile of tablets made from granules fabricated using melt granulation at 50 ºC (A) and 70 ºC (B) (T = processing temperature, A = agitator speed in the unit of RPM and C = chopper speed in the unit of RPM)

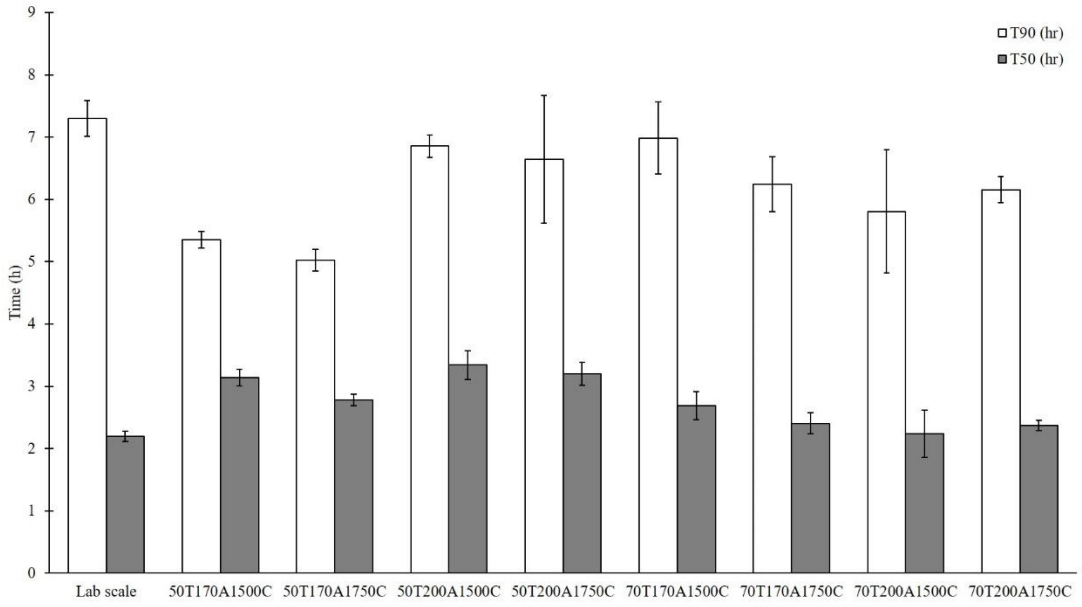

Figure 59. Comparison of dissolution parameters ($t_{50\%}$ and $t_{90\%}$) of tablet made from granules fabricated using melt granulation with different process parameters (T = processing temperature, A = agitator speed in the unit of RPM and C = chopper speed in the unit of RPM)

4.3.5.2 Dissolution performance

As illustrated in Tablet 16, similarity and dissolution efficiency were calculated and compared to investigate the effectiveness of scaling up using melt high-shear melt granulation. For similarity factor (f_2), drug release profile of eutectic tablet prepared using a beaker in circulating water bath was designated as reference product and dissolution profile of each tablet prepared using melt granulation was assigned as test product. The *f2* value should fall between 50 and 100, indicating both products exhibited similar drug release patterns [251]. Considering the distinct drug release patterns of tablets prepared using melt granulation at 50 ºC, as discussed earlier, the similarity factors for these tablets tended to be lower, ranging from 53.05 to 67.11. Conversely, tablets fabricated using melt granulation at 70 ºC exhibited higher values, ranging from 69.15 to 76.36. This suggests that melt granulation at the processing temperature of 70 ºC might be a suitable condition for scaling up the manufacturing of eutectic tablets. Furthermore, variations in the speed of the agitator and chopper had a negligible influence on the dissolution pattern.

The results of calculated DE are presented in Table 16. Tablets fabricated using melt granulation at 50 ºC exhibited DE value in range of 0.70 ± 0.01 to 0.71 ± 0.02 while the DE value of tablets prepared using melt granulation at 70 ºC exhibited higher value, ranging 0.72 ± 0.02 to 0.75 ± 0.02, which close to the eutectic tablet prepared with a beaker in circulating water bath. This observation supported the results of similarity factor and was consistent with the previous study [252].

Table 16. Similarity factor (f_2) and dissolution efficiency (DE) of tablet made from granules fabricated using melt granulation with different process parameters

Formulations	Similarity factor (f_2)	Dissolution efficiency (DE) (mean ± SD)
50T170A1500C	56.63	0.70 ± 0.01
50T170A1750C	67.11	0.71 ± 0.02
50T200A1500C	53.05	0.70 ± 0.01
50T200A1750C	56.78	0.70 ± 0.03
70T170A1500C	72.18	0.72 ± 0.02
70T170A1750C	76.22	0.75 ± 0.02
70T200A1500C	69.15	0.77 ± 0.04
70T200A1750C	76.36	0.74 ± 0.01
Eutectic_lab scale	NA	0.74 ± 0.01

Remark: T = processing temperature, A = agitator speed in the unit of RPM and C = chopper speed in the unit of RPM, NA = Not available

4.3.5.3 Summary

Granules containing the eutectic mixture of IBU, P407, and MCC were successfully fabricated using high-shear melt granulation, employing various process parameters such as processing temperature, agitator speed, and chopper speed. The granules, prepared under various conditions of high-shear melt granulation, exhibited a favorable appearance along with acceptable physical properties. Notably, the processing temperature emerged as a critical process parameter in high-shear melt granulation, significantly impacting the physical and physicochemical characteristics of the granules. This, in turn, led to modifications in the physical attributes and dissolution behavior of the eutectic tablets. Conversely, variations in the speed of the agitator and chopper exerted minimal influence on the properties of both granules and tablets.

CHAPTER 5
CONCLUSION

Effervescent matrix tablets containing eutectic mixture between IBU and P407 were successfully development using melt granulation techniques. The effervescent agents have a potential to modify the tablet surface and microstructure which influence the tablet behaviors during drug liberation. Various scales, spanning molecular and microscopic to macroscopic, were examined through a combination of traditional and cutting-edge methods. The eutectic mixture of Ibuprofen (IBU) and poloxamer 407 (P407) exhibited improved wetting characteristics and CO_2 liberation during effervescence, leading to increased tablet surface roughness through matrix erosion, as observed using a stereomicroscope. Effervescent agents (5-10% (w/w)) were investigated for their impact on tablet characteristics using texture analysis and imaging techniques. These agents prompted a rapid effervescence reaction, resulting in a high gel layer formation with low gel strength, as confirmed by texture analysis. Digital microscopy and SEM revealed enhanced surface roughness, porosity, and a microporous structure in the gel layer. SRXTM displayed interconnected pores, influencing the gel layer's strength, drug release patterns, and release mechanism. Real-time UV-visible imaging provided microscopic insights into tablet behavior and drug release. Effervescent matrix tablets demonstrated increased water penetration in HCl buffer, leading to finger-like and highly porous gel layer structures. Shifting to a phosphate buffer at pH 6.8 modified gel layer structures, significantly reducing the drug release rate and prolonging release. Numerical approximation, based on a developed mathematical model, estimated diffusion parameters during drug liberation studies. The mechanistic control of drug release in effervescent matrix tablets by effervescent agents and HPMC was clarified through the relationship between estimated diffusion parameters and drug release profiles. Scaling up *via* high-shear melt granulation was conducted to extend preformulation knowledge to the manufacturing phase. The IBU-P407 eutectic mixture served as a meltable binder, facilitating particle agglomeration into granules. Granules and tablets prepared at 70 ºC exhibited satisfactory appearance and physical characteristics. Variations in processing temperature significantly influenced granule properties, subsequently altering the physical attributes and dissolution behavior of the eutectic tablets. Understanding multiscale characteristics in pharmaceutical development provides valuable insights shaping future directions in pharmaceutical product design.

SUGGESTIONS

The implementation of multiscale characterization techniques aims to offer a multidimensional understanding of pharmaceutical product development. To further enhance our comprehension, it is recommended to employ computerized modeling, specifically utilizing the discrete element method (DEM) and computational fluid dynamics (CFD) in the context of high-shear melt granulation. This approach would yield valuable insights while minimizing material usage in comparison to experimental methods. Additionally, it is advisable to explore other pertinent experiments to augment our understanding of these systems. This includes the development of a more comprehensive mathematical model, the application of advanced techniques to characterize the impact of effervescent agents, and molecular modeling to study water and drug diffusion influenced by effervescent agents. Conducting comprehensive investigations will significantly contribute to a deeper insight into pharmaceutical product design and development.

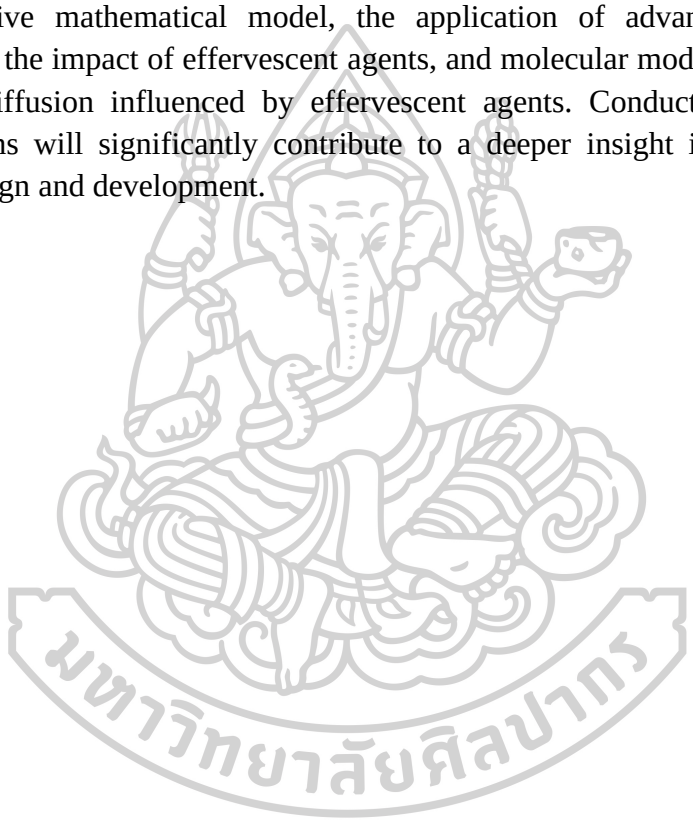

APPENDICES

Appendix I: Calibration curve for *in vitro* release study using dissolution apparatus II (paddle)

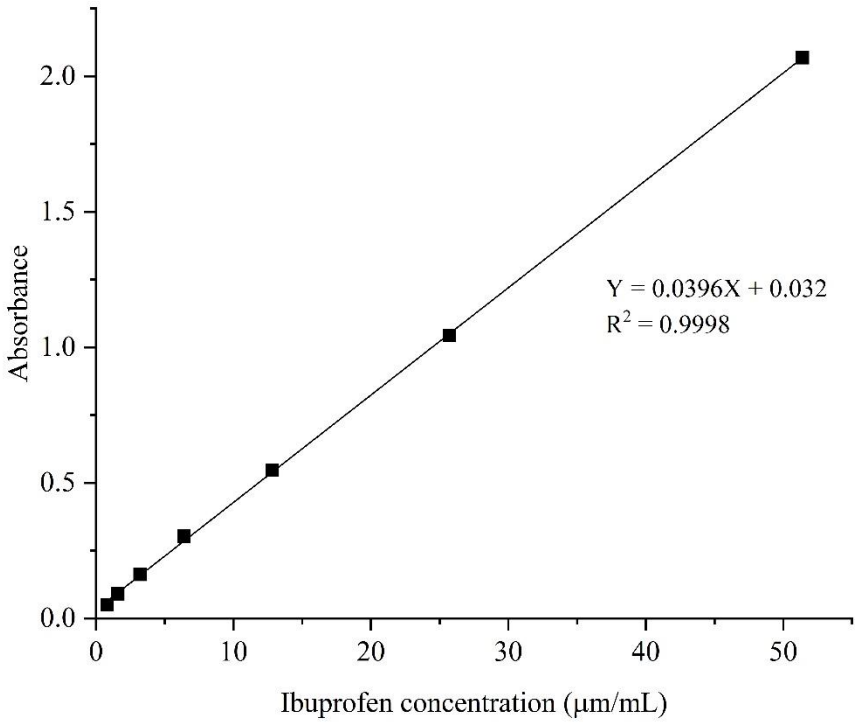

Figure 60. Calibration curve of IBU in 10% (v/v) methanol in 0.1 N HCl buffer pH 1.2

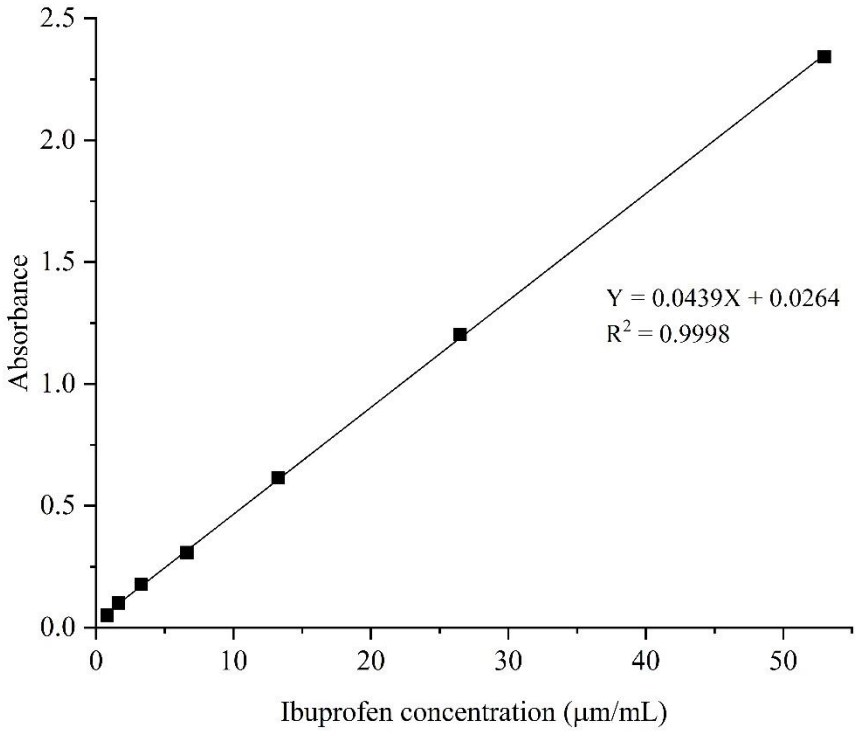

Figure 61. Calibration curve of IBU in 10% (v/v) methanol in phosphate buffer pH 6.8

Appendix II: Supplementary methods and data in UV-imaging technique

1. Selection of UV wavelength for quantification of ibuprofen concentration during dissolution experiment

To begin the study, UV spectra measurements of ibuprofen (IBU) were conducted in two different dissolution media: 0.1 N HCl buffer pH of 1.2 and 0.1 M phosphate buffer pH of 6.8. UV-Vis spectrophotometry was employed using a Cary 60 instrument from Agilent Technologies. IBU solutions with concentrations of 0.31 mM and 3.88 mM were prepared in the respective dissolution media.

The UV spectra of IBU revealed distinct characteristics in these two-dissolution media. In 0.1 N HCl buffer pH of 1.2, the highest absorbance of IBU solution was observed at around 220 nm. However, in the case of 0.1 M phosphate buffer pH of 6.8, the UV spectra displayed three peaks at wavelengths of 235 nm, 265 nm, and 273 nm. These findings were consistent with previous studies [253, 254]. While the SDi2 system could not provide the maximum wavelengths seen in the full UV spectra, it was determined that the wavelength of 255 nm could offer a sufficient signal for IBU quantification using the SDi2 system. Therefore, the wavelength of 255 nm was chosen for the UV calibration of IBU with the SDi2 system.

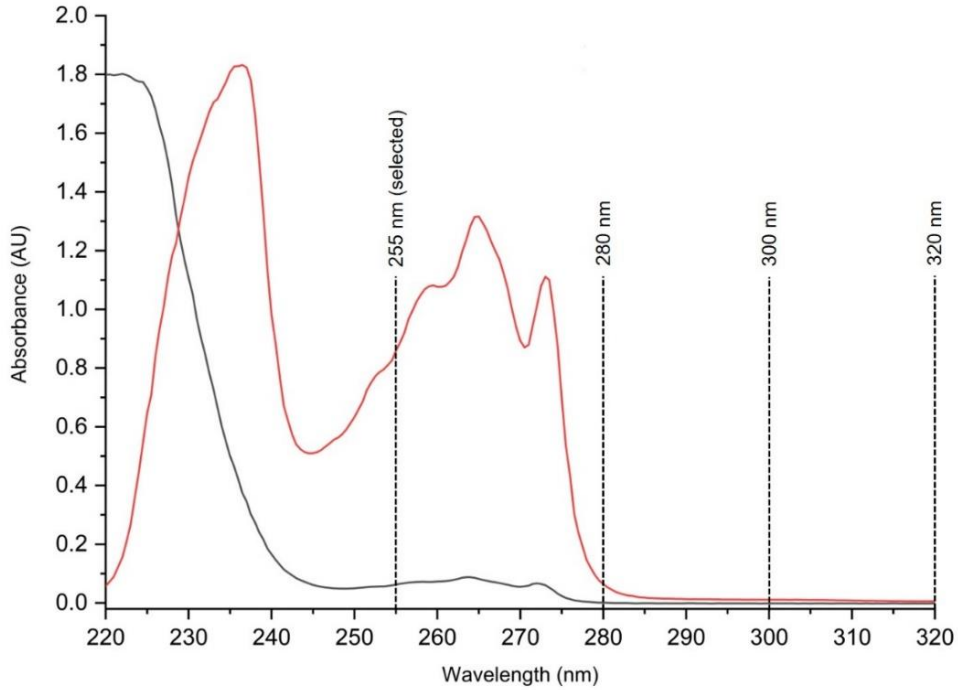

Figure 62. UV spectra of IBU in 0.1 N HCl buffer, pH 1.2 (red line; 0.31 mM of ibuprofen), and 0.1 M phosphate buffer, pH 6.8 (gray line; 3.88 mM of ibuprofen); using UV-Vis spectrophotometry.

2. Calibration of SDi2 system equipped with a USP IV type flow cell

In this study, UV calibration of ibuprofen (IBU) was performed using the whole dosage flow cell of the SDi2 system with two different dissolution media: 0.1 M phosphate buffer at pH 6.8 and 0.1 N HCl buffer at pH 1.2. Standard solutions of IBU were prepared at two different concentrations: 1.0 mg/mL for 0.1 M phosphate buffer at pH 6.8 and 0.1 mg/mL for 0.1 N HCl buffer at pH 1.2.

A whole dosage flow cell equipped with 1 mm glass beads was inserted into the SDi2 system, and a closed-loop configuration method was employed. Initially, the flow cell was filled with approximately 60 mL of the respective dissolution medium to capture the initial intensity (I_0) images. Then, the medium was pumped from the bottom to the top of the flow cell at a flow rate of 6.16 mL/min, with the experiments conducted at a temperature of 37°C. To establish a working standard concentration, a standard solution of IBU was introduced into the flow cell, creating a concentration range of 0.0012 to 0.0259 mg/mL in increments of 0.0012 mg/mL for 0.1 N HCl (pH 1.2) and 0.0165 to 0.2114 mg/mL in increments of 0.015 mg/mL for 0.1 M phosphate buffer (pH 6.8). The absorbance was continuously recorded at a wavelength of 255 nm for a duration of 5 minutes, with a 25-minute gap between each measurement of the working standard concentration. Data collection software was employed to record the measurements, and each working standard concentration was measured six times.

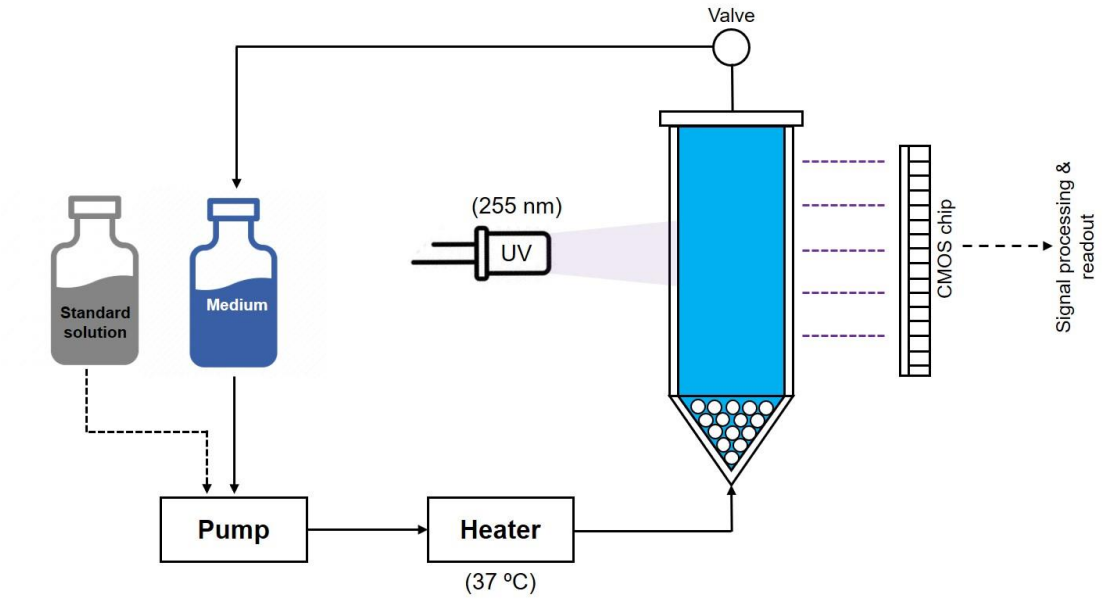

Figure 63. Set-up of SDi2 system equipped with USP IV type flow cell for IBU calibration

The calibration curve and representative UV images generated using different IBU concentrations in 0.1 N HCl buffer at pH 1.2 and 0.1 M phosphate buffer at pH 6.8 are presented in Figs. 63A and 63B, respectively. The calibration curves for IBU in

both acidic and neutral dissolution media exhibited a similar pattern and were fitted with a polynomial equation, as shown in Figs. 63A and 63B. The observed deviation from Beer's law at relatively low absorbance values, compared to conventional spectrophotometry, has been noted in previous studies. This limited linear range of UV imaging systems may be attributed to the design of the detector, which involves the conversion of UV light by a phosphorous layer into visible light that is then detected by the CMOS detector [255, 256].

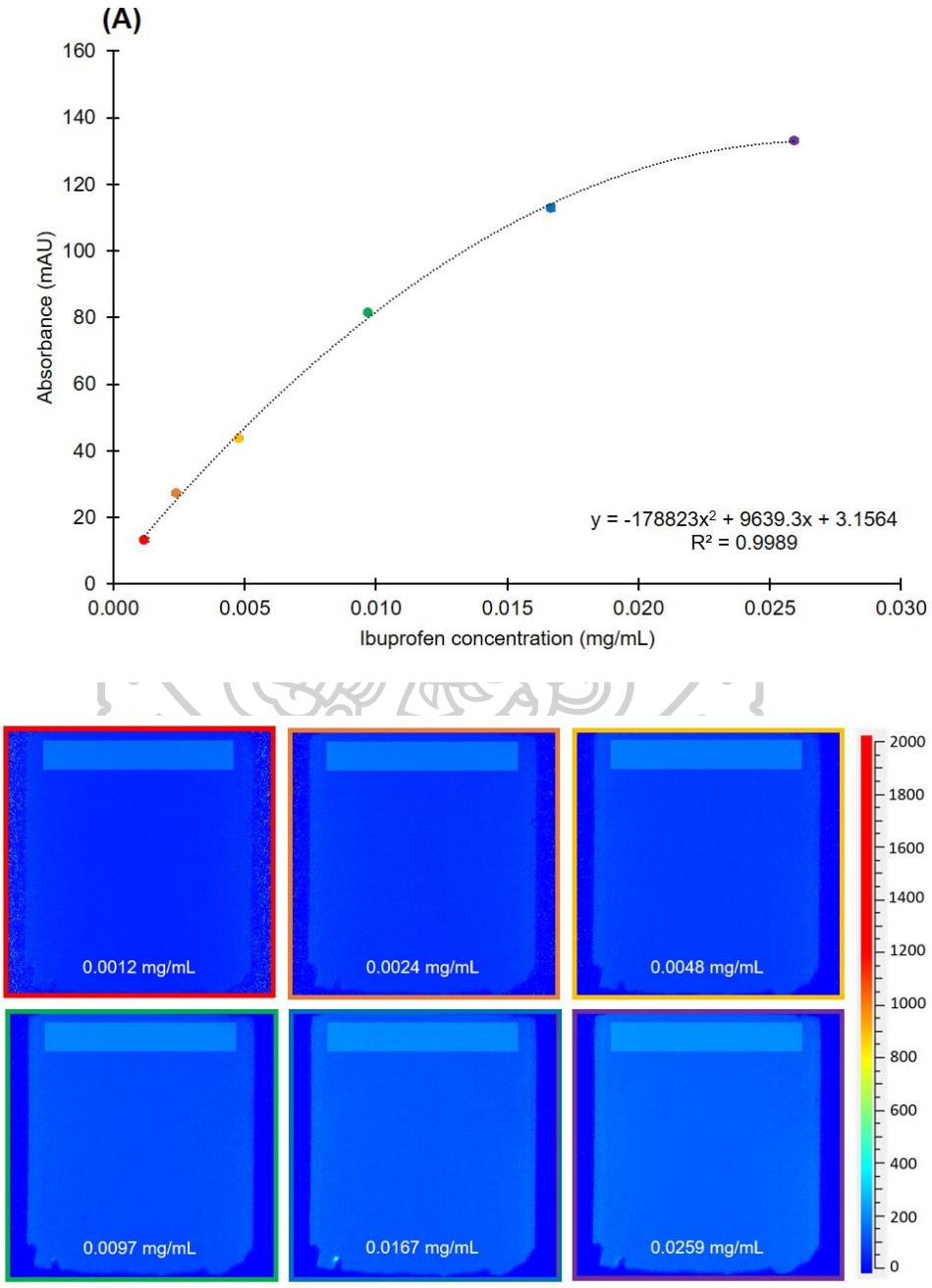

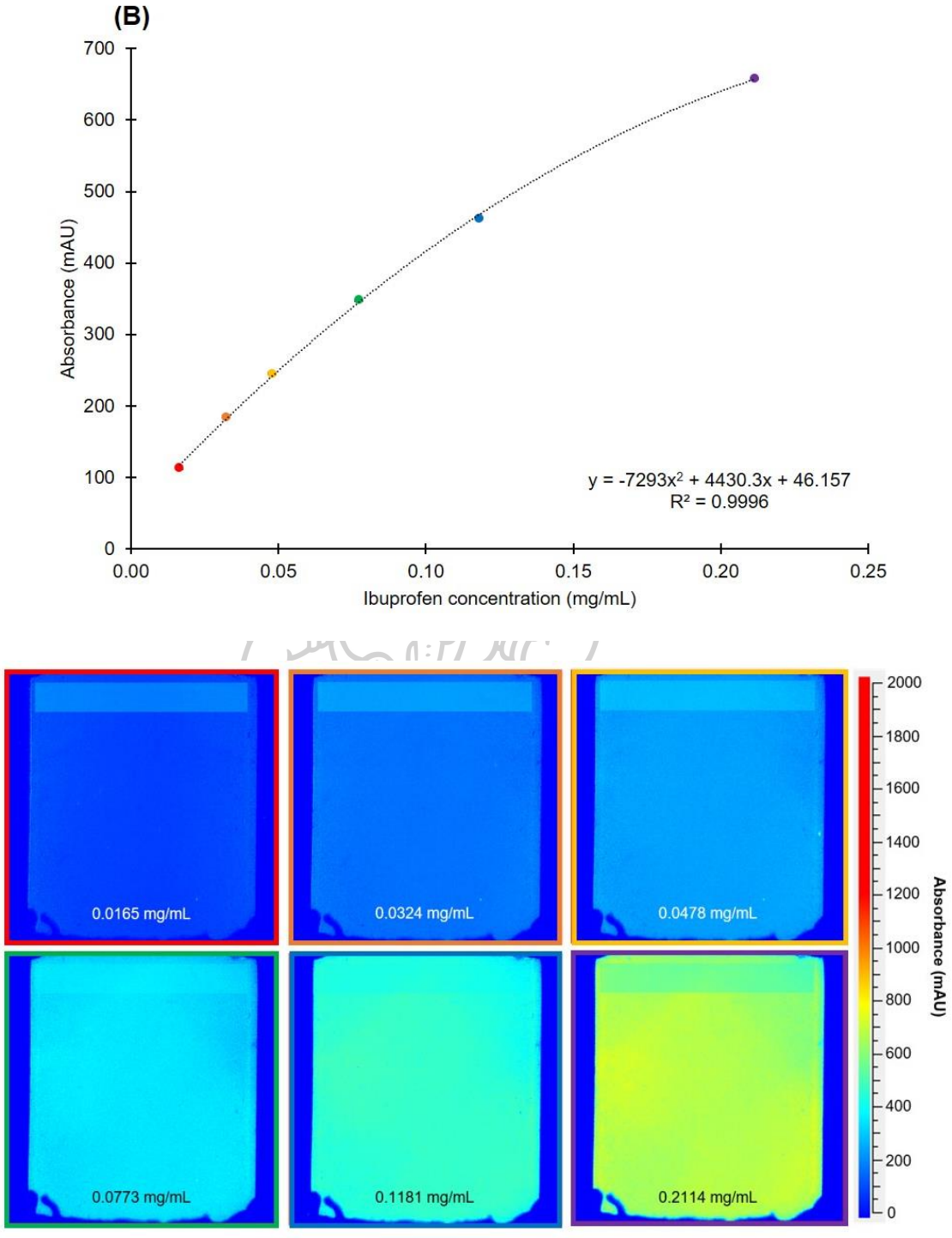

Figure 64. Calibration curve and representative UV images for IBU in 0.1 N HCl buffer, pH 1.2 (A) and 0.1 M phosphate buffer pH 6.8 (B). Wavelength used for UV analysis was 255 nm. Imaging area: 28×24 mm^2. Intense red color indicates high absorbance.

Appendix III: Differentiation processes and parameters substitution for estimation of water and drug diffusivities using numerical approximation based on mathematical model

1. Estimation of water diffusivity based on experimental data of water contents

Firstly, we have some hypotheses in modeling this system which are necessary to be noted:

(I) the radius and height of matrix tablet changes linearly with time

define: $$r = a_r t + b_r \quad (1)$$

$$z = a_z t + b_z \quad (2)$$

where a_r and a_z are the rate of tablet radius change and tablet height change with time, respectively, t is time and b_r and b_z denote the radius and height of matrix tablet at *t=0*, respectively.

(II) The change in tablet radius and height over time affects water concentration, as described by the following equations:

$$\frac{\partial C_w}{\partial r} = \frac{\partial C_w}{\partial t}\frac{\partial t}{\partial r} \quad (3)$$

$$\frac{\partial C_w}{\partial z} = \frac{\partial C_w}{\partial t}\frac{\partial t}{\partial z} \quad (4)$$

The first and second derivatives of Equations (3) and (4) can be calculated as following:

$$\frac{\partial C_w}{\partial r} = \frac{1}{a_r}\frac{\partial C_w}{\partial t} \quad (5)$$

$$\frac{\partial^2 C_w}{\partial r^2} = \left(\frac{1}{a_r}\right)^2 \frac{\partial^2 C_w}{\partial t^2} \quad (6)$$

$$\frac{\partial C_w}{\partial z} = \frac{1}{a_z}\frac{\partial C_w}{\partial t} \quad (7)$$

$$\frac{\partial^2 C_w}{\partial z^2} = \left(\frac{1}{a_z}\right)^2 \frac{\partial^2 C_w}{\partial t^2} \quad (8)$$

Considering: $$D_w = D_{w_{eq}} e^{-\beta_w\left(1-\frac{C_w}{C_{w_{eq}}}\right)} \quad (9)$$

The differentiation process of D_w in Equation (9) with respect to r and z, we obtain:

$$\frac{\partial D_w}{\partial r} = D_{w_{eq}} e^{-\beta_w\left(1-\frac{C_w}{C_{w_{eq}}}\right)} \frac{\beta_w}{C_{w_{eq}}} \frac{\partial C_w}{\partial r} = \frac{\beta_w}{C_{w_{eq}}} D_w \frac{\partial C_w}{\partial r} \qquad (10)$$

$$\frac{\partial D_w}{\partial z} = D_{w_{eq}} e^{-\beta_w\left(1-\frac{C_w}{C_{w_{eq}}}\right)} \frac{\beta_w}{C_{w_{eq}}} \frac{\partial C_w}{\partial z} = \frac{\beta_w}{C_{w_{eq}}} D_w \frac{\partial C_w}{\partial z} \qquad (11)$$

Considering Fick's second law:

$$\frac{\partial C_w}{\partial t} = \frac{\partial}{\partial r}\left(D_w \frac{\partial C_w}{\partial r}\right) + \frac{D_w}{r}\frac{\partial C_w}{\partial r} + \frac{\partial}{\partial z}\left(D_w \frac{\partial C_w}{\partial z}\right)$$

The Fick's second law can be expressed as follows:

$$\frac{\partial C_w}{\partial t} = D_w \frac{\partial}{\partial r}\left(\frac{\partial C_w}{\partial r}\right) + \frac{\partial D_w}{\partial r}\frac{\partial C_w}{\partial r} + \frac{D_w}{r}\frac{\partial C_w}{\partial r} + D_w \frac{\partial}{\partial z}\left(\frac{\partial C_w}{\partial z}\right) + \frac{\partial D_w}{\partial z}\frac{\partial C_w}{\partial z}. \qquad (12)$$

Substitute Equations (10) and (11) into Equation (12), we obtain:

$$\frac{\partial C_w}{\partial t} = D_w \frac{\partial^2 C_w}{\partial r^2} + \frac{\beta_w}{C_{w_{eq}}} D_w \left(\frac{\partial C_w}{\partial r}\right)^2 + \frac{D_w}{r}\frac{\partial C_w}{\partial r} + D_w \frac{\partial^2 C_w}{\partial z^2} + \frac{\beta_w}{C_{w_{eq}}} D_w \left(\frac{\partial C_w}{\partial z}\right)^2. \qquad (13)$$

Substitute Equations (3) and (4) into Equation (13), we acquire:

$$\frac{\partial C_w}{\partial t} = D_w \frac{\partial^2 C_w}{\partial r^2} + \frac{\beta_w}{C_{w_{eq}}} D_w \left(\frac{1}{a_r}\right)^2 \left(\frac{\partial C_w}{\partial t}\right)^2 + \frac{D_w}{r}\frac{1}{a_r}\frac{\partial C_w}{\partial t} + D_w \frac{\partial^2 C_w}{\partial z^2} + \frac{\beta_w}{C_{w_{eq}}} D_w \left(\frac{1}{a_z}\right)^2 \left(\frac{\partial C_w}{\partial t}\right)^2 \qquad (14)$$

Substitute Equations (6) and (8) into Equation (14), we have:

$$\frac{\partial C_w}{\partial t} = D_w \left(\frac{1}{a_r}\right)^2 \frac{\partial^2 C_w}{\partial t^2} + \frac{\beta_w}{C_{w_{eq}}} D_w \left(\frac{1}{a_r}\right)^2 \left(\frac{\partial C_w}{\partial t}\right)^2 + \frac{D_w}{r}\frac{1}{a_r}\frac{\partial C_w}{\partial t} + D_w \left(\frac{1}{a_z}\right)^2 \frac{\partial^2 C_w}{\partial t^2} + \frac{\beta_w}{C_{w_{eq}}} D_w \left(\frac{1}{a_z}\right)^2 \left(\frac{\partial C_w}{\partial t}\right)^2 \qquad (15)$$

After rearranging Equation (15), the resulting equation is:

$$\frac{\partial C_w}{\partial t} = \frac{1}{C_{w_{eq}}}\left(\left(\frac{1}{a_r}\right)^2 + \left(\frac{1}{a_z}\right)^2\right)\left(\frac{\partial C_w}{\partial t}\right)^2 \beta_w D_w + \left(\left(\frac{1}{a_r}\right)^2 \frac{\partial^2 C_w}{\partial t^2} + \frac{1}{r a_r}\frac{\partial C_w}{\partial t} + \left(\frac{1}{a_z}\right)^2 \frac{\partial^2 C_w}{\partial t^2}\right) D_w \quad (16)$$

Substitute Equation (9) into Equation (16), we have:

$$\frac{\partial C_w}{\partial t} = \frac{1}{C_{w_{eq}}}\left(\left(\frac{1}{a_r}\right)^2 + \left(\frac{1}{a_z}\right)^2\right)\left(\frac{\partial C_w}{\partial t}\right)^2 \beta_w D_{w_{eq}} e^{-\beta_w\left(1-\frac{C_w}{C_{w_{eq}}}\right)} + \left(\left(\frac{1}{a_r}\right)^2 \frac{\partial^2 C_w}{\partial t^2} + \frac{1}{r a_r}\frac{\partial C_w}{\partial t} + \left(\frac{1}{a_z}\right)^2 \frac{\partial^2 C_w}{\partial t^2}\right) D_{k_{eq}} e^{-\beta_w\left(1-\frac{C_w}{C_{w_{eq}}}\right)} \quad (17)$$

Define:

$$\tau = \left(\frac{1}{a_r}\right)^2 + \left(\frac{1}{a_z}\right)^2$$

Rearranging Equation (17), we obtain:

$$\frac{\partial C_w}{\partial t} = \frac{\tau}{C_{w_{eq}}}\left(\frac{\partial C_w}{\partial t}\right)^2 \beta_w D_{w_{eq}} e^{-\beta_w\left(1-\frac{C_w}{C_{w_{eq}}}\right)} + \left(\tau \frac{\partial^2 C_w}{\partial t^2} + \frac{1}{r_i a_r}\frac{\partial C_w}{\partial t}\right) D_{w_{eq}} e^{-\beta_w\left(1-\frac{C_w}{C_{w_{eq}}}\right)} \quad (18)$$

2. Estimation of drug diffusivity based on experimental data of water contents and drug release profiles

Firstly, we have some hypotheses in modeling this system which are necessary to be noted:

(I) the radius and height of matrix tablet changes linearly with time

Define: $$r = a_r t + b_r$$

$$z = a_z t + b_z$$

Where a_r and a_z are the rate of tablet radius change and tablet height change with time, respectively, t is time and b_r and b_z denote the radius and height of matrix tablet at *t=0*, respectively.

(II) The change in tablet radius and height over time affects drug concentration, as described by the following equations:

$$\frac{\partial C_d}{\partial r} = \frac{\partial C_d}{\partial t}\frac{\partial t}{\partial r} \quad (21)$$

$$\frac{\partial C_d}{\partial z} = \frac{\partial C_d}{\partial t}\frac{\partial t}{\partial z} \quad (22)$$

The first and second derivatives of Equations (21) and (22) can be calculated as following:

$$\frac{\partial C_d}{\partial r} = \frac{1}{a_r}\frac{\partial C_d}{\partial t} \quad (23)$$

$$\frac{\partial^2 C_d}{\partial r^2} = \left(\frac{1}{a_r}\right)^2 \frac{\partial^2 C_d}{\partial t^2} \quad (24)$$

$$\frac{\partial C_d}{\partial z} = \frac{1}{a_z}\frac{\partial C_d}{\partial t} \quad (25)$$

$$\frac{\partial^2 C_d}{\partial z^2} = \left(\frac{1}{a_z}\right)^2 \frac{\partial^2 C_d}{\partial t^2} \quad (26)$$

Considering: $$D_d = D_{d_{eq}} e^{-\beta_d\left(1-\frac{C_w}{C_{w_{eq}}}\right)} \quad (27)$$

The differentiation process of D_w in Equation (27) with respect to r and z, we obtain:

$$\frac{\partial D_d}{\partial r} = D_{d_{eq}} e^{-\beta_d\left(1-\frac{C_w}{C_{w_{eq}}}\right)} \frac{\beta_d}{C_{w_{eq}}}\frac{\partial C_w}{\partial r} = \frac{\beta_d}{C_{w_{eq}}} D_d \frac{\partial C_w}{\partial r} \quad (28)$$

$$\frac{\partial D_d}{\partial z} = D_{d_{eq}} e^{-\beta_d\left(1-\frac{C_w}{C_{w_{eq}}}\right)} \frac{\beta_d}{C_{w_{eq}}}\frac{\partial C_w}{\partial z} = \frac{\beta_d}{C_{w_{eq}}} D_d \frac{\partial C_w}{\partial z} \quad (29)$$

Considering Fick's second law:

$$\frac{\partial C_d}{\partial t} = \frac{\partial}{\partial r}\left(D_d \frac{\partial C_d}{\partial r}\right) + \frac{D_d}{r}\frac{\partial C_d}{\partial r} + \frac{\partial}{\partial z}\left(D_d \frac{\partial C_d}{\partial z}\right)$$

The Fick's second law can be expressed as follows:

$$\frac{\partial C_d}{\partial t} = D_d \frac{\partial}{\partial r}\left(\frac{\partial C_d}{\partial r}\right) + \frac{\partial D_d}{\partial r}\frac{\partial C_d}{\partial r} + \frac{D_d}{r}\frac{\partial C_d}{\partial r} + D_d \frac{\partial}{\partial z}\left(\frac{\partial C_d}{\partial z}\right) + \frac{\partial D_d}{\partial z}\frac{\partial C_d}{\partial z}. \quad (30)$$

Substitute Equations (28) and (29) into Equation (30), we obtain:

$$\frac{\partial C_d}{\partial t} = D_d \frac{\partial^2 C_d}{\partial r^2} + \frac{\beta_d}{C_{weq}} D_d \frac{\partial C_w}{\partial r}\frac{\partial C_d}{\partial r} + \frac{D_d}{r}\frac{\partial C_d}{\partial r} + D_d \frac{\partial^2 C_d}{\partial z^2} + \frac{\beta_d}{C_{weq}} D_d \frac{\partial C_w}{\partial z}\frac{\partial C_d}{\partial z}. \quad (31)$$

Substitute Equations (23) and (24) into Equation (31), we acquire:

$$\frac{\partial C_d}{\partial t} = D_d \frac{\partial^2 C_d}{\partial r^2} + \frac{\beta_d}{C_{weq}} D_d \left(\frac{1}{a_r}\right)^2 \frac{\partial C_w}{\partial t}\frac{\partial C_d}{\partial t} + \frac{D_d}{r}\frac{1}{a_r}\frac{\partial C_d}{\partial t} + D_d \frac{\partial^2 C_d}{\partial z^2} + \frac{\beta_d}{C_{weq}} D_d \left(\frac{1}{a_z}\right)^2 \frac{\partial C_w}{\partial t}\frac{\partial C_d}{\partial t} \quad (32)$$

Substitute Equations (24) and (26) into Equation (32), we have:

$$\frac{\partial C_d}{\partial t} = D_d \left(\frac{1}{a_r}\right)^2 \frac{\partial^2 C_d}{\partial t^2} + \frac{\beta_d}{C_{weq}} D_d \left(\frac{1}{a_r}\right)^2 \frac{\partial C_w}{\partial t}\frac{\partial C_d}{\partial t} + \frac{D_d}{r}\frac{1}{a_r}\frac{\partial C_d}{\partial t} + D_d \left(\frac{1}{a_z}\right)^2 \frac{\partial^2 C_d}{\partial t^2} + \frac{\beta_d}{C_{weq}} D_d \left(\frac{1}{a_z}\right)^2 \frac{\partial C_w}{\partial t}\frac{\partial C_d}{\partial t} \quad (33)$$

After rearranging Equation (33), the resulting equation is:

$$\frac{\partial C_d}{\partial t} = \frac{1}{C_{weq}}\left(\left(\frac{1}{a_r}\right)^2 + \left(\frac{1}{a_z}\right)^2\right)\frac{\partial C_w}{\partial t}\frac{\partial C_d}{\partial t}\beta_d D_d + \left(\left(\frac{1}{a_r}\right)^2 \frac{\partial^2 C_d}{\partial t^2} + \frac{1}{r a_r}\frac{\partial C_d}{\partial t} + \left(\frac{1}{a_z}\right)^2 \frac{\partial^2 C_d}{\partial t^2}\right) D_d \quad (34)$$

Substitute Equation (27) into Equation (34), we have:

$$\frac{\partial C_d}{\partial t} = \frac{1}{C_{w_{eq}}}\left(\left(\frac{1}{a_r}\right)^2 + \left(\frac{1}{a_z}\right)^2\right)\frac{\partial C_w}{\partial t}\frac{\partial C_d}{\partial t}\beta_d D_{d_{eq}} e^{-\beta_d\left(1-\frac{C_w}{C_{w_{eq}}}\right)} + \left(\left(\frac{1}{a_r}\right)^2\frac{\partial^2 C_d}{\partial t^2} + \frac{1}{r a_r}\frac{\partial C_d}{\partial t} + \left(\frac{1}{a_z}\right)^2\frac{\partial^2 C_d}{\partial t^2}\right) D_{d_{eq}} e^{-\beta_d\left(1-\frac{C_w}{C_{w_{eq}}}\right)} \quad (35)$$

Rearranging Equation (35), we obtain:

$$\frac{\partial C_d}{\partial t} = \frac{\tau}{C_{w_{eq}}}\frac{\partial C_w}{\partial t}\frac{\partial C_d}{\partial t}\beta_d D_{d_{eq}} e^{-\beta_d\left(1-\frac{C_w}{C_{w_{eq}}}\right)} + \left(\tau\frac{\partial^2 C_d}{\partial t^2} + \frac{1}{r_i a_r}\frac{\partial C_d}{\partial t}\right) D_{d_{eq}} e^{-\beta_d\left(1-\frac{C_w}{C_{w_{eq}}}\right)} \quad (36)$$

REFERENCES

1. Fuhrmann K, Fuhrmann G. Recent advances in oral delivery of macromolecular drugs and benefits of polymer conjugation. Curr Opin Colloid Interface Sci. 2017;31:67-74.
2. Zhou Z, Dunn C, Khadra I, Wilson CG, Halbert GW. Statistical investigation of simulated fed intestinal media composition on the equilibrium solubility of oral drugs. Eur J Pharm Sci. 2017;99:95-104.
3. Göke K, Lorenz T, Repanas A, Schneider F, Steiner D, Baumann K, et al. Novel strategies for the formulation and processing of poorly water-soluble drugs. Eur J Pharm Biopharm 2018:40-56.
4. Jermain SV, Brough C, Williams RO. Amorphous solid dispersions and nanocrystal technologies for poorly water-soluble drug delivery – An update. Int J Pharm 2018;535(1–2):379-92.
5. Leuner C, Dressman J. Improving drug solubility for oral delivery using solid dispersions. Eur J Pharm Biopharm. 2000;50(1):47-60.
6. Espíndola BD, Beringhs AOR, Sonaglio D, Stulzer HK, Silva MAS, Ferraz HG, et al. Liquisolid pellets: A pharmaceutical technology strategy to improve the dissolution rate of ritonavir. Saudi Pharm J 2019;27(5):702-12.
7. França MT, Marcos TM, Pereira RN, Stulzer HK. Could the small molecules such as amino acids improve aqueous solubility and stabilize amorphous systems containing Griseofulvin? Eur J Pharm Sci. 2020;143:105178.
8. Pinto JMO, Leão AF, Alves GF, Mendes C, França MT, Fernandes D, et al. New supersaturating drug delivery system as strategy to improve apparent solubility of candesartan cilexetil in biorelevant medium. Pharm Dev Technol. 2020;25(1):89-99.
9. Shi Q, Moinuddin SM, Cai T. Advances in coamorphous drug delivery systems. Acta Pharm Sin B. 2019;9(1):19-35.
10. Al-Dalaen SMI, Hamad AWR, Al-Hujran TA, Al-Btoush HA, Al-Halaseh L, Magharbeh MK, et al. Bioavailability and bioequivalence of two oral single dose of ibuprofen 400 mg to healthy volunteers. Biomed Pharmacol. 2021;14(1):435-44.
11. Tarabar S, Kelsh D, Vince B, Leyva R, Song D, Matschke K, et al. Phase I Pharmacokinetic Study of Fixed-Dose Combinations of Ibuprofen and Acetaminophen in Healthy Adult and Adolescent Populations. DRUGS R&D. 2020;20(1):23-37.
12. Guidance for industry, waiver of in vivo bioavailability and bioequivalence studies for immediate release solid oral dosage forms based on a biopharmaceutics classification system [Internet]. [cited 25 July 2021]. Available from: https: //www.fda.gov/downloads/Drugs/Guidances/ucm070246.pdf.
13. Potthast H, Dressman JB, Junginger HE, Midha KK, Oeser H, Shah VP, et al. Biowaiver Monographs for Immediate Release Solid Oral Dosage Forms: Ibuprofen. J Pharm Sci. 2005;94(10):2121-31.
14. Kabanov AV, Batrakova EV, Alakhov VY. Pluronic® block copolymers as novel polymer therapeutics for drug and gene delivery. J Control Release. 2002;82(2):189-212.

15. Takáts Z, Vékey K, Hegedüs L. Qualitative and quantitative determination of poloxamer surfactants by mass spectrometry. Rapid Commun Mass Spectrom. 2001;15(10):805-10.
16. Ghebremeskel AN, Vemavarapu C, Lodaya M. Use of Surfactants as Plasticizers in Preparing Solid Dispersions of Poorly Soluble API: Stability Testing of Selected Solid Dispersions. Pharm Res. 2006;23(8):1928-36.
17. Ali W, Williams AC, Rawlinson CF. Stochiometrically governed molecular interactions in drug: Poloxamer solid dispersions. Int J Pharm. 2010;391(1):162-8.
18. Al Masum MA, Sharmin F, Islam RB, Islam MA, Islam SMA. Application of solid dispersion technique in improving solubility of ibuprofen by poloxamers. BioMedRx. 2013;1(5):498-505.
19. Newa M, Bhandari KH, Oh DH, Kim YR, Sung JH, Kim JO, et al. Enhanced dissolution of ibuprofen using solid dispersion with poloxamer 407. Arch Pharm Res. 2008;31(11):1497-507.
20. Dugar RP, Gajera BY, Dave RH. Fusion Method for Solubility and Dissolution Rate Enhancement of Ibuprofen Using Block Copolymer Poloxamer 407. AAPS PharmSciTech. 2016;17(6):1428-40.
21. Phaechamud T. Variables Influencing Drug Release from Layered Matrix System Comprising Hydroxypropyl Methylcellulose. AAPS PharmSciTech. 2008;9(2):668-74.
22. Tiwari SB, Murthy TK, Raveendra Pai M, Mehta PR, Chowdary PB. Controlled release formulation of tramadol hydrochloride using hydrophilic and hydrophobic matrix system. AAPS PharmSciTech. 2003;4(3):18-23.
23. Maggi L, Segale L, Torre ML, Ochoa Machiste E, Conte U. Dissolution behaviour of hydrophilic matrix tablets containing two different polyethylene oxides (PEOs) for the controlled release of a water-soluble drug. Dimensionality study. Biomaterials. 2002;23(4):1113-9.
24. Conti S, Maggi L, Segale L, Ochoa Machiste E, Conte U, Grenier P, et al. Matrices containing NaCMC and HPMC: 1. Dissolution performance characterization. Int J Pharm. 2007;333(1):136-42.
25. Siahi-Shadbad MR, Asare-Addo K, Azizian K, Hassanzadeh D, Nokhodchi A. Release Behaviour of Propranolol HCl from Hydrophilic Matrix Tablets Containing Psyllium Powder in Combination with Hydrophilic Polymers. AAPS PharmSciTech. 2011;12(4):1176-82.
26. Dabbagh MA, Ford JL, Rubinstein MH, Hogan JE. Effects of polymer particle size, compaction pressure and hydrophilic polymers on drug release from matrices containing ethylcellulose. Int J Pharm. 1996;140(1):85-95.
27. Nerurkar J, Jun HW, Price JC, Park MO. Controlled-release matrix tablets of ibuprofen using cellulose ethers and carrageenans: effect of formulation factors on dissolution rates. Eur J Pharm Biopharm. 2005;61(1):56-68.
28. Obaidat AA, Obaidat RM. Controlled release of tramadol hydrochloride from matrices prepared using glyceryl behenate. Eur J Pharm Biopharm. 2001;52(2):231-5.
29. Jannin V, Pochard E, Chambin O. Influence of poloxamers on the dissolution performance and stability of controlled-release formulations containing Precirol® ATO 5. Int J Pharm. 2006;309(1):6-15.

30. Jannin V, Leccia E, Rosiaux Y, Doucet J. Evolution of the microstructure of sustained-release matrix tablets during dissolution and storage. Indian J Pharm Sci. 2018;80(6):1011-20.
31. Stepanek F, Loo A, Lim TS. Multiscale Modelling Methodology for Virtual Prototyping of Effervescent Tablets. J Pharm Sci. 2006;95(7):1614-25.
32. Avalle P, Pygall SR, Gower N, Midwinter A. The use of in situ near infrared spectroscopy to provide mechanistic insights into gel layer development in HPMC hydrophilic matrices. Eur J Pharm Sci. 2011;43(5):400-8.
33. Avalle P, Pygall SR, Pritchard J, Jastrzemska A. Interrogating erosion-based drug liberation phenomena from hydrophilic matrices using near infrared (NIR) spectroscopy. Eur J Pharm Sci. 2013;48(1):72-9.
34. Tomer G, Newton JM, Kinchesh P. Magnetic Resonance Imaging (MRI) as a Method to Investigate Movement of Water During the Extrusion of Pastes. Pharm Res. 1999;16(5):666-71.
35. Kaunisto E, Abrahmsen-Alami S, Borgquist P, Larsson A, Nilsson B, Axelsson A. A mechanistic modelling approach to polymer dissolution using magnetic resonance microimaging. J Control Release. 2010;147(2):232-41.
36. Kulinowski P, Dorożyński P, Młynarczyk A, Węglarz WP. Magnetic Resonance Imaging and Image Analysis for Assessment of HPMC Matrix Tablets Structural Evolution in USP Apparatus 4. Pharm Res. 2011;28(5):1065-73.
37. Ashraf M, luorno VL, Coffin-Beach D, Evans CA, Augsburger LL. A Novel Nuclear Magnetic Resonance (NMR) Imaging Method for Measuring the Water Front Penetration Rate in Hydrophilic Polymer Matrix Capsule Plugs and Its Role in Drug Release. Pharm Res. 1994;11(5):733-7.
38. Rajabi-Siahboomi AR, Bowtell RW, Mansfield P, Davies MC, Melia CD. Structure and Behavior in Hydrophilic Matrix Sustained Release Dosage Forms: 4. Studies of Water Mobility and Diffusion Coefficients in the Gel Layer of HPMC Tablets Using NMR Imaging. Pharm Res. 1996;13(3):376-80.
39. Markl D, Strobel A, Schlossnikl R, Bøtker J, Bawuah P, Ridgway C, et al. Characterisation of pore structures of pharmaceutical tablets: A review. Int J Pharm. 2018;538(1):188-214.
40. Yassin S, Su K, Lin H, Gladden LF, Zeitler JA. Diffusion and Swelling Measurements in Pharmaceutical Powder Compacts Using Terahertz Pulsed Imaging. J Pharm Sci. 2015;104(5):1658-67.
41. Pygall SR, Whetstone J, Timmins P, Melia CD. Pharmaceutical applications of confocal laser scanning microscopy: The physical characterisation of pharmaceutical systems. Adv Drug Deliv Rev. 2007;59(14):1434-52.
42. Melia CD, Marshall P, Stark P, Cunningham S, Kinahan A, Devane J. Investigating in Vitro Drug Release Mechanisms Inside Dosage Forms. In: Young D, Devane JG, Butler J, editors. In Vitro-in Vivo Correlations. Boston, MA: Springer US; 1997. p. 129-35.
43. Asare-Addo K, Walton K, Ward A, Totea A-M, Taheri S, Alshafiee M, et al. Direct imaging of the dissolution of salt forms of a carboxylic acid drug. Int J Pharm. 2018;551(1):290-9.
44. Asare-Addo K, Alshafiee M, Walton K, Ward A, Totea A-M, Taheri S, et al. Effect of preparation method on the surface properties and UV imaging of indomethacin solid dispersions. Eur J Pharm Biopharm. 2019;137:148-63.

45. Østergaard J, Meng-Lund E, Larsen SW, Larsen C, Petersson K, Lenke J, et al. Real-Time UV Imaging of Nicotine Release from Transdermal Patch. Pharm Res. 2010;27(12):2614-23.
46. Pajander J, Baldursdottir S, Rantanen J, Østergaard J. Behaviour of HPMC compacts investigated using UV-imaging. Int J Pharm. 2012;427(2):345-53.
47. Ward A, Walton K, Mawla N, Kaialy W, Liu L, Timmins P, et al. Development of a novel method utilising dissolution imaging for the measurement of swelling behaviour in hydrophilic matrices. Int J Pharm. 2019;1:100013.
48. Yin X, Li H, Liu R, Chen J, Ji J, Chen J, et al. Fractal structure determines controlled release kinetics of monolithic osmotic pump tablets. J Pharm Pharmacol. 2013;65(7):953-9.
49. Yin X, Li H, Guo Z, Wu L, Chen F, de Matas M, et al. Quantification of Swelling and Erosion in the Controlled Release of a Poorly Water-Soluble Drug Using Synchrotron X-ray Computed Microtomography. AAPS Journal. 2013;15(4):1025-34.
50. Maderuelo C, Zarzuelo A, Lanao JM. Critical factors in the release of drugs from sustained release hydrophilic matrices. J Control Release. 2011;154(1):2-19.
51. Colombo P, Bettini R, Santi P, Peppas NA. Swellable matrices for controlled drug delivery: gel-layer behaviour, mechanisms and optimal performance. Pharm Sci Tech Today. 2000;3(6):198-204.
52. Colombo P, Bettini R, Peppas NA. Observation of swelling process and diffusion front position during swelling in hydroxypropyl methyl cellulose (HPMC) matrices containing a soluble drug. J Control Release. 1999;61(1):83-91.
53. Hardy IJ, Windberg-Baarup A, Neri C, Byway PV, Booth SW, Fitzpatrick S. Modulation of drug release kinetics from hydroxypropyl methyl cellulose matrix tablets using polyvinyl pyrrolidone. Int J Pharm. 2007;337(1):246-53.
54. Siepmann J, Siepmann F. Mathematical modeling of drug delivery. Int J Pharm. 2008;364(2):328-43.
55. Siepmann J, Peppas NA. Hydrophilic Matrices for Controlled Drug Delivery: An Improved Mathematical Model to Predict the Resulting Drug Release Kinetics (the "sequential Layer" Model). Pharm Res. 2000;17(10):1290-8.
56. Siepmann J, Peppas NA. Modeling of drug release from delivery systems based on hydroxypropyl methylcellulose (HPMC). Adv Drug Deliv Rev. 2001;48(2):139-57.
57. Siepmann J, Podual K, Sriwongjanya M, Peppas NA, Bodmeier R. A New Model Describing the Swelling and Drug Release Kinetics from Hydroxypropyl Methylcellulose Tablets. J Pharm Sci. 1999;88(1):65-72.
58. Ramesh N, Davis PK, Zielinski JM, Danner RP, Duda JL. Application of free-volume theory to self diffusion of solvents in polymers below the glass transition temperature: A review. J Polym Sci B Polym Phys. 2011;49(23):1629-44.
59. Fujita H, editor Diffusion in polymer-diluent systems. Fortschritte Der Hochpolymeren-Forschung; 1961; Berlin, Heidelberg: Springer Berlin Heidelberg.
60. Wong TW, Cheong WS, Heng PWS. Melt granulation and pelletization. In: Parikh DM, editor. Handbook of Pharmaceutical Granulation Technology. 2 ed. Boca Raton: CRC Press; 2005.
61. Passerini N, Calogerà G, Albertini B, Rodriguez L. Melt granulation of pharmaceutical powders: A comparison of high-shear mixer and fluidised bed processes. Int J Pharm. 2010;391(1):177-86.

62. Daisy S, Mohit S, Sandeep K, Gupta G. Solubility enhancement – eminent role in poorly soluble drugs. Res J Pharm Technol. 2009;2(2):220-4.
63. Sareen S, Mathew G, Joseph L. Improvement in solubility of poor water-soluble drugs by solid dispersion. Int J Pharm Investig. 2012;2(1):12-7.
64. Choi J-S, Lee S-E, Jang WS, Byeon JC, Park J-S. Solid dispersion of dutasteride using the solvent evaporation method: Approaches to improve dissolution rate and oral bioavailability in rats. Mater Sci Eng C. 2018;90:387-96.
65. Xu W, Sun Y, Du L, Chistyachenko YS, Dushkin AV, Su W. Investigations on solid dispersions of valsartan with alkalizing agents: Preparation, characterization and physicochemical properties. J Drug Deliv Sci Technol. 2018;44:399-405.
66. Choi J-S, Kwon S-H, Lee S-E, Jang WS, Byeon JC, Jeong HM, et al. Use of acidifier and solubilizer in tadalafil solid dispersion to enhance the in vitro dissolution and oral bioavailability in rats. Int J Pharm. 2017;526(1):77-87.
67. Mohammadian M, Salami M, Momen S, Alavi F, Emam-Djomeh Z, Moosavi-Movahedi AA. Enhancing the aqueous solubility of curcumin at acidic condition through the complexation with whey protein nanofibrils. Food Hydrocoll. 2019;87:902-14.
68. Chen X, McClements DJ, Zhu Y, Chen Y, Zou L, Liu W, et al. Enhancement of the solubility, stability and bioaccessibility of quercetin using protein-based excipient emulsions. Int Food Res J. 2018;114:30-7.
69. Kim CH, Lee SG, Kang MJ, Lee S, Choi YW. Surface modification of lipid-based nanocarriers for cancer cell-specific drug targeting. J Pharm Investig. 2017;47(3):203-27.
70. Karashima M, Sano N, Yamamoto S, Arai Y, Yamamoto K, Amano N, et al. Enhanced pulmonary absorption of poorly soluble itraconazole by micronized cocrystal dry powder formulations. Eur J Pharm Biopharm. 2017;115:65-72.
71. Seo B, Kim T, Park HJ, Kim J-Y, Lee KD, Lee JM, et al. Extension of the Hansen solubility parameter concept to the micronization of cyclotrimethylenetrinitramine crystals by supercritical anti-solvent process. J Supercrit Fluids. 2016;111:112-20.
72. Wong JJL, Yu H, Lim LM, Hadinoto K. A trade-off between solubility enhancement and physical stability upon simultaneous amorphization and nanonization of curcumin in comparison to amorphization alone. Eur J Pharm Sci. 2018;114:356-63.
73. Park J-B, Park C, Piao ZZ, Amin HH, Meghani NM, Tran PHL, et al. pH-independent controlled release tablets containing nanonizing valsartan solid dispersions for less variable bioavailability in humans. J Drug Deliv Sci Technol. 2018;46:365-77.
74. Chen B-Q, Kankala RK, Wang S-B, Chen A-Z. Continuous nanonization of lonidamine by modified-rapid expansion of supercritical solution process. J Supercrit Fluids. 2018;133:486-93.
75. Huang Y, Zhang B, Gao Y, Zhang J, Shi L. Baicalein–Nicotinamide Cocrystal with Enhanced Solubility, Dissolution, and Oral Bioavailability. J Pharm Sci. 2014;103(8):2330-7.
76. Liu X, Feng X, Williams RO, Zhang F. Characterization of amorphous solid dispersions. J Pharm Investig. 2018;48(1):19-41.
77. Zhao Y, Xie X, Zhao Y, Gao Y, Cai C, Zhang Q, et al. Effect of plasticizers on manufacturing ritonavir/copovidone solid dispersions via hot-melt extrusion:

Preformulation, physicochemical characterization, and pharmacokinetics in rats. Eur J Pharm Sci. 2019;127:60-70.
78. Smeets A, Koekoekx R, Clasen C, Van den Mooter G. Amorphous solid dispersions of darunavir: Comparison between spray drying and electrospraying. Eur J Pharm Biopharm. 2018;130:96-107.
79. Cherukuvada S, Nangia A. Eutectics as improved pharmaceutical materials: design, properties and characterization. Chem Commun. 2014;50(8):906-23.
80. Zainal-Abidin MH, Hayyan M, Ngoh GC, Wong WF, Looi CY. Emerging frontiers of deep eutectic solvents in drug discovery and drug delivery systems. J Control Release. 2019;316:168-95.
81. Hyun S-M, Lee BJ, Abuzar SM, Lee S, Joo Y, Hong S-H, et al. Preparation, characterization, and evaluation of celecoxib eutectic mixtures with adipic acid/saccharin for improvement of wettability and dissolution rate. Int J Pharm. 2019;554:61-71.
82. Alshaikh RA, Essa EA, El Maghraby GM. Eutexia for enhanced dissolution rate and anti-inflammatory activity of nonsteroidal anti-inflammatory agents: Caffeine as a melting point modulator. Int J Pharm. 2019;563:395-405.
83. Bazzo GC, Mostafa D, França MT, Pezzini BR, Stulzer HK. How tenofovir disoproxil fumarate can impact on solubility and dissolution rate of efavirenz? Int J Pharm. 2019;570:118597.
84. Araya-Sibaja AM, Vega-Baudrit JR, Guillén-Girón T, Navarro-Hoyos M, Cuffini SL. Drug Solubility Enhancement through the Preparation of Multicomponent Organic Materials: Eutectics of Lovastatin with Carboxylic Acids. Pharmaceutics. 2019;11(3):112.
85. Bi M, Hwang S-J, Morris KR. Mechanism of eutectic formation upon compaction and its effects on tablet properties. Thermochim Acta. 2003;404(1):213-26.
86. Bazzo GC, Pezzini BR, Stulzer HK. Eutectic mixtures as an approach to enhance solubility, dissolution rate and oral bioavailability of poorly water-soluble drugs. Int J Pharm. 2020;588:119741.
87. Haneef J, Chadha R. Antioxidant-Based Eutectics of Irbesartan: Viable Multicomponent Forms for the Management of Hypertension. AAPS PharmSciTech. 2018;19(3):1191-204.
88. Hao H, Wang G, Sun J. Enantioselective Pharmacokinetics of Ibuprofen and Involved Mechanisms. Drug Metab Rev. 2005;37(1):215-34.
89. Moghimi SM, Hunter AC. Poloxamers and poloxamines in nanoparticle engineering and experimental medicine. Trends Biotechnol. 2000;18(10):412-20.
90. Kolašinac N, Kachrimanis K, Homšek I, Grujić B, Đurić Z, Ibrić S. Solubility enhancement of desloratadine by solid dispersion in poloxamers. Int J Pharm. 2012;436(1):161-70.
91. Shah TJ, Amin AF, Parikh JR, Parikh RH. Process optimization and characterization of poloxamer solid dispersions of a poorly water-soluble drug. AAPS PharmSciTech. 2007;8(2):E18-E24.
92. Takeda B, Jadhao U, Thakre V, Bhortake L. Formulation and evaluation of diclofenac sodium effervescent tablet. IPP. 2014;2:350-8.
93. Stahl H. Effervescent dosage manufacturing. Pharm Technol Europe. 2003;15(4):25-8.

94. Rajlakshmi G, Vamsi C, Balchandar R, Damodharan N. Formulation and evaluation of effervescent tablets of diclofenac potassium. Int J Pharm Biomed Res. 2011;2(4):237-43.
95. Lindberg N, Hansson H. Effervescent pharmaceuticals. In: Swarbrick J, editor. Encyclopedia of pharmaceutical technology. New York: Informa Healthcare; 2007. p. 1454-65.
96. Schmidt P, Brogmann B. Effervescent tablets: choice of a new binder for ascorbic acid. Acta Pharm Technol. 1988;34:22-6.
97. Wade A, Weller P. Handbook of Pharmaceutical Excipients. 2 ed. Washington and London: The American Pharmaceutical Association and the Pharmaceutical Society of Great Britain; 1994.
98. Chen X, Wen H, Park K. Challenges and new technologies of oral controlled release. In: Wen H, Park K, editors. Oral controlled release formulation design and drug delivery: theory to practice. New Jersey: John Wiley & Sons, Inc.; 2010.
99. Nair A, Vyas H, Kumar A. Controlled release matrix uncoated tablets of enalapril maleate using HPMC alone. J Basic Clin Pharm. 2010;1(2):71-5.
100. Rajput G, Majmudar F, Jayvadan P, Thakor R, Rajgor N. Stomach-specific mucoadhesive microsphere as a controlled drug delivery system. Sys Rev Pharm. 2010;1(1):36-44.
101. Kojima H, Yoshihara K, Sawada T, Kondo H, Sako K. Extended release of a large amount of highly water-soluble diltiazem hydrochloride by utilizing counter polymer in polyethylene oxides (PEO)/polyethylene glycol (PEG) matrix tablets. Eur J Pharm Biopharm. 2008;70(2):556-62.
102. Aulton's pharmaceutics; the design and manufacture of medicines. Philadelphia: Churchill Livingstone Elsevier; 2008.
103. Sudha BS, Sridhar BK, Srinatha A. Modulation of Tramadol Release from a Hydrophobic Matrix: Implications of Formulations and Processing Variables. AAPS PharmSciTech. 2010;11(1):433-40.
104. Reza M, Quadir M, Haider S. Comparative evaluation of plastic, hydrophobic and hydrophilic polymers as matrices for controlled-release drug delivery. J Pharm Sci. 2003;6(2):282-91.
105. Brady J, Dürig T, Shang S. Developing Solid Oral Dosage Forms Pharmaceutical Theory & Practice. New York: Esselvier; 2009.
106. Lee HY, Chan LW, Heng PWS. Influence of partially cross-linked alginate used in the production of alginate microspheres by emulsification. J Microencapsul. 2005;22(3):275-80.
107. Lee PI. Kinetics of drug release from hydrogel matrices. J Control Release. 1985;2:277-88.
108. Colombo P. Swelling-controlled release in hydrogel matrices for oral route. Adv Drug Deliv Rev. 1993;11(1):37-57.
109. Sai Cheong Wan L, Wan Sia Heng P, Fun Wong L. Matrix swelling: A simple model describing extent of swelling of HPMC matrices. Int J Pharm. 1995;116(2):159-68.
110. Amigo J, Ravn C. Direct quantification and distribution assessment of major and minor components in pharmaceutical tablets by NIR-chemical imaging. Eur J Pharm Sci. 2009;37:76-82.

111. Zeng Q, Wang L, Wu S, Fang G, Zhao M, Li Z, et al. Research progress on the application of spectral imaging technology in pharmaceutical tablet analysis. Int J Pharm. 2022;625.
112. Østergaard J, Lenke J, Sun Y, Ye F. UV imaging for in vitro dissolution and release studies: intial experiences. Dissol Technol. 2014;21:27-38.
113. Sun Y, Østergaard J. Application of UV Imaging in Formulation Development. Pharm Res. 2017;34(5):929-40.
114. Wu JX, Rehder S, Berg Fvd, Amigo JM, Carstensen JM, Rades T, et al. Chemical imaging and solid state analysis at compact surfaces using UV imaging. Int J Pharm. 2014;477(1):527-35.
115. Panakanti R, Narang AS. Impact of Excipient Interactions on Drug Bioavailability from Solid Dosage Forms. Pharm Res. 2012;29(10):2639-59.
116. Li Z, Sun Y, Bar-Shalom D, Mu H, Larsen SW, Jensen H, et al. Towards functional characterization of excipients for oral solid dosage forms using UV–vis imaging. Liberation, release and dissolution. J Pharm Biomed Anal. 2021;194:113789.
117. Zarmpi P, Flanagan T, Meehan E, Mann J, Fotaki N. Surface dissolution UV imaging for characterization of superdisintegrants and their impact on drug dissolution. Int J Pharm. 2020;577:119080.
118. Ye F, Yaghmur A, Jensen H, Larsen SW, Larsen C, Østergaard J. Real-time UV imaging of drug diffusion and release from Pluronic F127 hydrogels. Eur J Pharm Sci. 2011;43(4):236-43.
119. Brannon-Peppas L. Preparation and characterization of crosslinked hydrophilic networks. In: Brannon-Peppas L, Harland R, editors. Absorbent polymer technology. Amsterdam: Elsevier; 1990. p. 45–66.
120. am Ende M, am Ende D. Chemical engineering in the pharmaceutical Industry: drug product design, development, and modeling. New Jersey: John Wiley & Sons, Inc.; 2019.
121. Siepmann J, Kranz H, Peppas NA, Bodmeier R. Calculation of the required size and shape of hydroxypropyl methylcellulose matrices to achieve desired drug release profiles. Int J Pharm. 2000;201(2):151-64.
122. Higuchi T. Rate of Release of Medicaments from Ointment Bases Containing Drugs in Suspension. J Pharm Sci. 1961;50(10):874-5.
123. Siepmann J, Kranz H, Bodmeier R, Peppas NA. HPMC-Matrices for Controlled Drug Delivery: A New Model Combining Diffusion, Swelling, and Dissolution Mechanisms and Predicting the Release Kinetics. Pharm Res. 1999;16(11):1748-56.
124. Siepmann J, Streubel A, Peppas NA. Understanding and Predicting Drug Delivery from Hydrophilic Matrix Tablets Using the “Sequential Layer” Model. Pharm Res. 2002;19(3):306-14.
125. Lamberti G, Galdi I, Barba AA. Controlled release from hydrogel-based solid matrices. A model accounting for water up-take, swelling and erosion. Int J Pharm. 2011;407(1):78-86.
126. Caccavo D, Cascone S, Lamberti G, Barba AA. Controlled drug release from hydrogel-based matrices: Experiments and modeling. Int J Pharm. 2015;486(1):144-52.
127. Caccavo D, Lamberti G. PoroViscoElastic model to describe hydrogels' behavior. Mater Sci Eng C. 2017;76:102-13.

128. Siepmann F, Eckart K, Maschke A, Kolter K, Siepmann J. Modeling drug release from PVAc/PVP matrix tablets. J Control Release. 2010;141(2):216-22.
129. Barba AA, d'Amore M, Chirico S, Lamberti G, Titomanlio G. A general code to predict the drug release kinetics from different shaped matrices. Eur J Pharm Sci. 2009;36(2):359-68.
130. Krögel I, Bodmeier R. Development of a multifunctional matrix drug delivery system surrounded by an impermeable cylinder. J Control Release. 1999;61(1):43-50.
131. Siepmann J, Karrout Y, Gehrke M, Penz FK, Siepmann F. Predicting drug release from HPMC/lactose tablets. Int J Pharm. 2013;441(1):826-34.
132. Colombo P, Sonvico F, Colombo G, Bettini R. Novel Platforms for Oral Drug Delivery. Pharm Res. 2009;26(3):601-11.
133. Pavurala N, Achenie LEK. A mechanistic approach for modeling oral drug delivery. Comput Chem Eng. 2013;57:196-206.
134. Kaunisto E, Marucci M, Borgquist P, Axelsson A. Mechanistic modelling of drug release from polymer-coated and swelling and dissolving polymer matrix systems. Int J Pharm. 2011;418(1):54-77.
135. Schaefer T, Holm P, Kristensen H. Melt pelletization in high shear mixer. I. Effects of process variables and binder. Acta Pharm Nord. 1992;4:133–40.
136. Schaefer T, Holm P, Kristensen H. Melt pelletization in high shear mixer. II. Power consumption and granule growth. Acta Pharm Nord. 1992;4:141–8.
137. Schaefer T, Holm P, Kristensen H. Melt pelletization in high shear mixer. III. Effect of lactose quality. Acta Pharm Nord. 1992;4:245–52.
138. Passerini N, Albertini B, González-Rodríguez ML, Cavallari C, Rodriguez L. Preparation and characterisation of ibuprofen–poloxamer 188 granules obtained by melt granulation. Eur J Pharm Sci. 2002;15(1):71-8.
139. Passerini N, Albertini B, Perissutti B, Rodriguez L. Evaluation of melt granulation and ultrasonic spray congealing as techniques to enhance the dissolution of praziquantel. Int J Pharm. 2006;318(1):92-102.
140. Perissutti B, Rubessa F, Moneghini M, Voinovich D. Formulation design of carbamazepine fast-release tablets prepared by melt granulation technique. Int J Pharm. 2003;256(1):53-63.
141. Thies R, Kleinebudde P. Melt pelletisation of a hygroscopic drug in a high shear mixer: Part 1. Influence of process variables. Int J Pharm. 1999;188(2):131-43.
142. Voinovich D, Moneghini M, Perissutti B, Filipovic-Grcic J, Grabnar I. Preparation in high-shear mixer of sustained-release pellets by melt pelletisation. Int J Pharm. 2000;203(1):235-44.
143. Steffens KE, Brenner MB, Hartig MU, Monschke M, Wagner KG. Melt granulation: A comparison of granules produced via high-shear mixing and twin-screw granulation. Int J Pharm. 2020;591:119941.
144. Zhang Y, Huo M, Zhou J, Zou A, Li W, Yao C, et al. DDSolver: An Add-In Program for Modeling and Comparison of Drug Dissolution Profiles. The AAPS Journal. 2010;12(3):263-71.
145. Goldoozian S, Mohylyuk V, Dashevskiy A, Bodmeier R. Gel Strength of Hydrophilic Matrix Tablets in Terms of In Vitro Robustness. Pharm Res. 2021;38(7):1297-306.

146. Yin X, Li L, Gu X, Wang H, Wu L, Qin W, et al. Dynamic structure model of polyelectrolyte complex based controlled-release matrix tablets visualized by synchrotron radiation micro-computed tomography. Mater Sci Eng C. 2020;116:111137.
147. Vlassenbroeck J, Masschaele B, Cnudde V, Dierick M, Pieters K, Van Hoorebeke L, et al. Octopus 8: A High Performance Tomographic Reconstruction Package for X-ray Tube and Synchrotron micro-CT. Advances in X-ray Tomography for Geomaterials2006. p. 167-73.
148. Ajay L, editor Drishti: a volume exploration and presentation tool. ProcSPIE; 2012.
149. Hedsund C, Gregersen T, Joensson IM, Olesen HV, Krogh K. Gastrointestinal transit times and motility in patients with cystic fibrosis. Scand J Gastroenterol. 2012;47(8-9):920-6.
150. Lamberti G, Galdi I, Barba AA. Controlled release from hydrogel-based solid matrices. A model accounting for water up-take, swelling and erosion. Int JPharm. 2011;407(1):78-86.
151. Pavurala N, Achenie LEK. A mechanistic approach for modeling oral drug delivery. Computers & Chemical Engineering. 2013;57:196-206.
152. Wen Huey Lai, Kek SL, Tay KG. Solving Nonlinear Least Squares Problem Using Gauss-Newton Method. Int j innov sci eng technol. 2017;4(1):258-62.
153. Vogel CR. Computational Methods for Inverse Problems. Philadelphia, USA: Society for Industrial and Applied Mathematics; 2002.
154. Viceconti M, Pappalardo F, Rodriguez B, Horner M, Bischoff J, Musuamba Tshinanu F. In silico trials: Verification, validation and uncertainty quantification of predictive models used in the regulatory evaluation of biomedical products. Methods. 2021;185:120-7.
155. Schaefer T, Holm P, Kristensen HG. Melt Granulation in A Laboratory Scale High Shear Mixer. Drug Development and Industrial Pharmacy. 1990;16(8):1249-77.
156. Lerdkanchanaporn S, Dollimore D, Evans SJ. Phase diagram for the mixtures of ibuprofen and stearic acid. Thermochim Acta. 2001;367–368:1-8.
157. Bose S, Du Y, Takhistov P, Michniak-Kohn B. Formulation optimization and topical delivery of quercetin from solid lipid based nanosystems. Int J Pharm. 2013;441(1-2):56-66.
158. Leinonen UI, Jalonen HU, Vihervaara PA, Laine ESU. Physical and lubrication properties of magnusium stearate. J Pharm Sci. 1992;81(12):1194-8.
159. Yodkhum K, Phaechamud T. Thermal Analysis of Chitosan-Lactate and Chitosan-Aluminum Monostearate Composite System. Adv Mat Res. 2012;506:278-81.
160. Gordon RE, VanKoevering CL, Reits DJ. Utilization of differential scanning calorimetry in the compatibility screening of ibuprofen with the stearate lubricants and construction of phase diagrams. Int J Pharm. 1984;21(1):99-105.
161. Meltzer V, Pincu E. Thermodynamic characterization of binary liquid crystal mixtures. Analele UniversităŃii din Bucureti – Chimie. 2008;1(17):15-8.
162. Yue D, Jia Y, Yao Y, Sun J, Jing Y. Structure and electrochemical behavior of ionic liquid analogue based on choline chloride and urea. Electrochim Acta. 2012;65:30-6.
163. Perkins SL, Painter P, Colina CM. Molecular dynamic simulations and vibrational analysisof an ionic liquid analogue. J Phys Chem B 2013;117:10250-60.

164. Phaechamud T, Tuntarawongsa S, Charoensuksai P. Evaporation behavior and characterization of eutectic solvent and ibuprofen eutectic solution. AAPS PharmSciTech. 2016;17:1213-20.
165. Aburahma MH, Badr-Eldin SM. Compritol 888 ATO: a multifunctional lipid excipient in drug delivery systems and nanopharmaceuticals. Expert Opin Drug Deliv. 2014;11(12):1865-83.
166. Setyawan D, Isadiartuti D, Betari SD, Paramita DP. Physical chracterization of ibuprofen-stearic acid binary mixture due to compression force. Indonesian J Pharm. 2016;27(1):28-34.
167. Kumar A, Singh P, Nanda A. Hot stage microscopy and its applications in pharmaceutical characterization. Appl Microsc. 2020;50:1-11.
168. Mallick S, Pattnaik S, Swain K, De PK, Saha A, Mazumdar P, et al. Physicochemical characterization of interaction of ibuprofen by solid-state milling with aluminum hydroxide. Drug Dev Ind Pharm. 2008;34(7):726-34.
169. Delaney SP, Nethercott MJ, Mays CJ, Winquist NT, Arthur D, Calahan JL, et al. Characterization of synthesized and commercial forms of magnesium stearate using differential scanning calorimetry, thermogravimetric analysis, powder X-ray diffraction, and solid-state NMR spectroscopy. J Pharm Sci. 2017;106(1):338-47.
170. Fini A, Cavallari C, Ospitali F, Gonzalez-Rodriguez ML. Theophylline-loaded compritol microspheres prepared by ultrasound-assisted atomization. J Pharm Sci. 2011;100(2):743-57.
171. Dragan F, Kacso I, Dreve S, Martin F, Borodi G, Bratu I, et al. Compatibility study of ibuprofen with some excipients employed for solid dosage forms. Rev Chim. 2015;66(2):191-5.
172. Eloy JO, Marchetti JM. Solid dispersions containing ursolic acid in Poloxamer 407 and PEG 6000: A comparative study of fusion and solvent methods. Powder Technol. 2014;253:98-106.
173. Othman MF, Anuar N, Ad Rahman S, Ahmad Taifuddin NA. Cocrystal Screening of Ibuprofen with Oxalic Acid and Citric Acid via Grinding Method. IOP Conf Ser: Mater Sci Eng. 2018;358(1):012065.
174. Biedrzycka K, Marcinkowska A. The Use of Hot Melt Extrusion to Prepare a Solid Dispersion of Ibuprofen in a Polymer Matrix. Polymers. 2023;15(13).
175. Bley H, Fussnegger B, Bodmeier R. Characterization and stability of solid dispersions based on PEG/polymer blends. Int J Pharm. 2010;390(2):165-73.
176. Shimada Y, Tateuchi R, Chatani H, Goto S. Mechanisms underlying changes in indomethacin solubility with local anesthetics and related basic additives. J Mol Struct. 2018;1155:165-70.
177. Cristofoletti R, Dressman JB. Dissolution methods to increasing discriminatory power of in vitro dissolution testing for ibuprofen free acid and its salts. J Pharm Sci. 2017;106(1):92-9.
178. Lu Y, Tang N, Lian R, Qi J, Wu W. Understanding the relationship between wettability and dissolution of solid dispersion. Int J Pharm. 2014;465(1):25-31.
179. Kim KT, Lee JY, Lee MY, Song CK, Choi J, Kim DD. Solid dispersions as a drug delivery system. J Pharm Investig. 2011;41:125-42.
180. Prabhu P, Patravale V. Dissolution enhancement of atorvastatin calcium by co-grinding technique. Drug Deliv Transl Res. 2016;6(4):380-91.

181. Łyszczarz E, Hofmanová J, Szafraniec-Szczęsny J, Jachowicz R. Orodispersible films containing ball milled aripiprazole-poloxamer®407 solid dispersions. Int J Pharm. 2020;575:118955.
182. Szafraniec J, Antosik A, Knapik-Kowalczuk J, Chmiel K, Kurek M, Gawlak K, et al. The Self-Assembly Phenomenon of Poloxamers and Its Effect on the Dissolution of a Poorly Soluble Drug from Solid Dispersions Obtained by Solvent Methods. Pharmaceutics. 2019;11(3).
183. Desai PM, Liew CV, Heng PWS. Review of Disintegrants and the Disintegration Phenomena. J Pharm Sci. 2016;105(9):2545-55.
184. Huanbutta K, Sriamornsak P, Limmatvapirat S, Luangtana-anan M, Yoshihashi Y, Yonemochi E, et al. Swelling kinetics of spray-dried chitosan acetate assessed by magnetic resonance imaging and their relation to drug release kinetics of chitosan matrix tablets. Eur J Pharm Biopharm. 2011;77(2):320-6.
185. Berardi A, Bisharat L, Blaibleh A, Pavoni L, Cespi M. A Simple and Inexpensive Image Analysis Technique to Study the Effect of Disintegrants Concentration and Diluents Type on Disintegration. J Pharm Sci. 2018;107(10):2643-52.
186. Berardi A, Bisharat L, Quodbach J, Abdel Rahim S, Perinelli DR, Cespi M. Advancing the understanding of the tablet disintegration phenomenon – An update on recent studies. Int J Pharm. 2021;598:120390.
187. Gupta A, Hunt RL, Shah RB, Sayeed VA, Khan MA. Disintegration of Highly Soluble Immediate Release Tablets: A Surrogate for Dissolution. AAPS PharmSciTech. 2009;10(2):495-9.
188. Fouad SA, Malaak FA, El-Nabarawi MA, Abu Zeid K. Development of orally disintegrating tablets containing solid dispersion of a poorly soluble drug for enhanced dissolution: In-vitro optimization/in-vivo evaluation. PLOS ONE. 2021;15(12):e0244646.
189. Andhariya JV, Jog R, Shen J, Choi S, Wang Y, Zou Y, et al. In vitro-in vivo correlation of parenteral PLGA microspheres: Effect of variable burst release. J Control Release. 2019;314:25-37.
190. Chung CK, García-Couce J, Campos Y, Kralisch D, Bierau K, Chan A, et al. Doxorubicin Loaded Poloxamer Thermosensitive Hydrogels: Chemical, Pharmacological and Biological Evaluation. Molecules. 2020;25(9).
191. Bruschi ML. Mathematical models of drug release. In: Bruschi ML, editor. Strategies to Modify the Drug Release from Pharmaceutical Systems: Woodhead Publishing; 2015. p. 63-86.
192. Kalný M, Grof Z, Štěpánek F. Microstructure based simulation of the disintegration and dissolution of immediate release pharmaceutical tablets. Powder Technol. 2021;377:257-68.
193. Dvořák J, Tomas J, Lizoňová D, Schöngut M, Dammer O, Pekárek T, et al. Investigation of tablet disintegration pathways by the combined use of magnetic resonance imaging, texture analysis and static light scattering. Int J Pharm. 2020;587:119719.
194. Park C, Lee HJ, Jin G, Ngo VH, Park J-B, Tran TDT, et al. Release Kinetics of Hydroxypropyl Methylcellulose Governing Drug Release and Hydrodynamic Changes of Matrix Tablet. Curr Drug Deliv. 2022;19(5):520-33.
195. Quodbach J, Kleinebudde P. A critical review on tablet disintegration. Pharm Dev Technol. 2016;21(6):763-74.

196. Markl D, Zeitler JA. A Review of Disintegration Mechanisms and Measurement Techniques. Pharm Res. 2017;34(5):890-917.
197. Zuo J-y, Park C, Doschak M, Löbenberg R. Are the release characteristics of Erzhi pills in line with traditional Chinese medicine theory? A quantitative study. J Integr Med. 2021;19(1):50-5.
198. Herlina, Kuswardhani N, Belgis M, Tiara A. Characterization of Physical and Chemical Properties of Effervescent Tablets Temulawak (Curcuma zanthorrhiza) in the Various Proportion of Sodium Bicarbonate and Tartaric Acid. E3S Web Conf. 2020;142.
199. Zheng X, Wu F, Hong Y, Shen L, Lin X, Feng Y. Improvements in sticking, hygroscopicity, and compactibility of effervescent systems by fluid-bed coating. RSC Adv. 2019;9(54):31594-608.
200. Patel S, Kaushal AM, Bansal AK. Compression Physics in the Formulation Development of Tablets. Crit Rev Ther Drug Carrier Syst. 2006;23(1):1-66.
201. Hwang R-C, Peck GR. A systematic evaluation of the compression and tablet characteristics of various types of microcrystalline cellulose. Pharm Technol Europe. 2001;25:112-32.
202. Anis Yohana C, Sriwidodo S, Marline A. Microcrystalline Cellulose as Pharmaceutical Excipient. In: Usama A, Juber A, editors. Pharmaceutical Formulation Design. Rijeka: IntechOpen; 2019. p. Ch. 3.
203. Lamoudi L, Chaumeil JC, Daoud K. Swelling, erosion and drug release characteristics of Sodium Diclofenac from heterogeneous matrix tablets. J Drug Deliv Sci Technol. 2016;31:93-100.
204. Mašková E, Kubová K, Raimi-Abraham BT, Vllasaliu D, Vohlídalová E, Turánek J, et al. Hypromellose – A traditional pharmaceutical excipient with modern applications in oral and oromucosal drug delivery. J Control Release. 2020;324:695-727.
205. Jamzad S, Tutunji L, Fassihi R. Analysis of macromolecular changes and drug release from hydrophilic matrix systems. Int J Pharm. 2005;292(1):75-85.
206. Chaiya P, Okonogi S, Phaechamud T. Stereomicroscope with Imaging Analysis: A Versatile Tool for Wetting, Gel Formation and Erosion Rate Determinations of Eutectic Effervescent Tablet. Pharmaceutics. 2022;14(6).
207. Fakhari A, Corcoran M, Schwarz A. Thermogelling properties of purified poloxamer 407. Heliyon. 2017;3(8).
208. Bukhari SN, Hussain MA, Haseeb MT, Wahid A, Ahmad N, Hussain SZ, et al. Metal Complexation of Arabinoxylan Engenders a Smart Material Offering pH, Solvents, and Salt Responsive On-Off Swelling with the Potential for Sustained Drug Delivery. Gels. 2022;8(5).
209. Cheng Y, Qin H, Acevedo NC, Jiang X, Shi X. 3D printing of extended-release tablets of theophylline using hydroxypropyl methylcellulose (HPMC) hydrogels. Int J Pharm. 2020;591:119983.
210. Kaberova Z, Karpushkin E, Nevoralová M, Vetrík M, Šlouf M, Dušková-Smrčková M. Microscopic Structure of Swollen Hydrogels by Scanning Electron and Light Microscopies: Artifacts and Reality. Polymers. 2020;12(3).
211. Hollings AL, Hackett MJ. Mapping metals in brain tissue with X-ray fluorescence and X-ray absorption spectroscopy at synchrotron light sources. Spectrosc Eur. 2022;34:26-9.

212. Yang B, Liu D, Lu J, Meng X, Sun Y. Phosphate uptake behavior and mechanism analysis of facilely synthesized nanocrystalline Zn-Fe layered double hydroxide with chloride intercalation. Surf Interface Anal. 2018;50(3):378-92.
213. Karakosta E, Jenneson PM, Sear RP, McDonald PJ. Observations of coarsening of air voids in a polymer--highly-soluble crystalline matrix during dissolution. Phys Rev E. 2006;74(1):011504.
214. Laity PR, Cameron RE. Synchrotron X-ray microtomographic study of tablet swelling. Eur J Pharm Biopharm. 2010;75(2):263-76.
215. Laity PR, Mantle MD, Gladden LF, Cameron RE. Magnetic resonance imaging and X-ray microtomography studies of a gel-forming tablet formulation. Eur J Pharm Biopharm. 2010;74(1):109-19.
216. de Terris T, Andreau O, Peyre P, Adamski F, Koutiri I, Gorny C, et al. Optimization and comparison of porosity rate measurement methods of Selective Laser Melted metallic parts. Additive Manufacturing. 2019;28:802-13.
217. Hesaraki S, Moztarzadeh F, Sharifi D. Formation of interconnected macropores in apatitic calcium phosphate bone cement with the use of an effervescent additive. J Biomed Mater Res A 2007;83A(1):80-7.
218. Li CL, Martini LG, Ford JL, Roberts M. The use of hypromellose in oral drug delivery. J Pharm Pharmacol. 2005;57(5):533-46.
219. Hillery A, Park K. Drug Delivery: Fundamentals and Applications. Boca Raton: CRC Press.; 2016.
220. Colombo P, Bettini R, Santi P, De Ascentiis A, Peppas NA. Analysis of the swelling and release mechanisms from drug delivery systems with emphasis on drug solubility and water transport. J Control Release. 1996;39(2):231-7.
221. Tahara K, Yamamoto K, Nishihata T. Application of model-independent and model analysis for the investigation of effect of drug solubility on its release rate from hydroxypropyl methylcellulose sustained release tablets. Int J Pharm. 1996;133(1):17-27.
222. Xu H, Liu L, Li X, Ma J, Liu R, Wang S. Extended tacrolimus release via the combination of lipid-based solid dispersion and HPMC hydrogel matrix tablets. Asian J Pharm Sci. 2019;14(4):445-54.
223. Viridén A, Wittgren B, Larsson A. The consequence of the chemical composition of HPMC in matrix tablets on the release behaviour of model drug substances having different solubility. Eur J Pharm Biopharm. 2011;77(1):99-110.
224. Tajarobi F, Abrahmsén-Alami S, Carlsson AS, Larsson A. Simultaneous probing of swelling, erosion and dissolution by NMR-microimaging—Effect of solubility of additives on HPMC matrix tablets. Eur J Pharm Sci. 2009;37(2):89-97.
225. Zhang P, Yang LC, Li L, Qu QT, Wu YP, Shimizu M. Effects of preparation conditions on porous polymer membranes by microwave assisted effervescent disintegrable reaction and their electrochemical properties. J Membr Sci. 2010;362(1):113-8.
226. Griveau L, Lafont M, le Goff H, Drouglazet C, Robbiani B, Berthier A, et al. Design and characterization of an in vivo injectable hydrogel with effervescently generated porosity for regenerative medicine applications. Acta Biomater. 2022;140:324-37.
227. Milcovich G, Antunes FE, Farra R, Grassi G, Grassi M, Asaro F. Modulating carbohydrate-based hydrogels as viscoelastic lubricant substitute for articular cartilages. Int J Biol Macromol. 2017;102:796-804.

228. Xiong Z, Wu P, Wang N, Cong H, Chen XD. How bio-relevant buffering media affect dissolution and release kinetics of solid formula: Ibuprofen as a model. J Drug Deliv Sci Technol. 2023;87:104857.
229. Chaiya P, Rojviriya C, Pichayakorn W, Phaechamud T. New Insight into the Impact of Effervescence on Gel Layer Microstructure and Drug Release of Effervescent Matrices Using Combined Mechanical and Imaging Characterisation Techniques. Pharmaceutics. 2022;14(11).
230. He C, Kim SW, Lee DS. In situ gelling stimuli-sensitive block copolymer hydrogels for drug delivery. J Control Release. 2008;127(3):189-207.
231. Ahuja N, Katare OP, Singh B. Studies on dissolution enhancement and mathematical modeling of drug release of a poorly water-soluble drug using water-soluble carriers. Eur J Pharm Biopharm. 2007;65(1):26-38.
232. Okumu A, DiMaso M, Löbenberg R. Dynamic Dissolution Testing To Establish In Vitro/In Vivo Correlations for Montelukast Sodium, a Poorly Soluble Drug. Pharm Res. 2008;25(12):2778-85.
233. Fallingborg J, Pedersen P, Jacobsen BA. Small Intestinal Transit Time and Intraluminal pH in Ileocecal Resected Patients with Crohn's Disease. Dig Dis Sci. 1998;43(4):702-5.
234. Wehbe M, Haslam AJ, Jackson G, Galindo A. Phase behaviour and pH-solubility profile prediction of aqueous buffered solutions of ibuprofen and ketoprofen. Fluid Phase Equilib. 2022;560:113504.
235. Janus E, Ossowicz P, Klebeko J, Nowak A, Duchnik W, Kucharski Ł, et al. Enhancement of ibuprofen solubility and skin permeation by conjugation with l-valine alkyl esters. RSC Adv. 2020;10(13):7570-84.
236. Zhang Y-h, Huang Z-y, editors. Preparation of a Kind of Honey Effervescent Tablets. Proceedings of 2013 4th International Asia Conference on Industrial Engineering and Management Innovation (IEMI2013); 2014 2014//; Berlin, Heidelberg: Springer Berlin Heidelberg.
237. Chaiya P, Phaechamud T. Effect of matrix-forming agent ratios on drug release, water sorption and erosion behaviors of shellac wax-poloxamer matrix tablet. Mater Today: Proc. 2022;52:2439-43.
238. Ghimire M, Hodges LA, Band J, O'Mahony B, McInnes FJ, Mullen AB, et al. In-vitro and in-vivo erosion profiles of hydroxypropylmethylcellulose (HPMC) matrix tablets. J Control Release. 2010;147(1):70-5.
239. Costa P, Sousa Lobo JM. Modeling and comparison of dissolution profiles. Eur J Pharm Sci. 2001;13(2):123-33.
240. Tanigawara Y, Yamaoka K, Nakagawa T, Uno T. New Method for the Evaluation of in Vitro Dissolution Time and Disintegration Time. Chem Pharm Bull. 1982;30(3):1088-90.
241. Podczeck F. Comparison of in vitro dissolution profiles by calculating mean dissolution time (MDT) or mean residence time (MRT). Int J Pharm. 1993;97(1):93-100.
242. Saeidipour F, Mansourpour Z, Mortazavian E, Rafiee-Tehrani N, Rafiee-Tehrani M. New comprehensive mathematical model for HPMC-MCC based matrices to design oral controlled release systems. Eur J Pharm Biopharm. 2017;121:61-72.

243. Chirico S, Dalmoro A, Lamberti G, Russo G, Titomanlio G. Analysis and modeling of swelling and erosion behavior for pure HPMC tablet. J Control Release. 2007;122(2):181-8.
244. Bi YX, Sunada H, Yonezawa Y, Danjo K. Evaluation of rapidly disintegrating tablets prepared by a direct compression method. Drug Dev Ind Pharm. 1999;25(5):571-81.
245. Ly A, Achouri IE, Gosselin R, Abatzoglou N. Rheological behavior of porous pharmaceutical materials: Linking torque profiles during wet massing to water diffusion coefficients and penetration time. Chem Eng Process: Process Intensif. 2020;157:108152.
246. Kikuchi S, Onuki Y, Kuribayashi H, Takayama K. Relationship between Diffusivity of Water Molecules Inside Hydrating Tablets and Their Drug Release Behavior Elucidated by Magnetic Resonance Imaging. Chem Pharm Bull. 2012;60(4):536-42.
247. Shah RB, Tawakkul MA, Khan MA. Comparative evaluation of flow for pharmaceutical powders and granules. AAPS PharmSciTech. 2008;9(1):250-8.
248. Hamdani J, Moës AJ, Amighi K. Development and evaluation of prolonged release pellets obtained by the melt pelletization process. Int J Pharm. 2002;245(1-2):167-77.
249. Macho O, Gabrišová Ľ, Guštafík A, Jezso K, Juriga M, Kabát J, et al. The Influence of Wet Granulation Parameters on the Compaction Behavior and Tablet Strength of a Hydralazine Powder Mixture. Pharmaceutics. 2023;15(8).
250. Kitazawa S, Johno I, Ito Y, Teramura S, Okado J. Effects of hardness on the disintegration time and the dissolution rate of uncoated caffeine tablets. J Pharm Pharmacol. 1975;27(10):765-70.
251. Ngwuluka NC, Lawal KA, Olorunfemi PO, Ochekpe NA. Post-market in vitro bioequivalence study of six brands of ciprofloxacin tablets/caplets in Jos, Nigeria. Sci Res Essays. 2009;4:298-305.
252. Fouad SA, Malaak FA, El-Nabarawi MA, Abu Zeid K, Ghoneim AM. Preparation of solid dispersion systems for enhanced dissolution of poorly water soluble diacerein: In-vitro evaluation, optimization and physiologically based pharmacokinetic modeling. PLOS ONE. 2021;16(1):e0245482.
253. Frade T, Gomes A. ZnO Nanostructured Thin Films Applied on Ibuprofen Photoelectrodegradation. Solid State Phenom. 2013;194:258-61.
254. Susilo SP, Pertiwi SH, Ainurofiq A. Development and validation of analytical methods for multicomponent crystals of ibuprofen with malic and tartaric acid using spectrophotometry. J Phys Conf Ser. 2022;2190(1):012033.
255. Jensen SS, Jensen H, Goodall DM, Østergaard J. Performance characteristics of UV imaging instrumentation for diffusion, dissolution and release testing studies. J Pharm Biomed Anal. 2016;131:113-23.
256. Bock F, Bøtker JP, Larsen SW, Lu X, Østergaard J. Methodological Considerations in Development of UV Imaging for Characterization of Intra-Tumoral Injectables Using cAMP as a Model Substance. Int J Mol Sci. 2022;23(7):3599.

มหาวิทยาลัยศิลปากร

VITA

NAME	Mr. Pornsit Chaiya
INSTITUTIONS ATTENDED	2019 - 2023; Doctor of Philosophy (Pharmaceutical Engineering), Faculty of Pharmacy, Silpakorn University, Thailand (Under RGJ-Ph.D. scholarship) 2022, January - 2022, June; Guest Ph.D. student, Application of UV-vis imaging for real-time monitoring of matrix tablet behavior under the supervision of Prof.Jesper Østergaard, Department of Pharmacy, University of Copenhagen, København Ø, Copenhagen, Denmark. 2018-current: Lecturer, Department of Industrial Pharmacy, School of Pharmacy, Walailak University, Thailand. 2009-2014; Pharm D., School of Pharmacy, Walailak University, Thailand (First class honors with GPA: 3.60) Major in Pharmaceutical Science
PUBLICATION	Chaiya P, Rojviriya C, Pichayakorn W, Phaechamud T. New insight into the impact of effervescence on gel layer microstructure and drug release of effervescent matrices using combined mechanical and imaging characterisation techniques. Pharmaceutics. 2022;14:2299. Chaiya P, Okonogi S, Phaechamud T. Stereomicroscope with imaging analysis: A versatile tool for wetting, gel formation and erosion rate determinations of eutectic effervescent tablet. Pharmaceutics. 2022;14:1280. Chaiya P, Chinpaisal C, Limmatvapirat S, Phaechamuand T. Alteration of crystallinity and thermal properties from incompatibility between ibuprofen and boundary lubricants. Mater. Today: Proc. 2021;47:3500-3508.